AD-A134 845 EVALUATION OF A BIAXIAL TEST FIXTURE(U) ANAMET LABS INC 1/2
SAN CARLOS CA APPLIED MECHANICS DIV J A HOLST JAN 83
ANAMET-1082.1A AFWAL-TR-82-3109 F33615-81-C-3201
UNCLASSIFIED F/G 11/4 NL

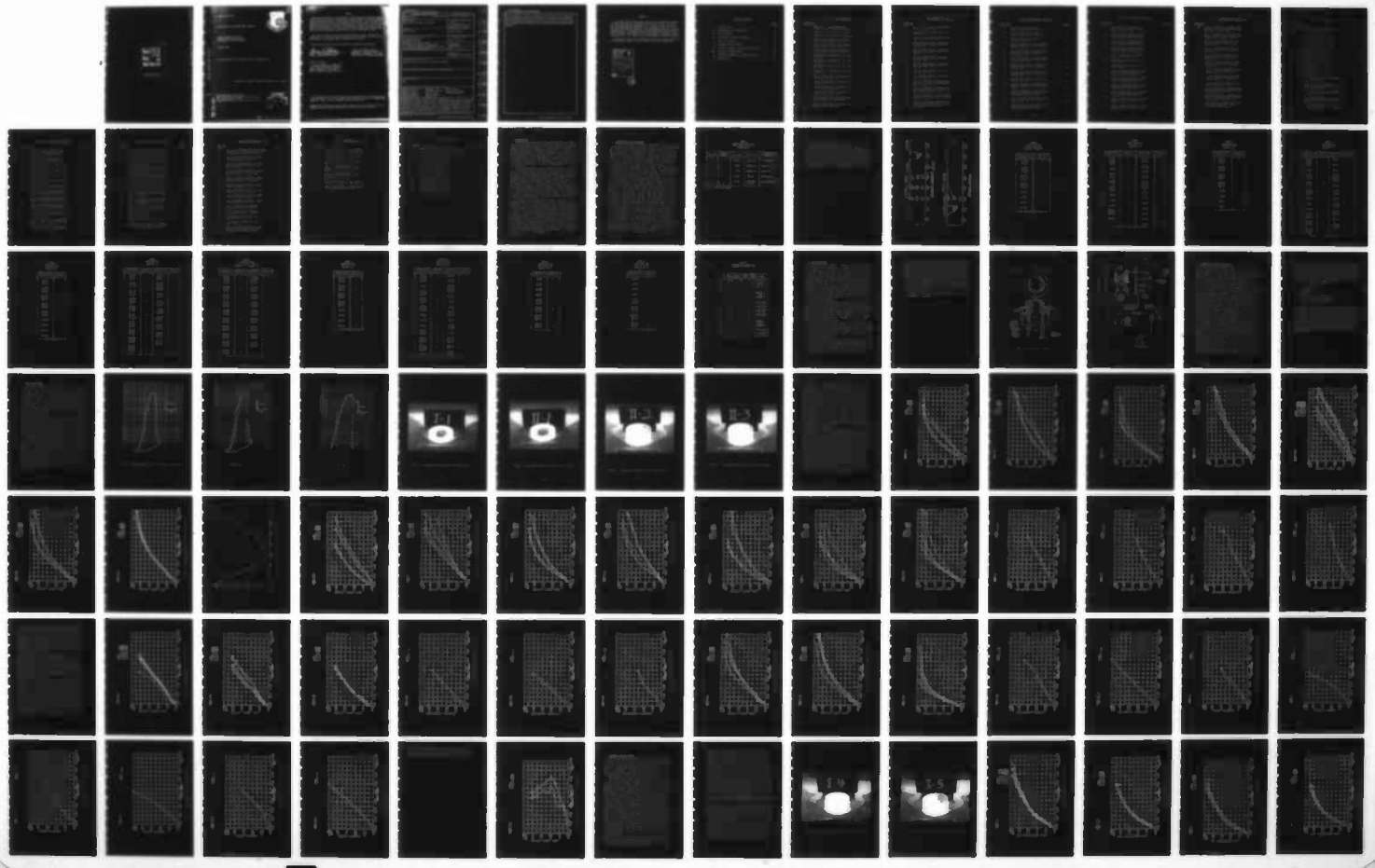

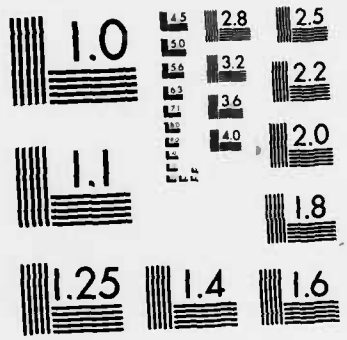

MICROCOPY RESOLUTION TEST CHART
NATIONAL BUREAU OF STANDARDS-1963-A

AFWAL-TR-82-3109

EVALUATION OF A BIAXIAL TEST FIXTURE

Anamet Laboratories, Inc.
Applied Mechanics Division
San Carlos, California 94070

January 1983

Interim Report for Period April 1981 - October 1982

Approved for public release; distribution unlimited

Flight Dynamics Laboratory
Air Force Wright Aeronautical Laboratories
Air Force Systems Command
Wright-Patterson Air Force Base, Ohio 45433

AD-A134 945

DTIC FILE COPY

DTIC ELECTE NOV 21 1983

83 11 15 105

NOTICE

When Government drawings, specifications, or other data are used for any purpose other than in connection with a definitely related Government procurement operation, the United States Government thereby incurs no responsibility nor any obligation whatsoever; and the fact that the government may have formulated, furnished, or in any way supplied the said drawings, specifications, or other data, is not to be regarded by implication or otherwise as in any manner licensing the holder or any other person or corporation, or conveying any rights or permission to manufacture use, or sell any patented invention that may in any way be related thereto.

This report has been reviewed by the Office of Public Affairs (ASD/PA) and is releasable to the National Technical Information Service (NTIS). At NTIS, it will be available to the general public, including foreign nations.

This technical report has been reviewed and is approved for publication.

James R. Johnson

JAMES R. JOHNSON, Project Engineer
Design & Analysis Methods Group

Fred A. Picchioni

FREDERICK A. PICCHIONI, Lt Col, USAF
Chief, Analysis & Optimization Branch

FOR THE COMMANDER

Ralph L. Kuster Jr.

RALPH L. KUSTER, JR., Col, USAF
Chief, Structures & Dynamics Division

"If your address has changed, if you wish to be removed from our mailing list, or if the addressee is no longer employed by your organization please notify AFWAL/FIBRA, W-PAFB, OH 45433 to help us maintain a current mailing list".

Copies of this report should not be returned unless return is required by security considerations, contractual obligations, or notice on a specific document.

UNCLASSIFIED

SECURITY CLASSIFICATION OF THIS PAGE (When Data Entered)

REPORT DOCUMENTATION PAGE

READ INSTRUCTIONS BEFORE COMPLETING FORM

1. REPORT NUMBER: AFWAL-TR-82-3109	2. GOVT ACCESSION NO.
3. RECIPIENT'S CATALOG NUMBER	
4. TITLE (and Subtitle): EVALUATION OF A BIAXIAL TEST FIXTURE	5. TYPE OF REPORT & PERIOD COVERED: INTERIM, Apr 81 - Oct 82
6. PERFORMING ORG. REPORT NUMBER: Anamet Lab. No. 1082.1A	
7. AUTHOR(s): James A. Holst	8. CONTRACT OR GRANT NUMBER(s): F33615-81-C-3201
9. PERFORMING ORGANIZATION NAME AND ADDRESS: Anamet Laboratories, Inc. 100 Industrial Way San Carlos, CA 94070	10. PROGRAM ELEMENT, PROJECT, TASK AREA & WORK UNIT NUMBERS: 62201F 2401 02 45
11. CONTROLLING OFFICE NAME AND ADDRESS: Flight Dynamics Laboratory (AFWAL/FIBRA) Air Force Wright Aeronautical Laboratories (AFSC) Wright-Patterson AFB, OH 45433	12. REPORT DATE: January 1983 13. NUMBER OF PAGES: 166
14. MONITORING AGENCY NAME & ADDRESS (if different from Controlling Office)	15. SECURITY CLASS. (of this report): Unclassified 15a. DECLASSIFICATION DOWNGRADING SCHEDULE

16. DISTRIBUTION STATEMENT (of this Report)

Approved for public release, distribution unlimited

17. DISTRIBUTION STATEMENT (of the abstract entered in Block 20, if different from Report)

18. SUPPLEMENTARY NOTES

NONE

19. KEY WORDS (Continue on reverse side if necessary and identify by block number)

Composite Cylinders	Structural Test	Ring Specimens
Biaxial Testing	Test Instrumentation	Biaxial Test Fixtures
Composite Laminates	Static Testing	Laminated Composites
Advanced Composites	Biaxial Stresses	
Composite Testing	Strain Gages	

20. ABSTRACT (Continue on reverse side if necessary and identify by block number)

This report evaluates a test system for examining laminated composite materials subjected to a biaxial state of stress. The system utilizes short, thin-walled cylindrical specimens loaded with combinations of axial compression, internal pressure and external pressure. Fourteen instrumented specimens were tested with gages of five different pattern designs and eleven different gage layouts depending on the type of load applied to the specimens. The test data is reported and the performance, validity and repeatability of the test system is evaluated in the report. It was found that the system was best suited for

DD FORM 1 JAN 73 1473 EDITION OF 1 NOV 65 IS OBSOLETE

SECURITY CLASSIFICATION OF THIS PAGE (When Data Entered)

testing specimens with internal pressure only. The next best test results were obtained with axial load only. Combinations of internal pressure with axial load produced good results, however there was little correlation between the biaxial stress ratio and the shape of the failure envelopes. Very poor and unpredictable results were obtained from the tests using external pressure loads. These specimens failed in buckling at very low loads due to compressive hoop stresses.

FOREWORD

This report presents the results of the tests of fourteen short composite cylindrical specimens when subjected to biaxial states of stress, as applied by a test system which was developed under a previous contract. The tests were performed by Anamet Laboratories, Inc., San Carlos, California, for the Air Force Flight Dynamics Laboratory, Air Force Wright Aeronautical Laboratories, Wright-Patterson Air Force Base, Ohio, as ASIAC Problem No. 403 under Contract F33615-81-C-3201, "The Aerospace Structures Information and Analysis Center," which is operated under contract for the Flight Dynamics Laboratory by Anamet Laboratories, Inc. Mr. James R. Johnson (AFWAL/FIBRA) is the project engineer.

The work was done by the Applied Mechanics Division of Anamet Laboratories. Program Manager is Edward B. Flora. James A. Holst was the investigator.

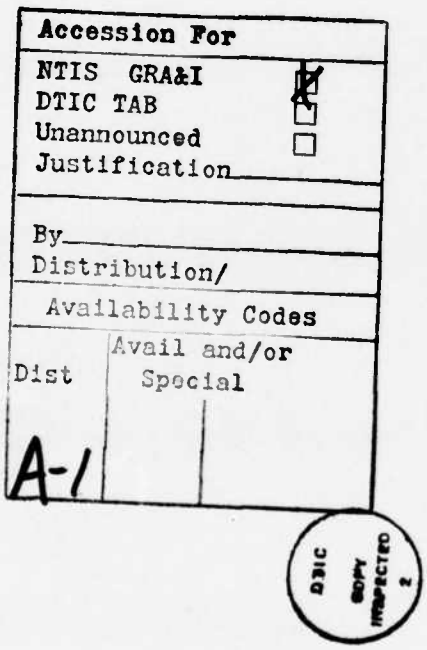

TABLE OF CONTENTS

LIST OF ILLUSTRATIONS

LIST OF ILLUSTRATIONS (Continued)

LIST OF ILLUSTRATIONS (Continued)

LIST OF ILLUSTRATIONS (Continued)

LIST OF ILLUSTRATIONS (Continued)

LIST OF ILLUSTRATIONS (Continued)

LIST OF ILLUSTRATIONS (Continued)

LIST OF ILLUSTRATIONS (Continued)

LIST OF ILLUSTRATIONS (Continued)

LIST OF ILLUSTRATIONS (Concluded)

LIST OF TABLES

I. INTRODUCTION

The Aerospace Structures Information and Analysis Center (ASIAC) has designed and fabricated a test system for examining composite materials subjected to biaxial states of stress. The system was designed for examining quadrants II, III and IV of the biaxial stress plane. Theoretical aspects of the system have been discussed in Anamet Laboratories, Inc. Report No. 277.502, "Technical Proposal for Test System for Conducting Biaxial Tests of Composite Laminates." The development of the system is described in ASIAC Report No. 180.1A, "Development of a Biaxial Test Fixture."

The system utilizes short, thin-wall cylindrical specimens. The ring specimens may be loaded with combinations of axial compression, internal pressure and external pressure. The axial compressive load is applied through the high pressure lubricant trapped between the specimen ends and the upper and lower parallel platens. The system is loaded with a standard 110 kip universal test machine. The internal and external pressure is produced by a manual or electric hydraulic 10,000 psi power supply. The internal pressure is retained within the volume between the specimen and the inner core of the fixture. The external pressure is retained with the aid of an external pressure collet placed around the specimen.

The goal of this project was to develop a relatively inexpensive method of conducting valid tests on composite materials subjected to biaxial states of stress. This required that the test procedure, test fixtures and specimens be simple and easily produced. Also, the resulting test data had to be valid and reducible to definable relationships between macroscopic stresses and applied loads. The method selected uses the classical relationships of thin-wall cylinders subjected to axial load, internal pressure and external pressure. Fourteen specimens instrumented with bonded resistive-foil type strain gages were tested under various load combinations. This evaluation is a review of this test data and investigates the performance, validity and repeatability of the test system.

II. INSTRUMENTED TEST SPECIMENS

A total of fourteen instrumented specimens and several uninstrumented specimens were tested. The uninstrumented specimens were used to develop setup procedures before testing the instrumented specimens. The specimens were made of a graphite epoxy composite with a ± 45 degree layup. The specimens were manufactured by IIT (Illinois Institute of Technology). Details of the specimens' construction were not provided. It is assumed that there were two specific types of construction marked I and II. The specimens were cylindrical with an inside diameter of 3.92 inches and a wall thickness of 0.045 inches. This corresponds to a cross-sectional area of 0.554 square inches. Both 1-inch and 2-inch specimen lengths were tested. The ends of the specimens were ground flat and parallel to ± 0.0005 inches.

The specimens were instrumented with bonded resistive-foil type strain gages of five different pattern designs. The gage type, pattern design, gage length and model numbers are listed in Table 1. In some cases type 5 gages were substituted for type 4 gages. The gages were bonded to both the inside and outside surface of the specimens. A code system was devised to identify each gage element on the specimen. The code consisted of a two or three digit number followed by a three character string. The first two or three digits represent the angular position of the element around the circumference. The angular locations used in these tests were 0°, 45°, 90°, 135°, 180°, 225°, 270° and 315°. The first character in the string indicated if the gage element was on the internal or external surface of the specimen. This first character will be (E) for external or (I) for internal. The second character of the string indicated the lengthwise location of the gage. This second character will be (T) for top, (U) for upper, (C) for center, (L) for lower and (B) for bottom. Gages in the upper and lower position lie mid-way between the top and center and the bottom and center, respectively. The third character represents the measurement direction of the element. This character will be (A) for axial strain, (D) for diagonal

TABLE 1

BONDED RESISTIVE-FOIL TYPE

STRAIN GAGES

Gage Type	Number of Elements	Gage Length	Pattern Type	Micro-Measurements Pattern No.
1	2	0.060"	90° cross	CEA-06-062WT-350
2	1	0.062"	single axis	FAE-06S-35-S6ES*
3	1	0.125"	single axis	EA-06-125AC-350
4	2	0.125"	90° tee	CEA-06-125UT-350
5	3	0.125"	0°-45°-90° rosette	CEA-03-125UR-350

*BLH Electronics part number

strain and (T) for tangential or hoop strain. A typical example of a gage layout is shown in Figure 1.

There were eleven different gage layouts used depending on the type of load applied to the specimen. These gage layouts are listed in Tables 2 through 12. Table 13 list the test number, specimen type, gage layout and load condition for all the instrumented specimens tested. The specimens were loaded with combinations of axial compression, internal pressure and external pressure. Different ratios of axial compression and pressure were used to obtain different ratios of axial stress (σ_x) and hoop stress (σ_θ).

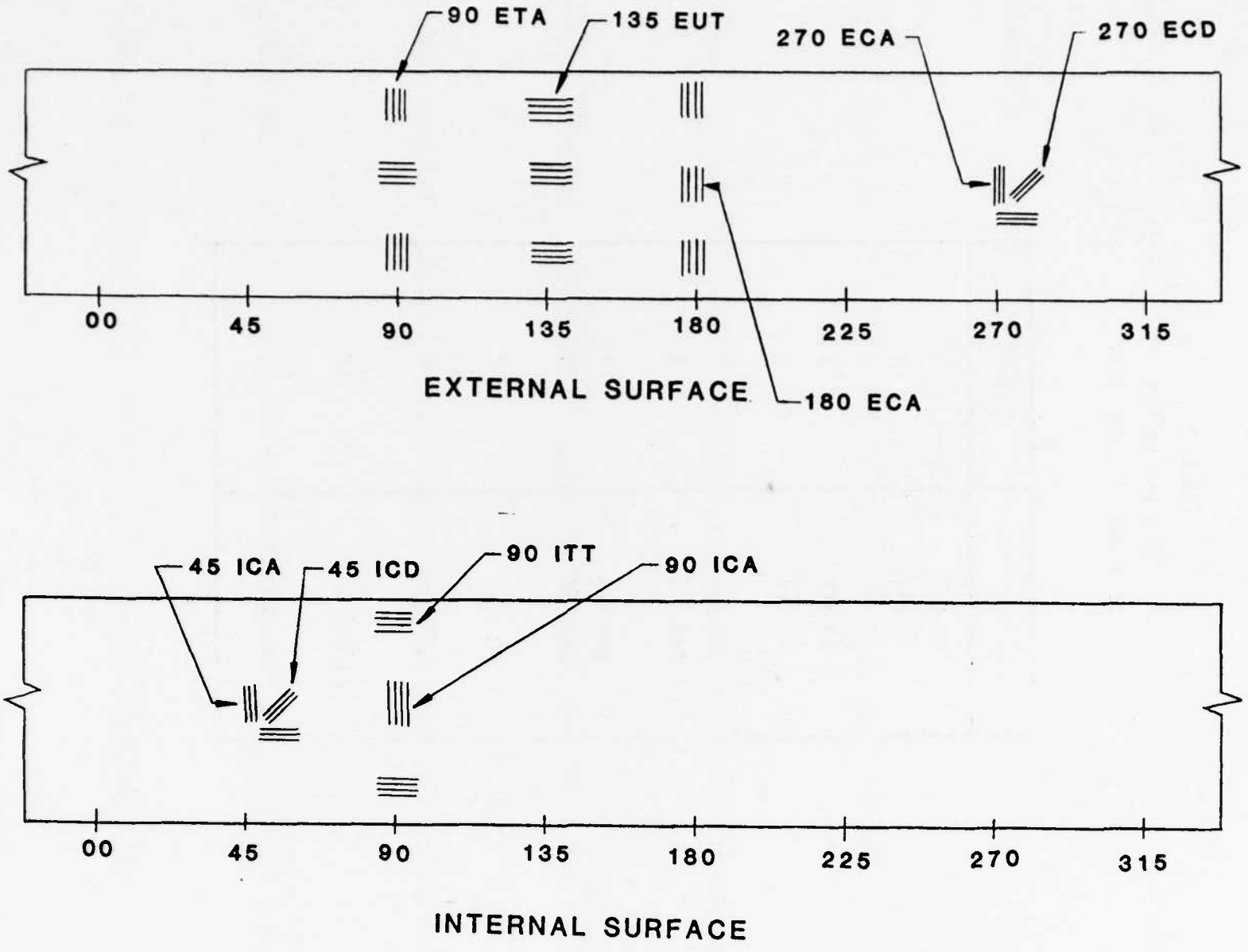

Figure 1 Sketch of a Typical Gage Layout Showing Element Identification Codes

TABLE 2

GAGE LAYOUT FOR

TEST NOS. I-1 AND II-1

Gage Position	Gage Type
90 ETA	1
90 ETT	1
90 ECA	1
90 ECT	1
180 ETA	1
180 ETT	1
180 ECA	1
180 ECT	1
90 ITA	2
90 ICA	2
180 ITA	2
180 ICA	2

TABLE 3
GAGE LAYOUT FOR
TEST NO. II-2

Gage Position	Gage Type	Gage Position	Gage Type
00 ECA	5	180 ECA	1
00 ECD	5	180 ECT	1
00 ECT	5		
		180 ELA	2
45 ECA	3		
		180 EBA	2
90 ETA	1		
90 ETT	1	225 ECA	3
90 EUA	2	270 ECA	5
		270 ECD	5
90 ECA	1	270 ECT	5
90 ECT	1		
		315 ECA	3
90 ELA	2		
		90 ITA	2
90 EBA	2		
		90 ICA	3
135 ECA	3		
		90 IBA	2
180 ETA	1		
180 ETT	1	180 ITA	2
180 EUA	2	180 ICA	3
		180 IBA	2

TABLE 4
GAGE LAYOUT FOR
TEST NO. II-3

Gage Position	Gage Type
90 ETA	1
90 ETT	1
90 ECA	4
90 ECT	4
180 ETA	1
180 ETT	1
180 ECA	4
180 ECT	4
90 ITA	2
90 ICA	3
180 ITA	2
180 ICA	3

TABLE 5
GAGE LAYOUT FOR
TEST NO. I-4

Gage Position	Gage Type	Gage Position	Gage Type
00 ECA	5	225 EUT	3
00 ECD	5		
00 ECT	5	225 ECT	3
45 ECT	3	225 ELT	3
90 ETA	1	270 ECA	5
90 ETT	1	270 ECD	5
		270 ECT	5
90 ECA	4		
90 ECT	4	315 ECT	3
90 EBA	1	90 ITA	1
90 EBT	1	90 ITT	1
135 EUT	3	90 ICT	3
135 ECT	3	90 IBA	1
		90 IBT	1
135 ELT	3		
		180 ITA	1
180 ETA	1	180 ITT	1
180 ETT	1		
		180 ICT	3
180 ECA	4		
180 ECT	4	180 IBA	1
		180 IBT	1
180 EBA	1		
180 EBT	1		

TABLE 6
GAGE LAYOUT FOR
TEST NO. I-5

Gage Position	Gage Type
90 ETA	1
90 ETT	1
90 ECA	4
90 ECT	4
180 ETA	1
180 ETT	1
180 ECA	4
180 ECT	4
270 ECA	5
270 ECT	5
90 ITA	2
90 ICT	3
180 ITA	2
180 ICT	3

TABLE 7

GAGE LAYOUT FOR

TEST NO. I-6

Gage Position	Gage Type	Gage Position	Gage Type
00 ECA	4	270 ECA	4
00 ECT	4	270 ECT	4
45 ECA	4	315 ECA	5
45 ECT	4	315 ECD	5
		315 ECT	5
90 ETA	1		
90 ETT	1	90 ITA	1
		90 ITT	1
90 ECA	4		
90 ECT	4	90 ICA	4
		90 ICT	4
90 EBA	1		
90 EBT	1	90 IBA	1
		90 IBT	1
135 ECA	4		
135 ECT	4	180 ITA	1
		180 ITT	1
180 ETA	1		
180 ETT	1	180 ICA	4
		180 ICT	4
180 ECA	4		
180 ECT	4	180 IBA	1
		180 IBT	1
180 EBA	1		
180 EBT	1	315 ICA	4
		315 ICT	4
225 ECA	5		
225 ECD	5		
225 ECT	5		

TABLE 8

GAGE LAYOUT FOR

TEST NOS. I-7, I-8 AND II-12

Gage Position	Gage Type	Gage Position	Gage Type
00 ECA	5	270 ECA	5
00 ECD	5	270 ECD	5
00 ECT	5	270 ECT	5
45 ECA	4	315 ECA	4
45 ECT	4	315 ECT	4
90 ETA	1	90 ITA	1
90 ETT	1	90 ITT	1
90 ECA	4	90 ICA	4
90 ECT	4	90 ICT	4
90 EBA	1	90 IBA	1
90 EBT	1	90 IBT	1
135 ECA	4	180 ITA	1
135 ECT	4	180 ITT	1
180 ETA	1	180 ICA	4
180 ETT	1	180 ICT	4
180 ECA	4	180 IBA	1
180 ECT	4	180 IBT	1
180 EBA	1	315 ICA	4
180 EBT	1	315 ICT	4
225 ECA	4		
225 ECT	4		

TABLE 9
GAGE LAYOUT FOR
TEST NO. I-9

Gage Position	Gage Type
90 ETA	1
90 ETT	1
90 ECA	4
90 ECT	4
180 ETA	1
180 ETT	1
180 ECA	4
180 ECT	4
90 ITA	2
90 ICA	3
180 ITA	2
180 ICT	3

TABLE 10

GAGE LAYOUT FOR

TEST NO. II-10

Gage Position	Gage Type	Gage Position	Gage Type
00 ECA	5	225 ECT	3
00 ECD	5		
00 ECT	5	225 ELT	3
45 ECT	3	270 ECA	5
		270 ECD	5
90 ETA	1	270 ECT	5
90 ETT	1		
		315 ECT	3
90 ECA	4		
90 ECT	4	00 ICT	3
90 EBA	1	45 ICT	3
90 EBT	1		
		90 ITA	1
135 EUT	3	90 ITT	1
135 ECT	3	90 ICT	3
135 ELT	3	90 IBA	1
		90 IBT	1
180 ETA	1		
180 ETT	1	135 ICT	3
180 ECA	4	180 ITA	1
180 ECT	4	180 ITT	1
180 EBA	1	180 ICT	3
180 EBT	1		
		180 IBA	1
225 EUT	3	180 IBT	1

TABLE 11
GAGE LAYOUT FOR
TEST NO. II-11

Gage Position	Gage Type
90 ETA	2
90 ECT	3
180 ETA	2
180 ECT	3
90 ITA	1
90 ITT	1
90 ICA	4
90 ICT	4
180 ITA	1
180 ITT	1
180 ICA	4
180 ICT	4

TABLE 12
GAGE LAYOUT FOR
TEST NO. II-13

Gage Position	Gage Type
90 ETA	2
90 ECA	3
180 ETA	2
180 ECT	3
90 ITA	1
90 ITT	1
90 ICA	4
90 ICT	4
180 ITA	1
180 ITT	1
180 ICA	4
180 ICT	4

TABLE 13

INSTRUMENTED SPECIMENS TESTED

Test No.	Specimen Length	Material Construction	Gage Layout Table No.	Number of Gage Elements	Load Condition
I-I	I5/I6"	I	2	I2	Axial Load ($-\sigma_x$)
II-I	15/16"	II	2	I2	Axial Load ($-\sigma_x$)
II-2	2"	II	3	30	Axial Load ($-\sigma_x$)
II-3	2"	II	4	I2	Axial Load ($-\sigma_x$)
I-4	2"	I	5	36	Internal Pressure ($+\sigma_\theta$)
I-5	2"	I	6	I4	Internal Pressure ($+\sigma_\theta$)
I-6	2"	I	7	40	Axial & Internal ($-\sigma_x = \frac{1}{2}\sigma_\theta$)
I-7	2"	I	8	40	Axial & Internal ($-\sigma_x = \sigma_\theta$)
I-8	2"	I	8	40	Axial & Internal ($-\sigma_x = 2\sigma_\theta$)
I-9	2"	I	9	I2	Axial & Internal ($-\sigma_x = \sigma_\theta$)
II-I0	2"	II	I0	39	External Pressure ($-\sigma_\theta$)
II-II	2"	II	II	I2	External Pressure ($-\sigma_\theta$)
II-I2	2"	II	8	40	Axial & External ($-\sigma_x = -\sigma_\theta$)
II-I3	2"	II	I2	I2	Axial & External ($-\sigma_x = -\sigma_\theta$)

III. TEST EQUIPMENT

The biaxial test fixture consisted of a hollow cylinder acting as the lower platen while a stepped solid cylinder served as the upper platen and inner core. The specimen was placed around the inner core and was loaded between the two platen surfaces. The load was transmitted through high pressure lubricant trapped between the specimen ends and the platen surfaces. The internal pressure was retained within the volume between the specimen and the inner core. A special molded rubber gasket was also used to help retain hydraulic pressure. The inner core reduced the wetted hydraulic area normal to the specimen axis. This reduced the axial load required to overcome the resultant axial load from the internal hydraulic pressure. The external pressure was retained with the aid of an external pressure collet placed around the specimen.

The axial load was provided by an MTS Model 810, 110 kip servocontrolled, universal testing machine. The axial load was measured using a strain gage load cell, MTS Model 661.23A-02 with MTS Model 440 signal conditioning. The internal and external pressure was produced using a manual high pressure pump. The pressure was monitored using a strain gage pressure transducer, Datronic Model 502-3000-G with a Honeywell Model 218 bridge amplifier as signal conditioning.

Both the load and pressure signal were used as feedback to the servocontroller. This setup allowed the operator to manually control the pressure while the servo-system automatically applied a proportional load with respect to pressure. The ratio between axial load and pressure could be adjusted to obtain the desired biaxial stress condition.

A SUN Model AD-1-SCE 10/32 data acquisition system was used to digitize the axial load, pressure and strain gage data. This system has sixty-four input channels which are multiplexed through an Analog to Digital Converter (ADC) to a digital serial output port. The input channels can be individually programmed as analog voltage inputs or can provide internal bridge

completion and excitation for the bonded strain gages. Amplifier gain and scale factors can also be programmed for individual channels. During the test, the data from the SUN system was sent directly to a PDP 11/34 mini-computer. The data was transferred at a rate of 12 1/2 channels per second. The computer transfers the data to a hard disk magnetic storage medium for future processing. A special computer program was written which converts the raw data into engineering units and allows plots to be made for a graphical presentation of the results. Loads corresponding to strain values were found through linear interpolation with time. The plots were produced using a Tektronix graphics terminal and hardcopy unit.

Figure 2 is a sketch of the biaxial test fixture. Figure 3 is a schematic of the test system.

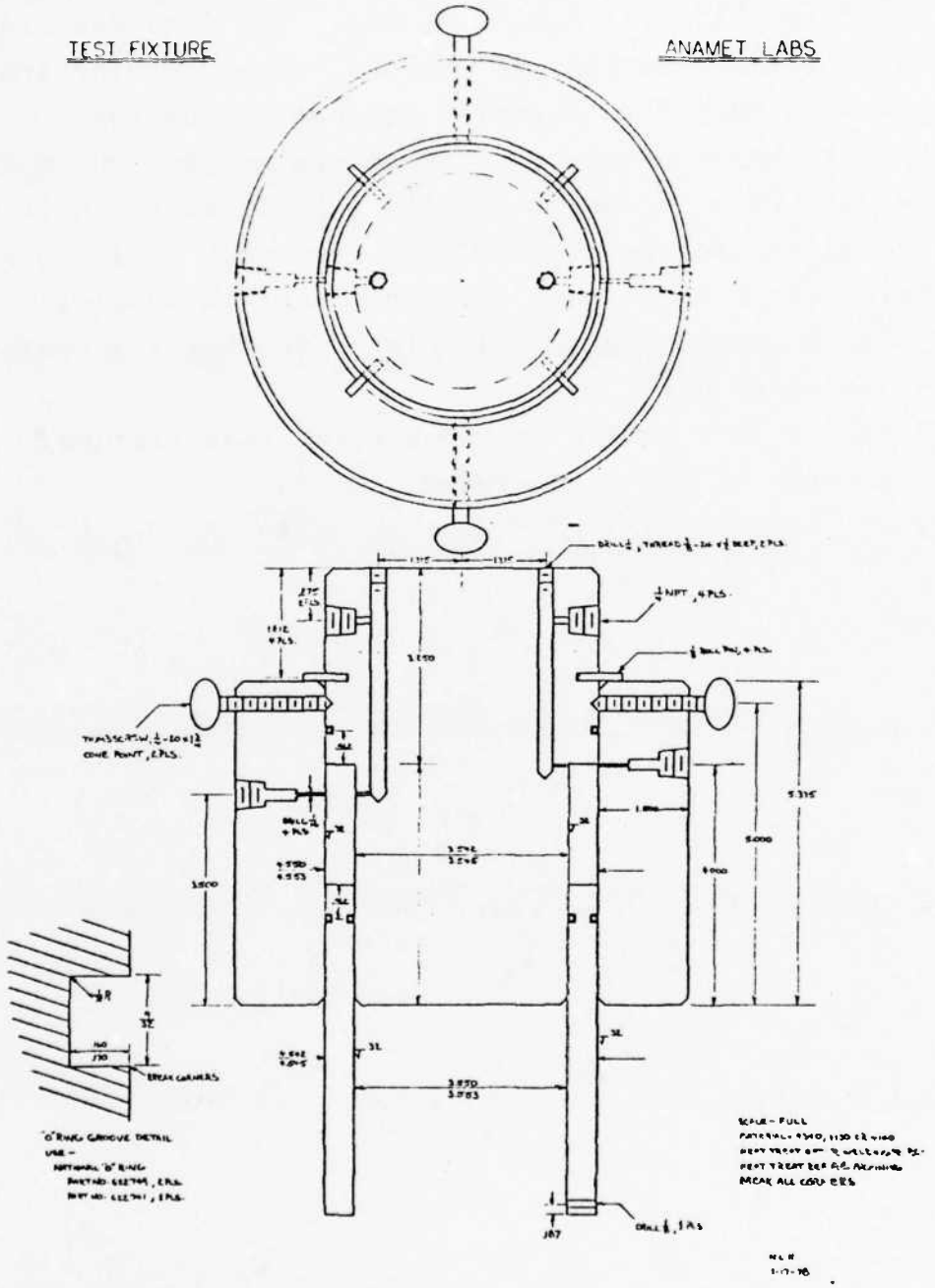

Figure 2 Sketch of the Biaxial Test Fixture

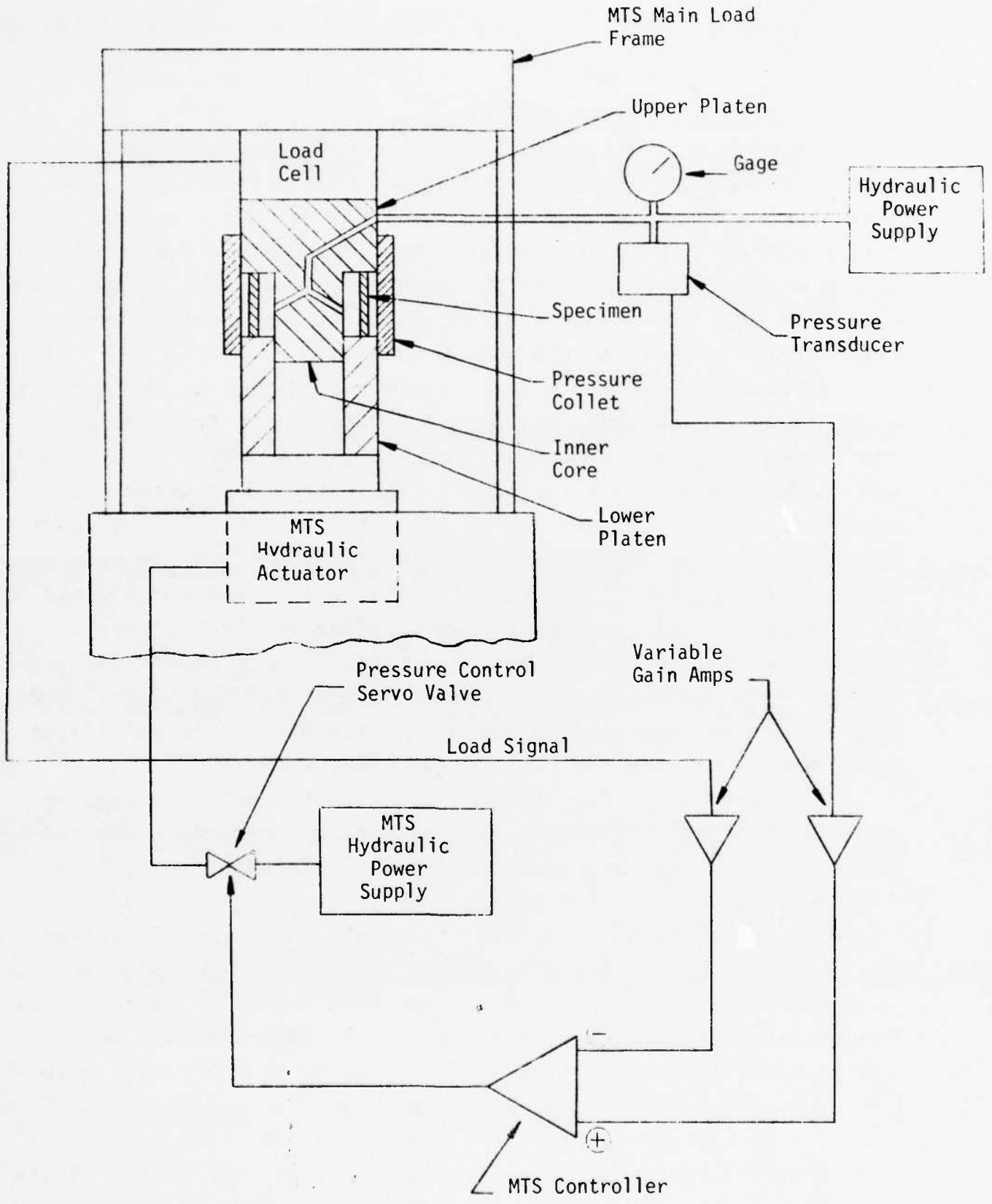

Figure 3 Schematic of the Biaxial Loading System

IV. EVALUATION OF GASKET MATERIALS

The most critical assumption made in the design of this system is that the short ring specimens have sufficiently free boundary conditions at the ends to emulate thin-wall cylinder stress theory. It is also assumed that the contact stress at the specimen ends is uniform and the resultant axial load is not eccentric with the specimen axis. These assumptions are most critical for materials with a high Poisson's ratio.

In order to provide a free boundary condition at the ends it is necessary to minimize the friction between the specimen and the platen surfaces. This must be accomplished while axial loads and surface pressures are applied. The system must allow the specimen to freely deform due to Poisson's effect. It was decided to use a solid high pressure lubricant between the specimen ends and the platens. The radial and torsional restraint would be governed by the viscous or plastic shear strength of the lubricant. The lubricant must also function as a gasket to help retain hydraulic surface pressure as well as equalizing the loading to the specimen ends to compensate for slight irregularities and mismatch between the platens and specimen.

A procedure was developed to evaluate the relative performance of different lubricants by measuring and recording the radial deformation of the specimens subjected to axial load. The radial displacements were measured at the end of the specimen near the gasket surface and simultaneously at mid-length of the specimen. These measurements indicated "barreling" or "hourglassing" of the specimen under load. The amount of barreling or hourglassing is a relative measure of the constraints on the specimen ends. Ideally, the ratio of top to middle radial deformation would be unity, indicating that the entire cylindrical specimen is expanding uniformly. In the case of barreling, the top to middle radial deformation ratio is less than unity. A top to middle deformation ratio of less than zero indicates hourglassing. Radial displacements were measured using two linear variable differential transformers (LVDT). The load was measured

using a strain gage load cell attached to the actuator of the test machine. The LVDT and load cell data were recorded on an FM analog data recorder. The data was then plotted on an analog X-Y recorder for a graphical representation of gasket performance.

Several gasket and lubrication material configurations were tested. Each configuration used single or sandwich layer combinations of polyethelene, teflon and lead foil. The following is a list of the gasket configurations tested.

.001" polyethelene
.001" teflon
.005" teflon
.001" lead/.004" polyethelene/.001" lead
.001" lead/.001" teflon/.001" lead
.001" lead/.005" teflon/.001" lead
.001" teflon/.004" polyethelene/.001" teflon

The sandwich gaskets performed much better than any of the single layer gaskets. In general, the gaskets using teflon showed more stick-slip frictional behavior than the polyethelene gaskets. In tests using the thicker teflon, the specimen tended to "dig-in" to the gasket, preventing sliding as the specimen expanded. None of the gasket configurations proved to be clearly superior; however, the best results were obtained using a .001" lead/.004" polyethelene/.001" lead sandwich construction. The remaining tests presented in this evaluation were conducted using this gasket configuration.

V. AXIAL LOAD TESTS

Four instrumented specimens were tested with compressive axial load only. These were Test Nos. I-1, II-1, II-2 and II-3. Test Nos. I-1 and II-1 specimens were 1 inch in length. They were instrumented with twelve strain gage elements using the gage layout listed in Table 2. The gages were at the 90° and 180° locations. Test Nos. II-2 and II-3 were 2 inches in length. Test No. II-2 was instrumented with thirty strain gage elements using the gage layout listed in Table 3. The gages on Test No. II-2 were spaced 45° apart around the specimen circumference. Test No. II-3 was instrumented with twelve strain gage elements using the gage layout listed in Table 4. The gages were at the 90° and 180° locations.

The specimens were loaded with compressive axial load between the two platens of the biaxial test fixture. The lead/-polyethelene/lead sandwich gasket lubrication was used at both platen surfaces. Neither internal or external pressure loads were applied, thus the pressure feedback to the controller was not used. The MTS system was operated in actuator displacement control. The strain gage and load cell data were recorded via the SUN system to the PDP 11/34 computer.

As the specimens were axially loaded, the load vs. machine cross-head displacement was recorded on an analog X-Y recorder (except for Test No. II-3). These plots are shown in Figures 4 through 6. As can be seen from the plots, the first three specimens failed at a maximum axial load of -11,000 lbs. With a specimen cross-sectional area of 0.554 square inches, this corresponds to an axial stress (σ_x) of -19.86 ksi. Test No. II-3 failed at a slightly higher load of -11,875 lbs. which corresponds to an axial stress (σ_x) of -21.44 ksi. The failure in all of the specimens resulted in separation between the ply layups. There was also some blooming at the ends of the specimens. Figures 7 through 10 are photographs of the specimens after testing.

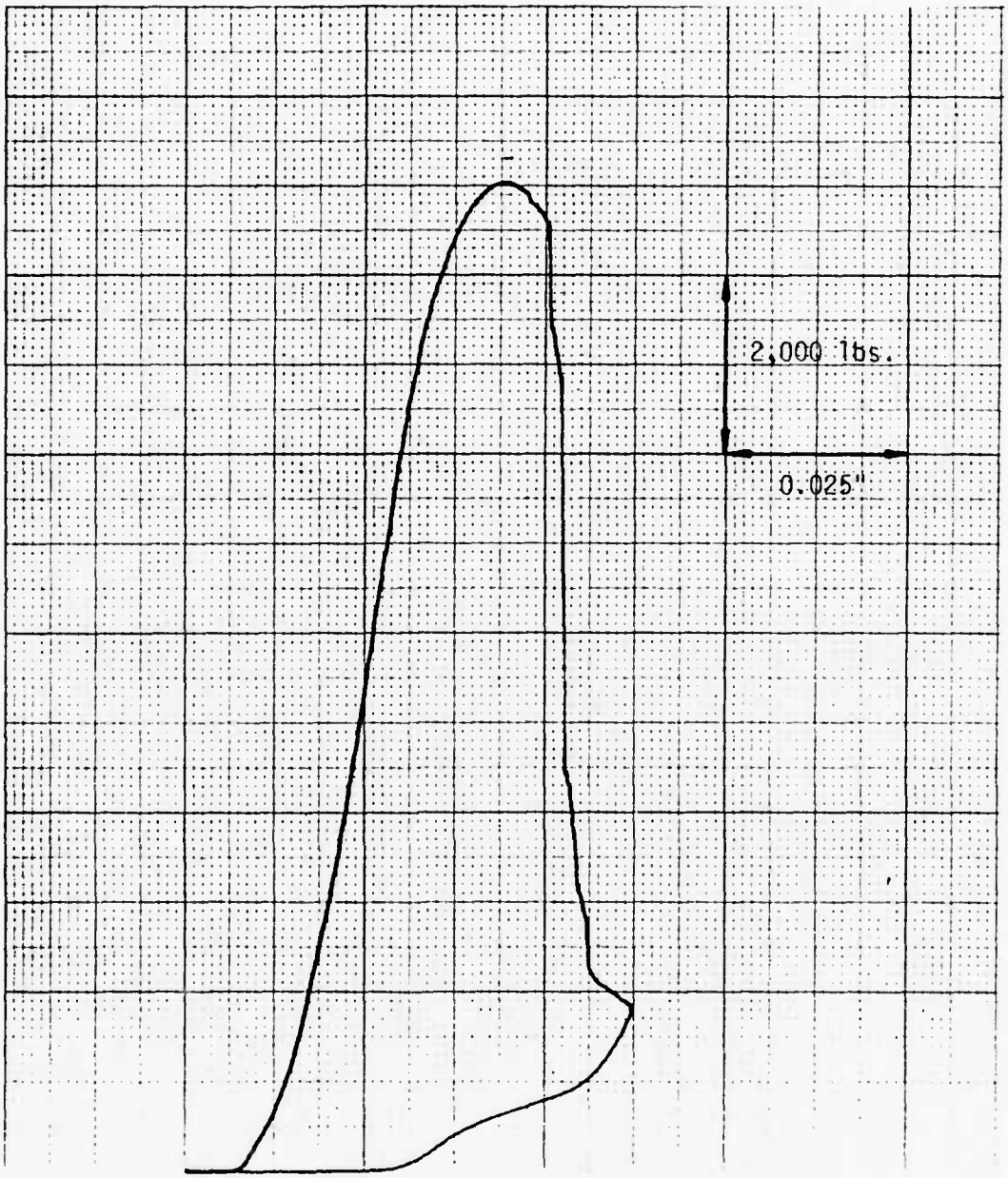

Figure 4 Plot of Axial Load vs. MTS Actuator Displacement for Test No. I-1

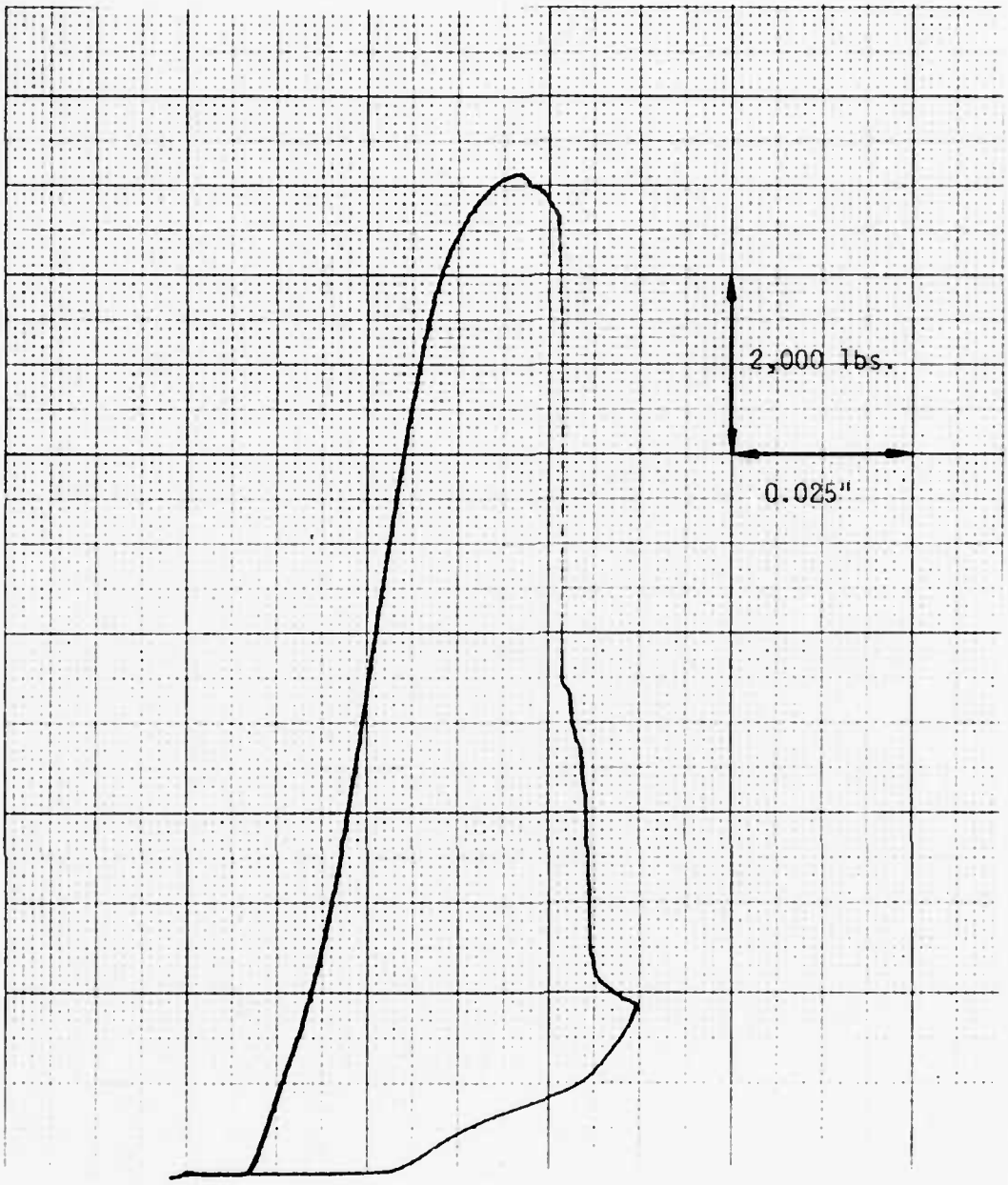

Figure 5 Plot of Axial Load vs. MTS Actuator Displacement for Test No. II-1

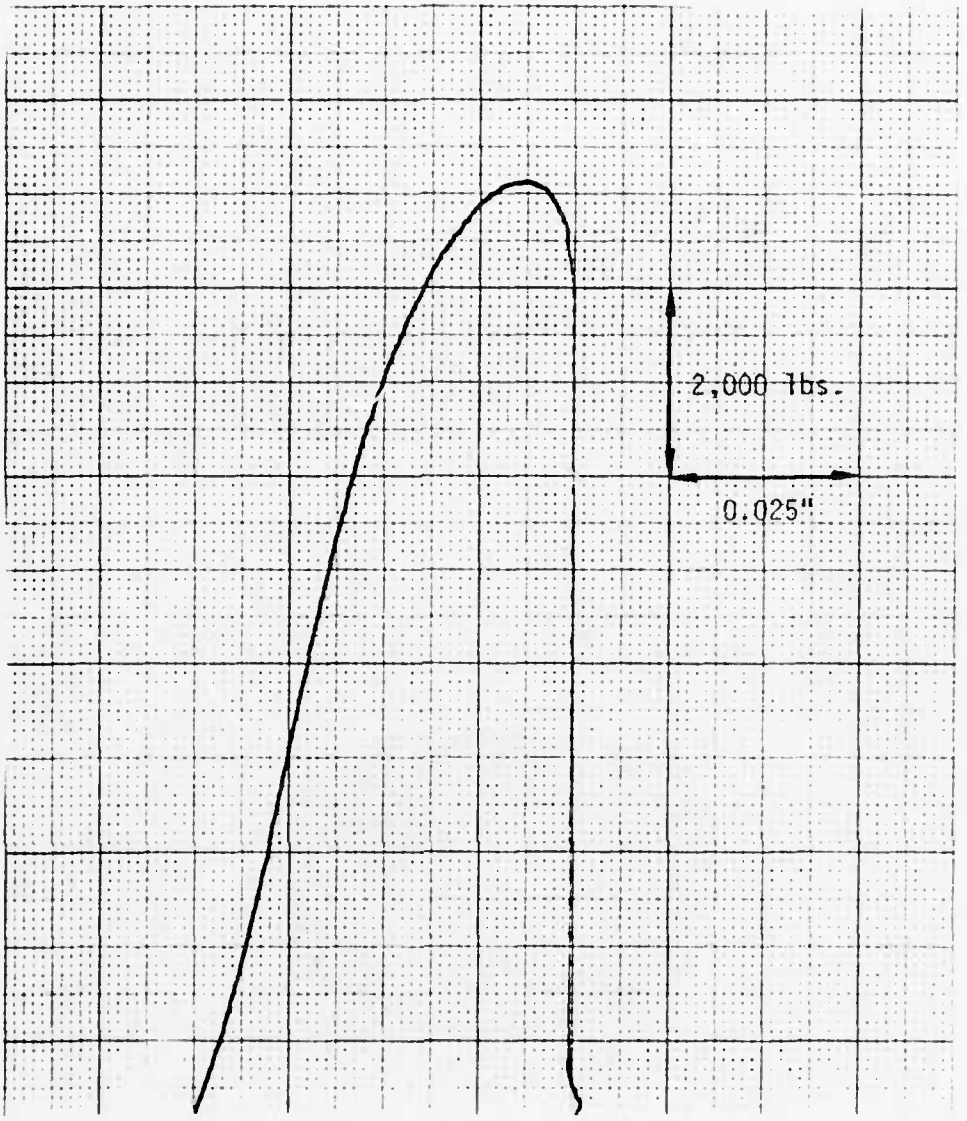

Figure 6 Plot of Axial Load vs. MTS Actuator Displacement for Test No. II-2

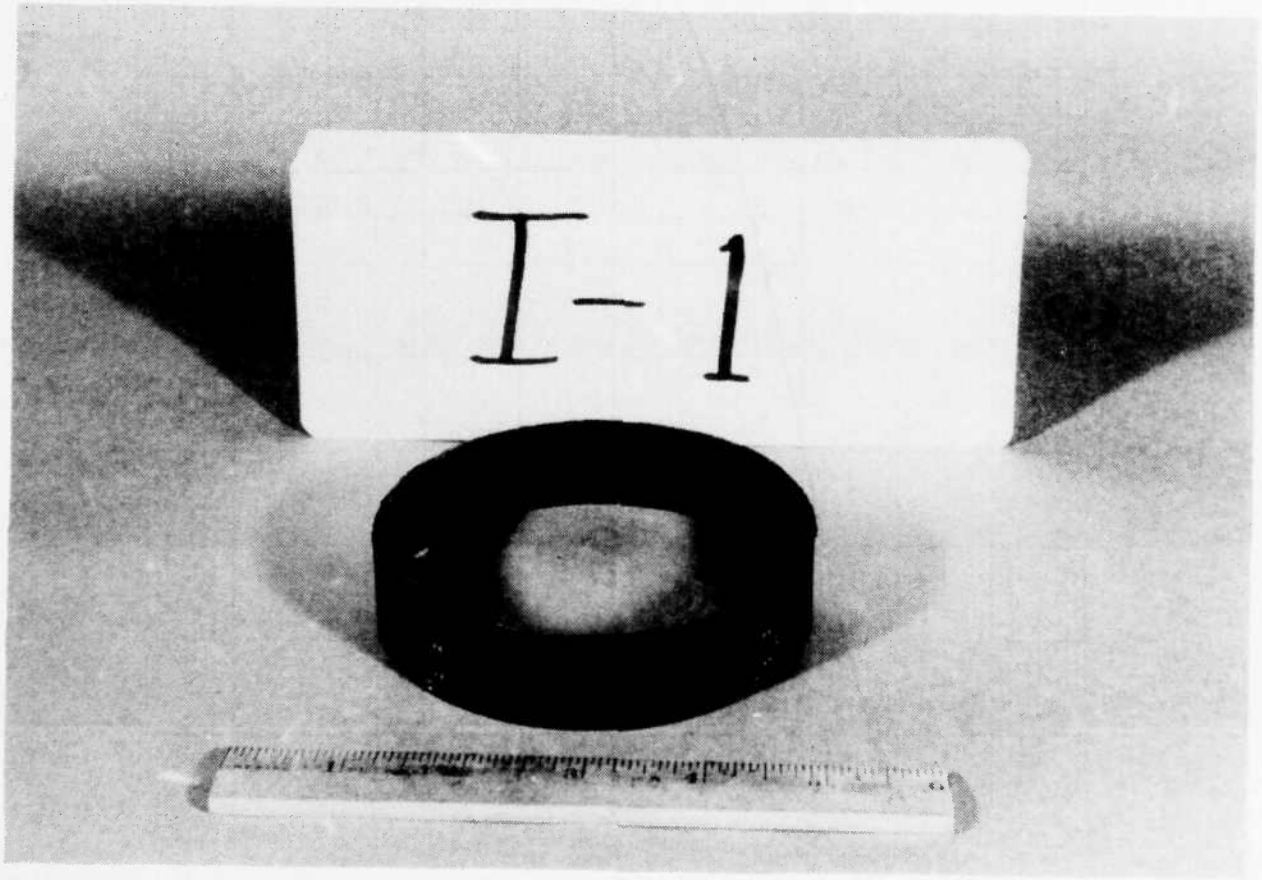

Figure 7 Photograph of Specimen No. I-1 After Testing

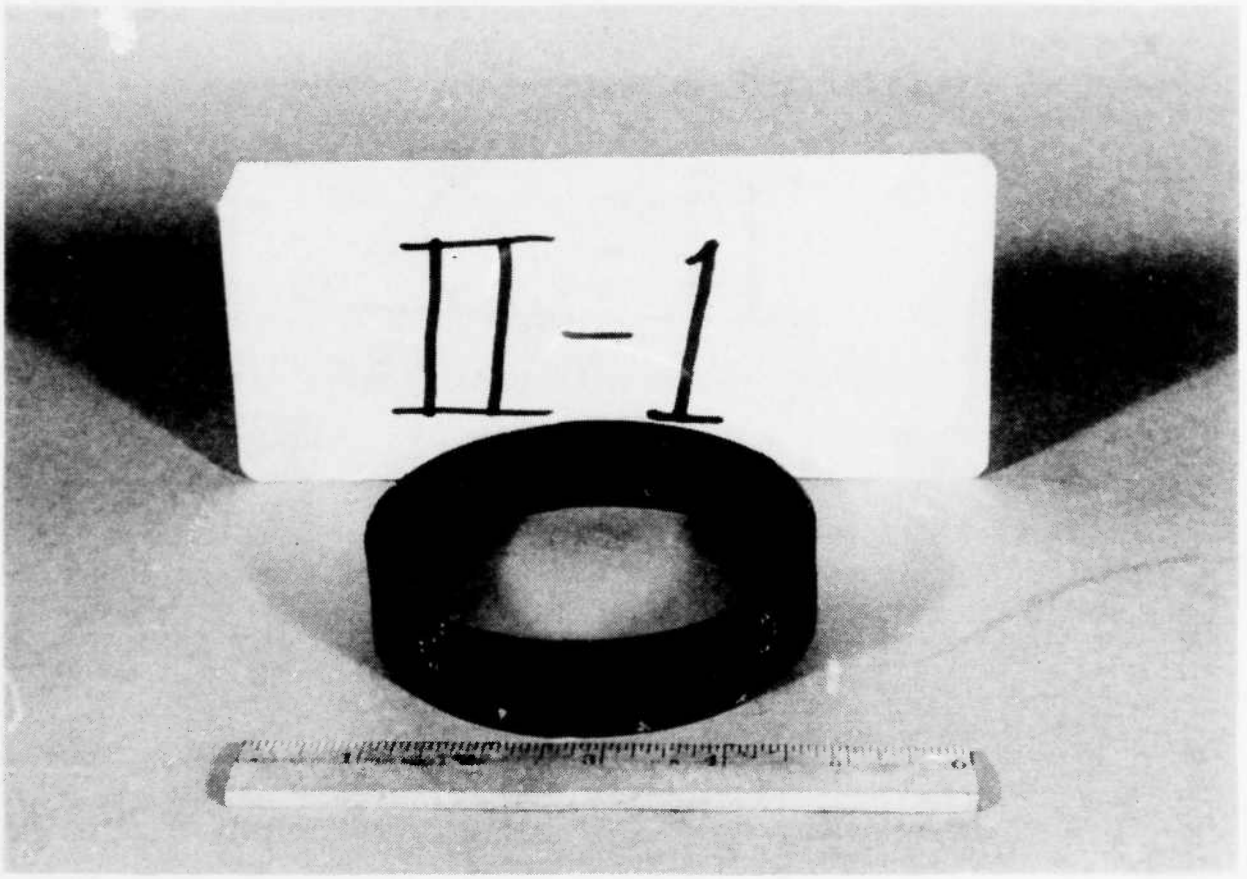

Figure 8 Photograph of Specimen No. II-1 After Testing

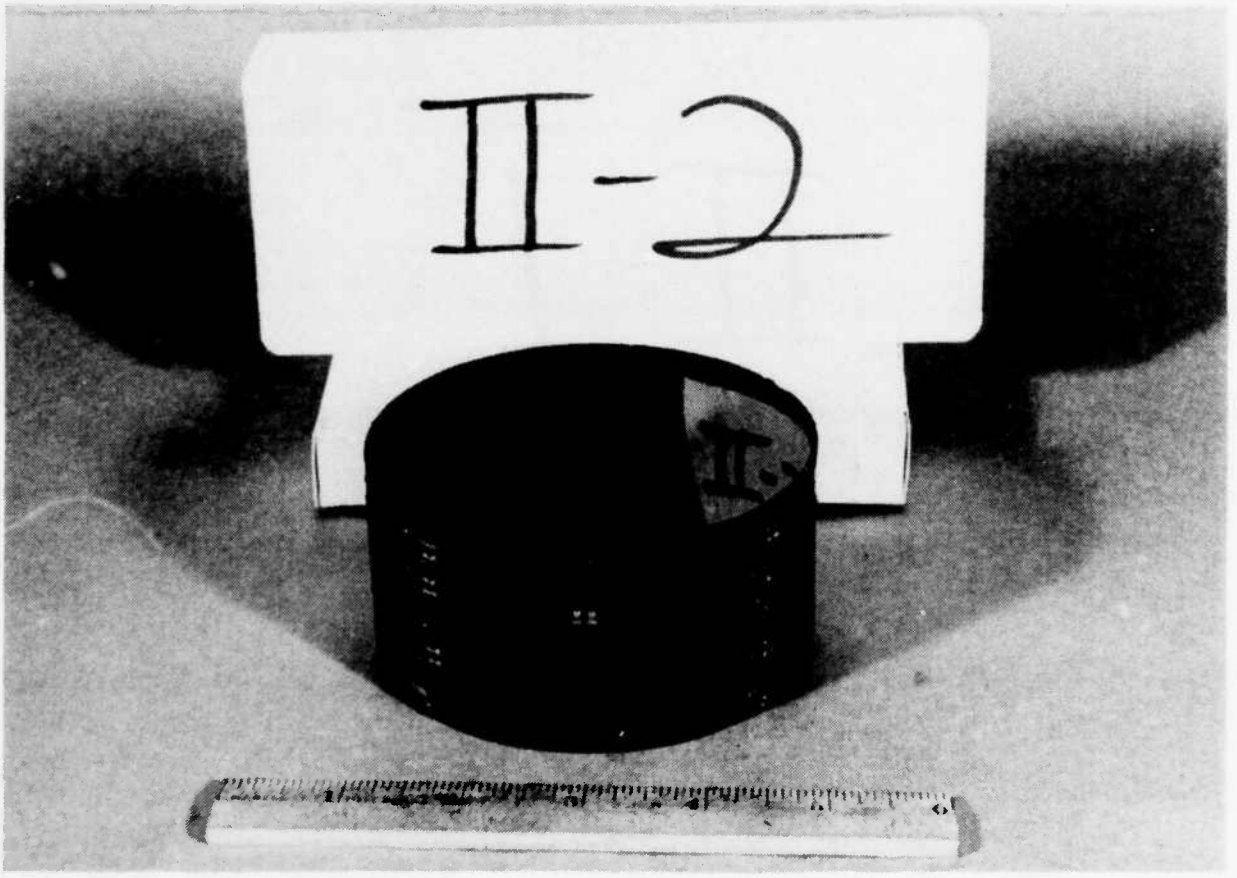

Figure 9 Photograph of Specimen No. II-2 After Testing

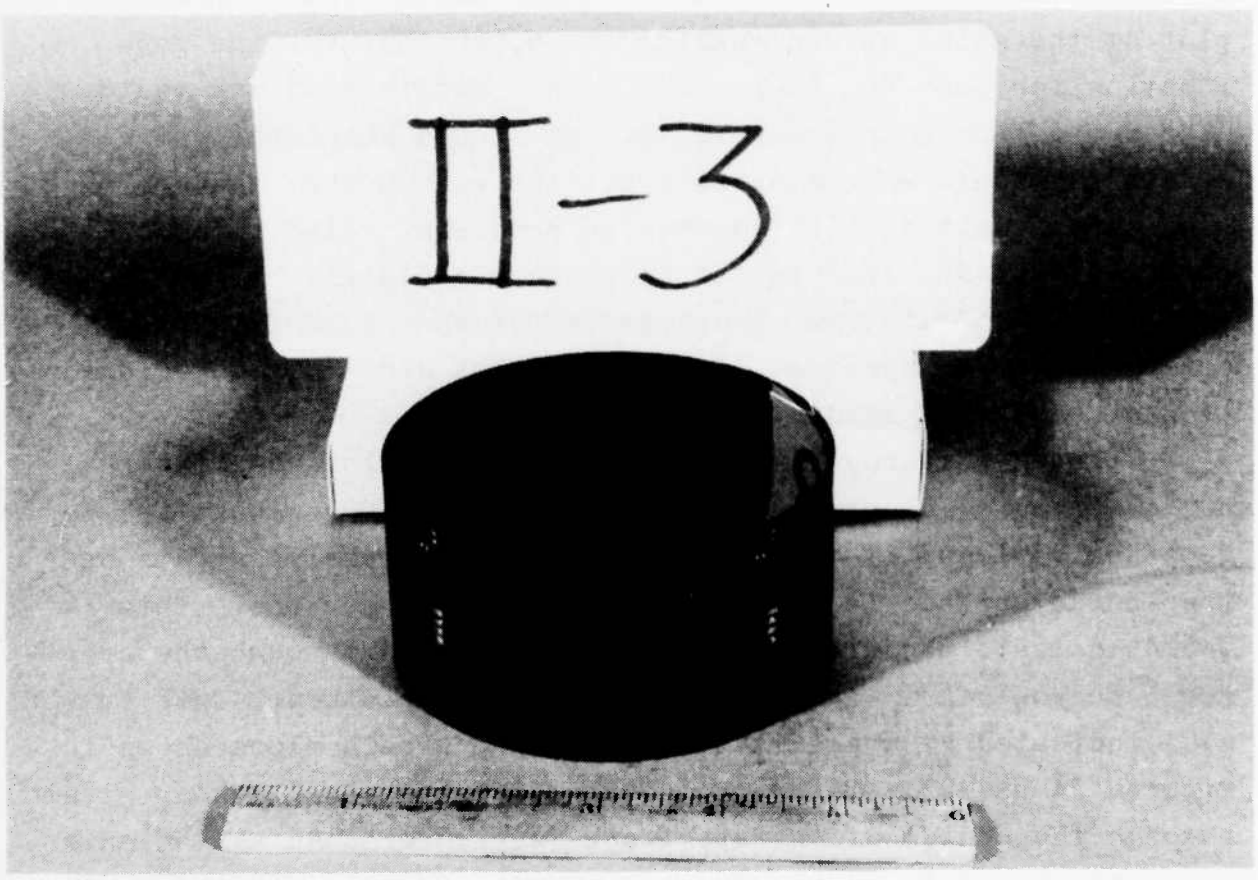

Figure 10 Photograph of Specimen No. II-3 After Testing

Figures 11 through 17 are plots of axial load vs. axial strain for the four test specimens. The plots show there was some variation in the load distribution around the specimens' circumference. Test Nos. I-1, II-1 and II-3 show more compressive strain at the 90° location than at the 180° location. Also, Test No. II-2 shows high strain near 315° and 00° locations and low strain values near the 135° location. This would indicate that the axial load was slightly eccentric with respect to the specimen axis. This is better illustrated in Figure 18 with a plot of the axial strain reading at -6,000 lbs. vs. the gage location for Test No. II-2. The higher strain readings would correspond to higher local loads. It should be noted that no strain gage data was recorded after the -6,000 lbs. load for Test II-2 as a result of instrumentation problems. Also, some of the gages in Test No. II-2 failed to produce a signal. Figure 19 is a plot of axial load vs. hoop strain for the gages around the circumference of specimen II-2. This plot also show some indication of eccentric loading.

Figures 20 through 23 are plots of axial load vs. internal and external axial strain at the 90° and 180° gage locations for Test Nos. I-1 and II-1. In general, the compressive strain on the inside surface is higher than the outside surface. This would indicate there was some bending stresses through the specimens' length resulting in barreling of the specimen. This is also indicated by the axial load vs. hoop strain plots shown in Figures 24 and 25. These plots show that the tensile hoop strain through the center of the specimens is greater than at the ends. A relative measure of the bending can be made by plotting the ratio of external axial strain vs. internal axial strain. Ideally, the ratio of external vs. internal strain should be unity. When barreling or bending stresses occur, the internal compressive strain becomes greater than the external compressive strain and the ratio drops below unity. Plots of external axial vs. internal axial strain for the 180° gage location of Test Nos. I-1 and II-1 are given in Figures 26 through 29.

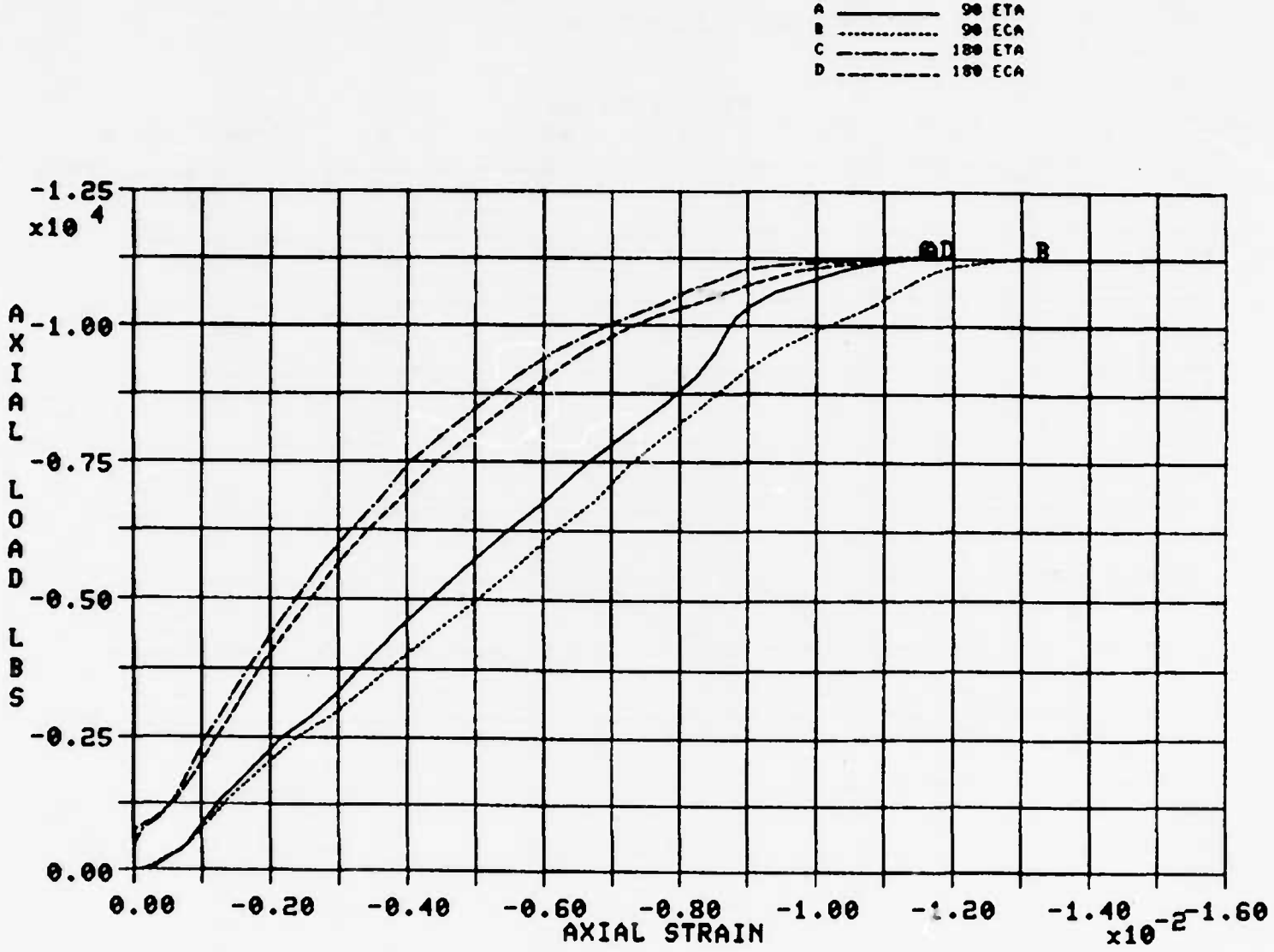

Figure 11 Plot of Axial Load vs. External Axial Strain for Test No. I-1

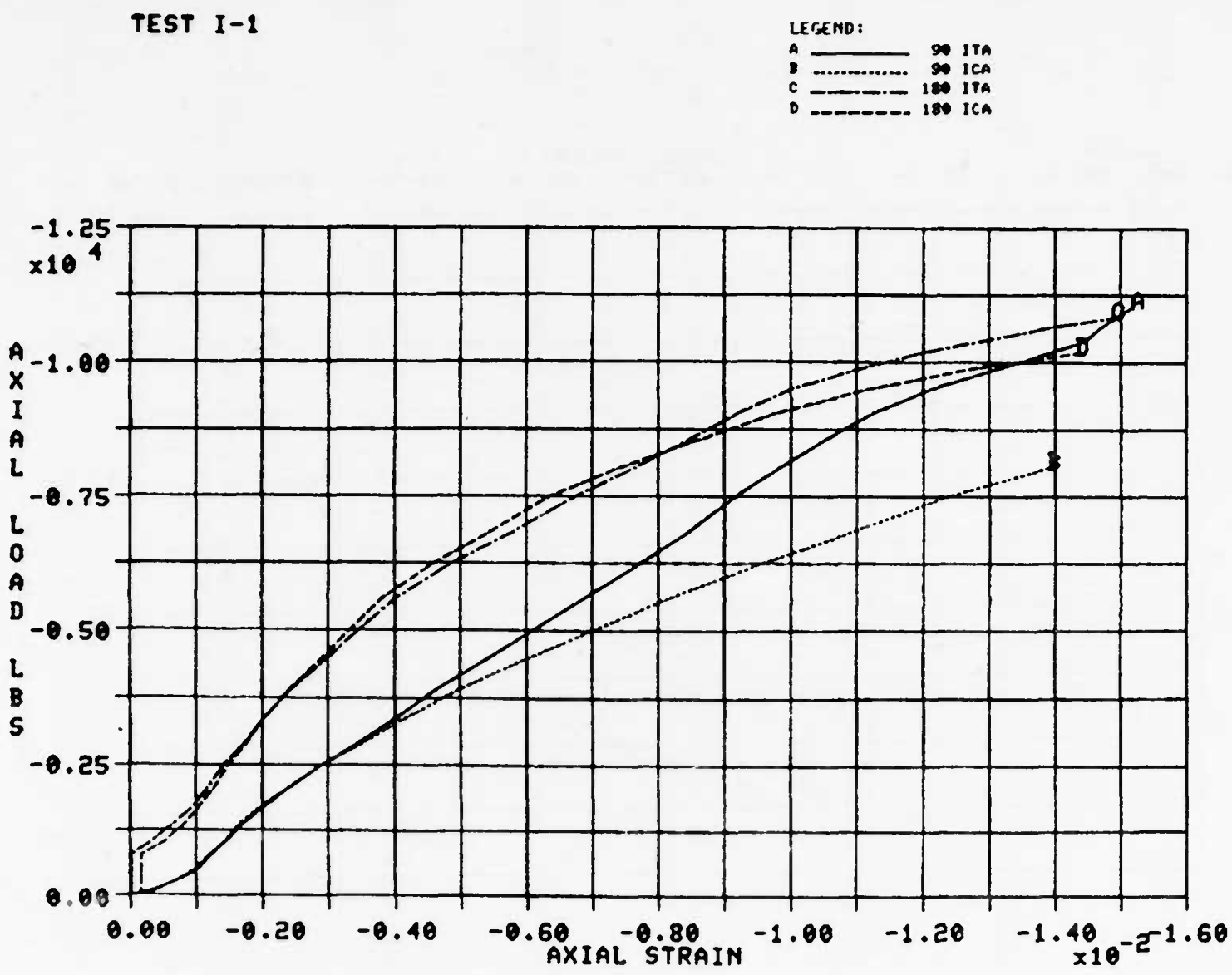

Figure 12 Plot of Axial Load vs. Internal Axial Strain for Test No. I-1

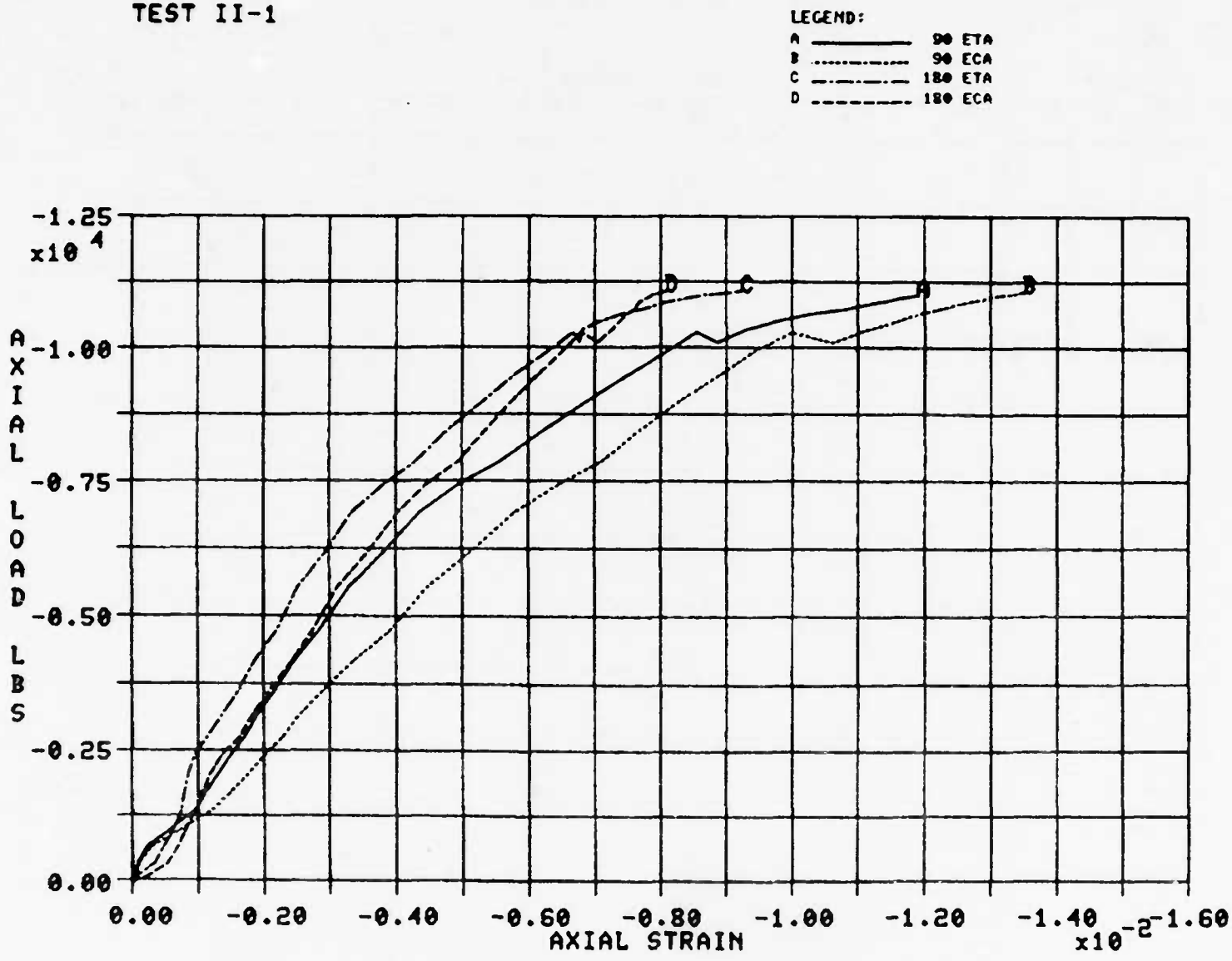

Figure 13 Plot of Axial Load vs. External Axial Strain for Test No. II-1

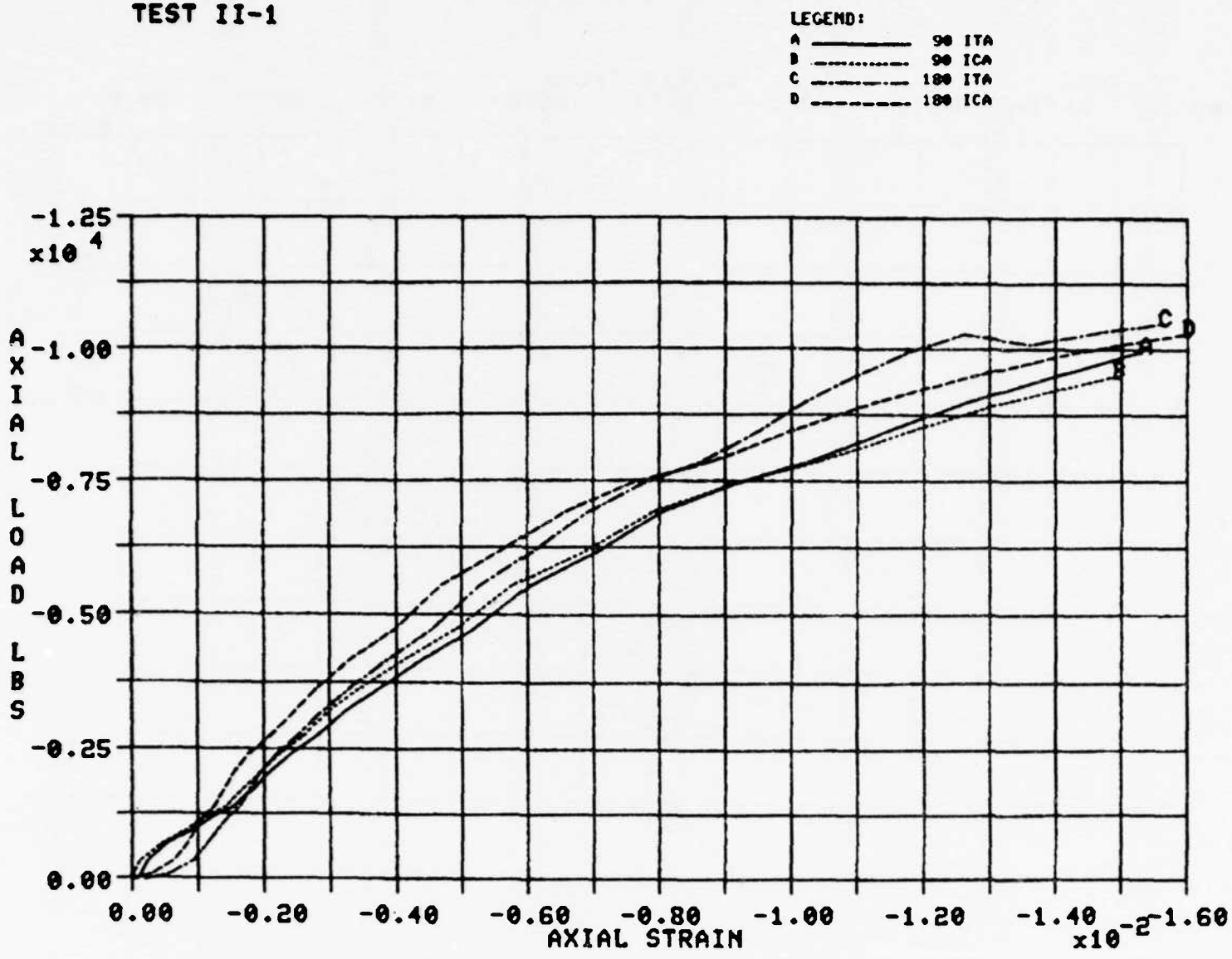

Figure 14 Plot of Axial Load vs. Internal Axial Strain for Test No. II-1

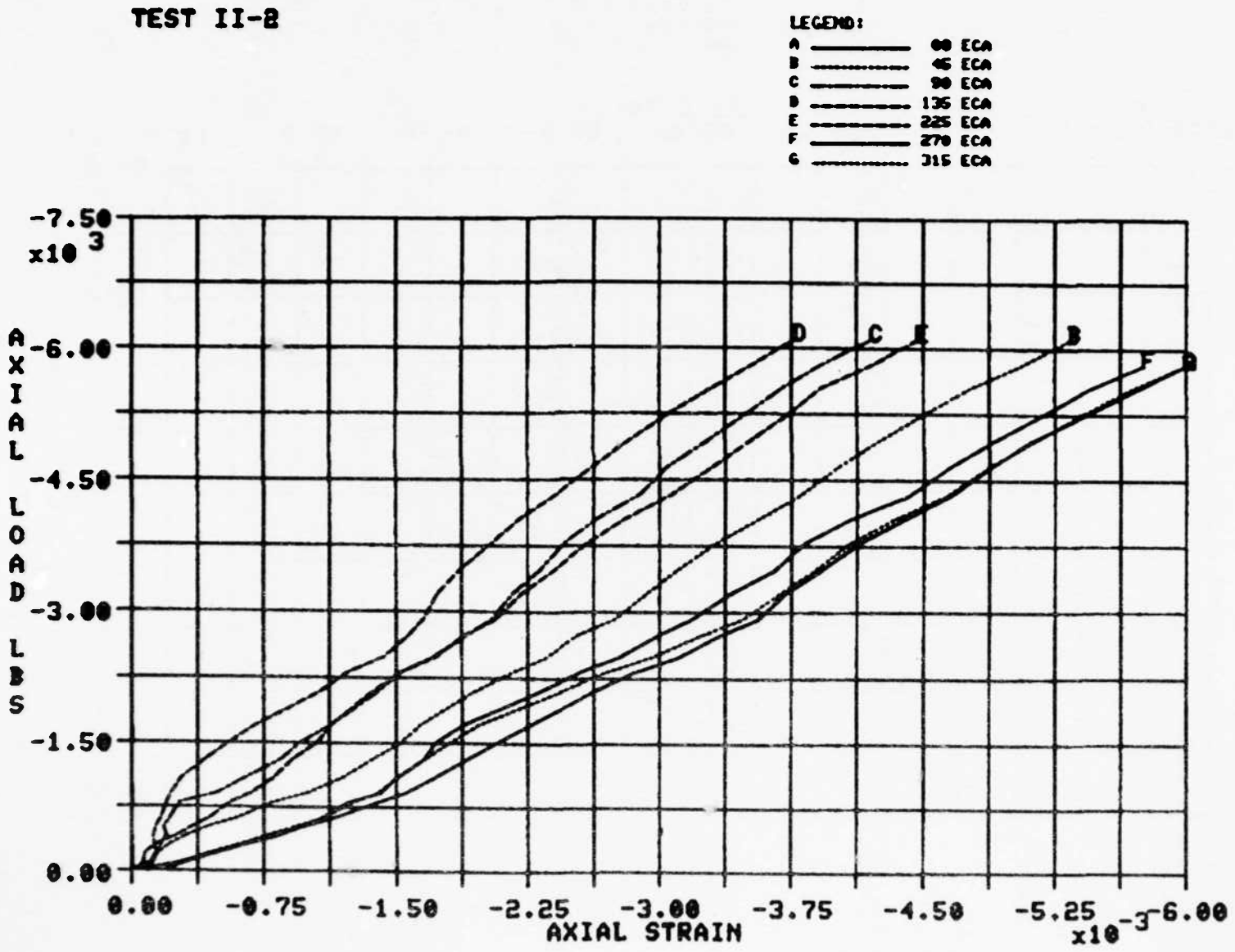

Figure 15 Plot of Axial Load vs. External Axial Strain Around the Circumference of Test No. II-2

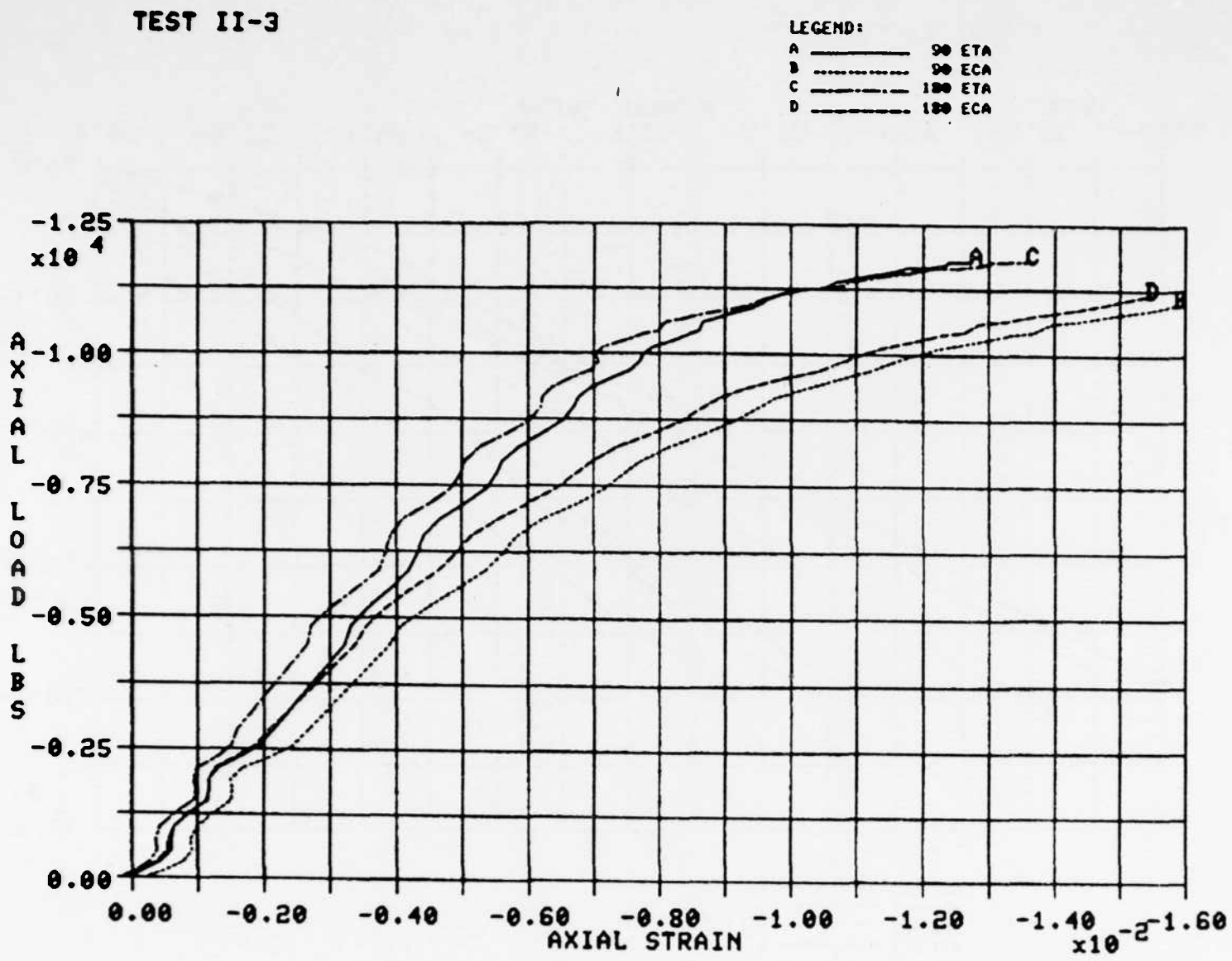

Figure 16 Plot of Axial Load vs. External Axial Strain for Test No. II-3

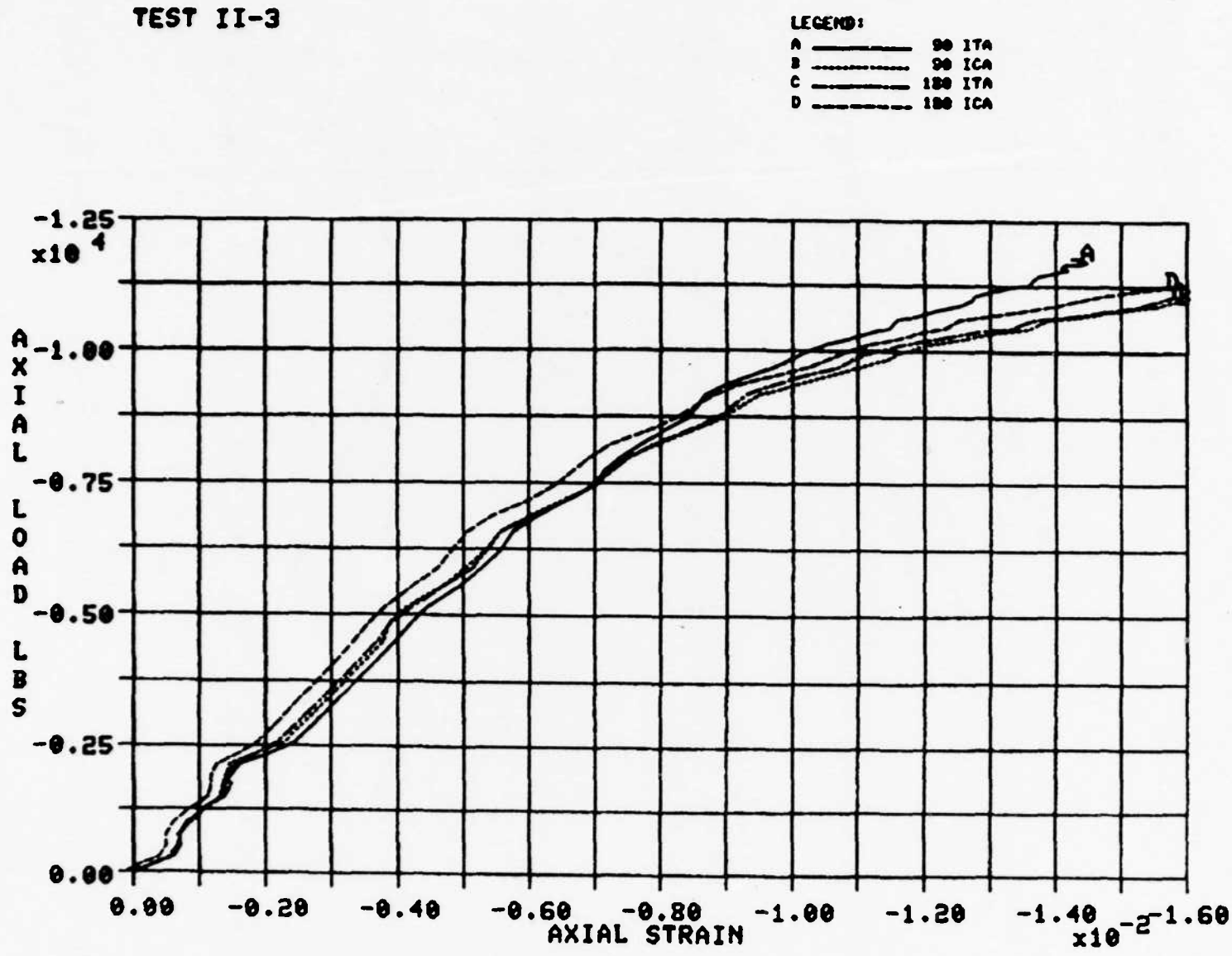

Figure 17 Plot of Axial Load vs. Internal Axial Strain for Test No. II-3

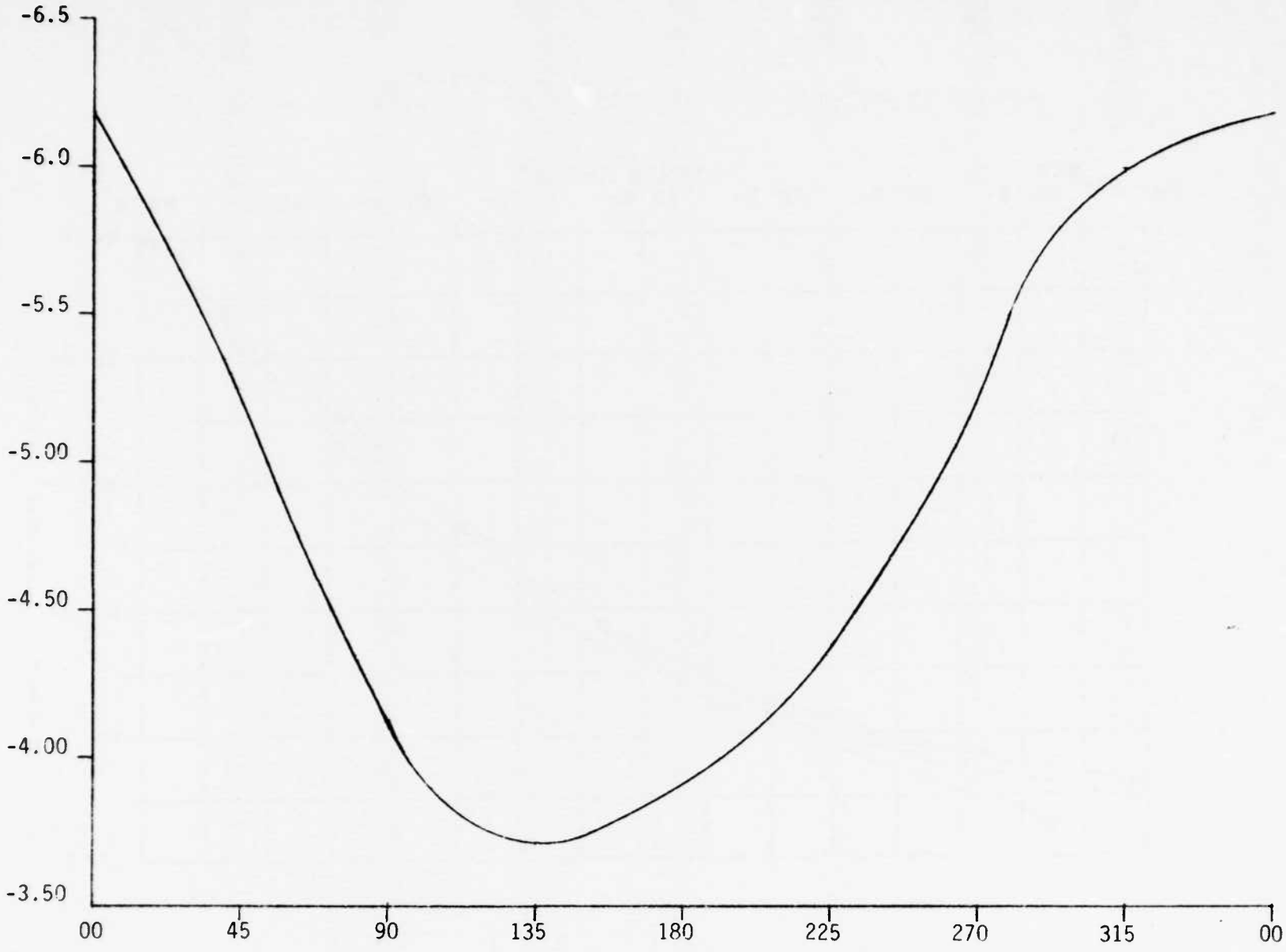

Figure 18 Axial Strain vs. Gage Location for Test No. II-2

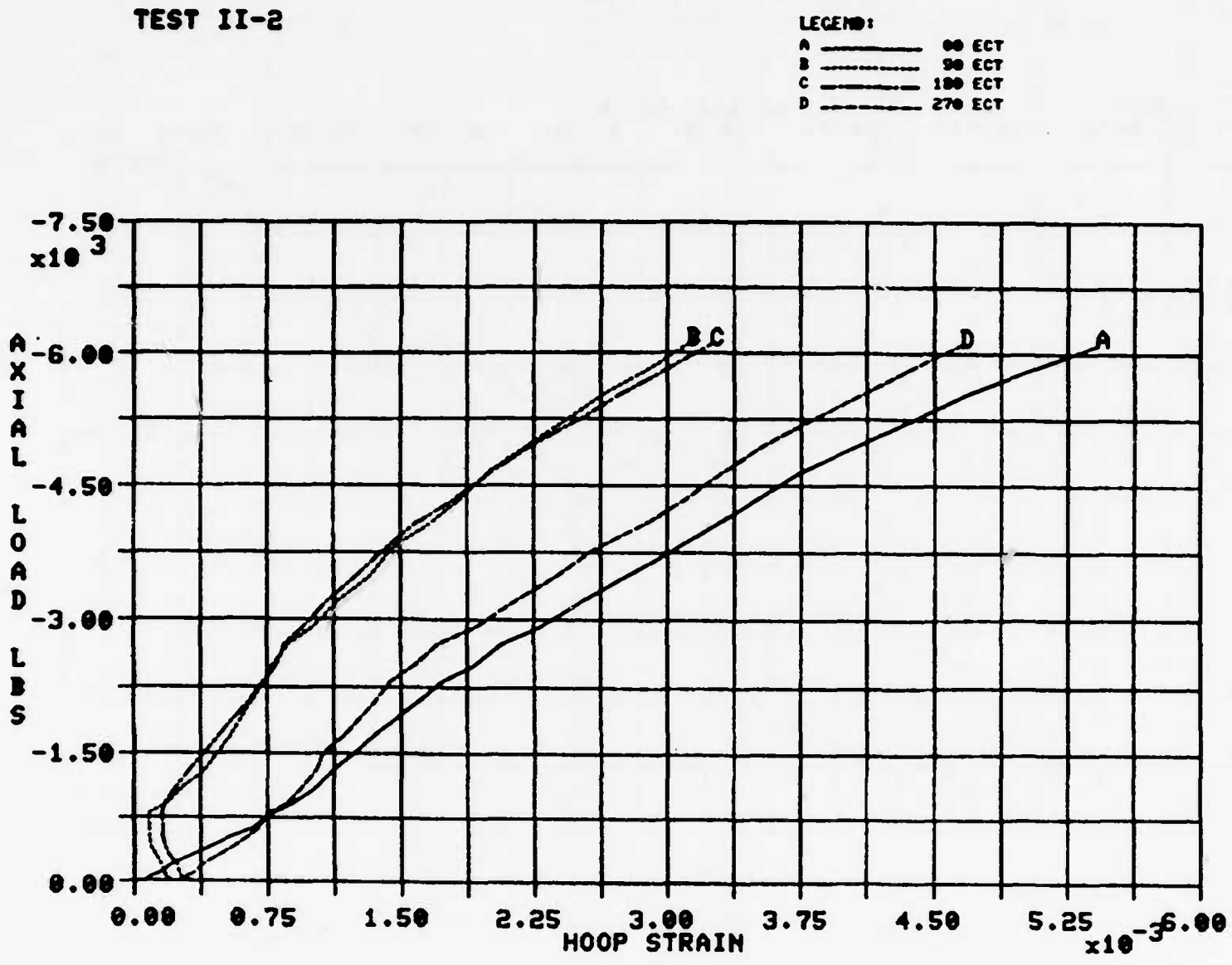

Figure 19 Plot of Axial Load vs. External Hoop Strain for Test No. II-2

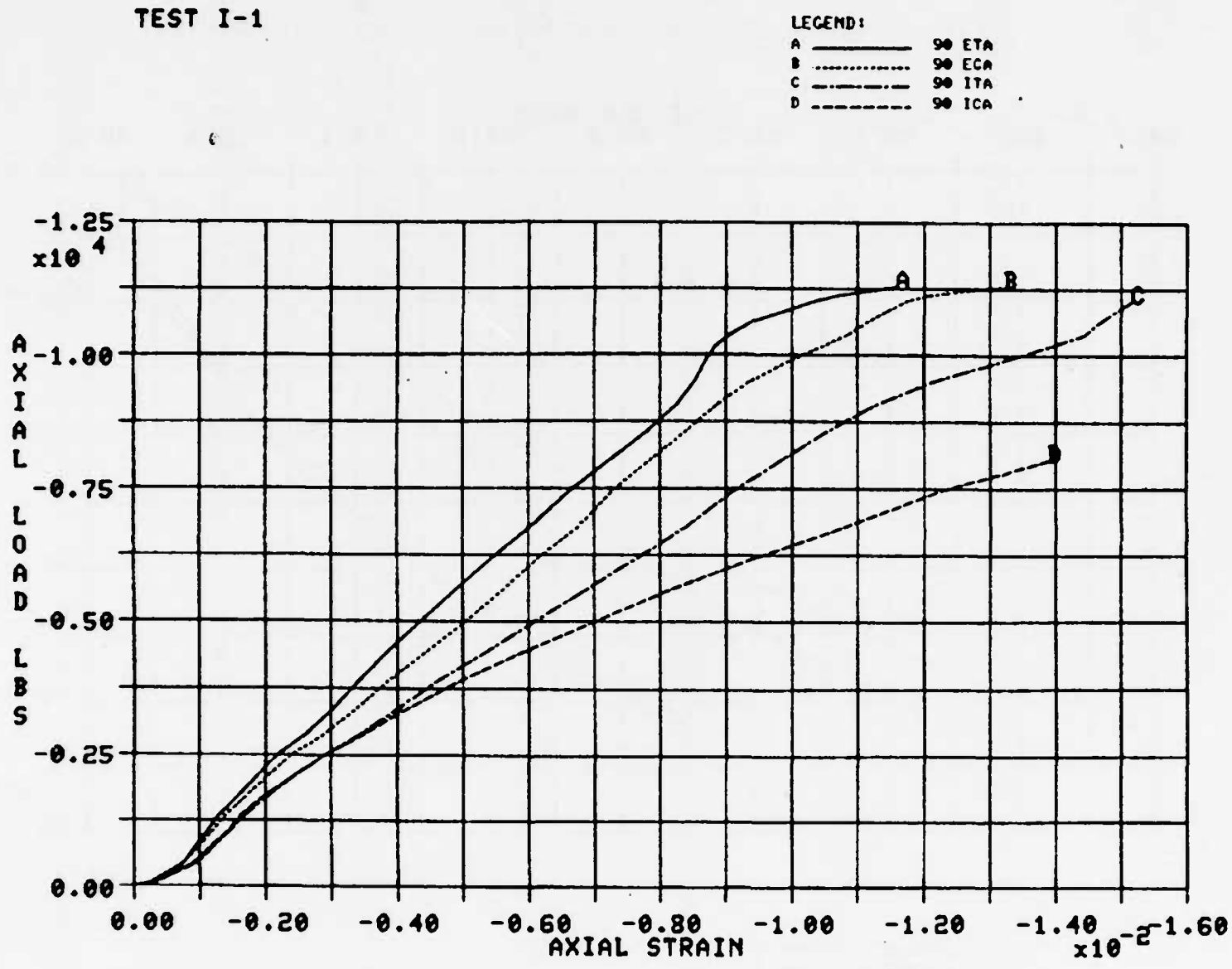

Figure 20 Plot of Axial Load vs. Internal and External Axial Strain at 90° for Test No. I-1

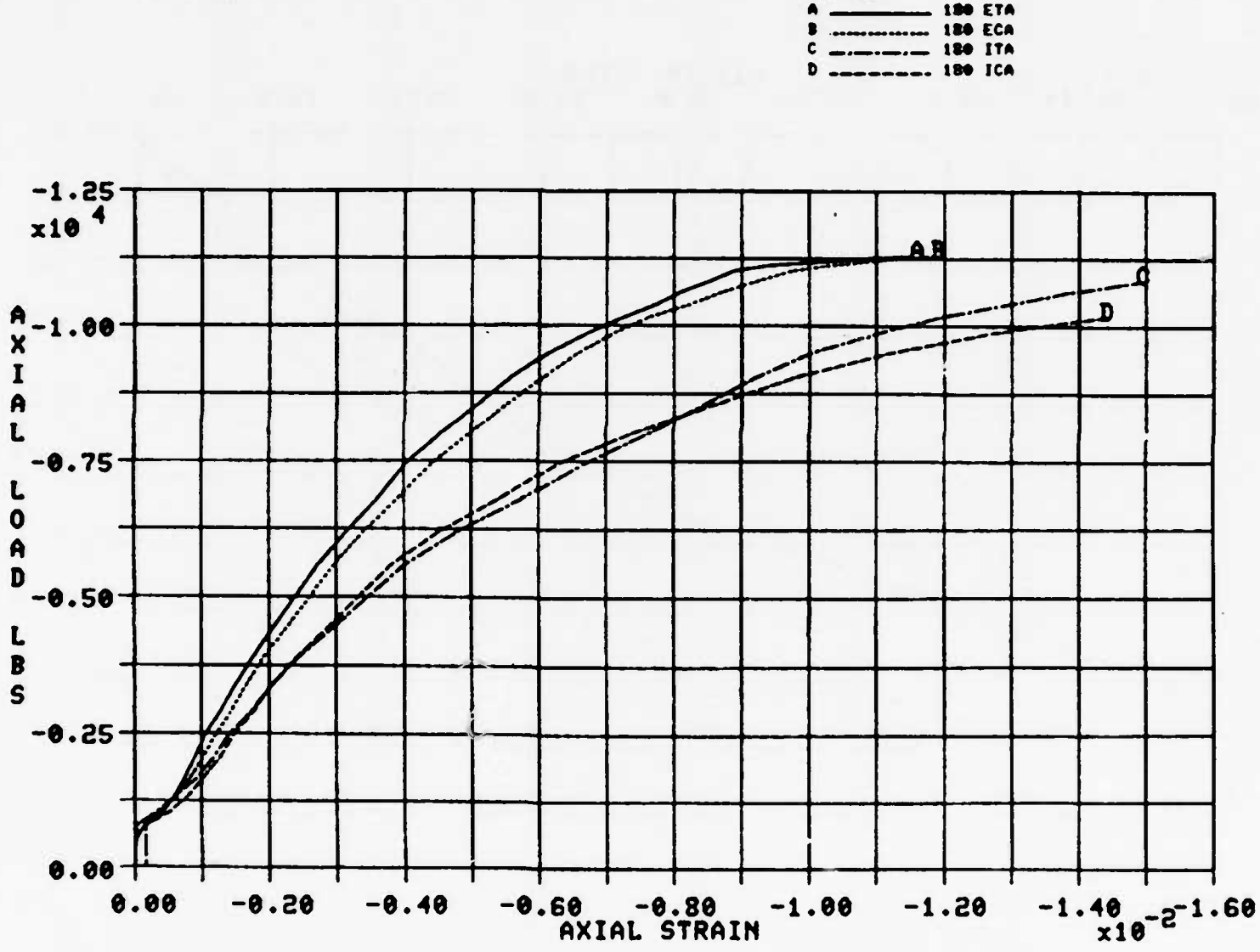

Figure 21 Plot of Axial Load vs. Internal and External Axial Strain at 180° for Test No. I-1

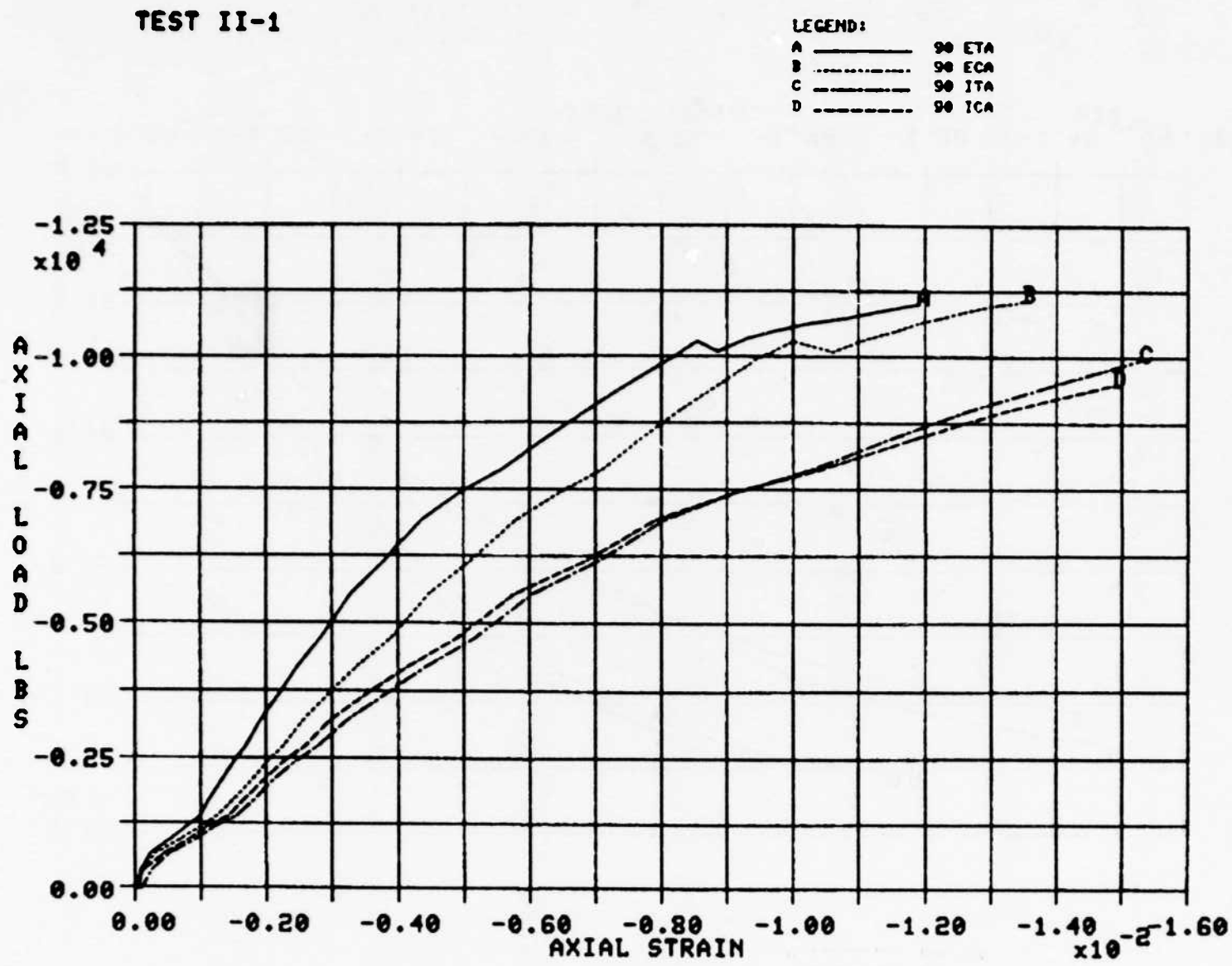

Figure 22 Plot of Axial Load vs. Internal and External Axial Strain at 90° for Test No. II-1

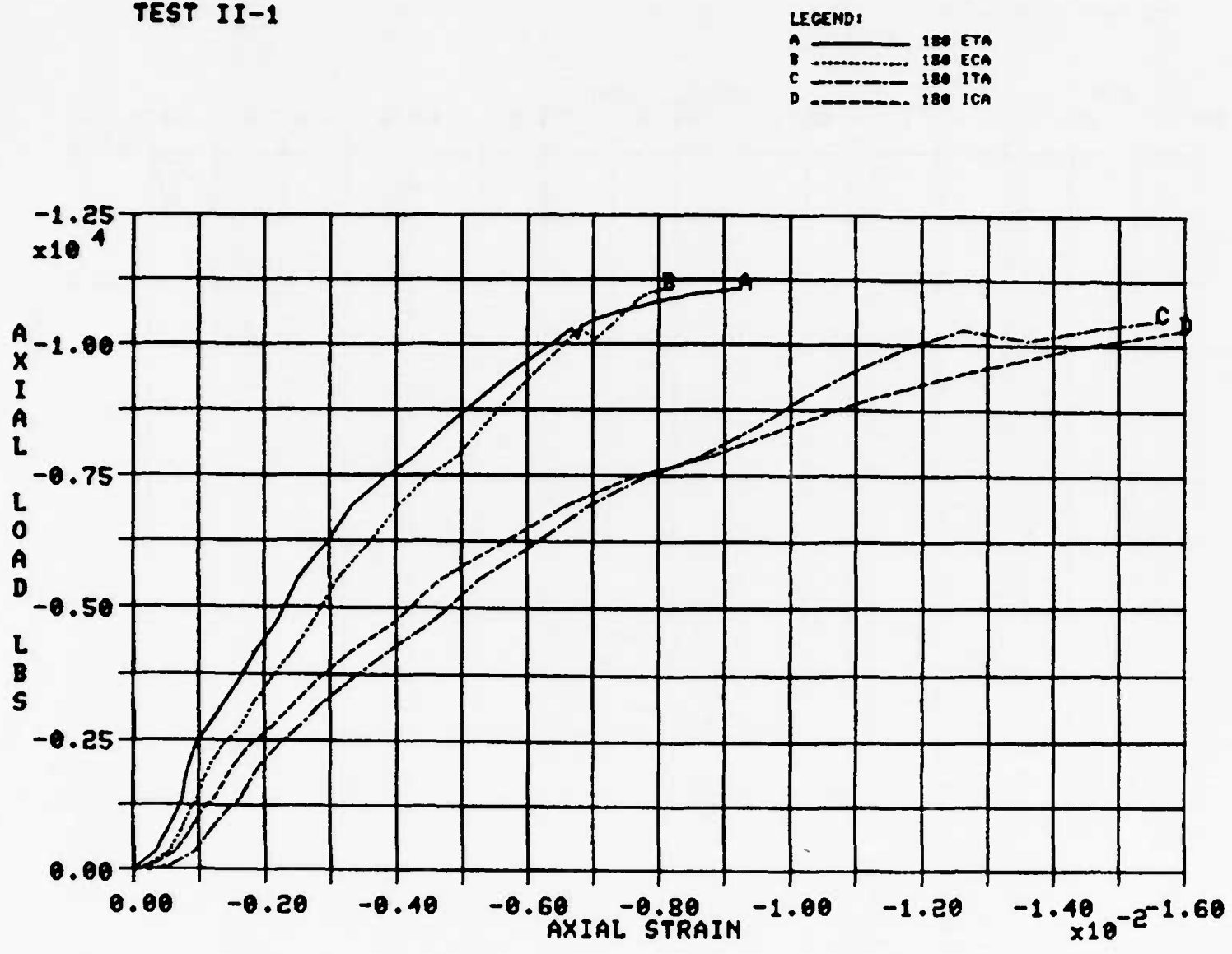

Figure 23 Plot of Axial Load vs. Internal and External Axial Strain at 180° for Test No. II-1

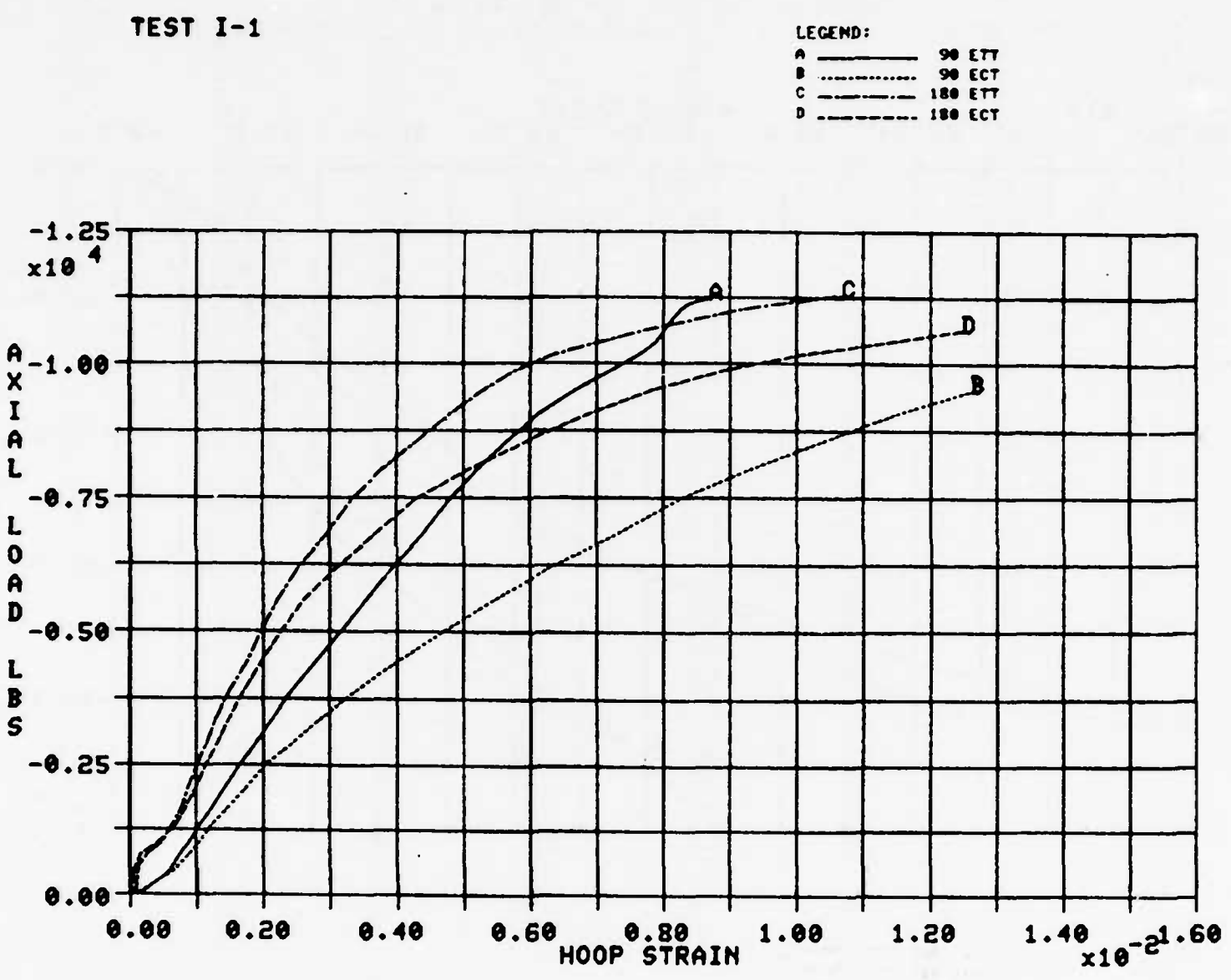

Figure 24 Plot of Axial Load vs. Hoop Strain for Test No. I-1

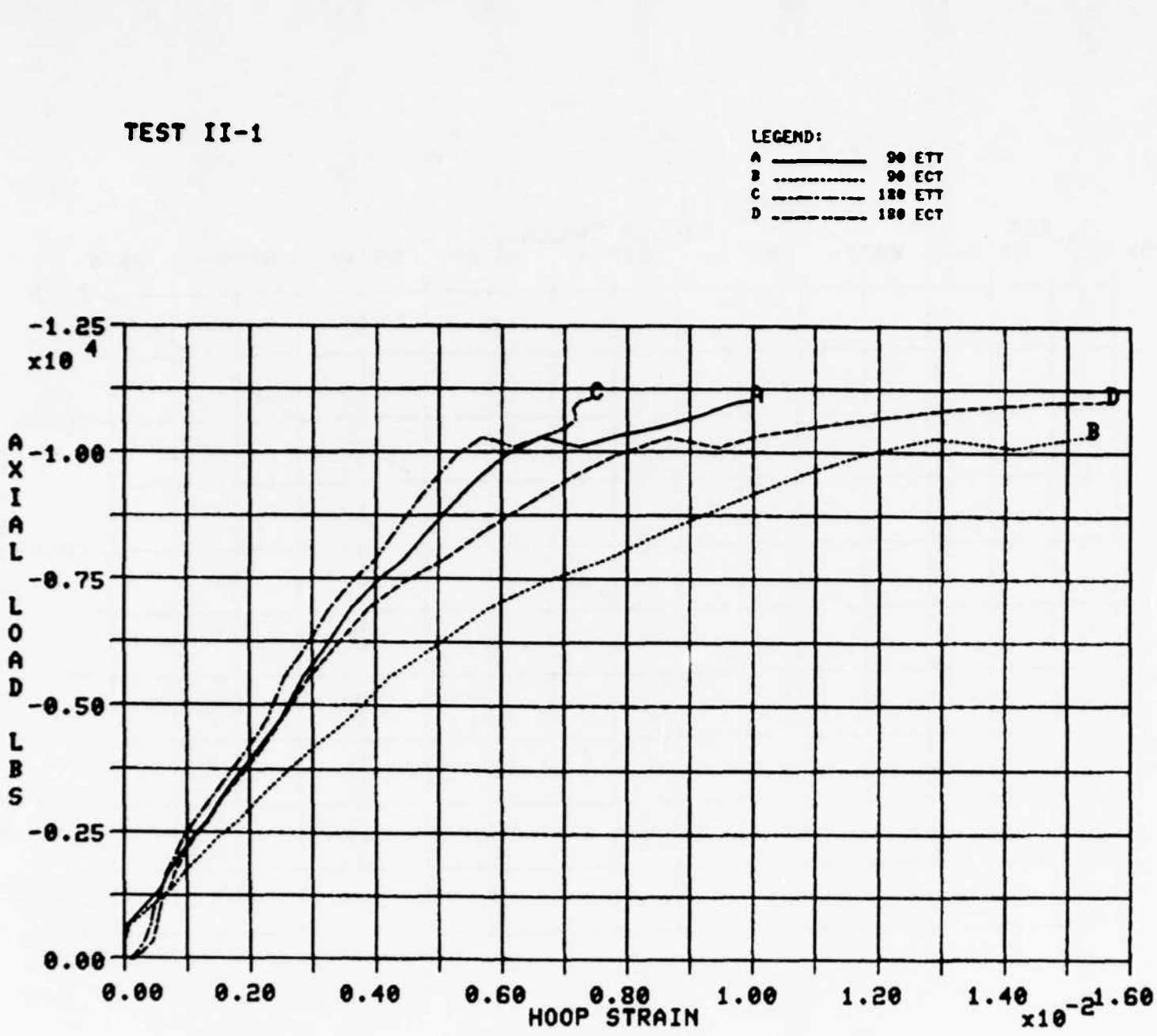

Figure 25 Plot of Axial Load vs. Hoop Strain for Test No. II-1

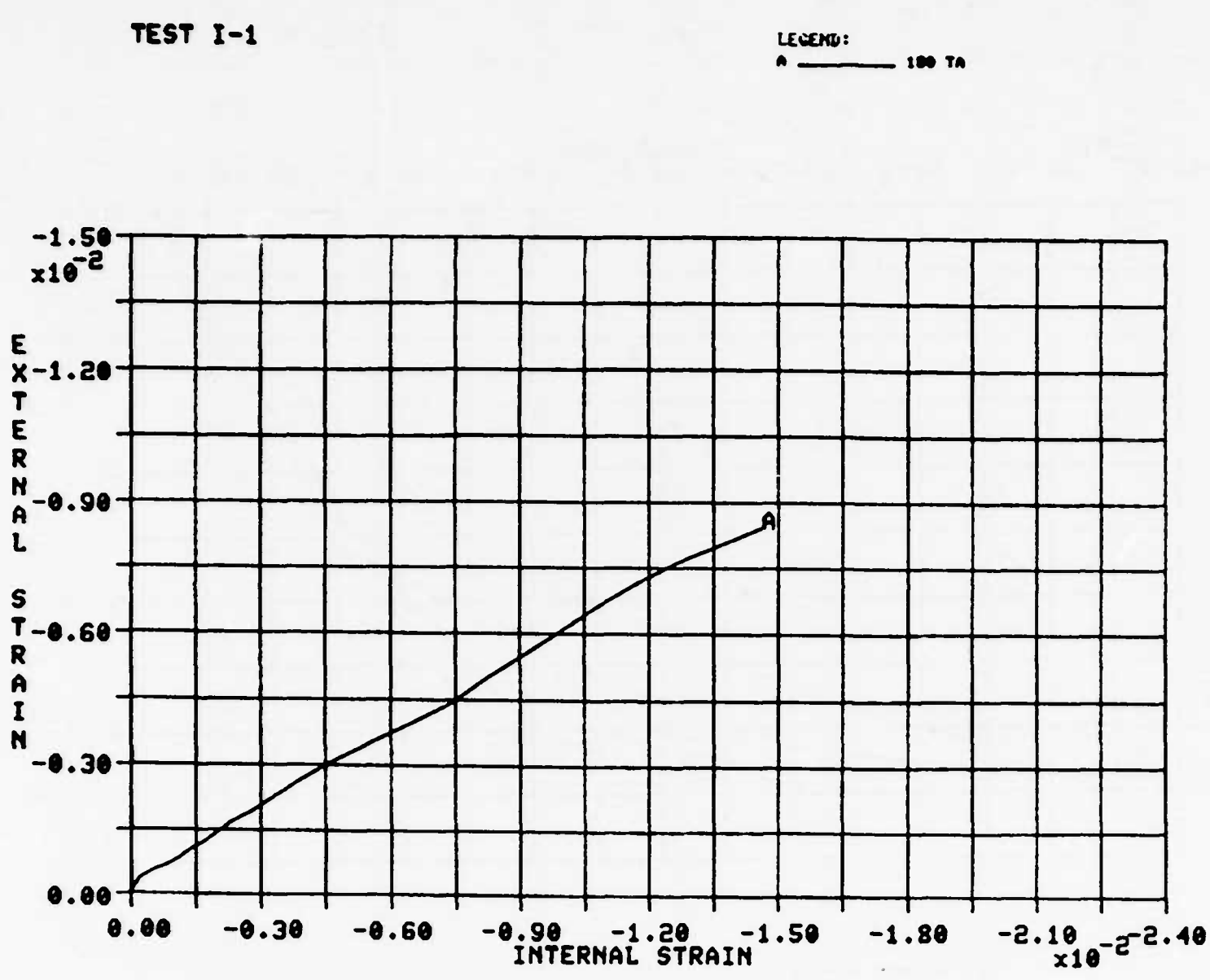

Figure 26 Plot of External vs. Internal Axial Strain at 180° Near the Top Edge of Test No. I-1

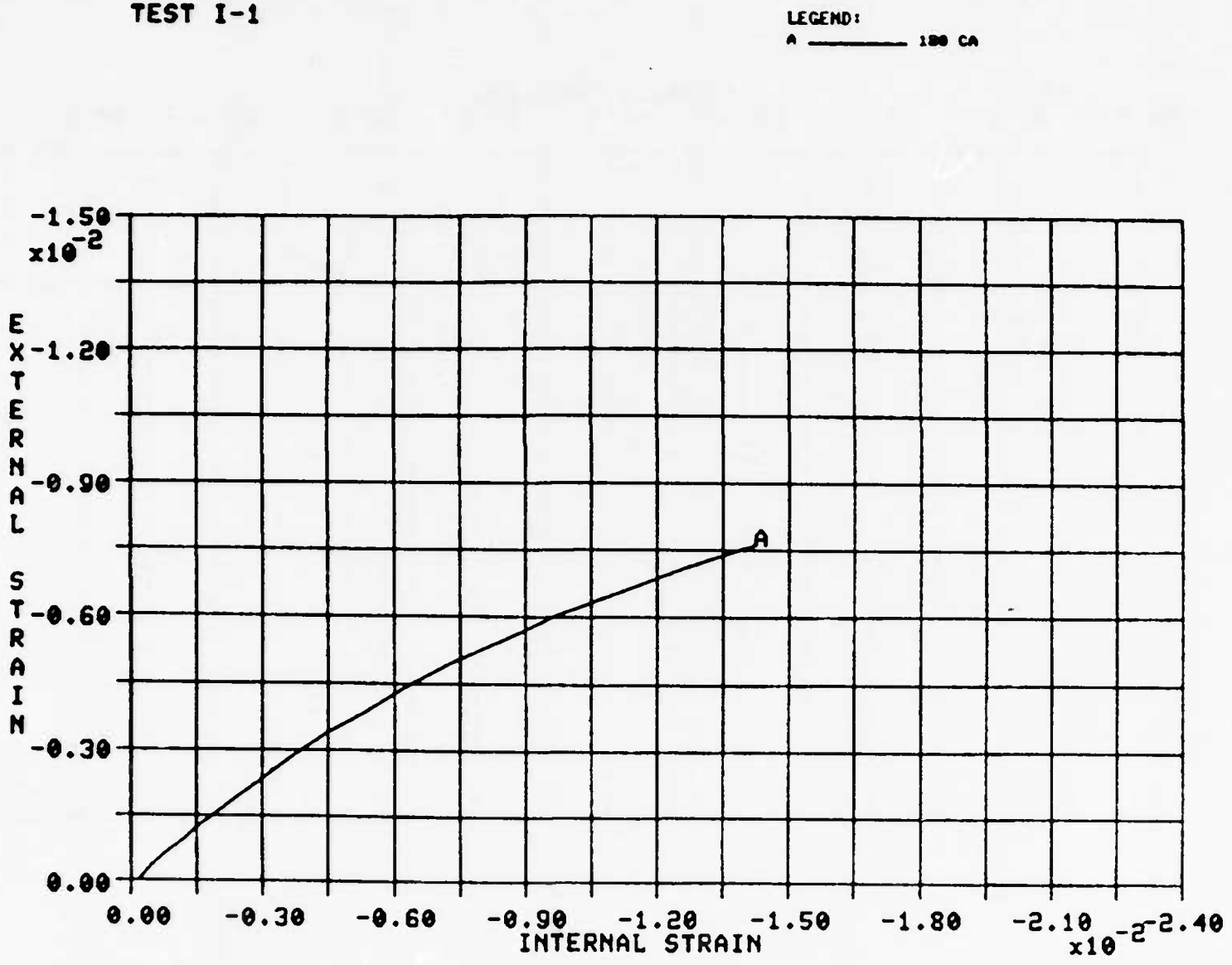

Figure 27 Plot of External vs. Internal Axial Strain at 180° Near the Center or Mid-length of Test No. I-1

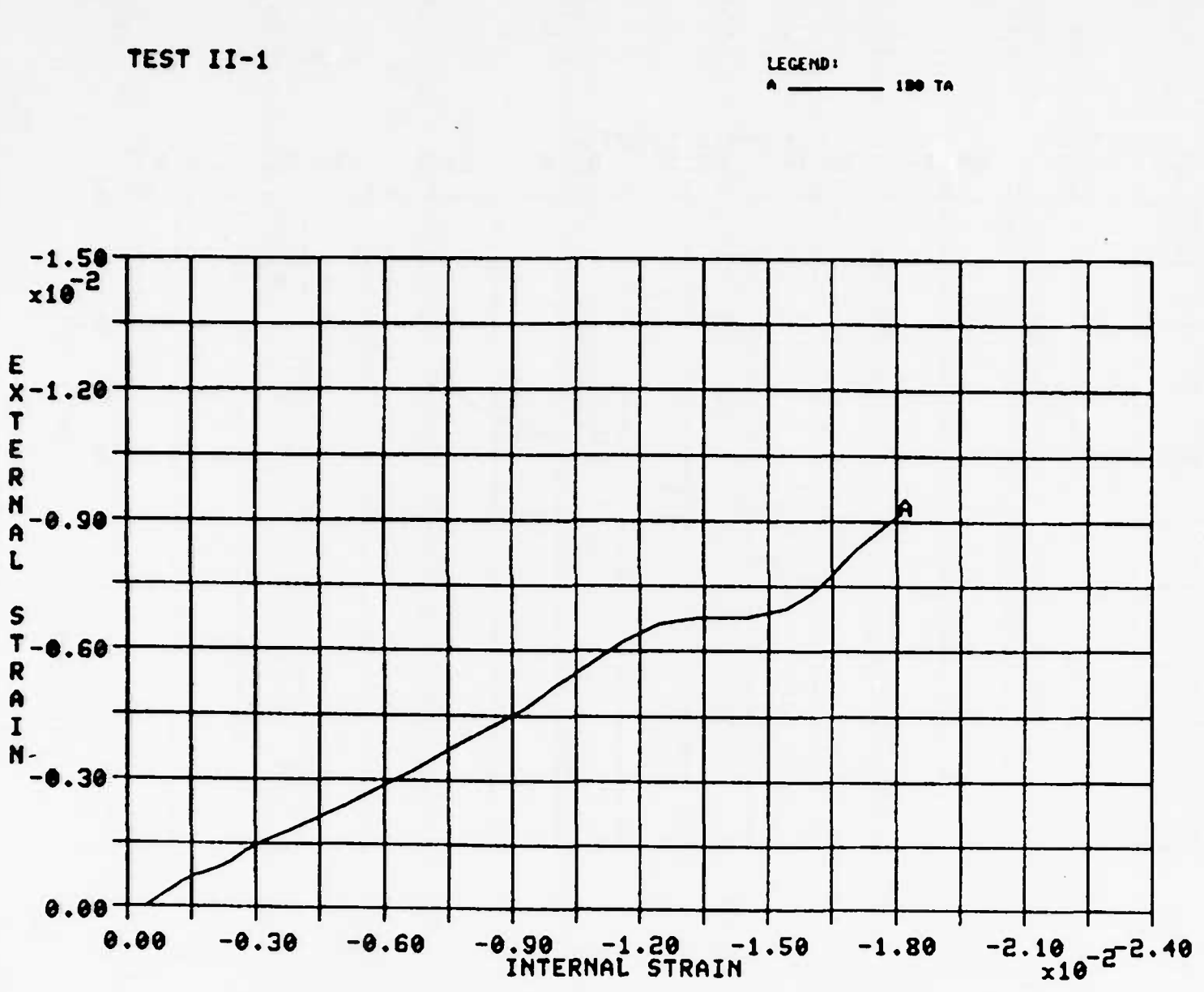

Figure 28 Plot of External vs. Internal Axial Strain at 180° Near the Top Edge of Test No. II-1

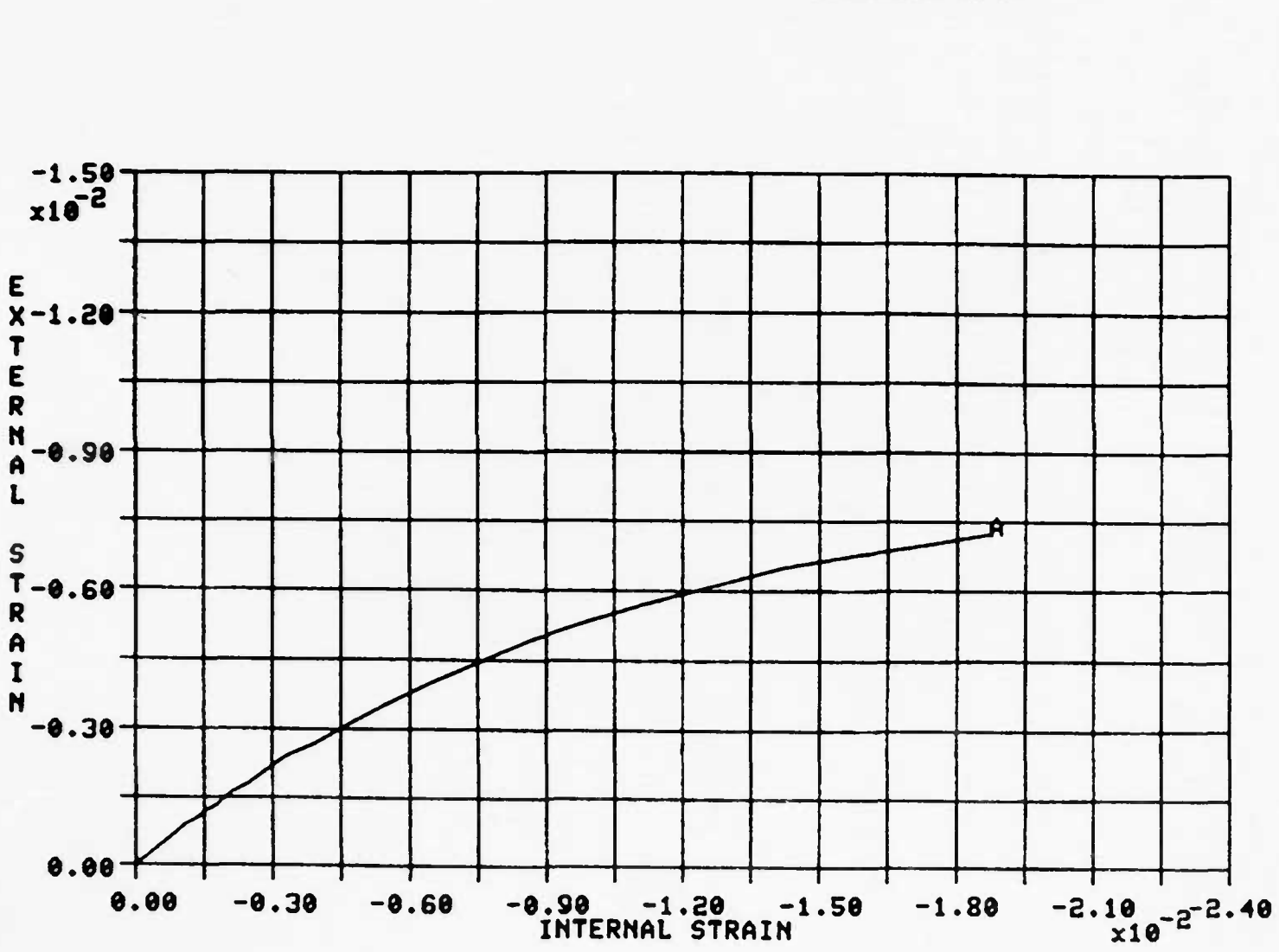

Figure 29 Plot of External vs. Internal Axial Strain at 180° Near the Center or Mid-length of Test No. II-1

Figures 30 and 31 are plots of axial load vs. internal and external axial strain at the 90° and 180° gage locations for Test No. II-2. These plots show good agreement between internal and external axial strain indicating very little bending stress or barreling of the specimen. This is also indicated by the plot of axial load vs. hoop strain shown in Figure 32 where equal strain at the center and edge of the specimen indicate the cylinder is expanding uniformly through out its length. The plots of external axial strain vs. internal axial strain shown in Figures 33 through 35 show a slope of almost unity. This would also indicate very small bending stresses.

Plots of axial load vs. external and internal axial strain for Test No. II-3 are given in Figures 36 and 37. These plots show indications of bending stresses at the top edge. This may be a result of the blooming along the edges of the specimen. Figure 38 is a plot of axial load vs. hoop strain which also shows some indication that the specimen was barreling under load. Figures 39 and 40 are plots of external axial vs. internal axial strain. These plots are in agreement with Figures 36 and 37 showing indications of bending stresses near the top edge and no bending through the center.

With only a uniaxial load applied, the Poisson's ratio can be measured by plotting hoop strain vs. axial strain at various gage locations. The slope of these plots are a measure of Poisson's ratio. Figures 41 and 42 are plots of hoop vs. axial strain for Test No. I-1 at the 90° location. These plots indicate the Poisson's ratio is 0.80 at the start of the test and increases to greater than 1.0 at the test end. Figures 43 and 44 are similar plots for Test No. II-1. These plots indicate a Poisson's ratio of 0.87 at the beginning increasing to greater than 1.0 at the test end. Figures 45 and 46 are plots of hoop vs. axial strain for Test Nos. II-2 and II-3. Test No. II-2 has a Poisson's ratio of 0.51 increasing to 1.00, while Test No. II-3 has a ratio of 0.90 at the start increasing to 1.19 at the test end. There appears to be better agreement between different gage

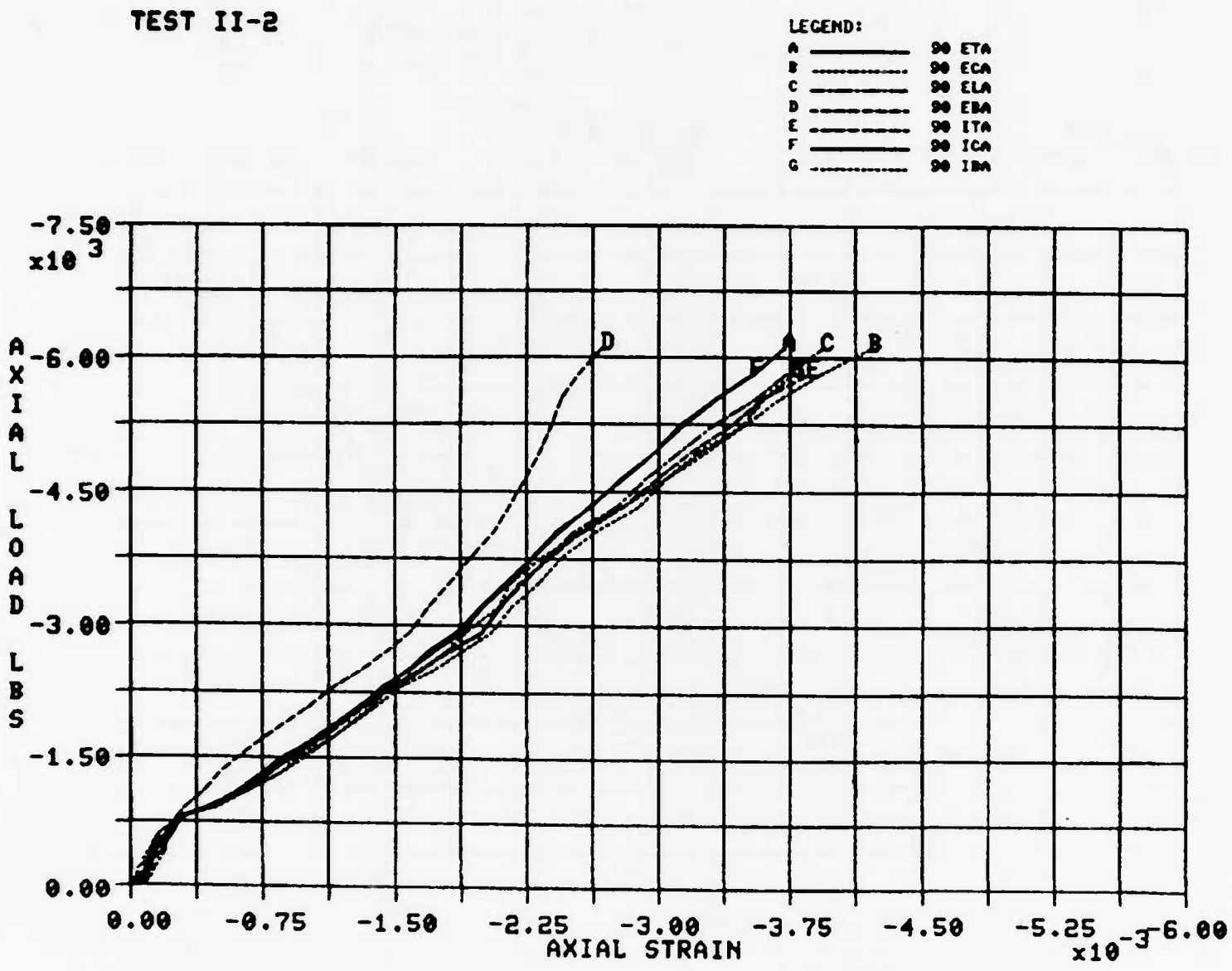

Figure 30 Plot of Axial Load vs. Axial Strain at 90° for Test No. II-2

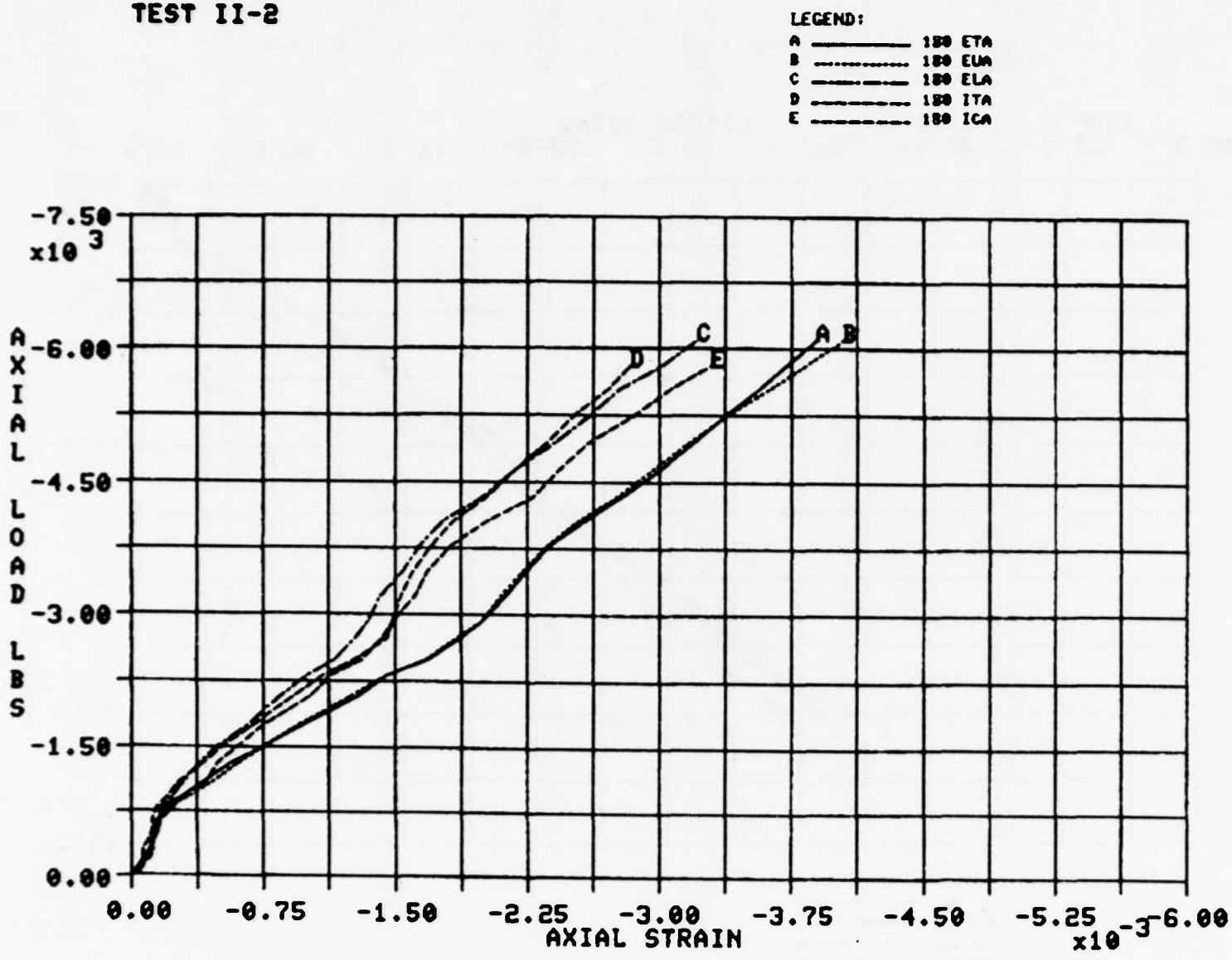

Figure 31 Plot of Axial Load vs. Axial Strain at 180° for Test No. II-2

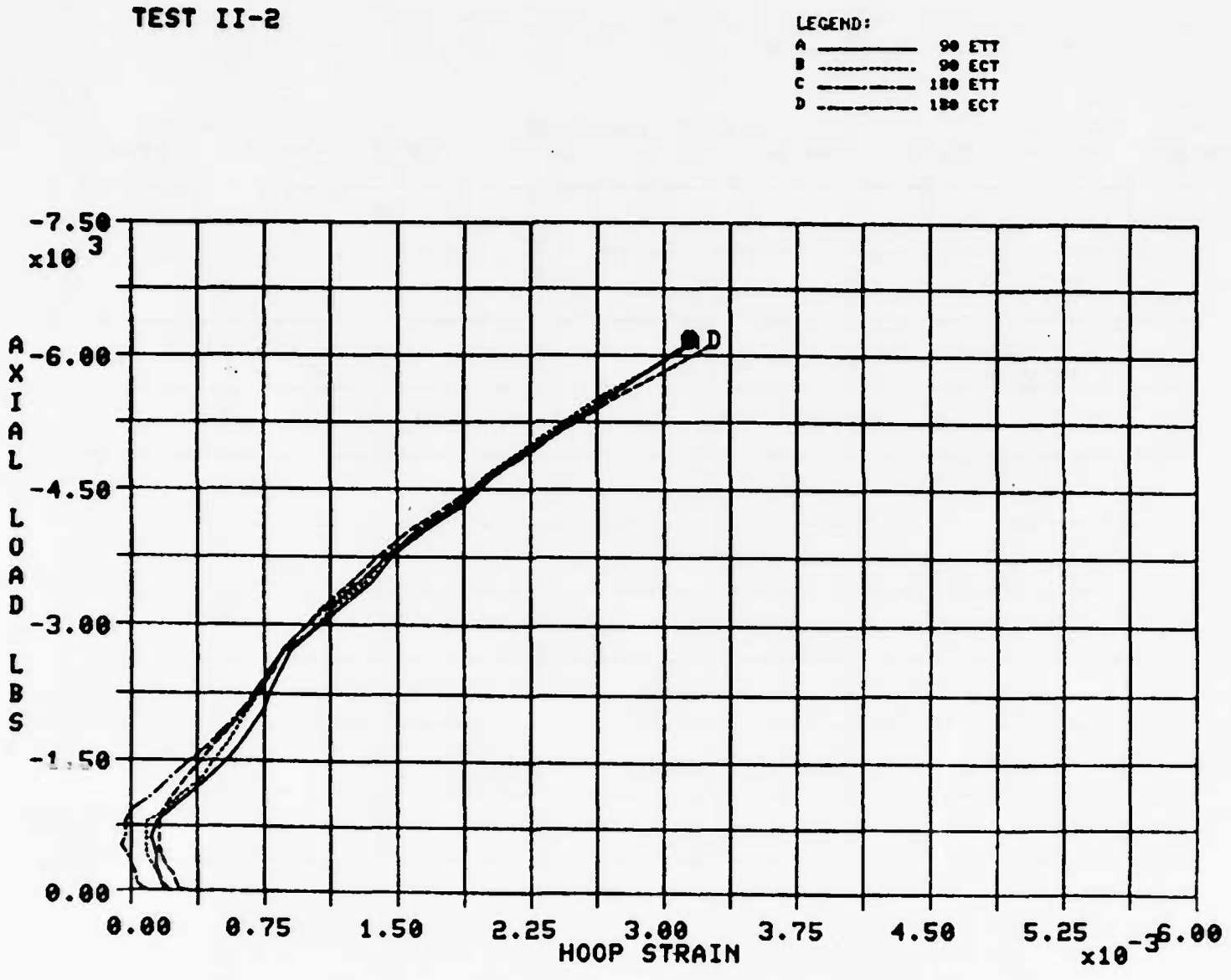

Figure 32 Plot of Axial Load vs. Hoop Strain for Test No. II-2

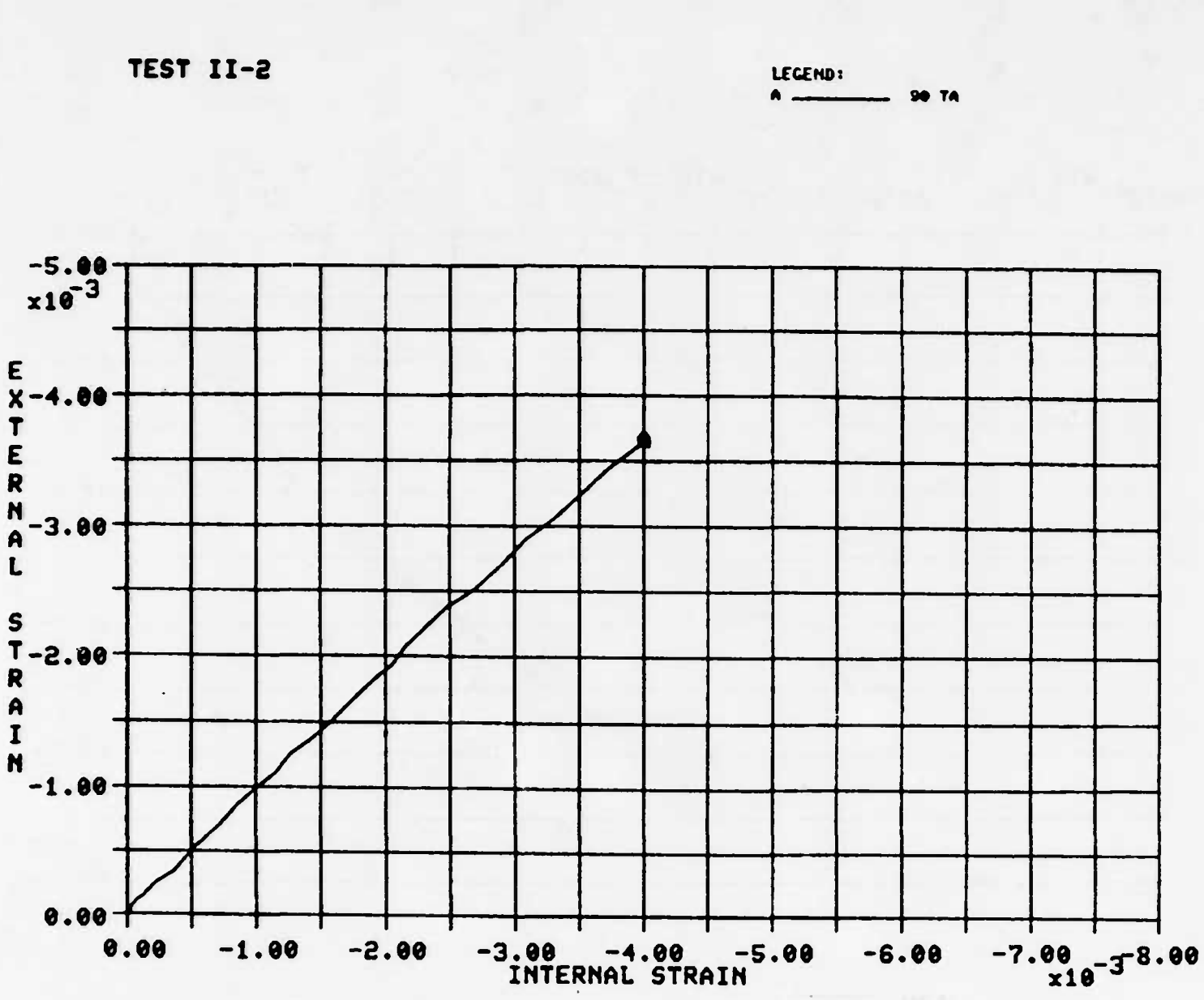

Figure 33 Plot of External vs. Internal Axial Strain at 90° Near the Top Edge of Test No. II-2

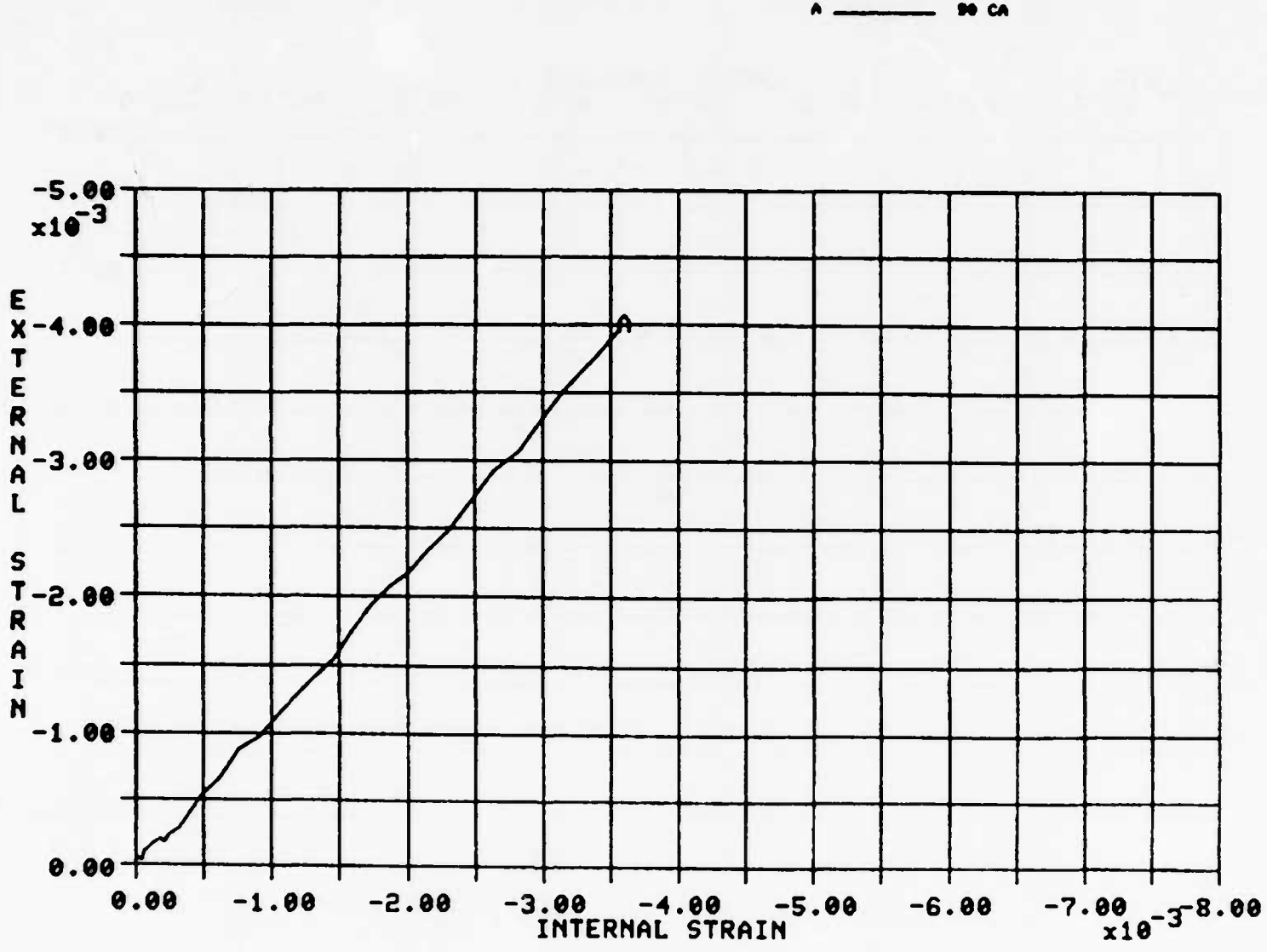

Figure 34 Plot of External vs. Internal Axial Strain at 90° Near the Center or Mid-length of Test No. II-2

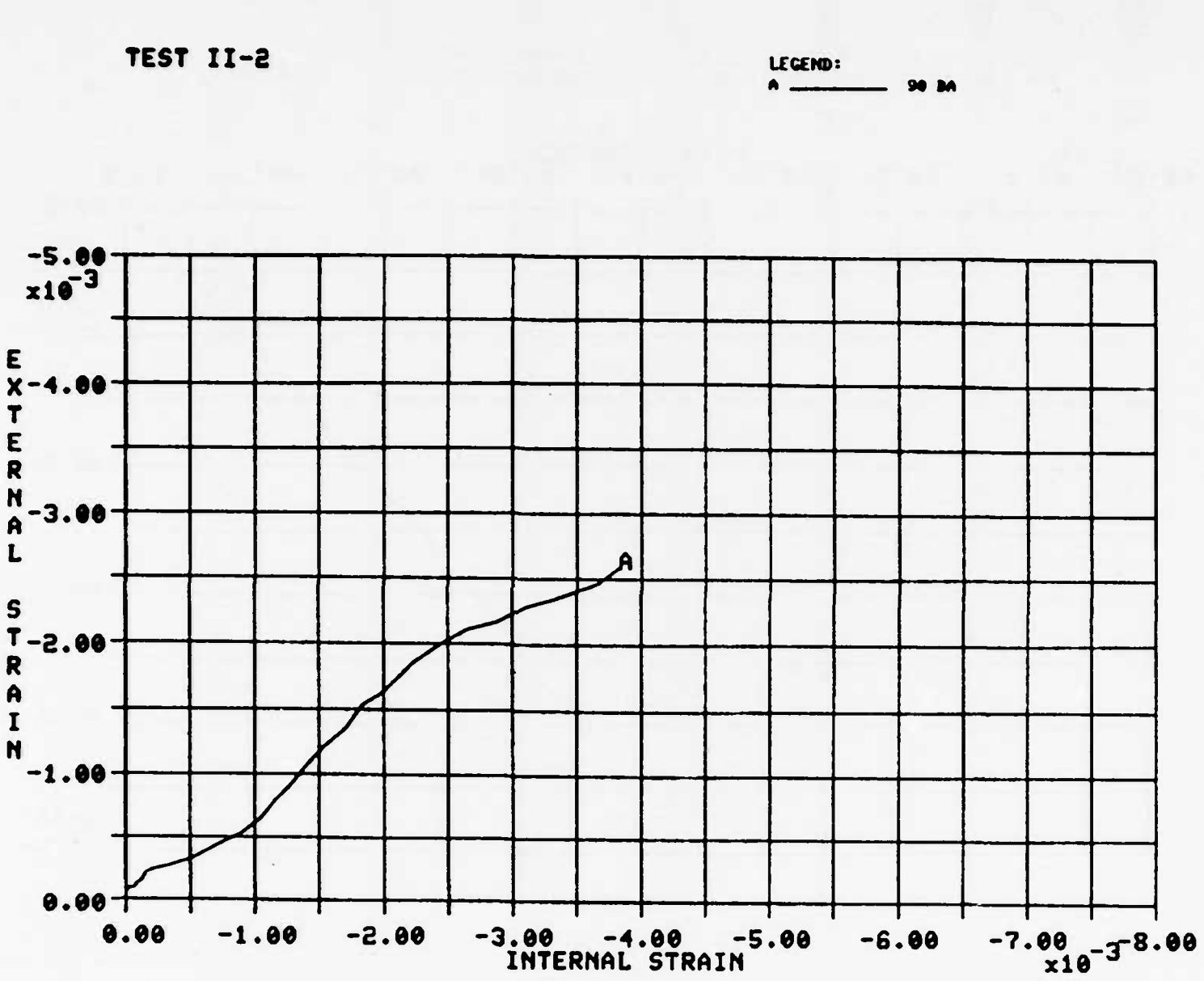

Figure 35 Plot of External vs. Internal Axial Strain at 90° Near the Bottom Edge of Test No. II-2

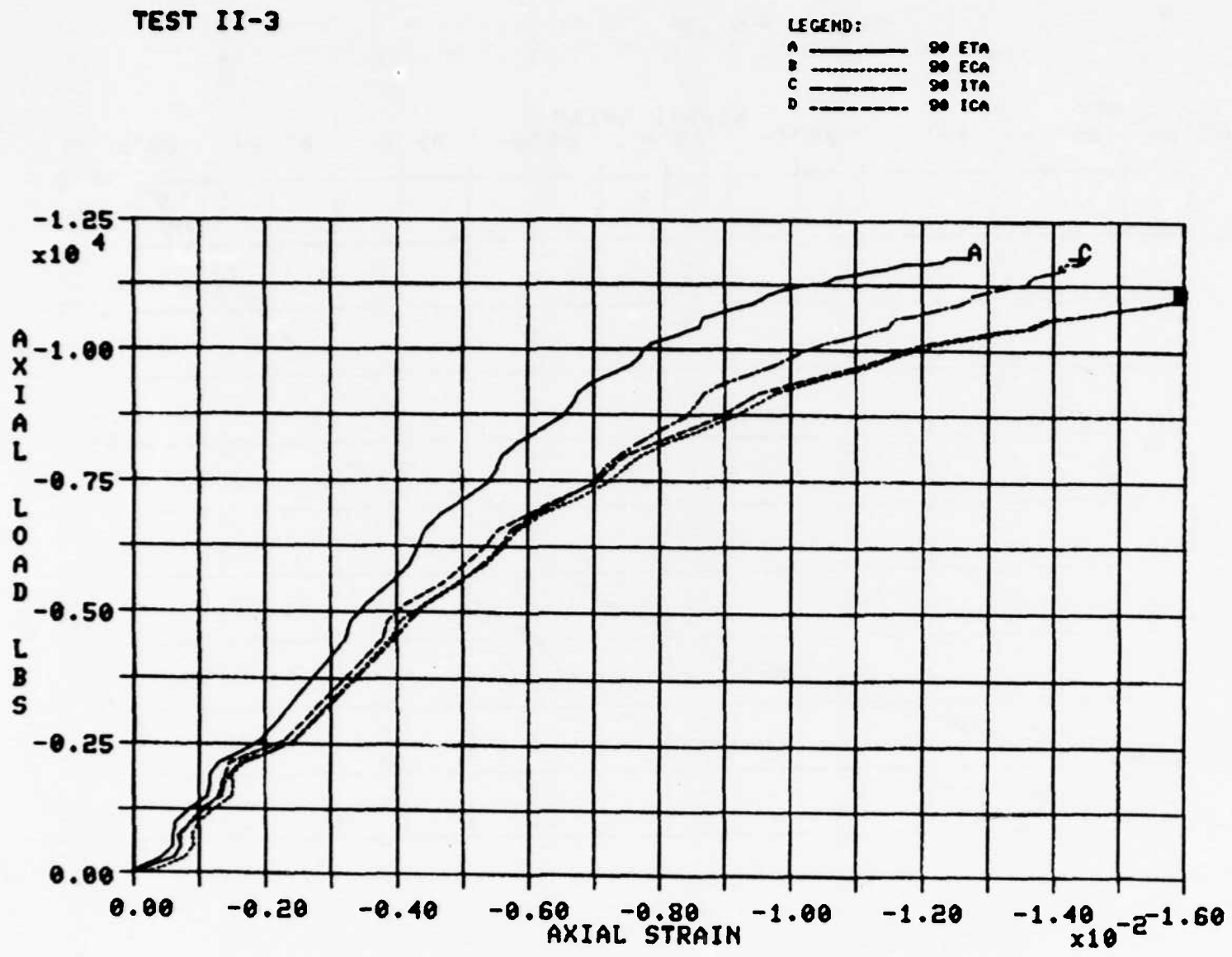

Figure 36 Plot of Axial Load vs. Internal and External Axial Strain at 90° for Test No. II-3

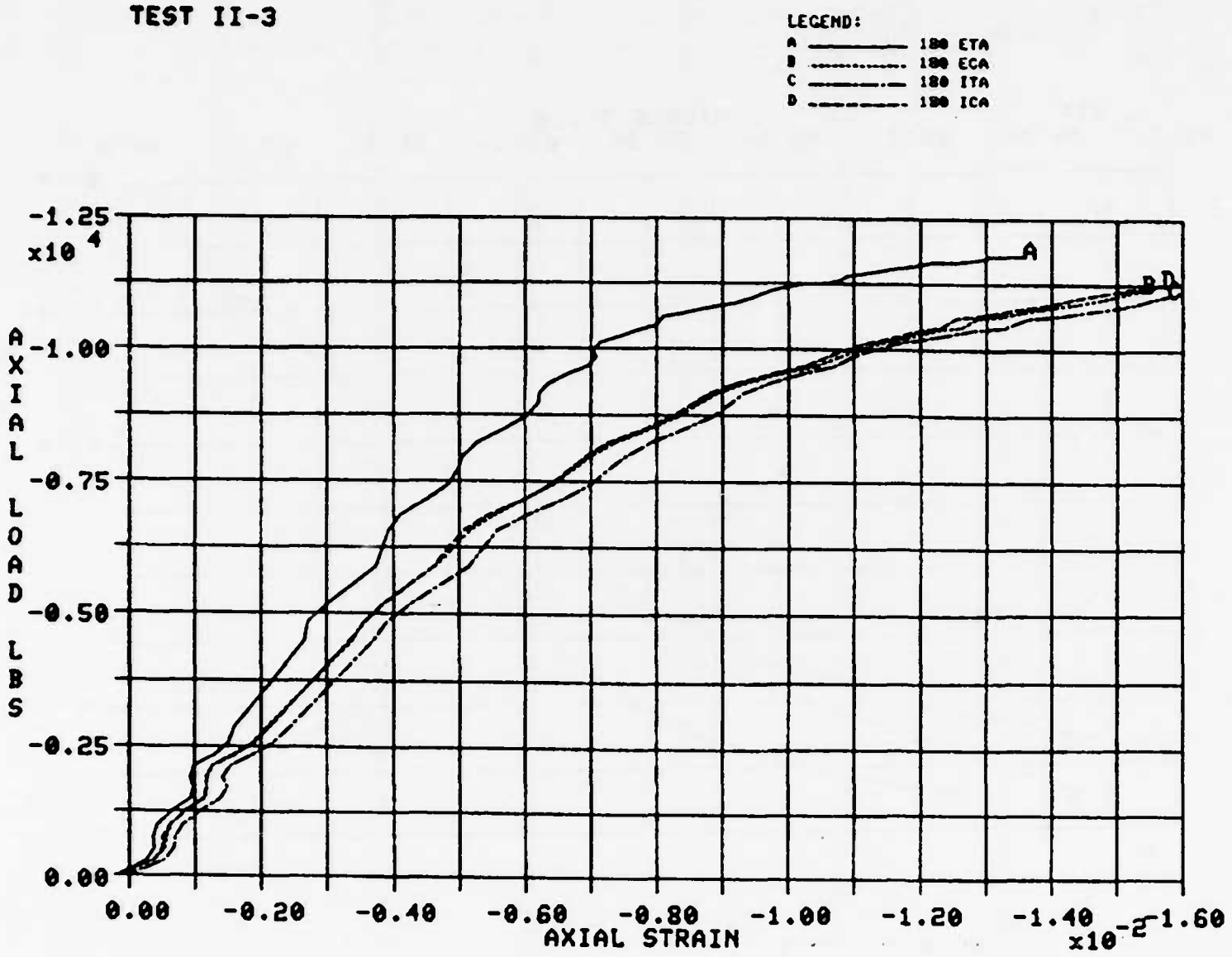

Figure 37 Plot of Axial Load vs. Internal and External Axial Strain at 180° for Test No. II-3

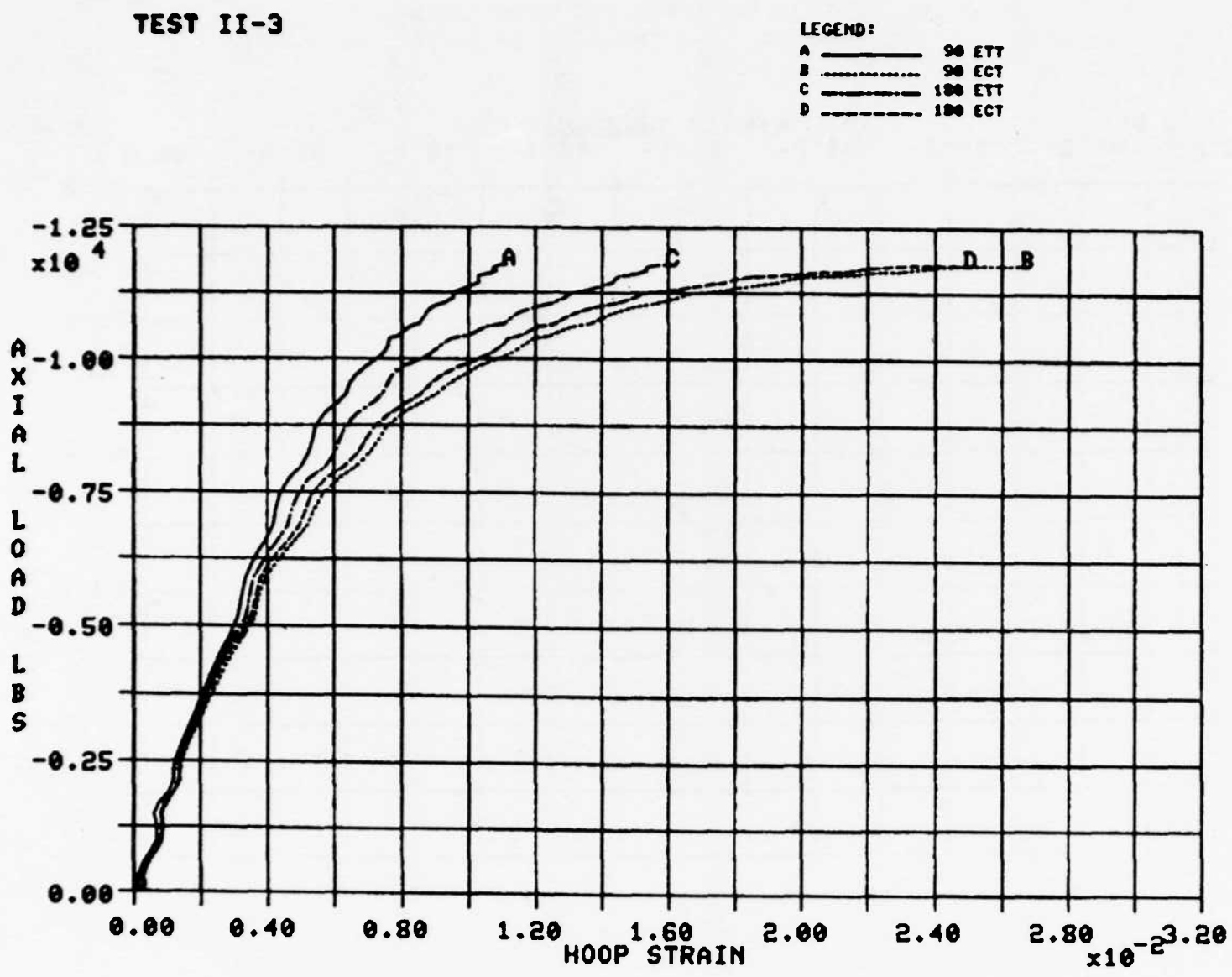

Figure 38 Plot of Axial Load vs. Hoop Strain for Test No. II-3

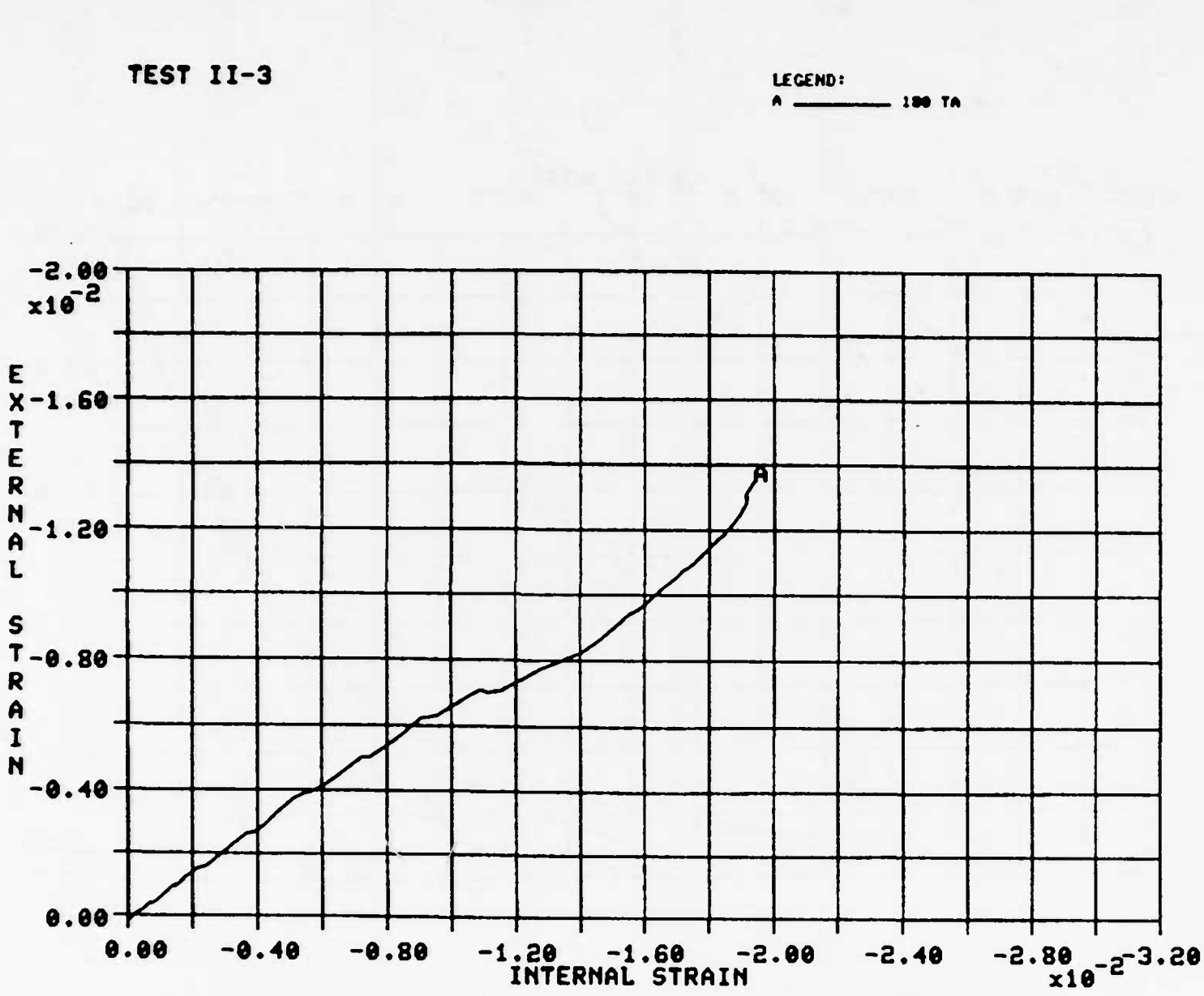

Figure 39 Plot of External vs. Internal Axial Strain at 180° Near the Top Edge of Test No. II-3

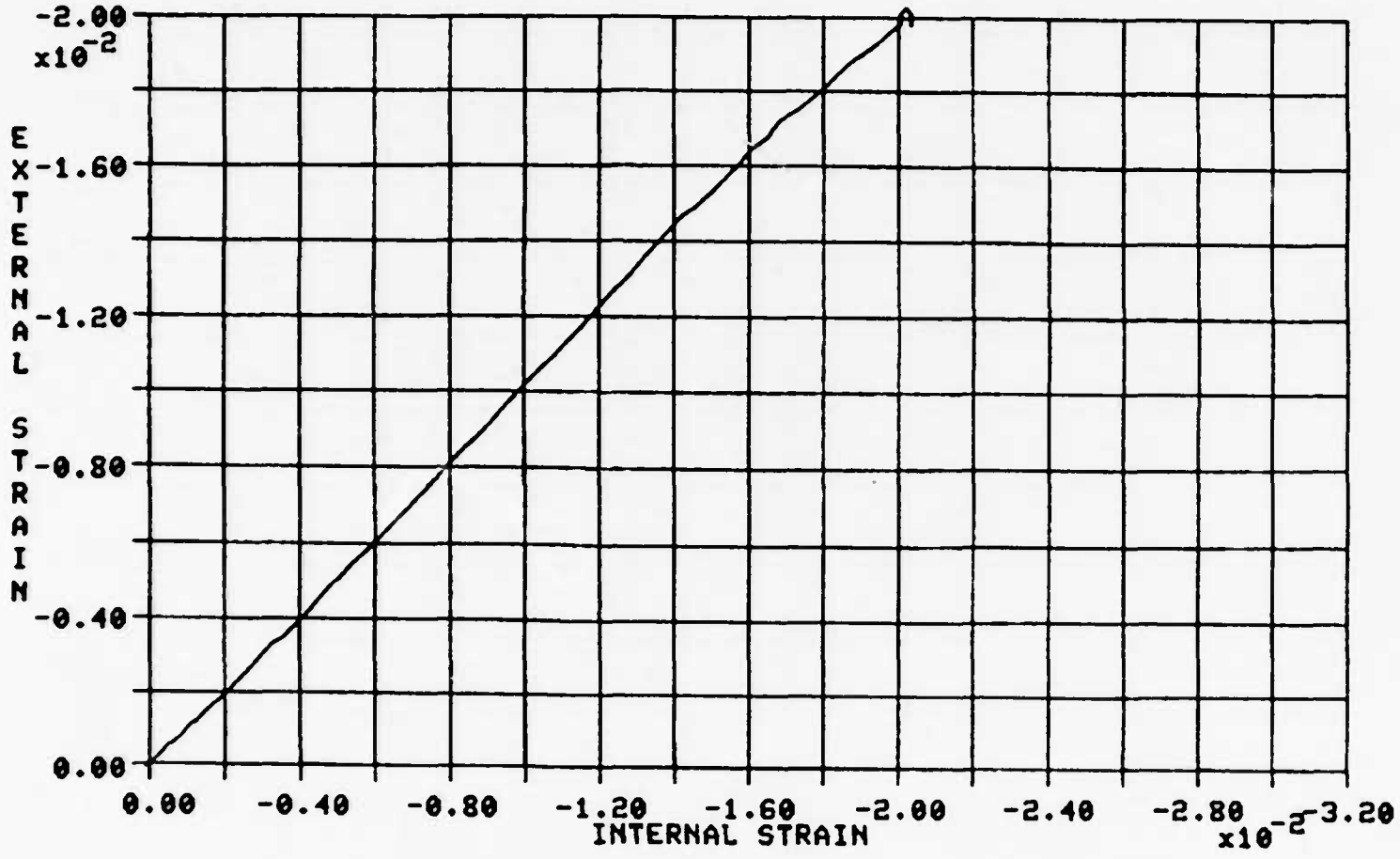

Figure 40 Plot of External vs. Internal Axial Strain at 180° Near the Center or Mid-length of Test No. II-3

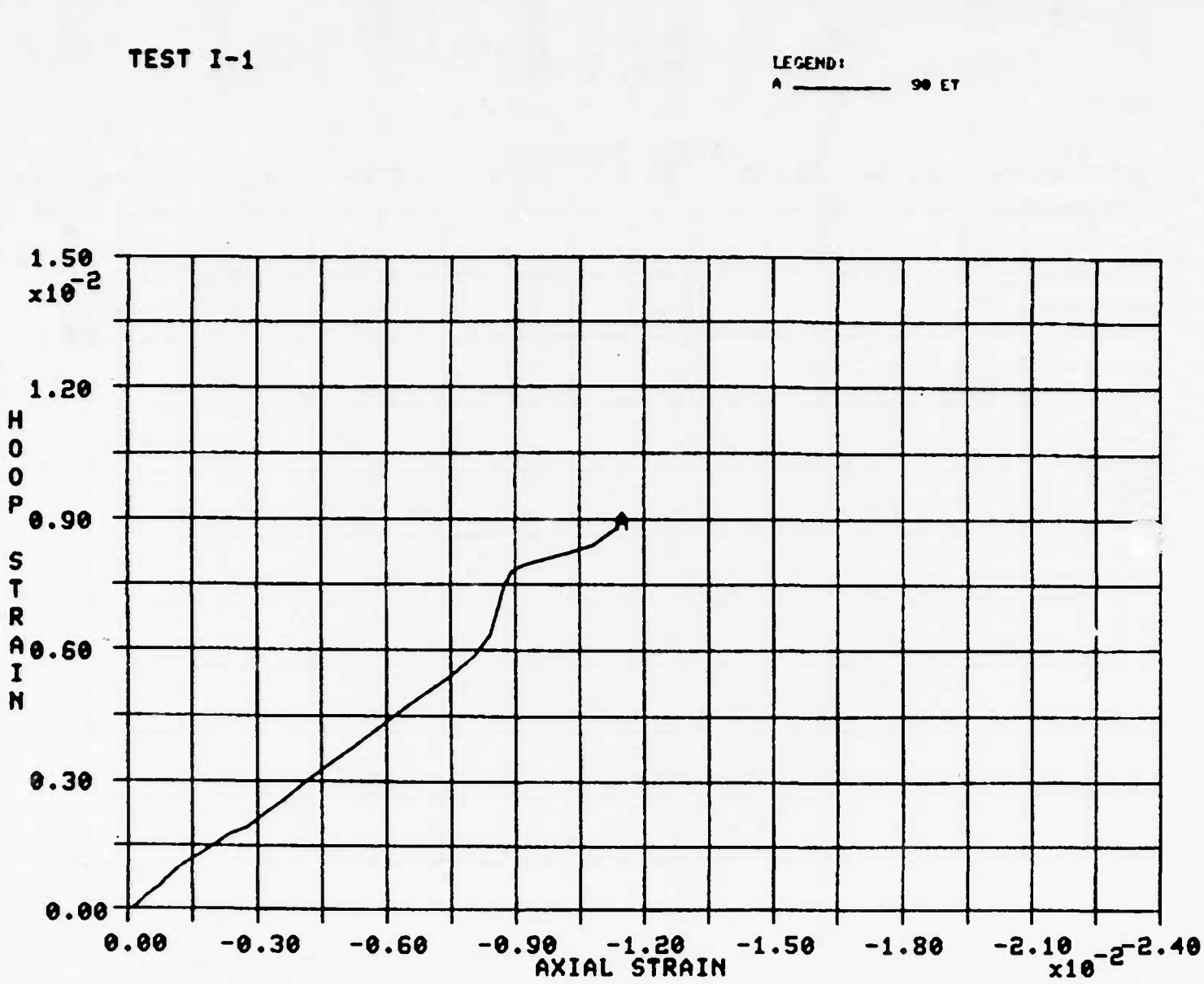

Figure 41 Plot of Hoop vs. Axial Strain at the 90° Location Near the Top Edge of Test No. I-1

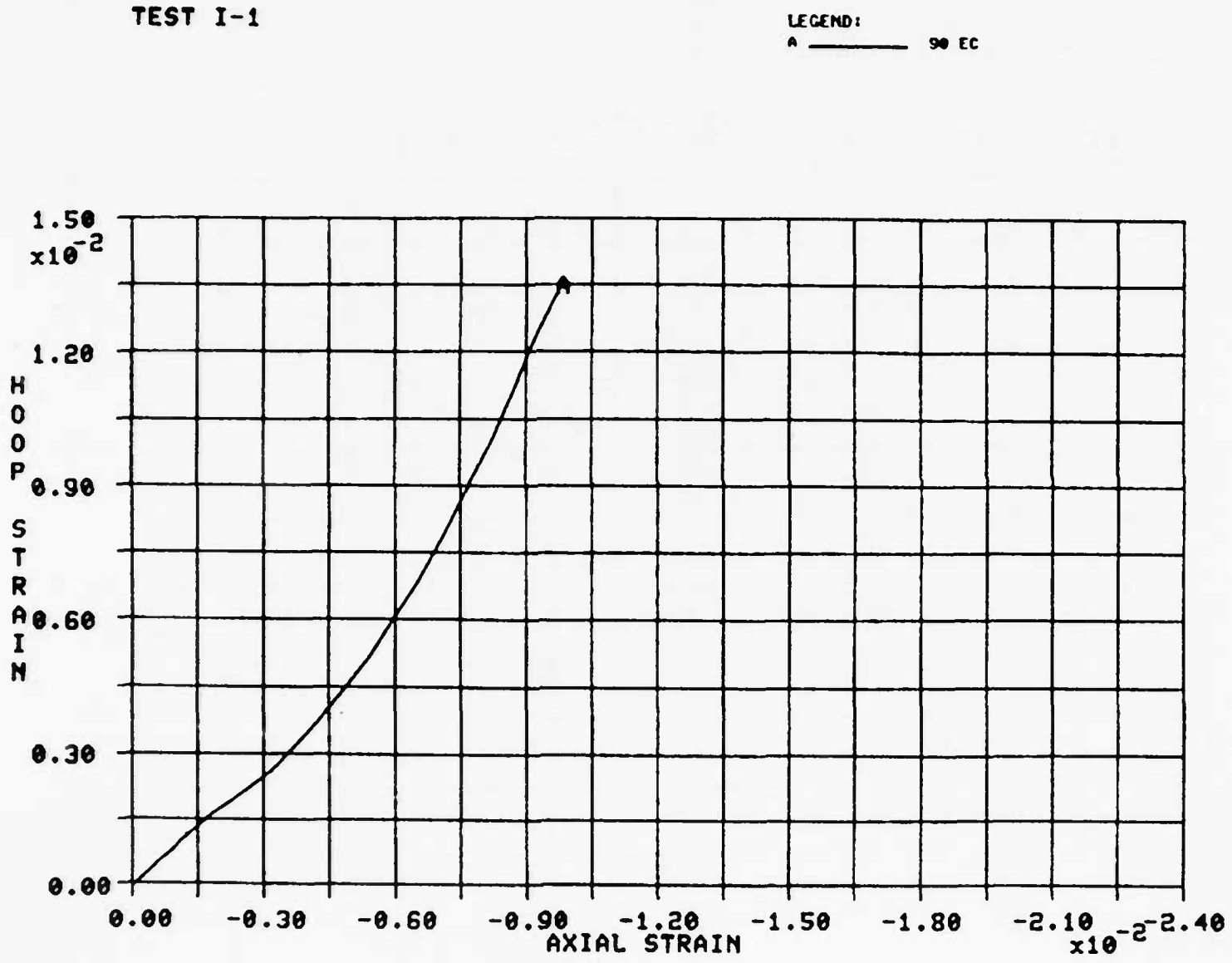

Figure 42 Plot of Hoop vs. Axial Strain at the 90° Location Near the Center or Mid-length of Test No. I-1

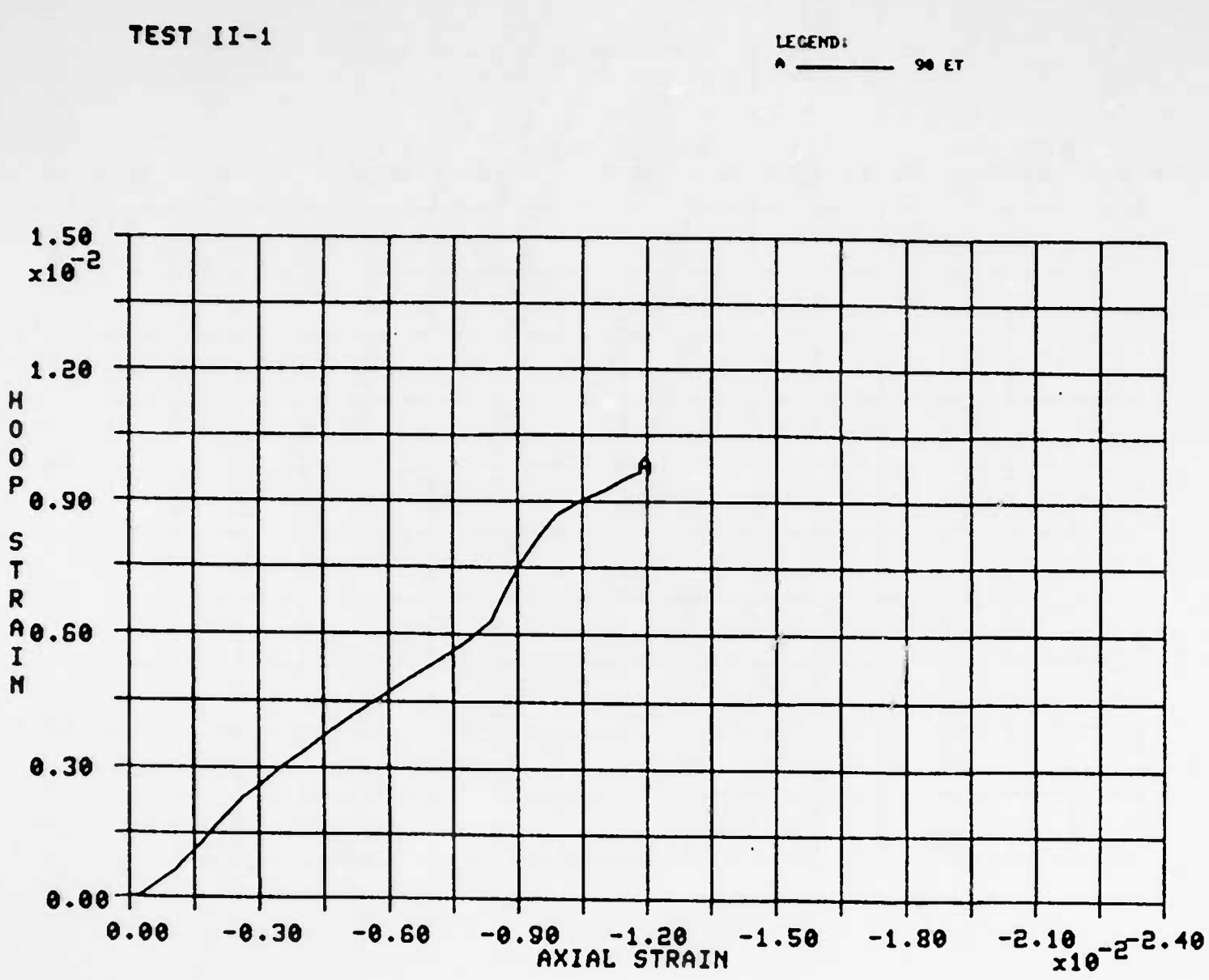

Figure 43 Plot of Hoop vs. Axial Strain at the 90° Location Near the Top Edge of Test No. II-1

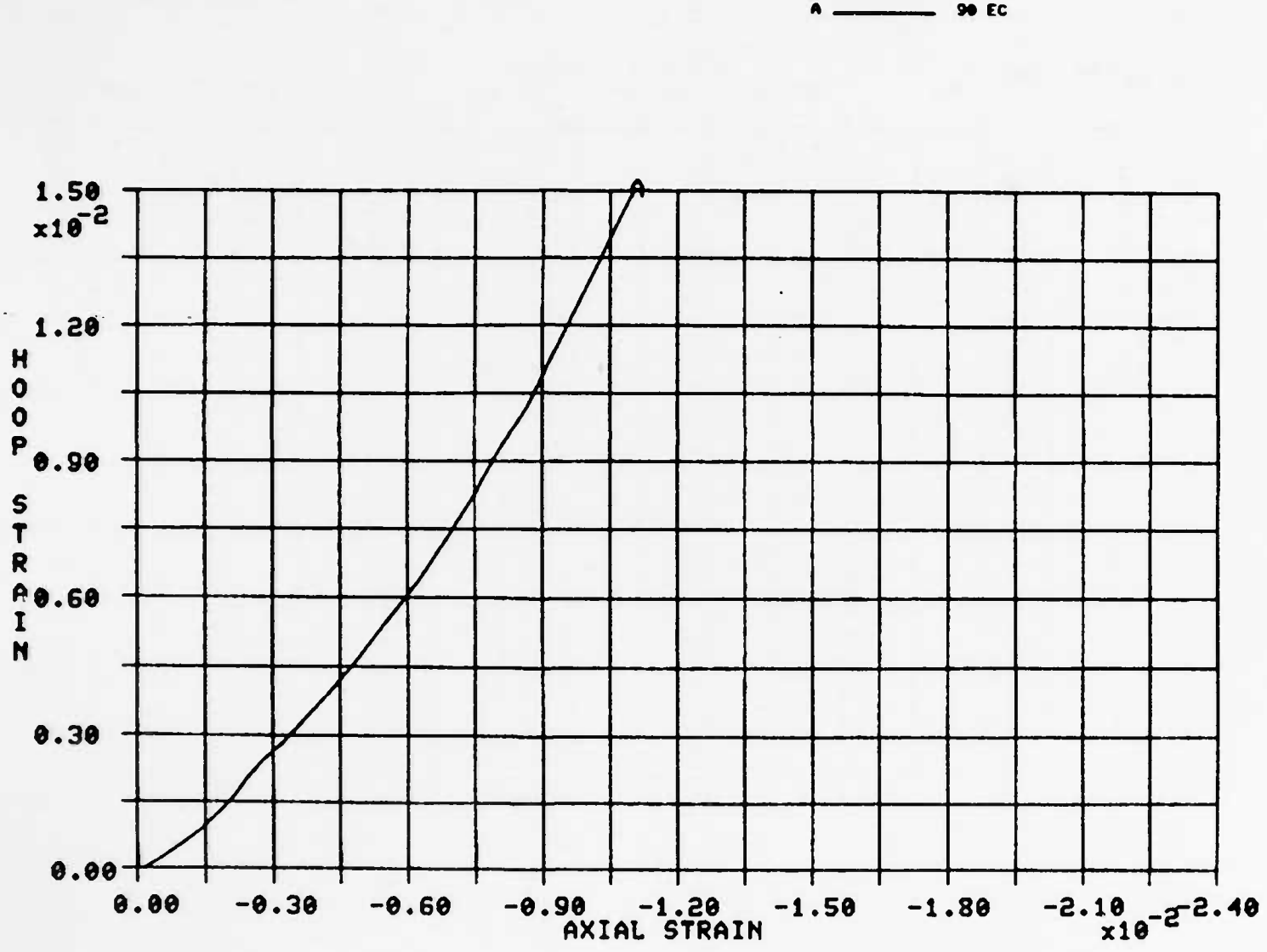

Figure 44 Plot of Hoop vs. Axial Strain at the 90° Location Near the Center or Mid-length of Test No. II-1

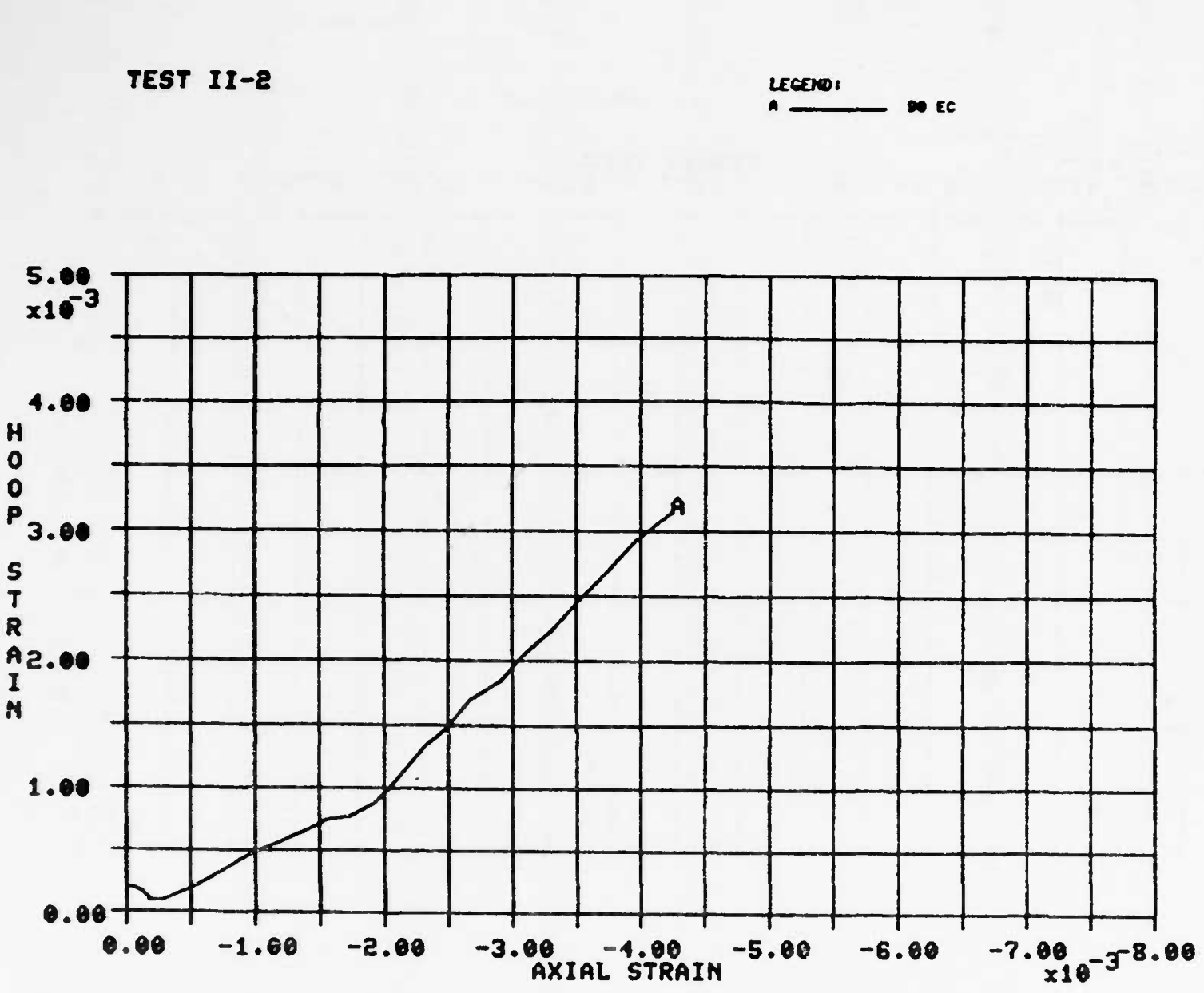

Figure 45 Plot of Hoop vs. Axial Strain at the 90° Location Near the Center or Mid-length of Test No. II-2

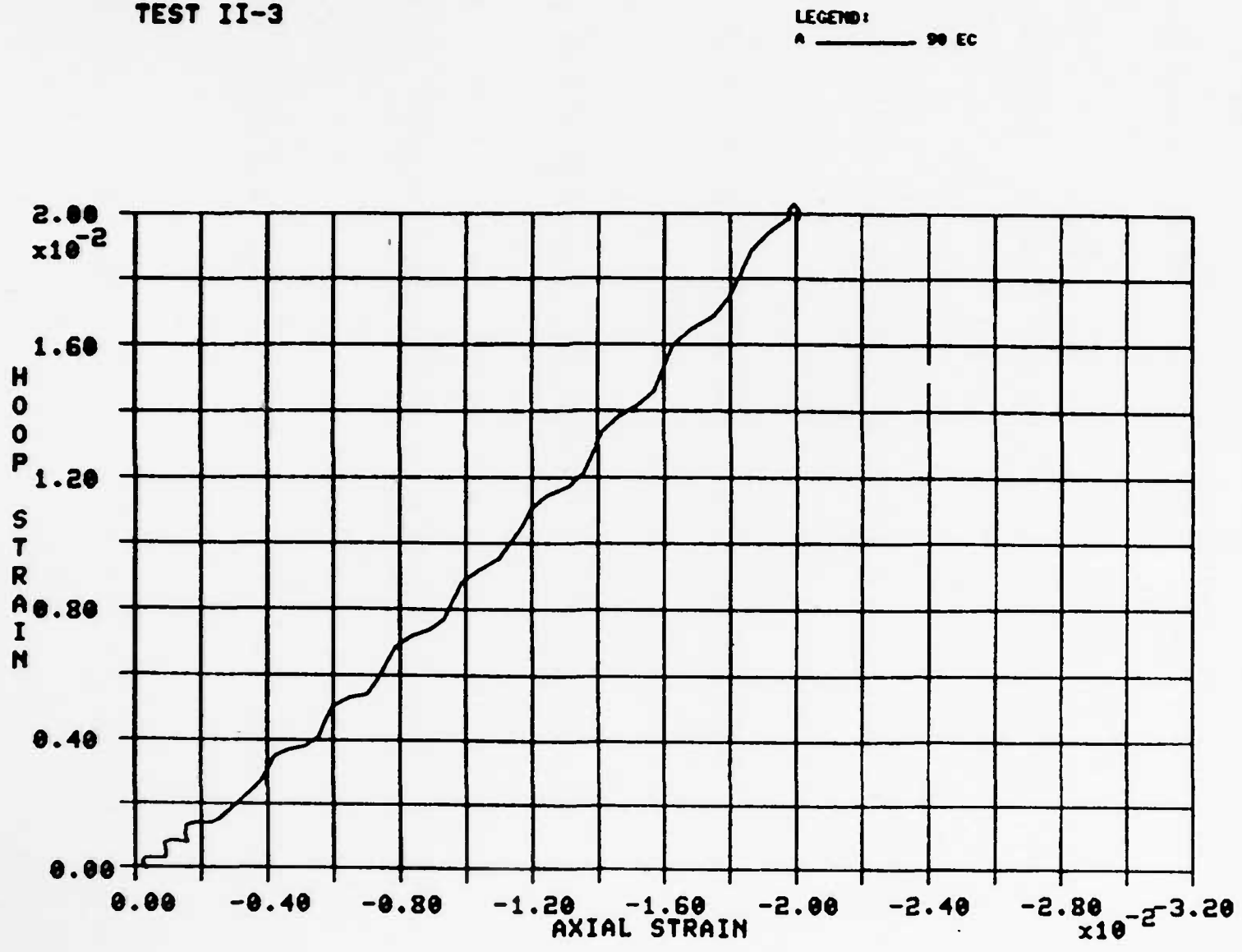

Figure 46 Plot of Hoop vs. Axial Strain at the 90° Location Near the Center or Mid-length of Test No. II-3

location for the 2-inch specimen than the 1-inch specimens. Figure 47 is a plot of axial load vs. diagonal strain for Test No. II-2. It can be seen that as the Poisson's ratio approaches unity the diagonal gages do not increase in output.

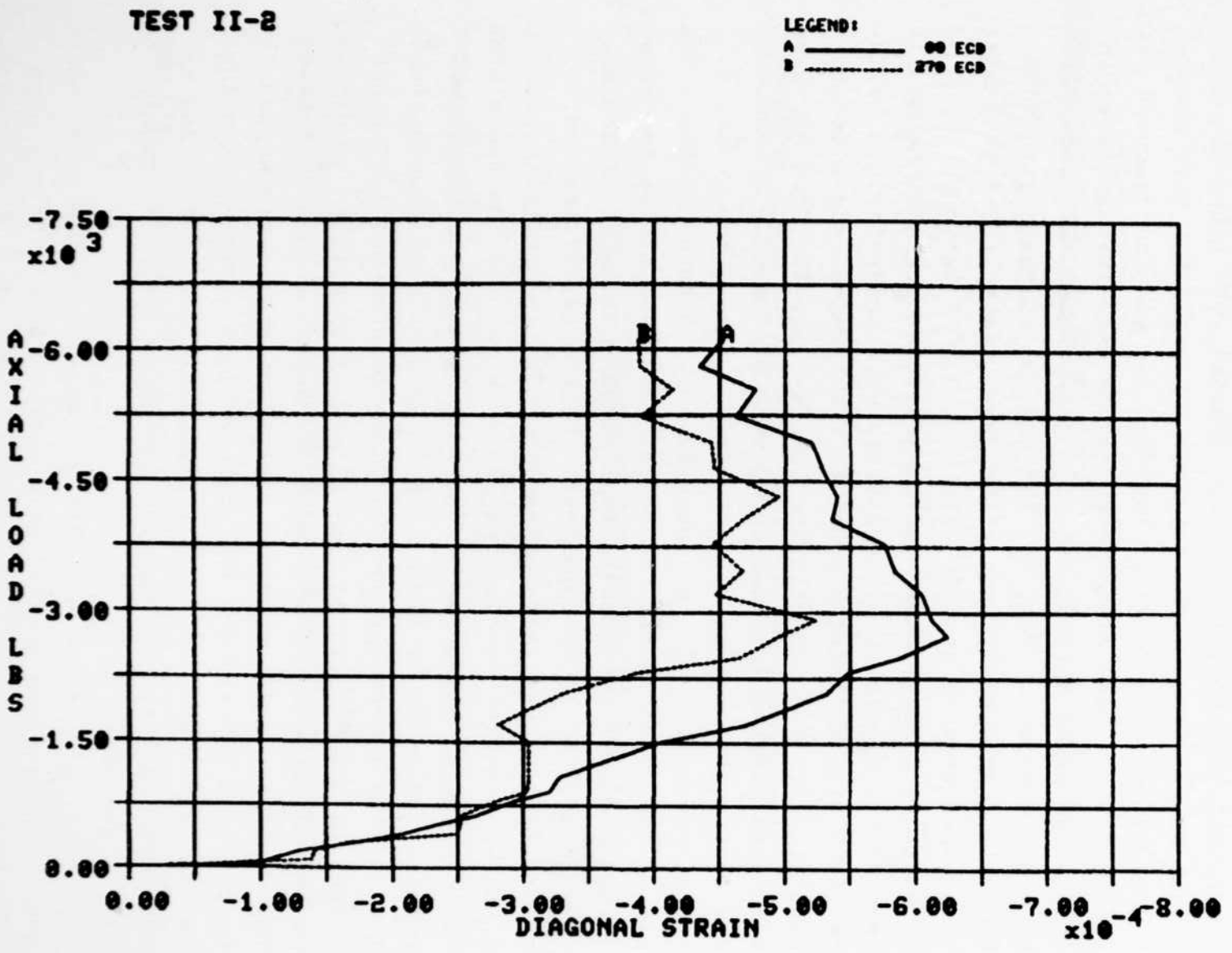

Figure 47 Plot of Axial Load vs. Diagonal Strain for Test No. II-2

VI. INTERNAL PRESSURE TESTS

Two instrumented specimens were tested with internal pressure load only. These were Test Nos. I-4 and I-5. Both specimens were 2 inches in length. Test No. I-4 was instrumented with thirty-six strain gage elements using the gage layout listed in Table 5. The gages were spaced 45° apart around the circumference of the specimen. Test No. I-5 was instrumented with fourteen strain gage elements using the gage layout listed in Table 6. The gages were at the 90°, 180° and 270° locations.

Two special-made rubber gaskets were used on the inside surface of the specimens. The gaskets were molded into a cylindrical tube with a diameter equal to the specimen and a length slightly longer than one-half the specimen length. Two of these gaskets were stacked together inside the specimens. Cut-outs were made for the instrumentation wires. All of the seams and cut-outs were sealed with silicone rubber. Because of the extra length of the gasket pair, the gaskets could be preloaded between the two platens of the biaxial test fixture with only a small axial load applied to the specimen. This provided the seal necessary for internal pressurization. The lead/polyethelene/-lead sandwich gasket lubrication was also used at the two platen surfaces. The pressure was produced using a manual, handwheel-operated, single-stroke piston pump. This allowed smooth steady control of the internal pressure. The pressure and load signal were sent to the MTS system controller. The ratio in gain between the pressure and load signal was adjusted such that the system would produce a constant preload on the specimen plus the force required to overcome the pressure load acting on the internal platen surfaces. The strain gage, load cell and pressure transducer data were recorded via the SUN system and sent to the PDP 11/34 computer.

An axial preload of -200 lbs was applied to Specimen I-4. Internal pressure was applied at a rate of approximately 5 psi per second. It was found that the specimen could not be loaded past 300 psi without loss of hydraulic pressure. The pressure

load was then released and the axial preload was increased to -400 lbs. If it were assumed that the entire axial load was supported by the specimen and not the internal gasket, this would correspond to an initial axial sress (σ_x) of -0.72 ksi. The internal pressure was increased again slowly. The specimen failed at a pressure of 575 psi. With a cylinder diameter of 3.92 inches and a wall thickness of 0.045 inches, this corresponds to a hoop stress (σ_θ) of 25.04 ksi. The specimen failed as a result of tensile hoop stresses at the 90° gage location. The fracture left a jagged edge with local separation between plies. All other areas of the specimen appeared to be undamaged. The next specimen was Test No. I-5. An axial preload of -400 lbs. was applied. The internal pressure could not be increased past 520 psi without loss of the pressure seal. The axial load was increased; however, the gasket was permanently damaged and the specimen could not be failed under internal hydraulic pressure. The strain gage data indicates the specimen was near failure. The pressure of 520 psi corresponds to a hoop stress (σ_θ) of 22.65 ksi. There was no apparent damage to the specimen after testing. Photographs of the specimen are shown in Figures 48 and 49.

Figures 50 and 51 are plots of internal pressure vs. hoop strain at mid-length around the circumference of the specimens. These plots show a good distribution of hoop stress around the specimens' circumference. Plots of internal pressure vs. axial strain around the circumference, as shown in Figures 52 and 53, also indicate good load distribution.

Figures 54 and 55 are plots of internal pressure vs. internal and external axial strain at 90° and 180° gage locations for Test No. I-4. This data shows good agreement between internal and external gages; however, the internal strain is generally higher than the external strain indicating a small amount of bending through the length of the specimen. This is also indicated by the plots of external vs. internal strain shown in Figures 56 and 57. These plots have a slope slightly less than

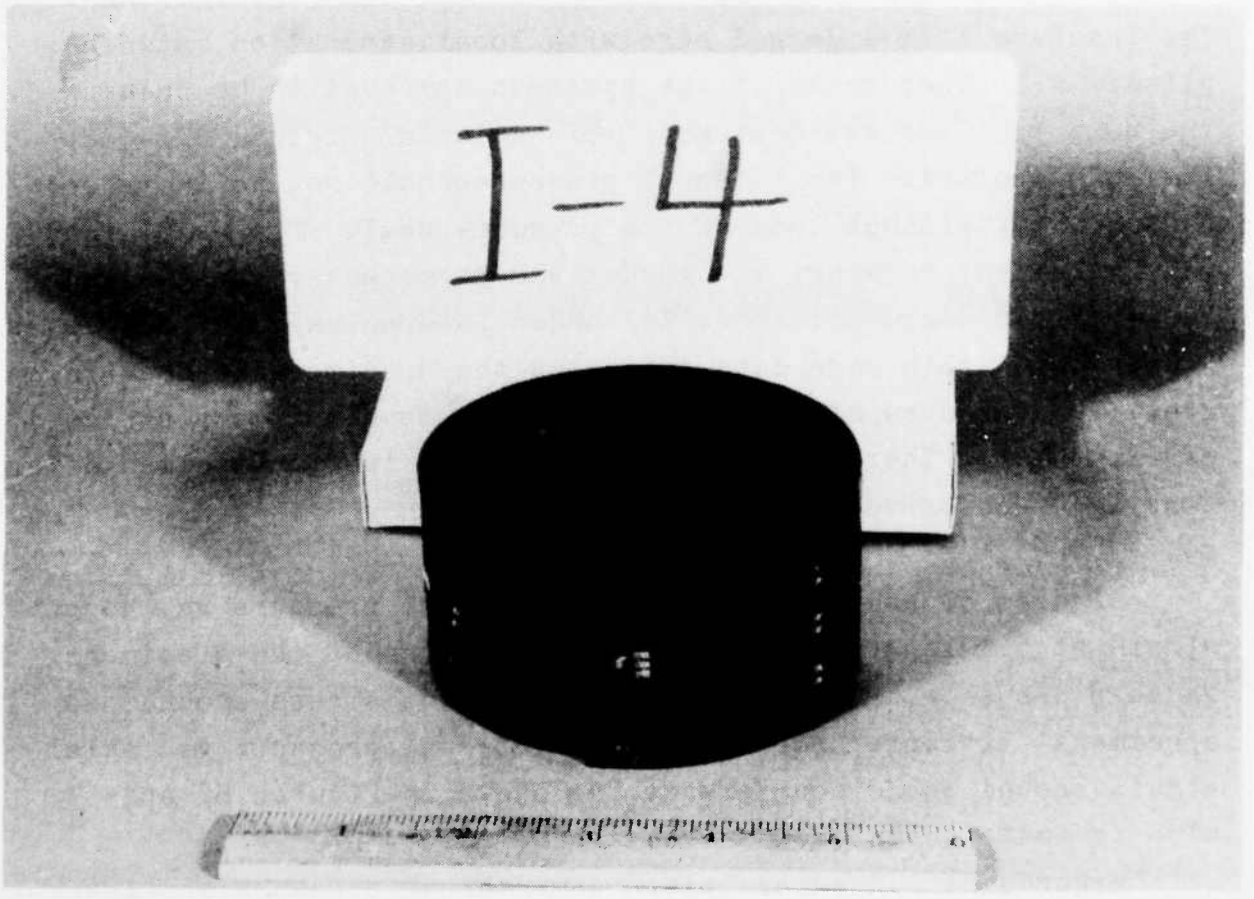

Figure 48 Photograph of Specimen No. I-4 After Testing

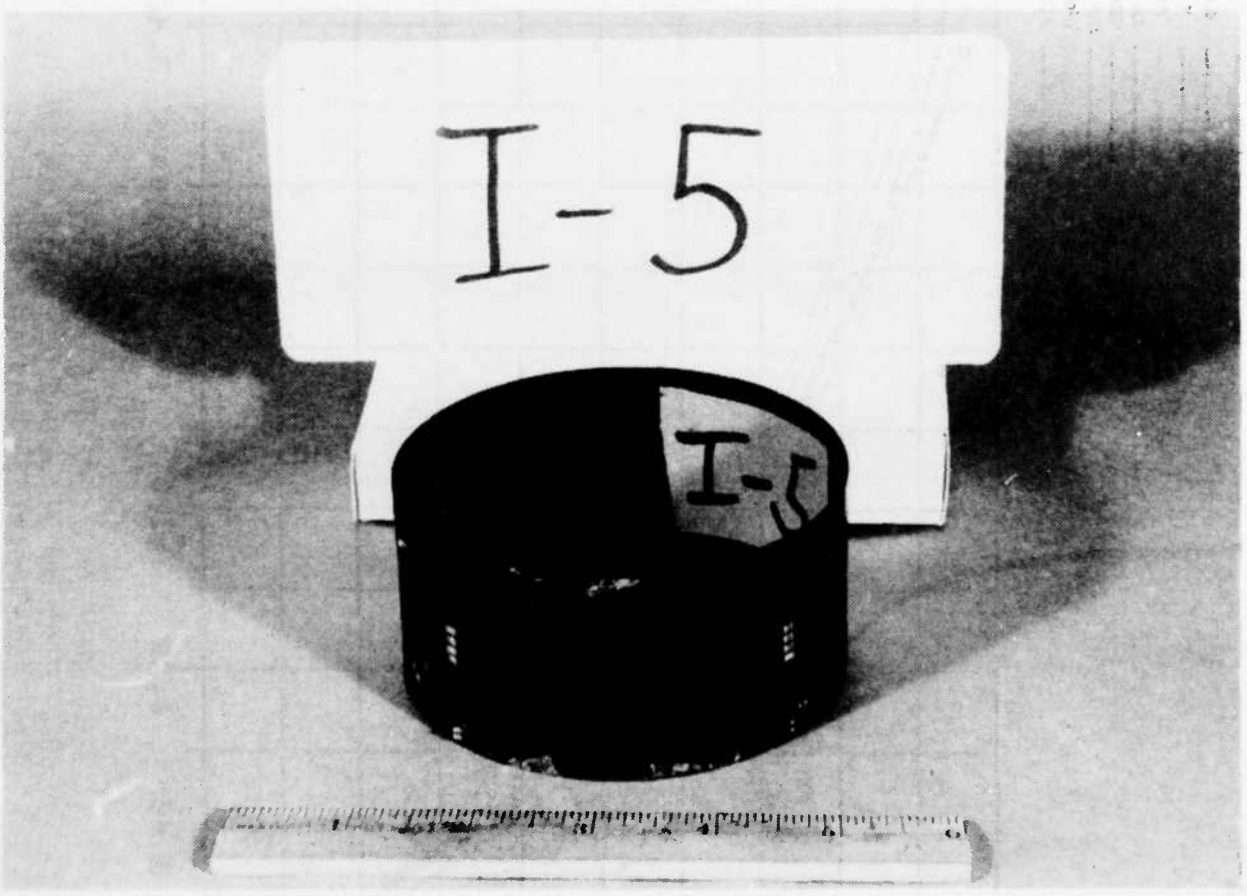

Figure 49 Photograph of Specimen No. I-5 After Testing

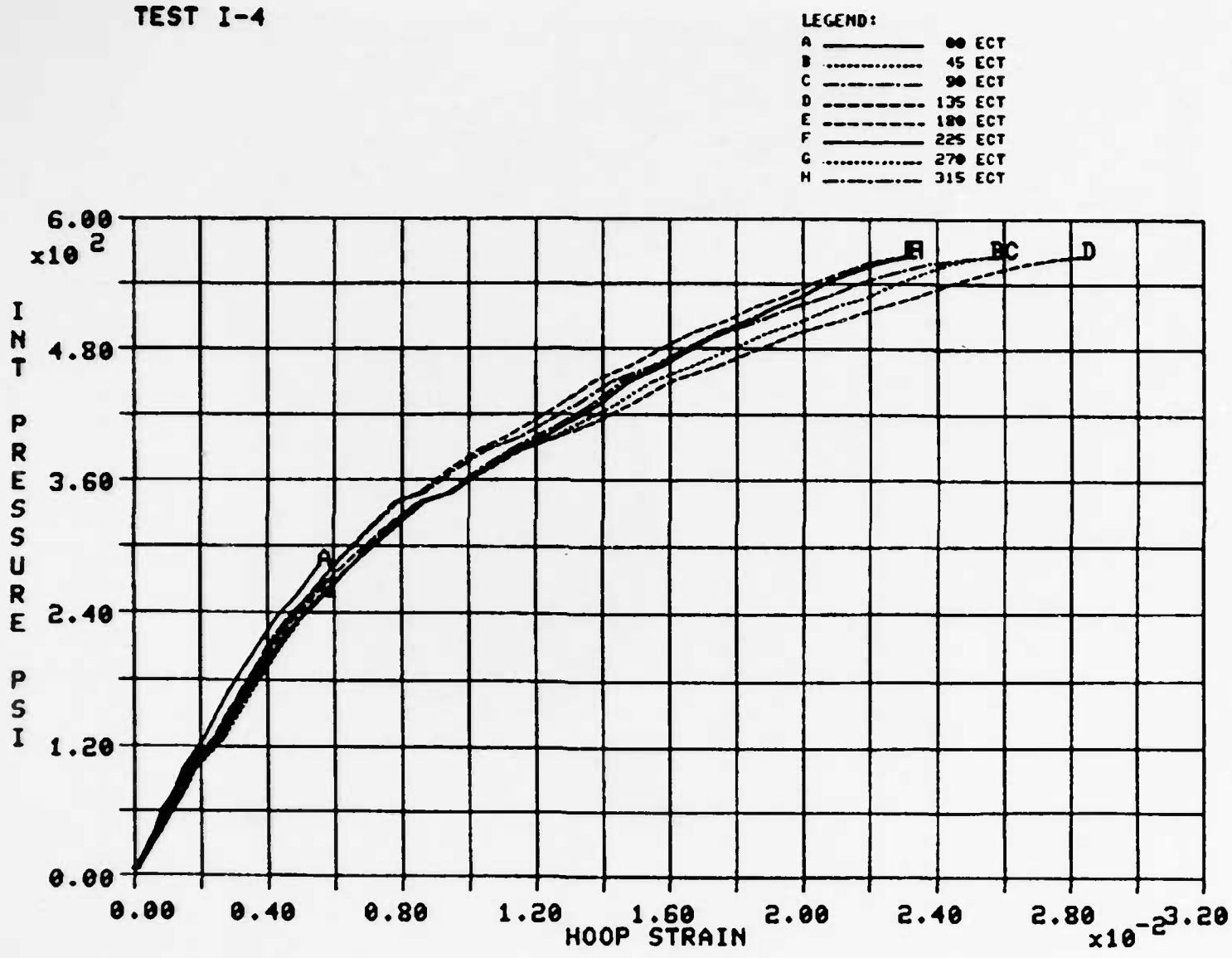

Figure 50 Plot of Internal Pressure vs. Hoop Strain at Mid-length Around the Circumference of Test No. I-4

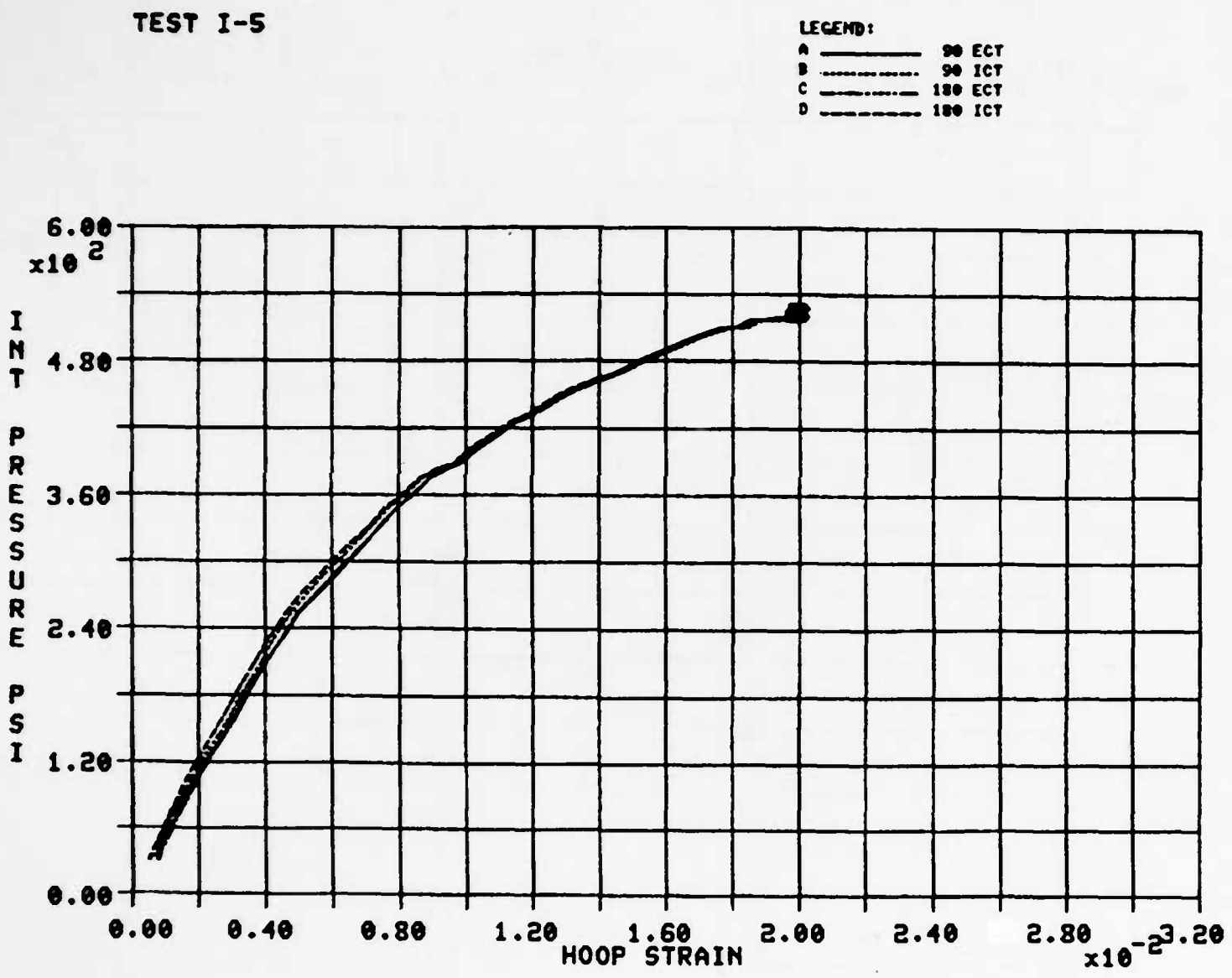

Figure 51 Plot of Internal Pressure vs. Hoop Strain at Mid-length Around the Circumference of Test No. I-5

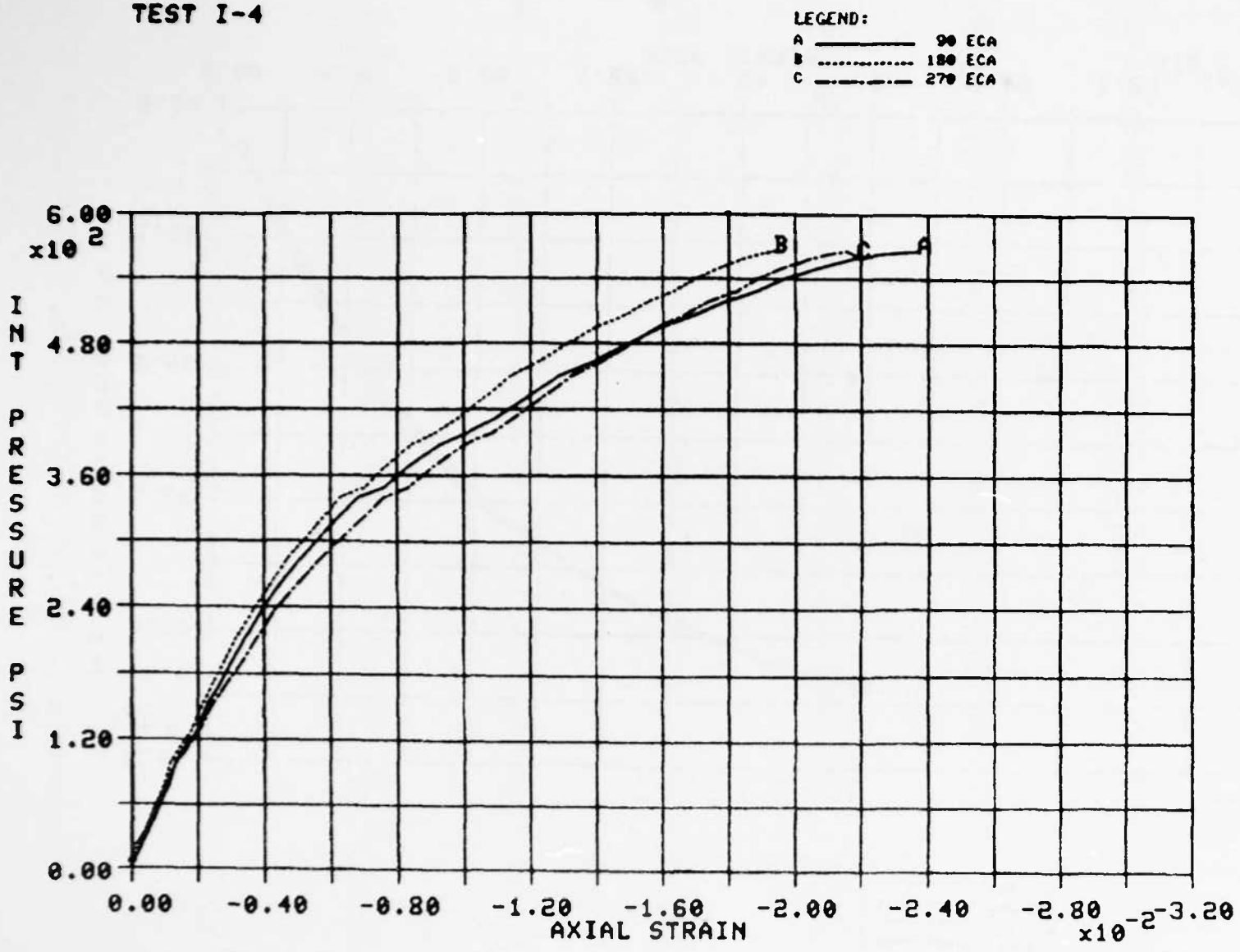

Figure 52 Plot of Internal Pressure vs. Axial Strain at Mid-length Around the Circumference of Test No. I-4

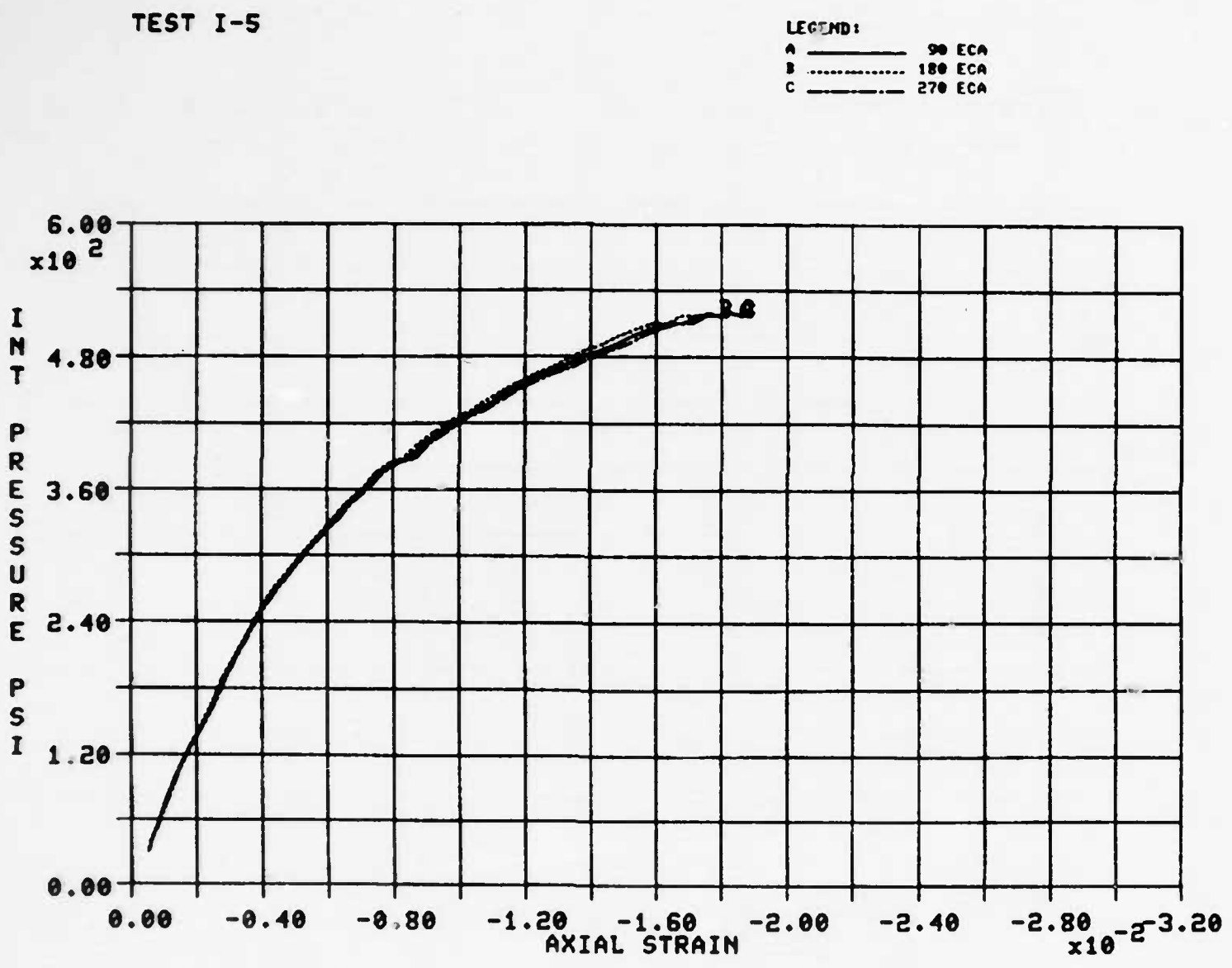

Figure 53 Plot of Internal Pressure vs. Axial Strain at Mid-length Around the Circumference of Test No. I-5

AD-A134 845 EVALUATION OF A BIAXIAL TEST FIXTURE(U) ANAMET LABS INC 2/2
SAN CARLOS CA APPLIED MECHANICS DIV J A HOLST JAN 83
ANAMET-1082.1A AFWAL-TR-82-3109 F33615-81-C-3201
UNCLASSIFIED F/G 11/4 NL

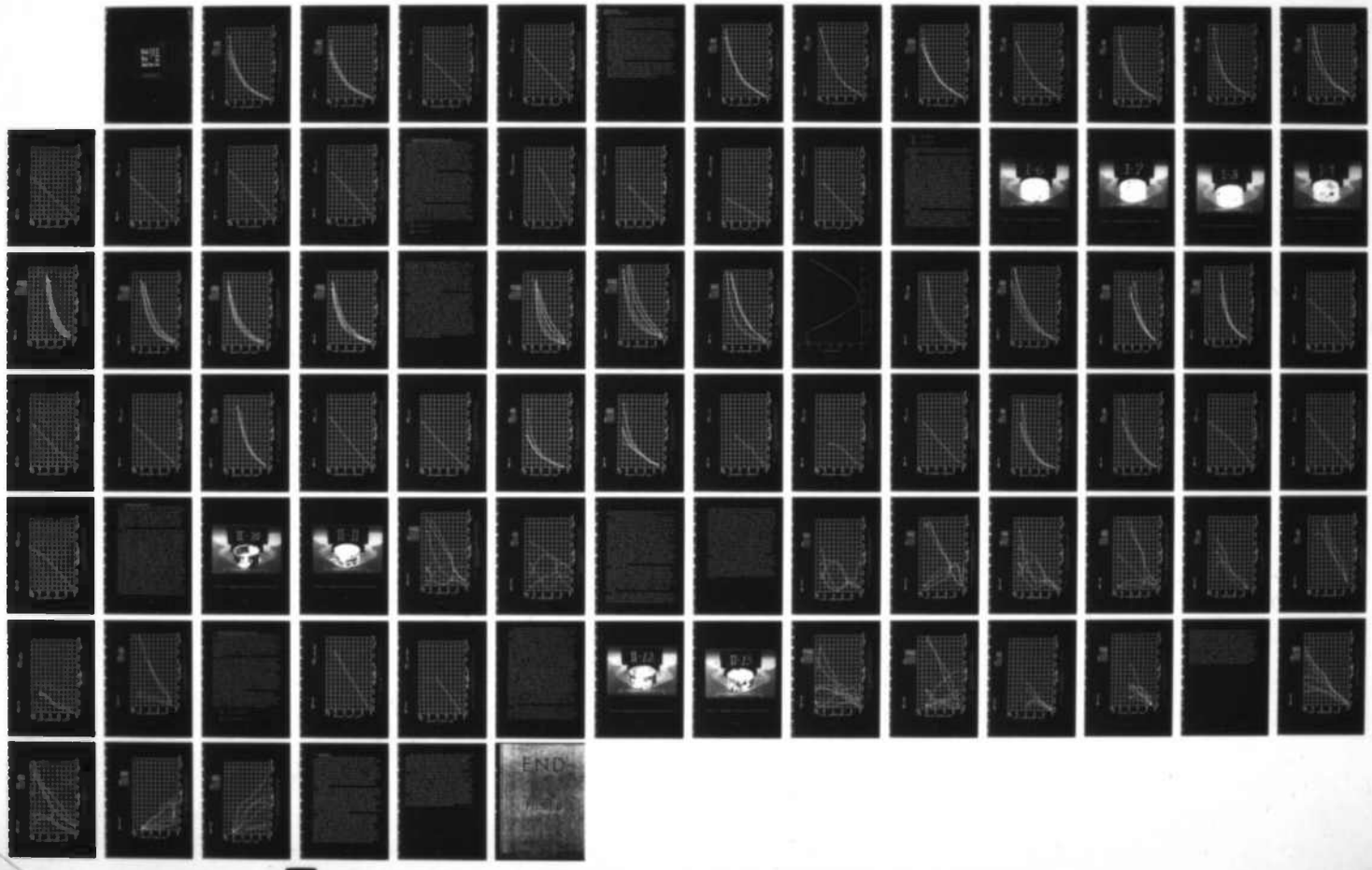

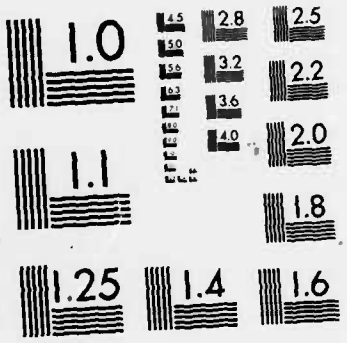

MICROCOPY RESOLUTION TEST CHART
NATIONAL BUREAU OF STANDARDS-1963-A

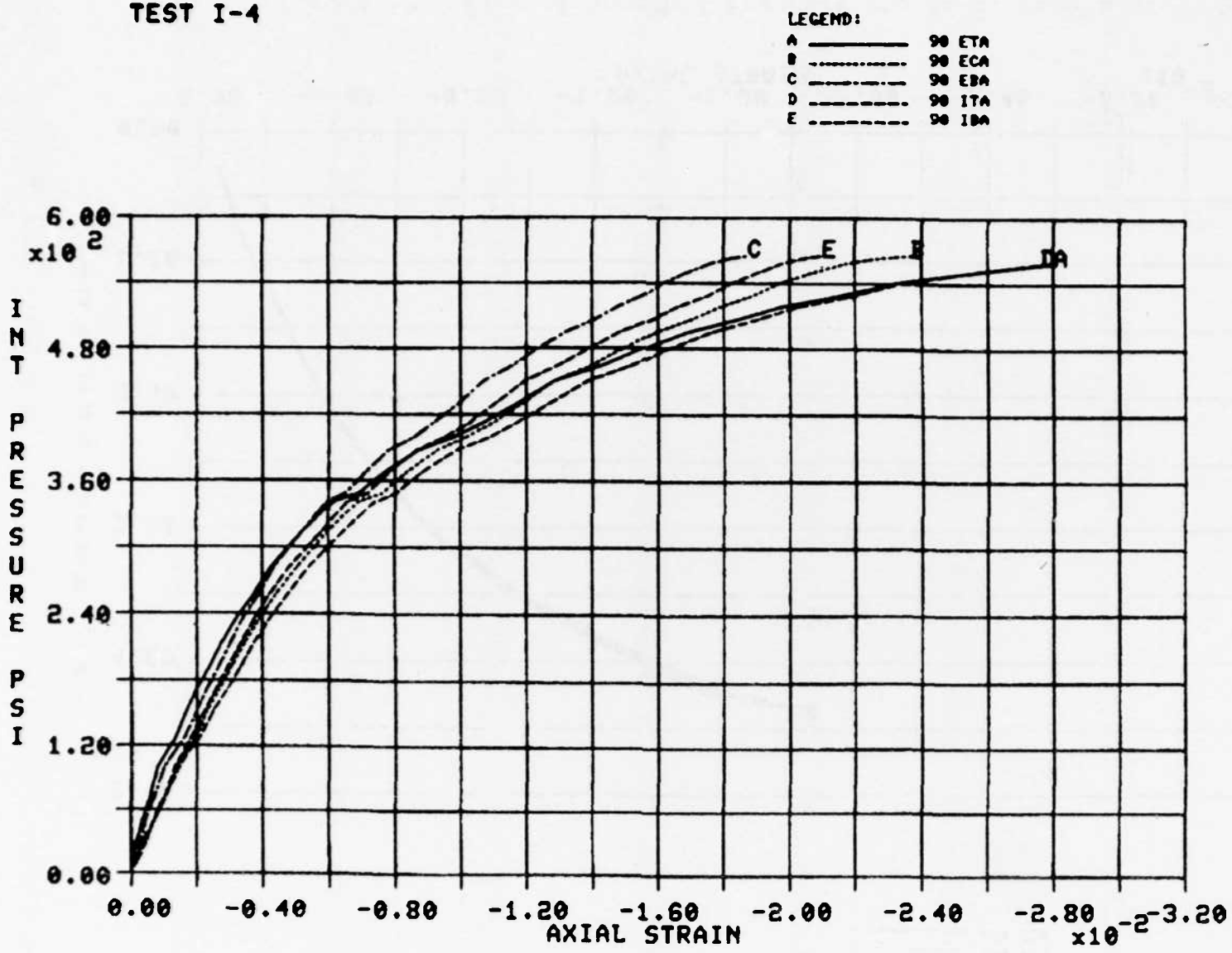

Figure 54 Plot of Internal Pressure vs. Axial Strain at the 90° Location for Test No. I-4

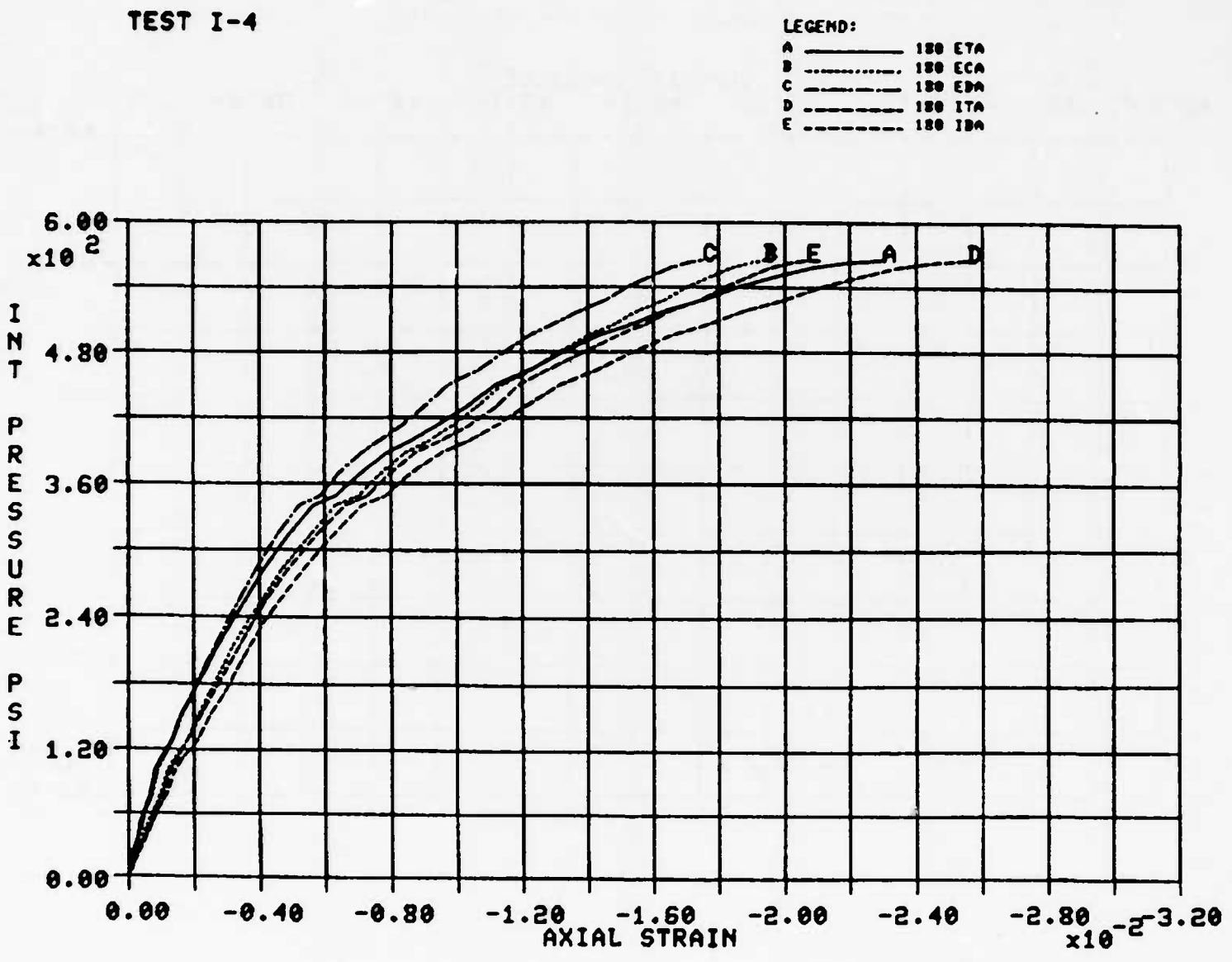

Figure 55 Plot of Internal Pressure vs. Axial Strain at the 180° Location for Test No. I-4

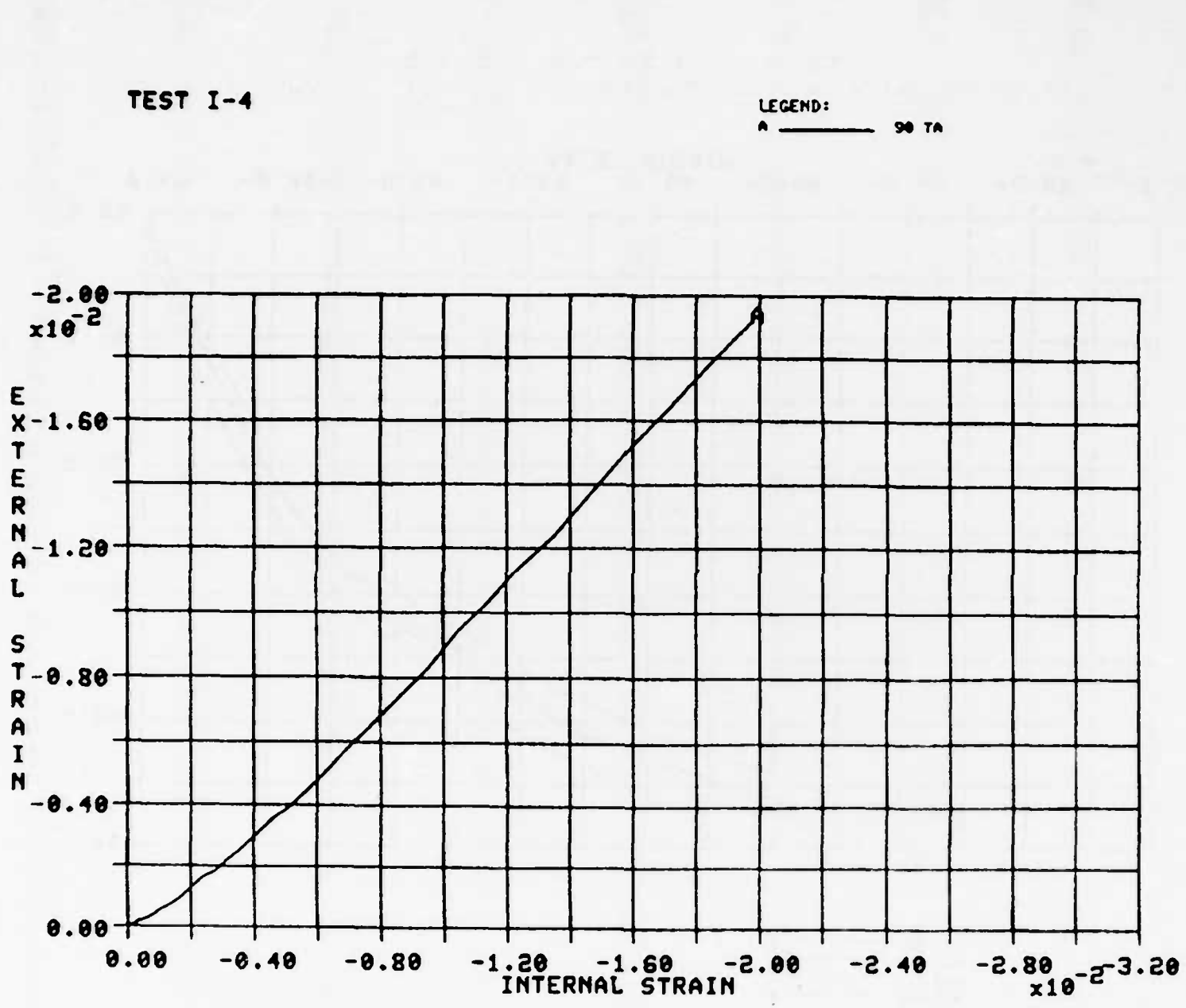

Figure 56 Plot of External vs. Internal Axial Strain at the 90° Location Near the Top Edge of Test No. I-4

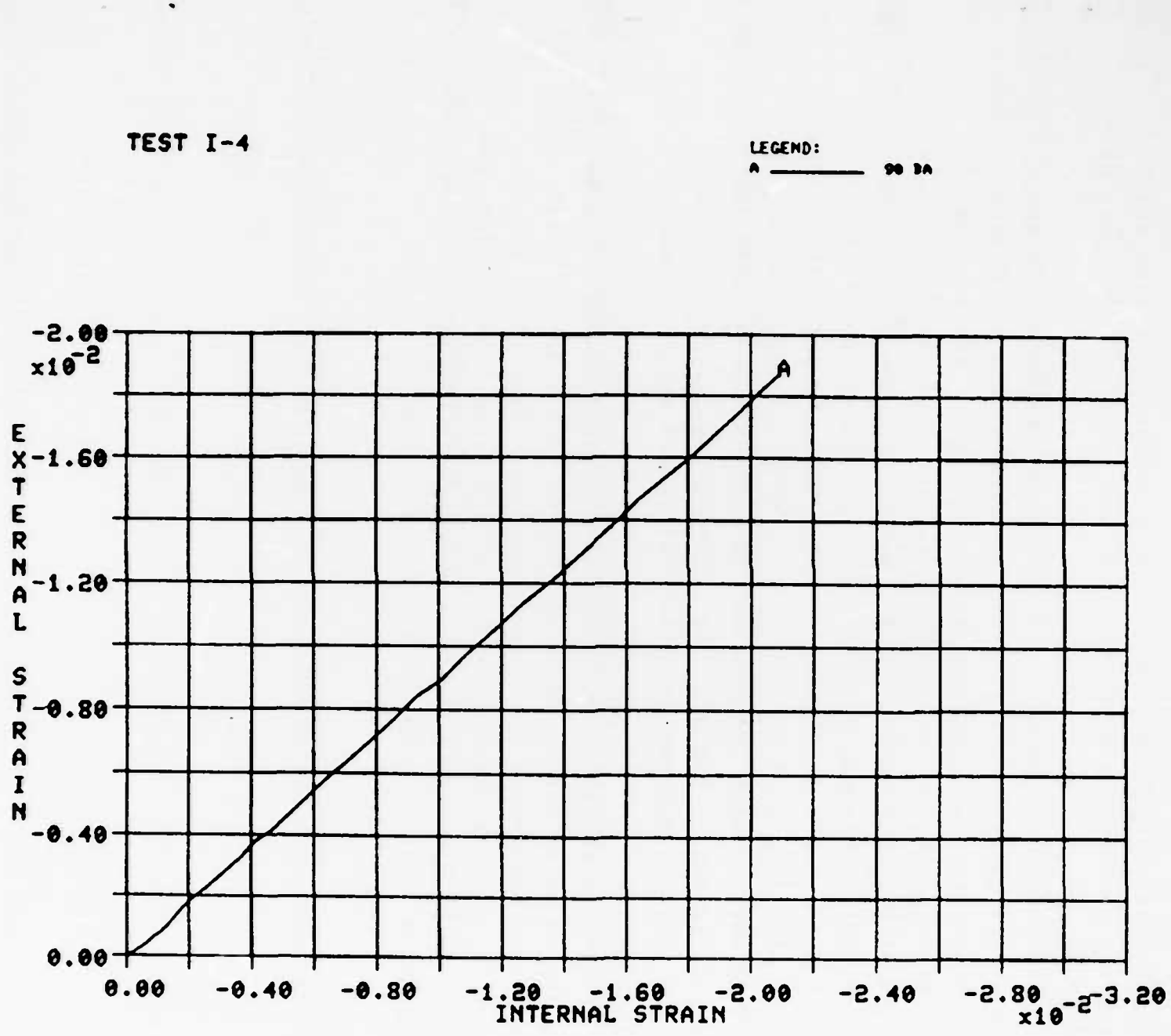

Figure 57 Plot of External vs. Internal Axial Strain at the 90° Location Near the Bottom Edge of Test No. I-4

unity, indicating a small amount of bending. Figures 58 through 61 are plots of internal pressure vs. hoop strain. These plots do not indicate any barreling of the specimen. Barreling would be evident from higher hoop strain at the center of the specimen than at the ends.

Figures 62 through 64 are plots of internal pressure vs. axial strain and internal pressure vs. hoop strain for Test No. I-5. These plots show higher strain readings at the specimen ends than through the center or mid-length. This would indicate hourglassing of the specimen under load. This can also be seen when comparing internal and external axial strain readings where the external strain is slightly greater than the internal strain. This is also indicated by the plots of external vs. internal strain where the slope is greater than unity. These plots are shown in Figures 65 and 66. The effect of hourglassing could explain why the specimen could not retain hydraulic pressure during testing.

With uniaxial loading, the Poisson's ratio can be measured by plotting axial strain vs. hoop strain. The slope of these plots are a measure of the Poisson's ratio. Figures 67 and 68 are plots of axial strain vs. hoop strain. For Test No. I-4, the ratio starts at 0.84 and increases slightly to 0.95. Test I-5 starts at a ratio of 0.78 and increases to 1.04.

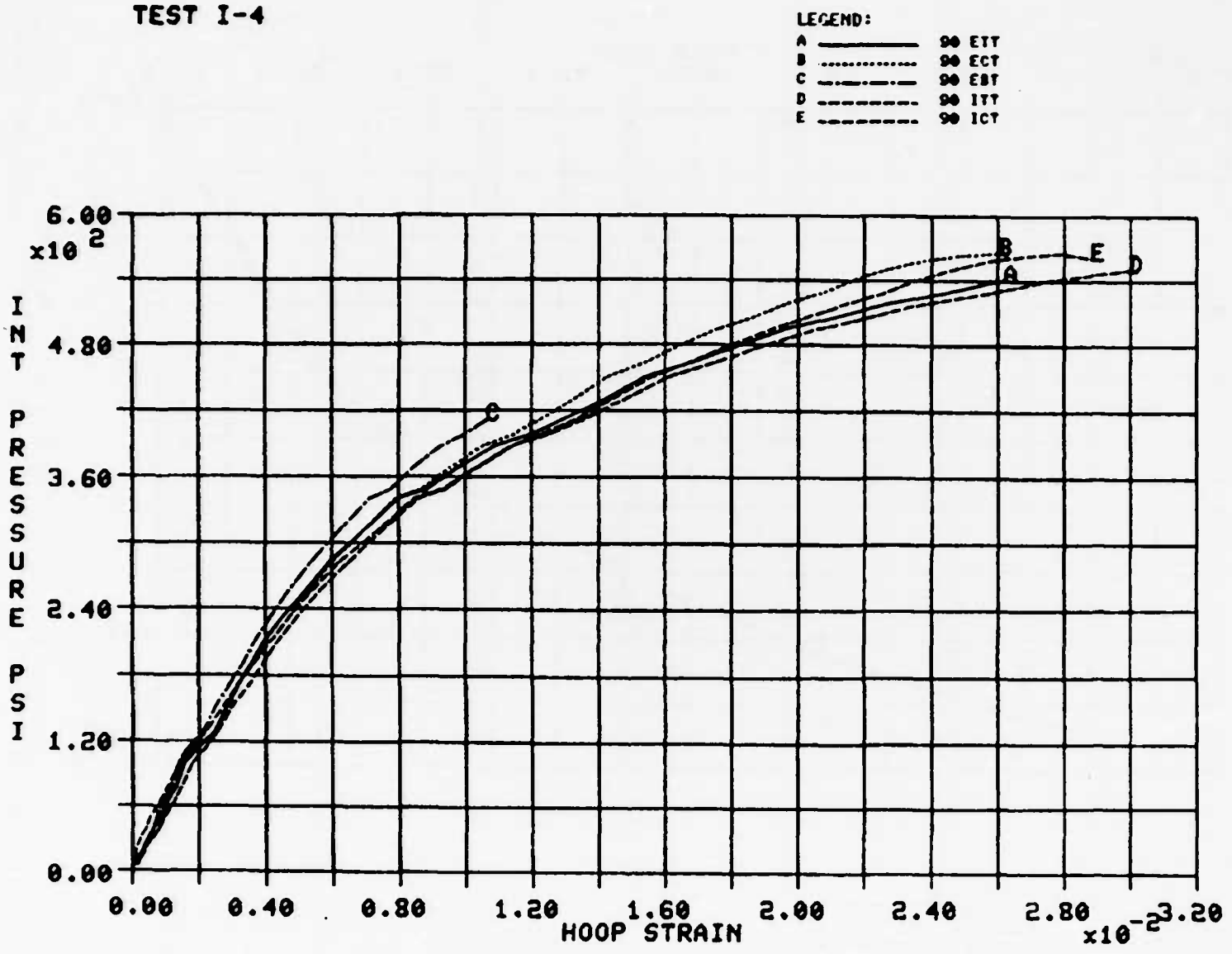

Figure 58 Plot of Internal Pressure vs. Hoop Strain at the 90° Location for Test No. I-4

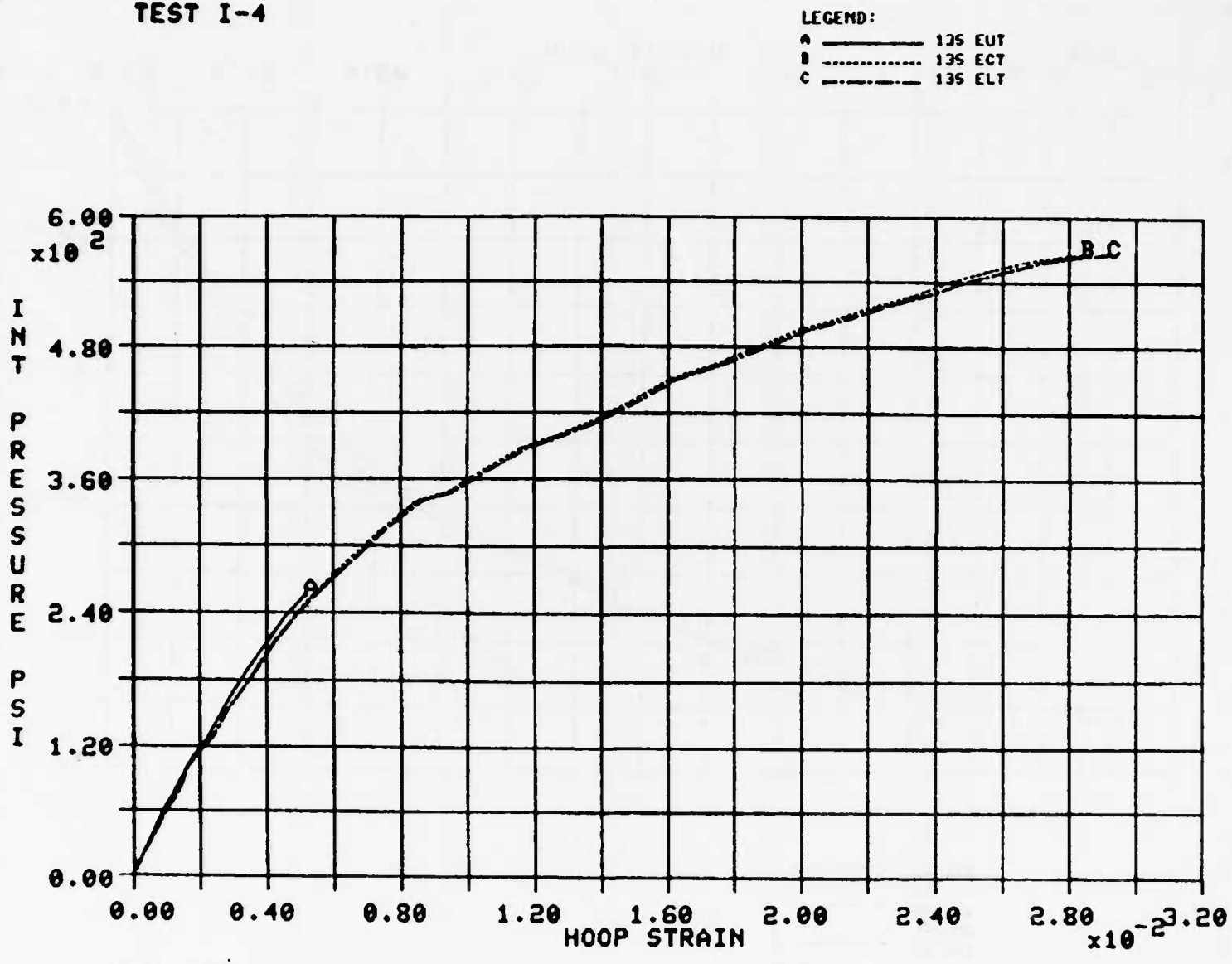

Figure 59 Plot of Internal Pressure vs. Hoop Strain at the 135° location for Test No. I-4

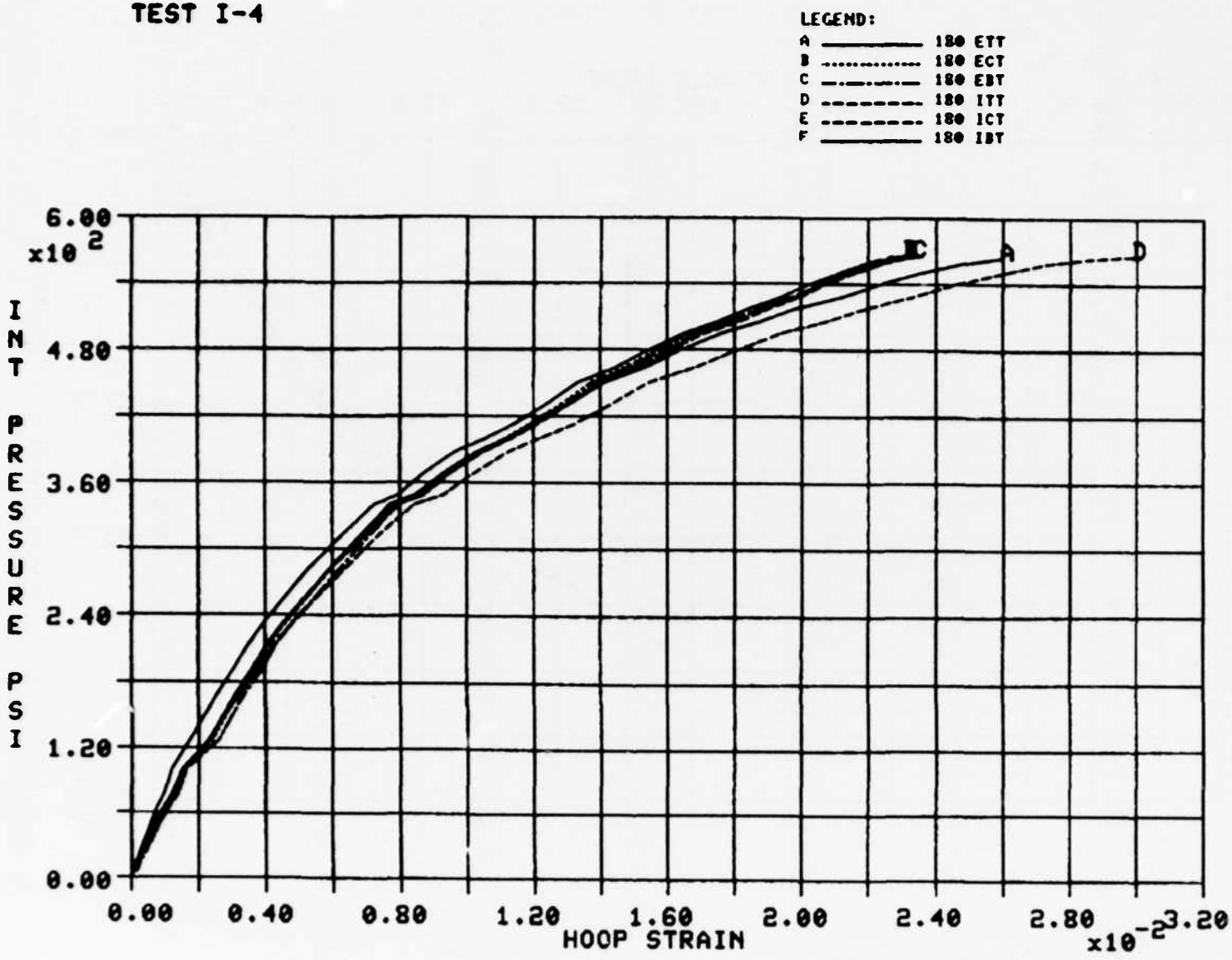

Figure 60 Plot of Internal Pressure vs. Hoop Strain at the 180° Location for Test No. I-4

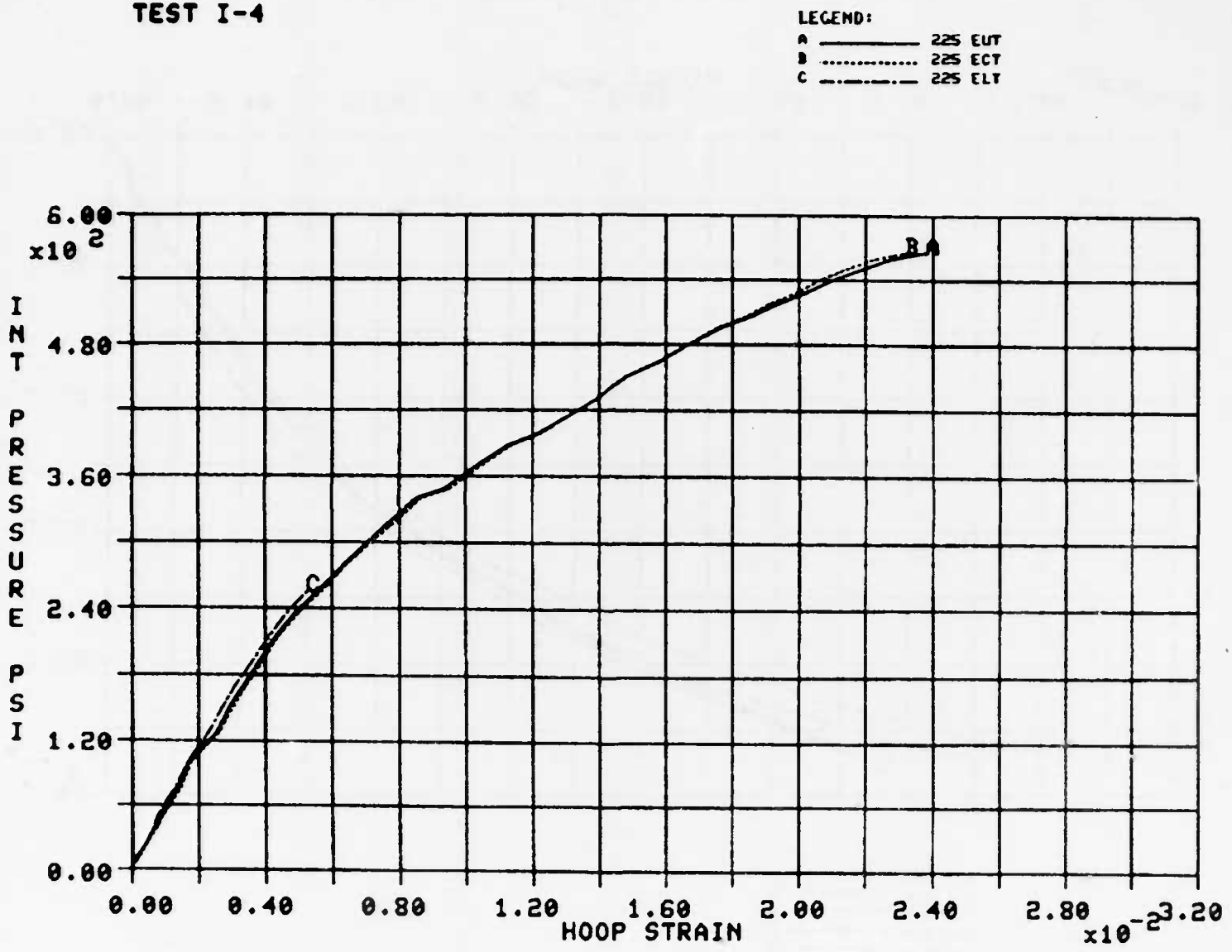

Figure 61 Plot of Internal Pressure vs. Hoop Strain at the 225° Location for Test No. I-4

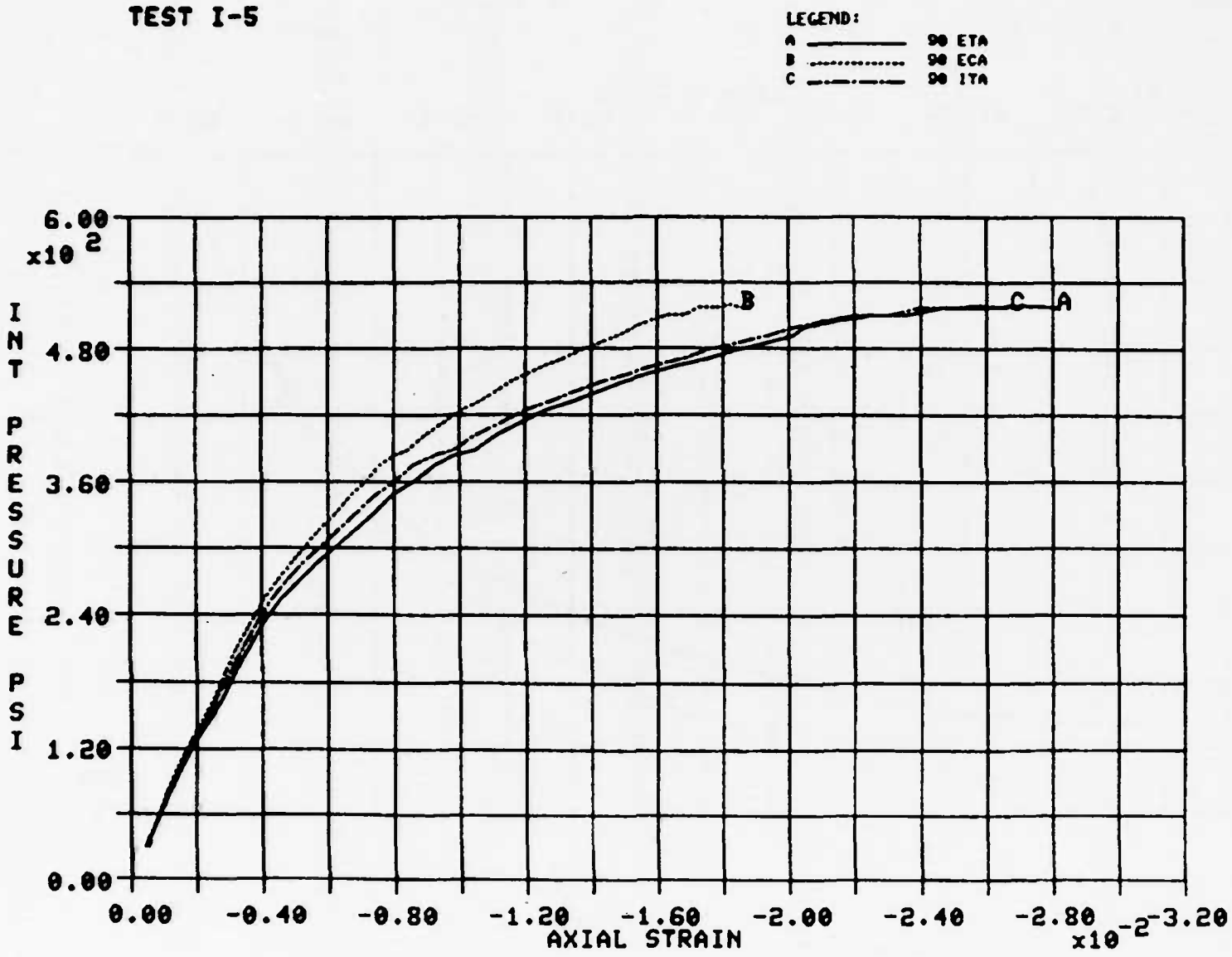

Figure 62 Plot of Internal Pressure vs. Axial Strain at the 90° Location for Test No. I-5

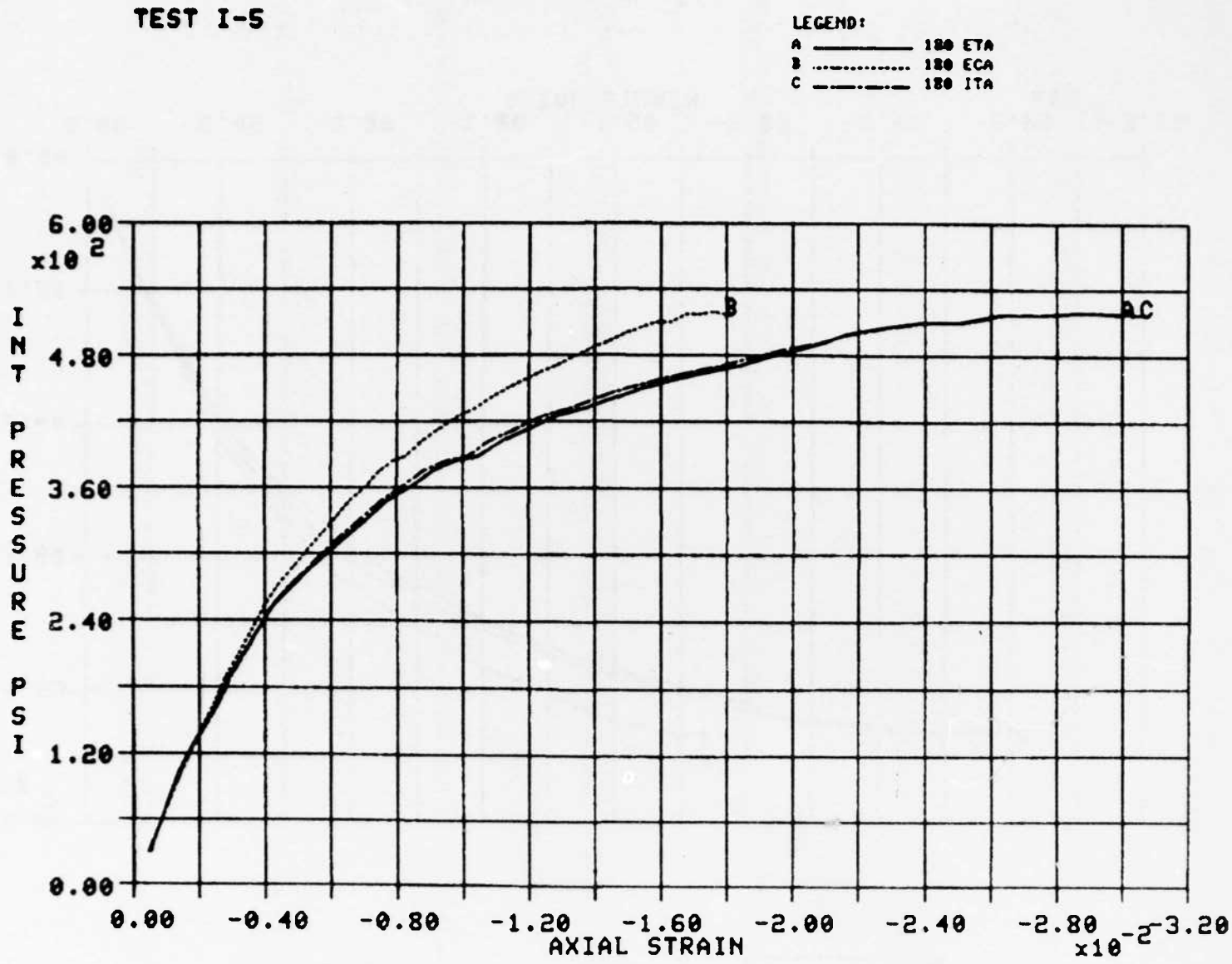

Figure 63 Plot of Internal Pressure vs. Axial Strain at the 180° Location for Test No. I-5

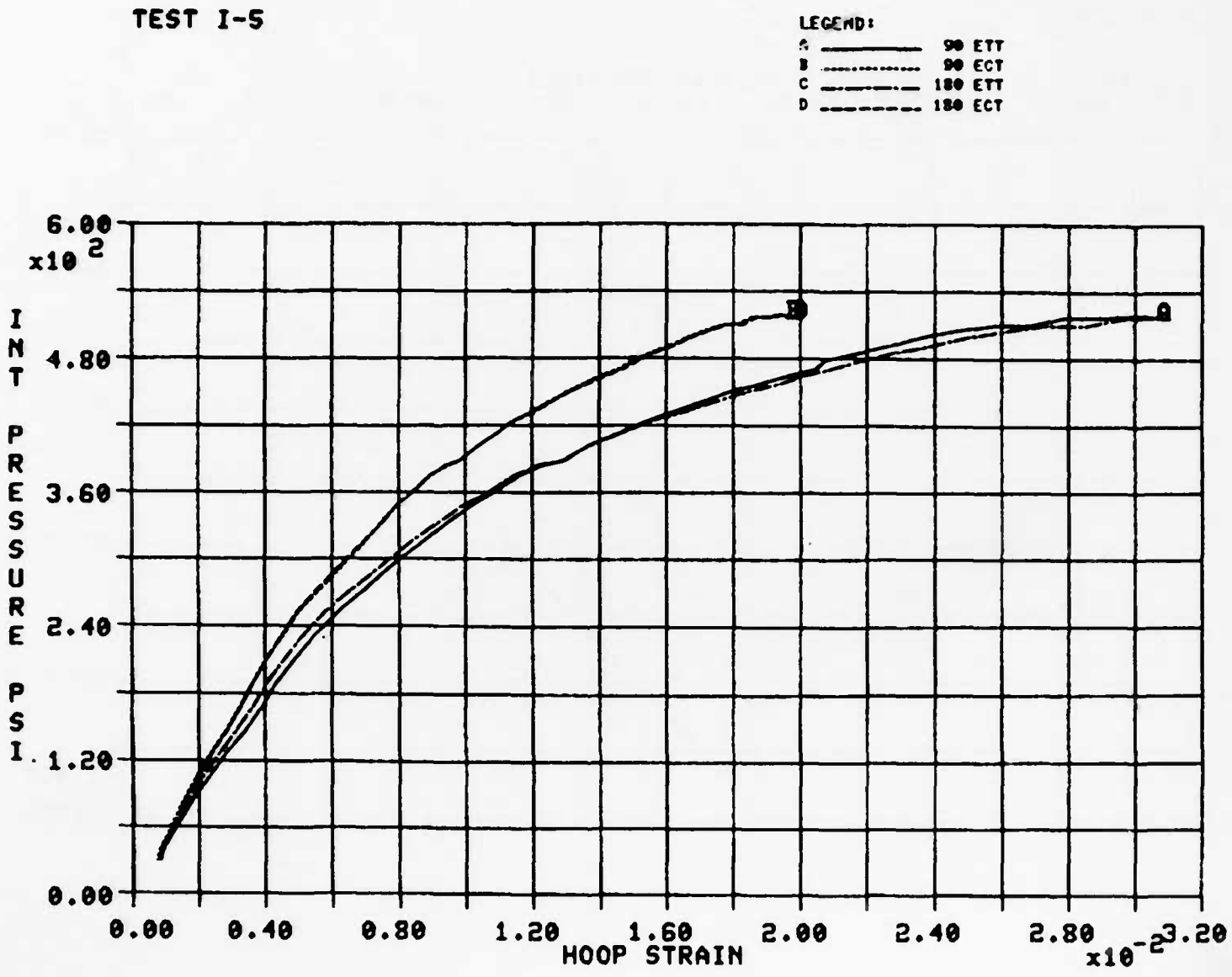

Figure 64 Plot of Internal Pressure vs. Hoop Strain for Test No. I-5

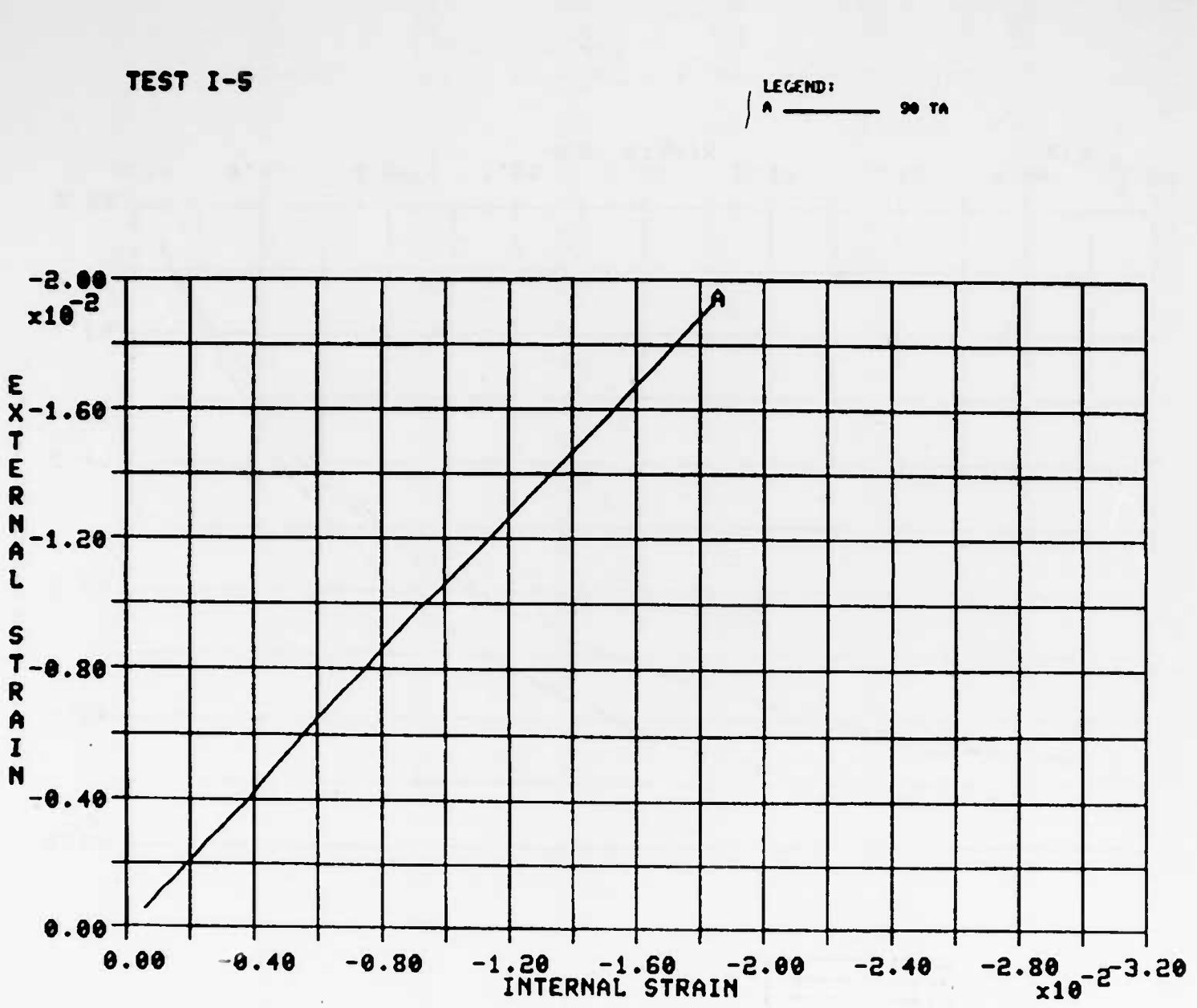

Figure 65 Plot of External vs. Internal Axial Strain at the 90° Location Near the Top Edge of Test No. I-5

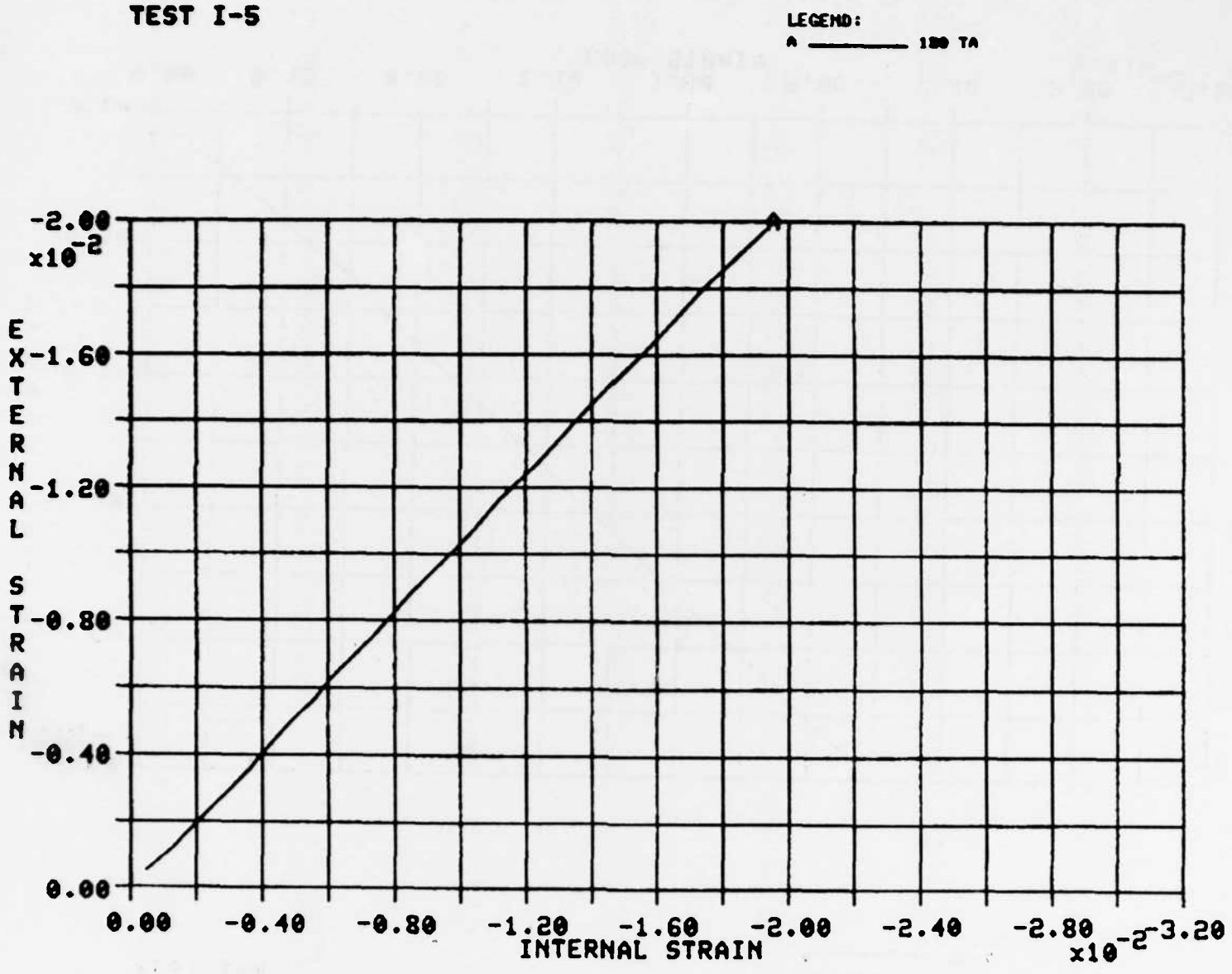

Figure 66 Plot of External vs. Internal Axial Strain at the 180° Location Near the Top Edge of Test No. I-5

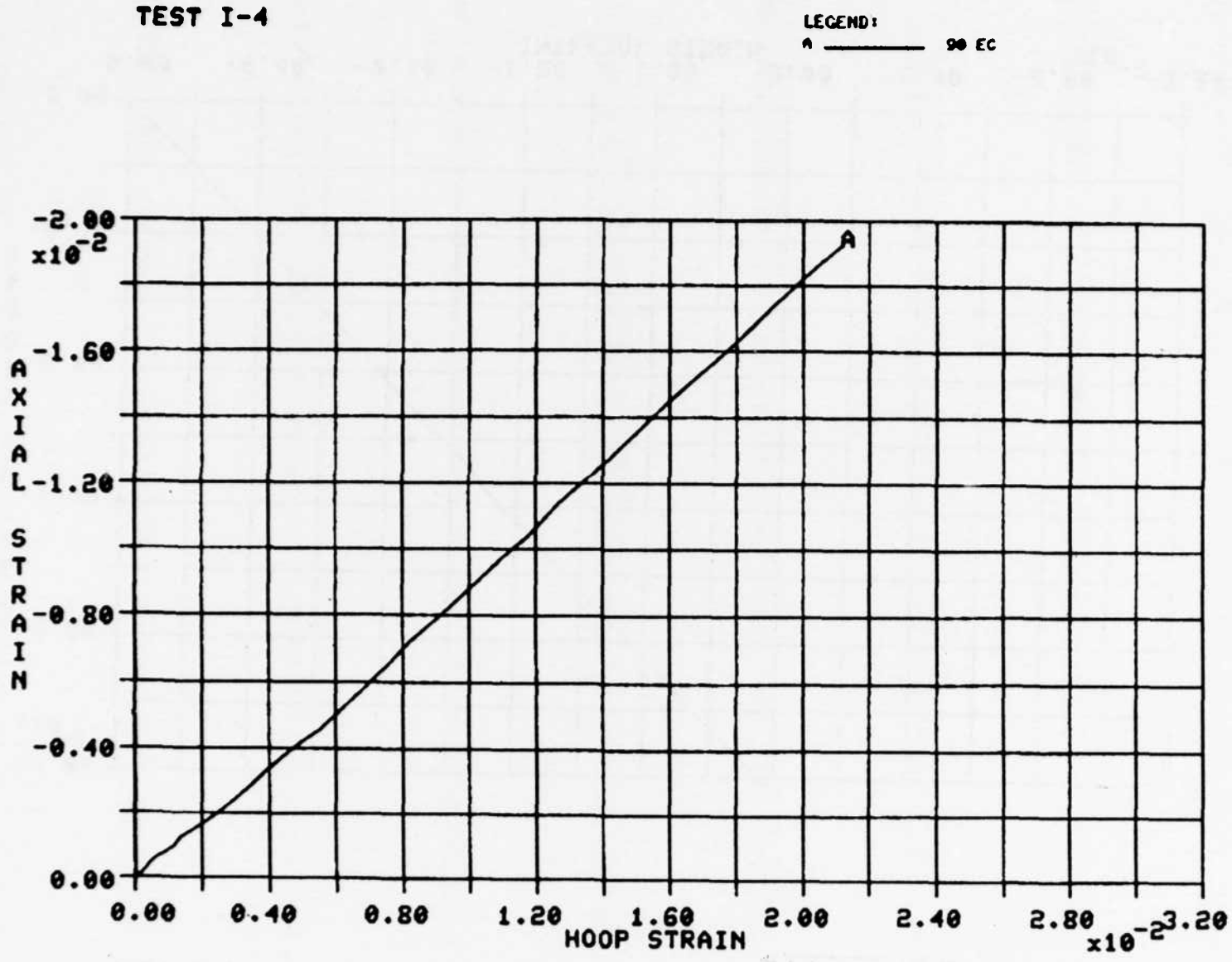

Figure 67 Plot of Axial vs. Hoop Strain at the 90° Location Near the Center or Mid-length of Test No. I-4

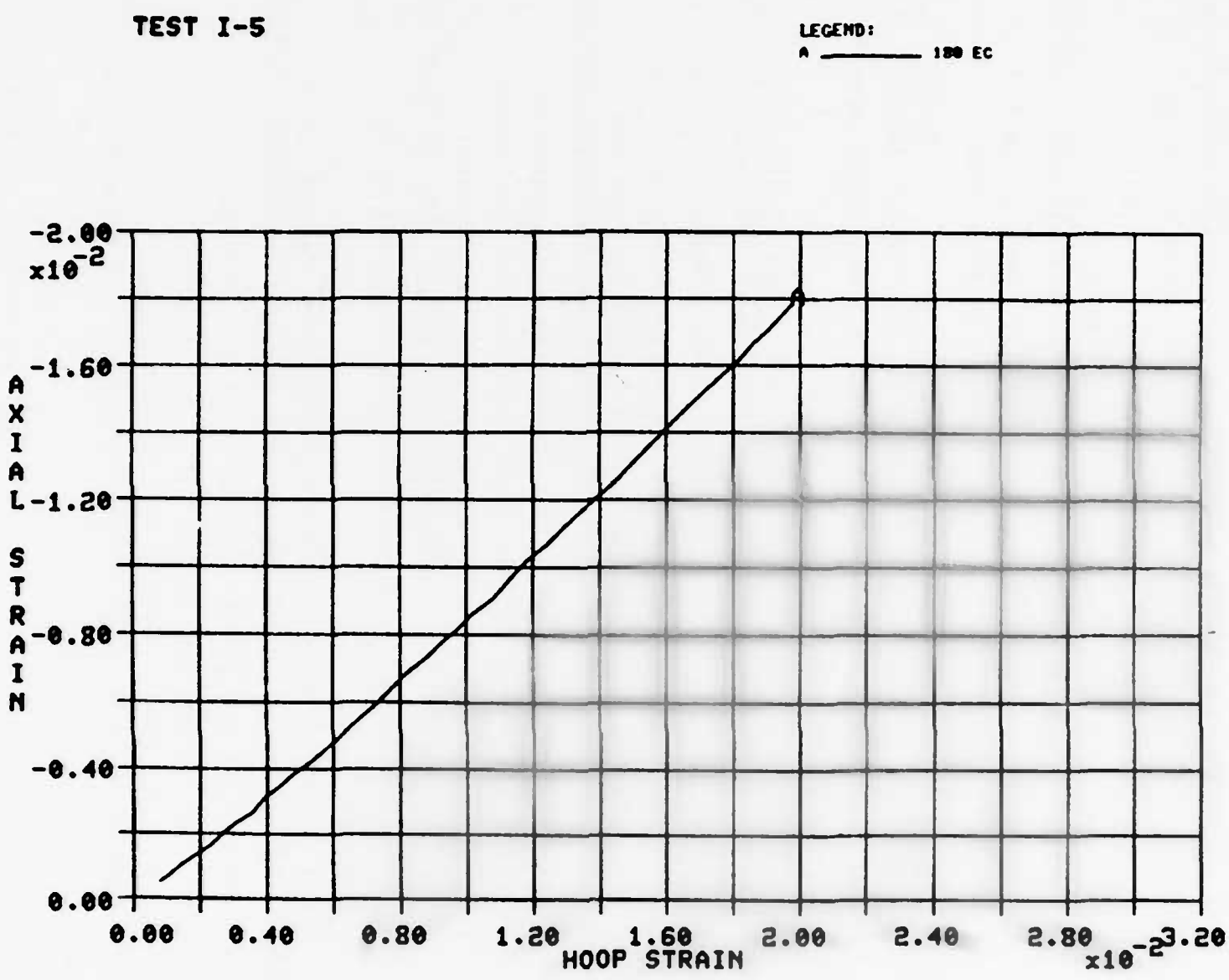

Figure 68 Plot of Axial vs. Hoop Strain at the 180° Location Near the Center or Mid-length of Test No. I-5

VII. INTERNAL PRESSURE PLUS AXIAL LOAD TESTS

A total of four instrumented specimens were tested with combinations of internal pressure and axial loads. The specimens were loaded with different ratios of internal pressure and axial load to produce various biaxial stress conditions. These were Test Nos. I-6, I-7, I-8 and I-9. All four specimens were 2 inches in length. Specimen Nos. I-6, I-7 and I-8 were instrumented with forty strain gage elements. The gages were installed using similar gage layouts as listed in Tables 7 and 8. The gages were spaced 45° apart around the circumference of the specimens. Specimen No. I-9 was instrumented with only twelve gage elements using the gage layout listed in Table 9. The gages were at the 90° and 180° locations.

Two special-made molded rubber gaskets were used on the inside surface of the specimens as in previous tests performed with internal pressure only. The lead/polyethelene/lead sandwich gasket lubrication was also used at the two plated surfaces. The axial load and internal pressure signals were both sent to the MTS controller through two variable gain amplifiers. The gain on the amplifiers were adjusted such that the system would produce the correct ratio between axial and hoop stresses plus the force required to overcome the pressure load acting on the internal surface area of the platens. The strain gage, axial load, and pressure data were digitized via the SUN system and sent to the PDP 11/34 computer.

The simultaneous application of internal pressure and axial compressive load produced different biaxial stress conditions. Figures 69 through 72 are plots of axial load vs. internal pressure from the four tests. Using the 0.554 in^2 axial cross-sectional area, 3.92 inch diameter and 0.045 inch wall thickness, the ratio of axial stress (σ_x) vs. hoop stress (σ_θ) is calculated as

$$\frac{-\sigma_x}{\sigma_\theta} = 0.59, \text{ Test I-6}$$

$$\frac{-\sigma_x}{\sigma\theta} = 1.01, \text{ Test I-7}$$

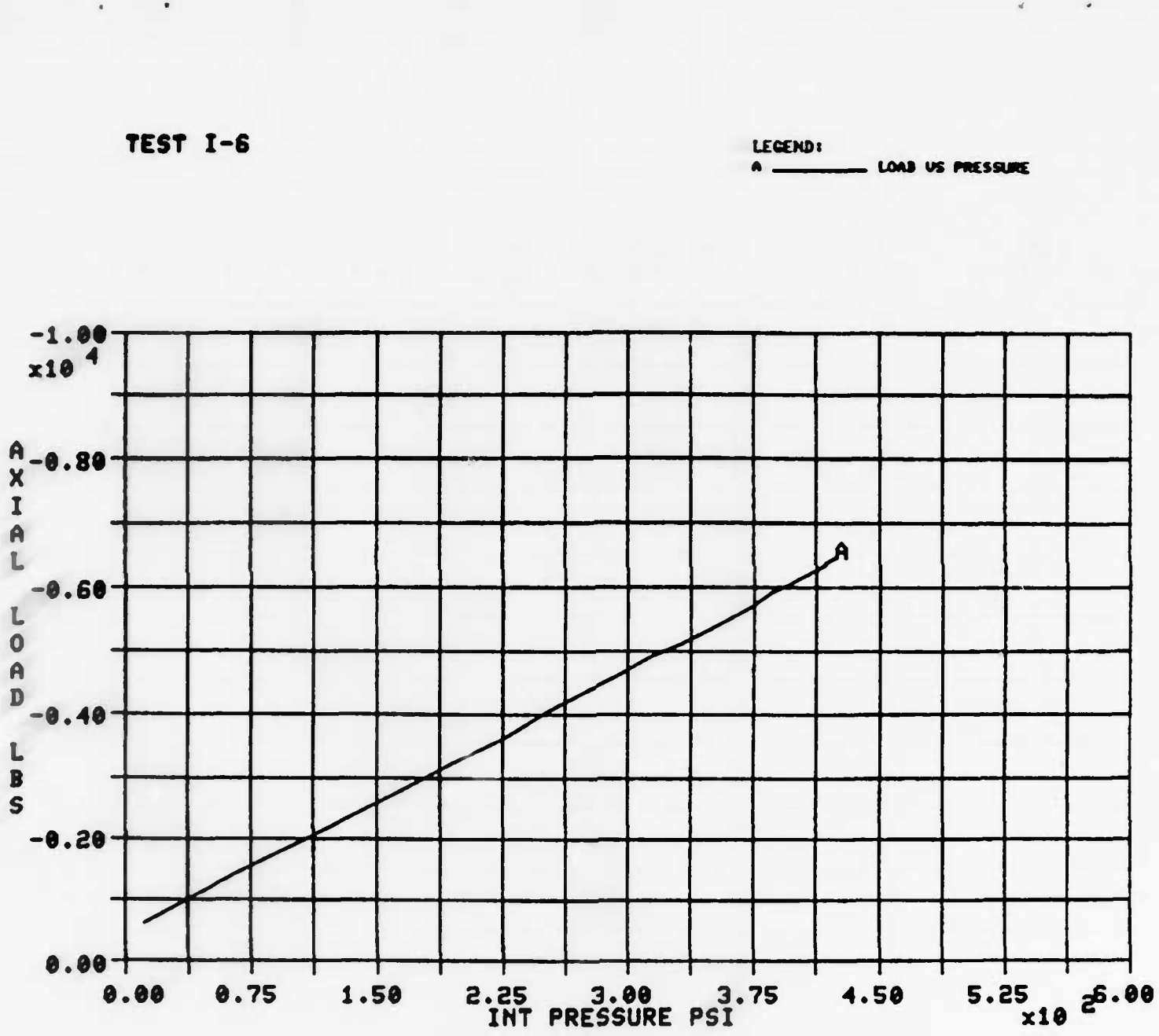

Figure 69 Plot of Axial Load vs. Internal Pressure for Test No. I-6

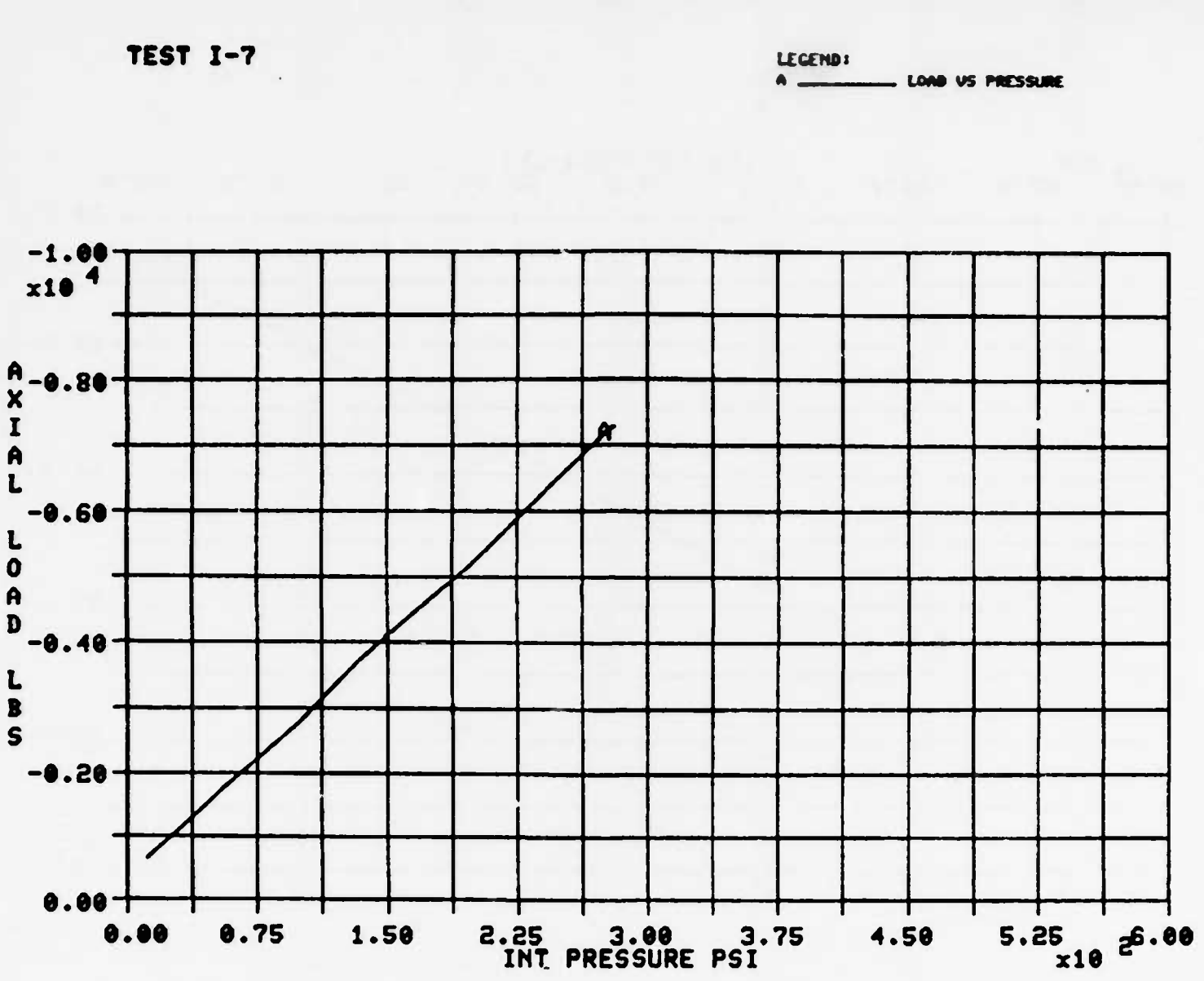

Figure 70 Plot of Axial Load vs. Internal Pressure for Test No. I-7

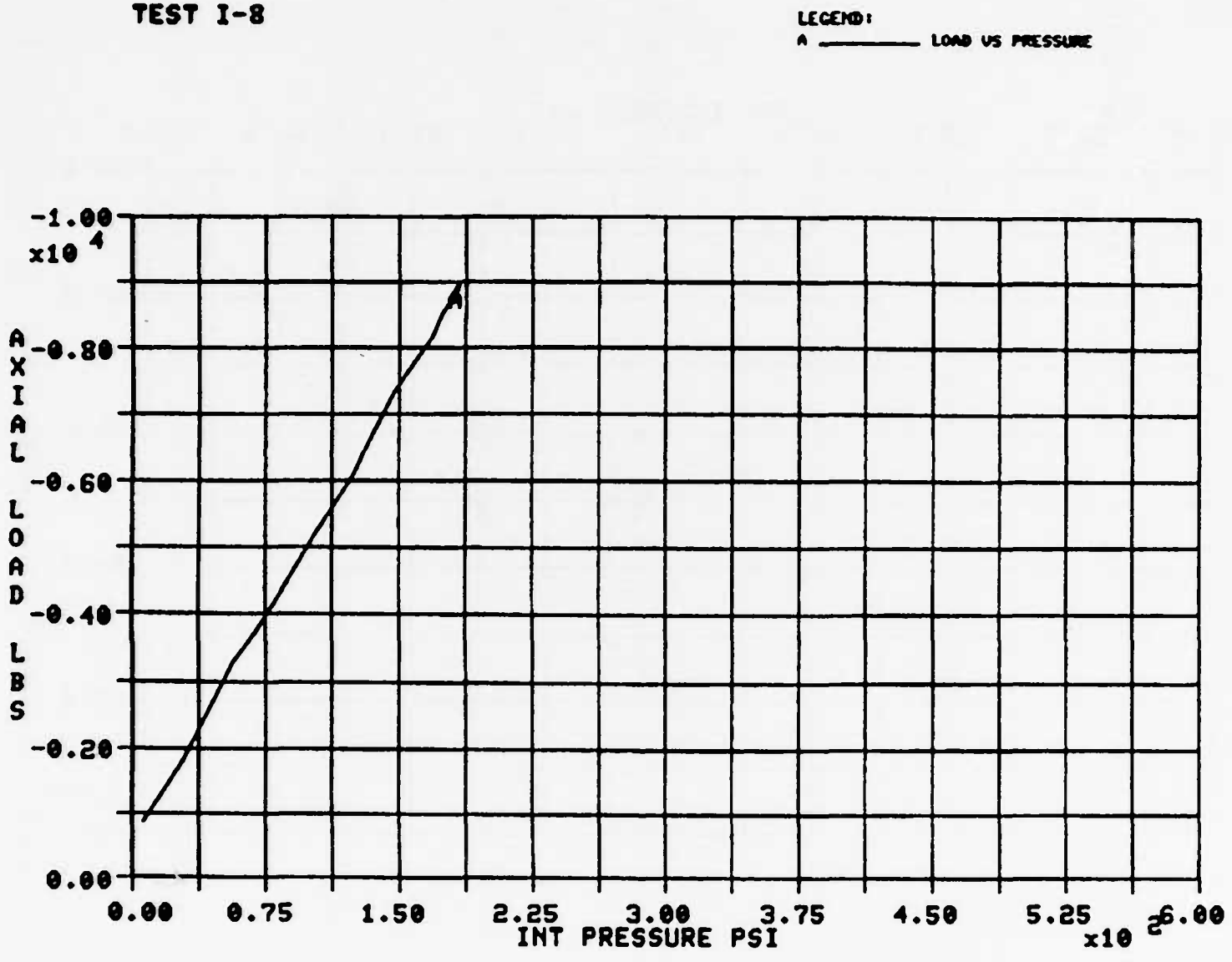

Figure 71 Plot of Axial Load vs. Internal Pressure for Test No. I-8

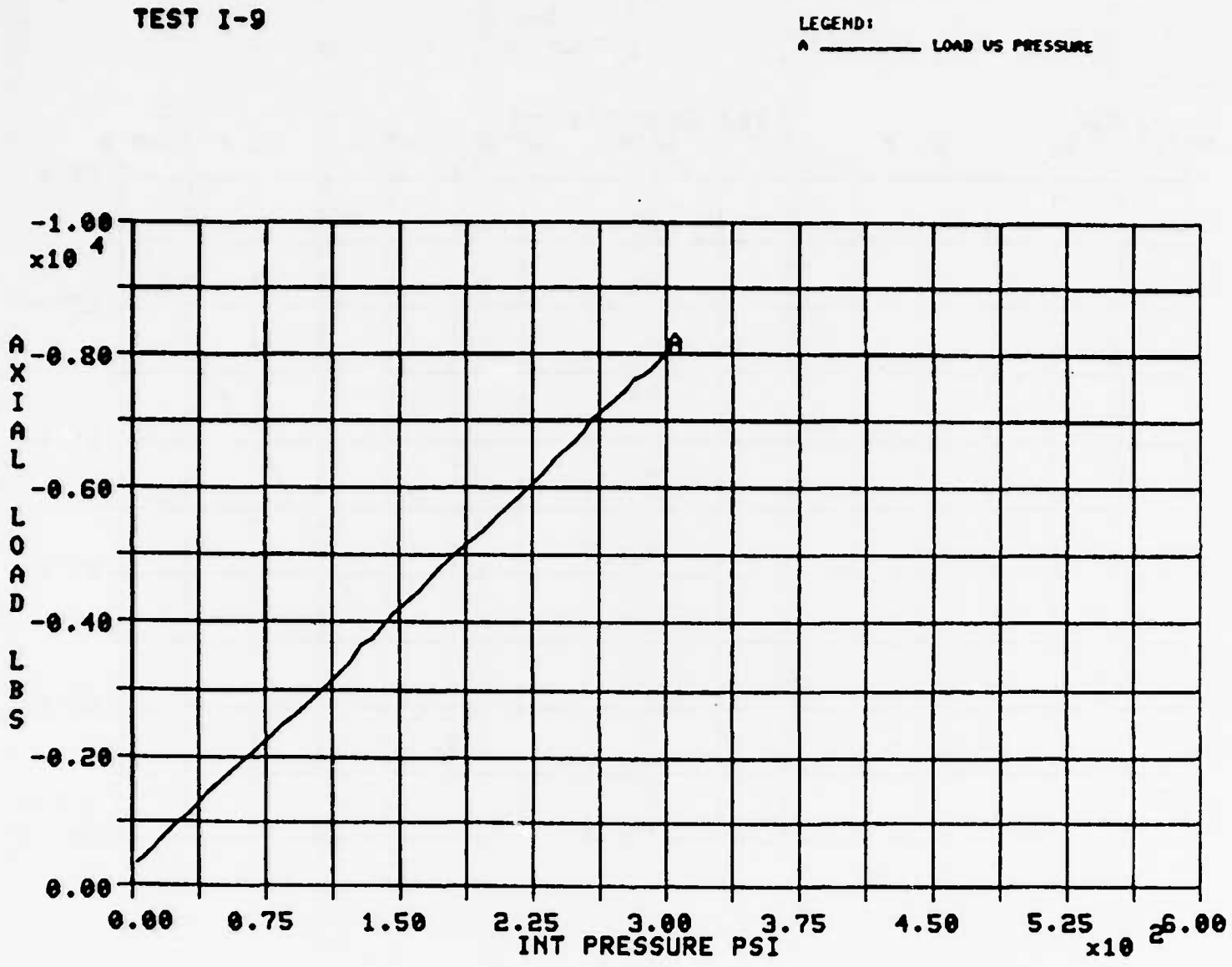

Figure 72 Plot of Axial Load vs. Internal Pressure for Test No. I-9

$$\frac{-\sigma_x}{\sigma_\theta} = 1.86, \text{ Test I-8}$$

$$\frac{-\sigma_x}{\sigma_\theta} = 1.07, \text{ Test I-9}$$

An initial preload of approximately -400 lbs. was also applied to the specimens. This is equivalent to an axial stress level of -0.72 ksi.

Specimen No. I-6 failed with an axial load of -6,563 lbs. at an internal pressure of 424 psi. This corresponds to an axial stress (σ_x) of -11.85 ksi and a hoop stress (σ_θ) of 18.47 ksi. Specimen No. I-7 failed with an axial load of -7,250 lbs. at an internal pressure of 280 psi. This is equivalent to -13.09 ksi axial stress and 12.20 ksi hoop stress. Specimen No. I-8 failed with an axial load of -9,000 lbs. at an internal pressure of 185 psi. The corresponding stresses are -16.25 ksi axial stress and 8.06 ksi hoop stress. Specimen No. I-9 failed with an axial load of -8,000 lbs. at an internal pressure of 300 psi. This is equivalent to an axial stress of -14.44 ksi and a hoop stress of 13.07 ksi. The ultimate failure in all four of the specimens appeared to be the result of the tensile hoop stresses. The specimens fractured along the length of the specimen wall generally parallel with the specimen axis. There was also some buckling in the walls, blooming at the ends, separation between ply layups and splinters in the inside and outside surface fibers as a result of axial loading. In general, the specimens subjected to the higher relative axial loads showed more respective damage. Figures 73 through 76 are photographs of the specimens after testing.

Figures 77 through 80 are plots of axial and pressure loads vs. axial and hoop strain, respectively, for Test Nos. I-6 and I-8. These plots are from the external gages at mid-length around the specimens circumference. Discounting the initial strain, the plots appear to be in good agreement, indicating good load distribution around the specimens circumference. Similar

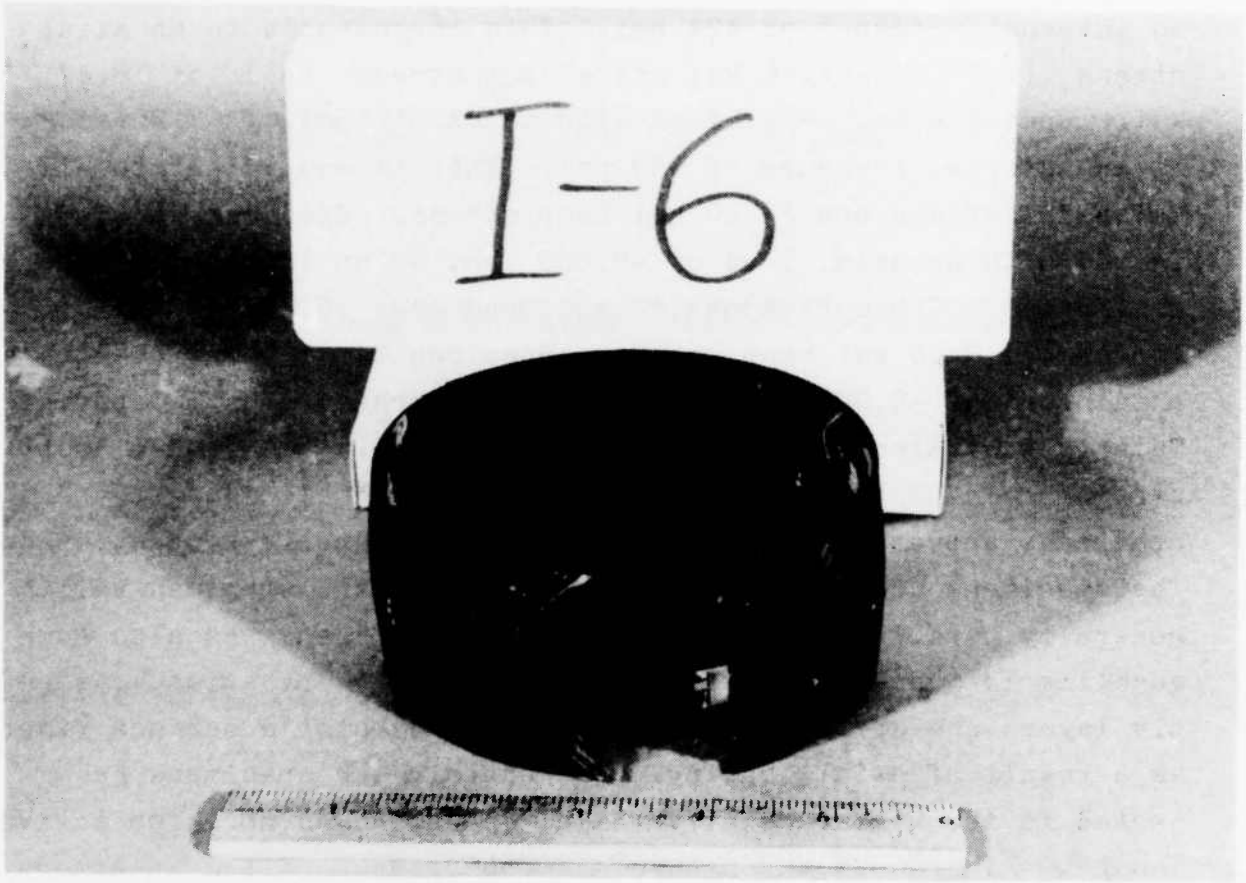

Figure 73 Photograph of Specimen No. I-6 After Testing

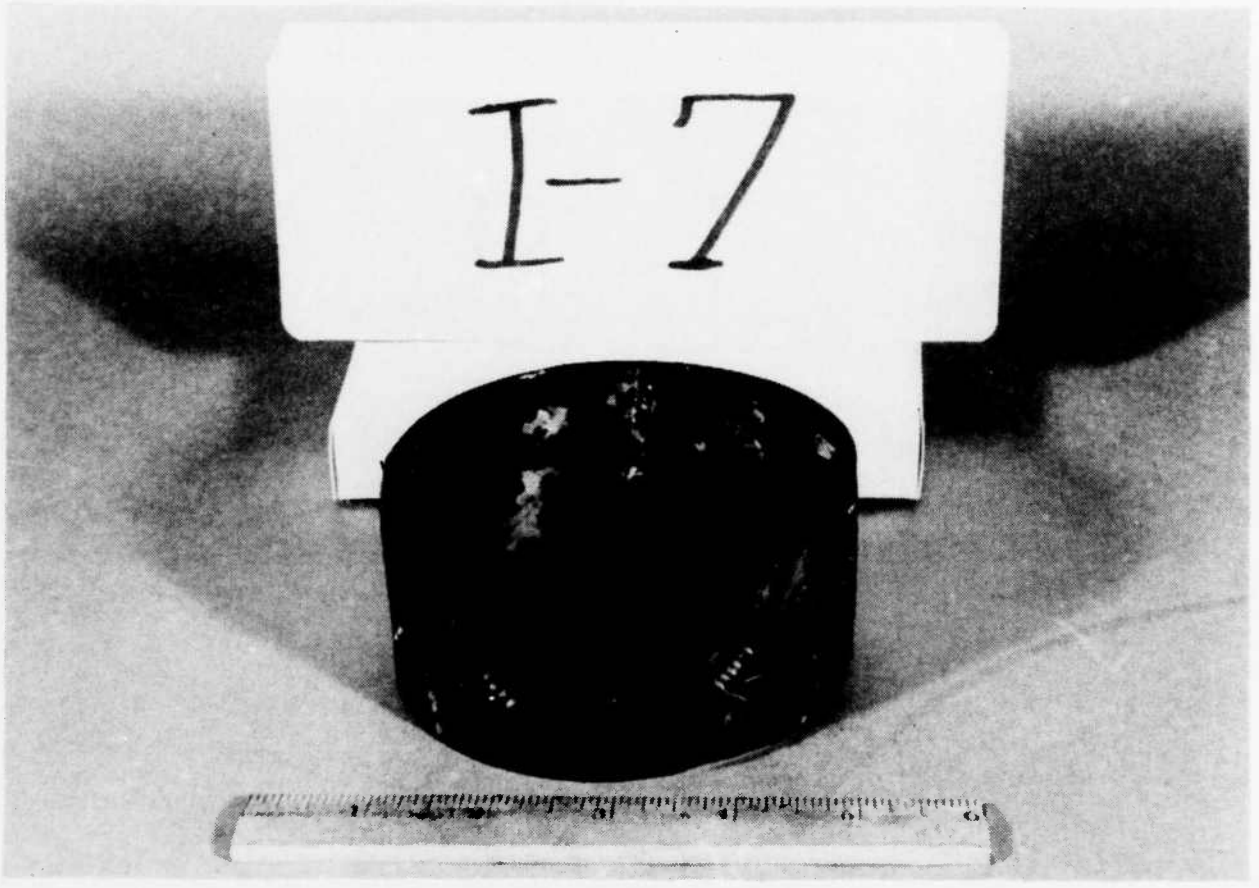

Figure 74 Photograph of Specimen No. I-7 After Testing

Figure 75 Photograph of Specimen No. I-8 After Testing

Figure 76 Photograph of Specimen No. I-9 After Testing

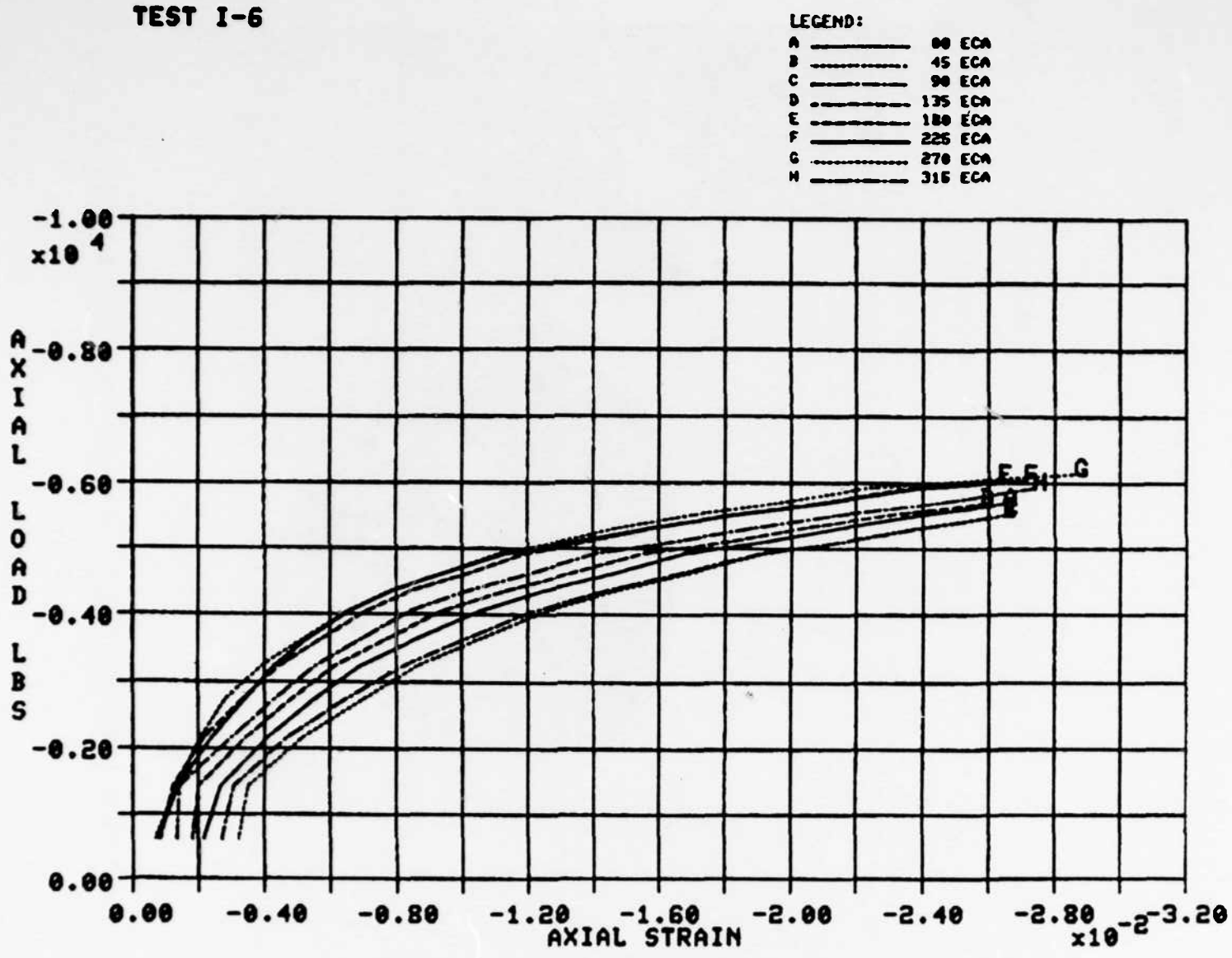

Figure 77 Plot of Axial Load vs. Axial Strain at Mid-length Around the Circumference of Test No. I-6

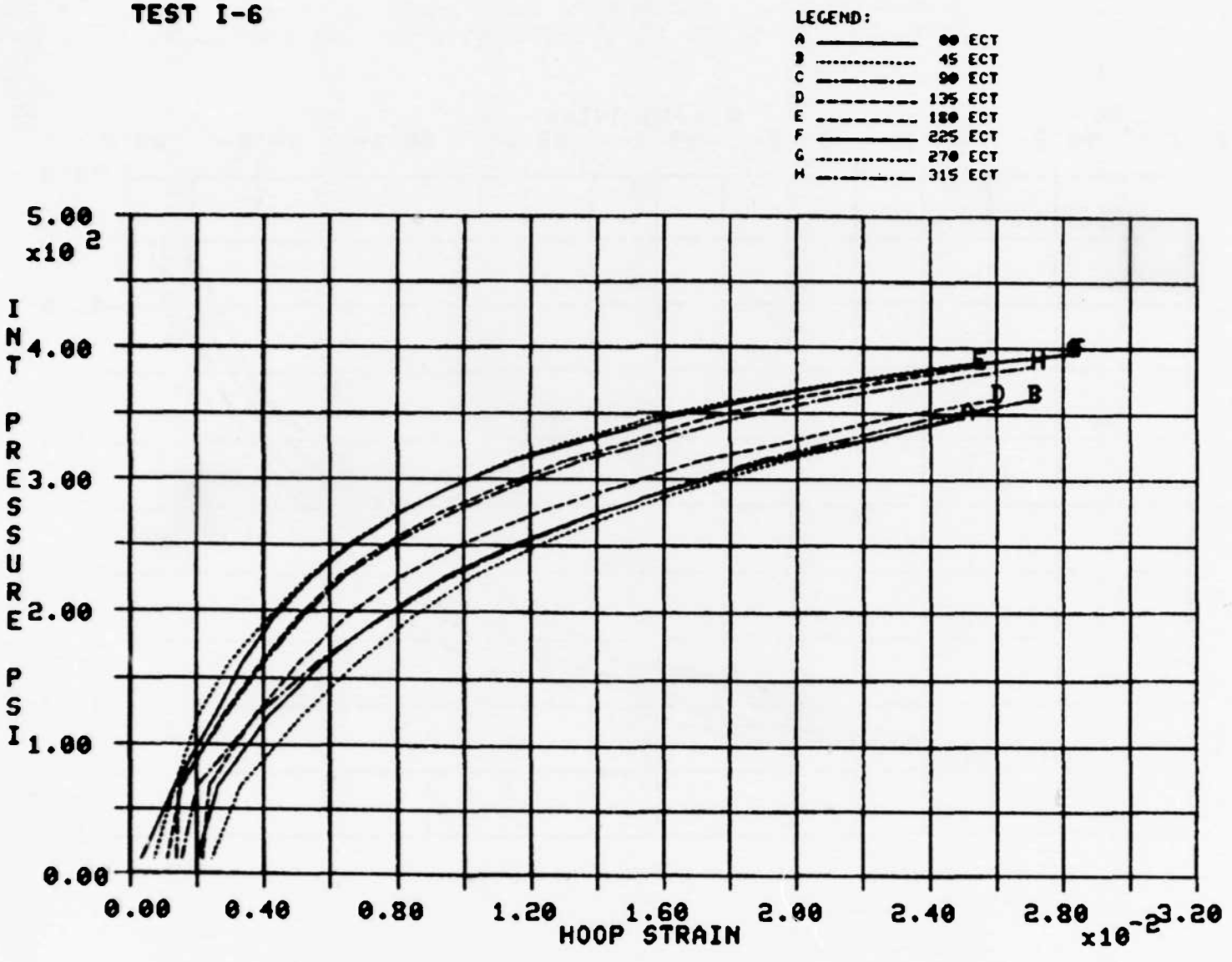

Figure 78 Plot of Internal Pressure vs. Hoop Strain at Mid-length Around the Circumference of Test No. I-6

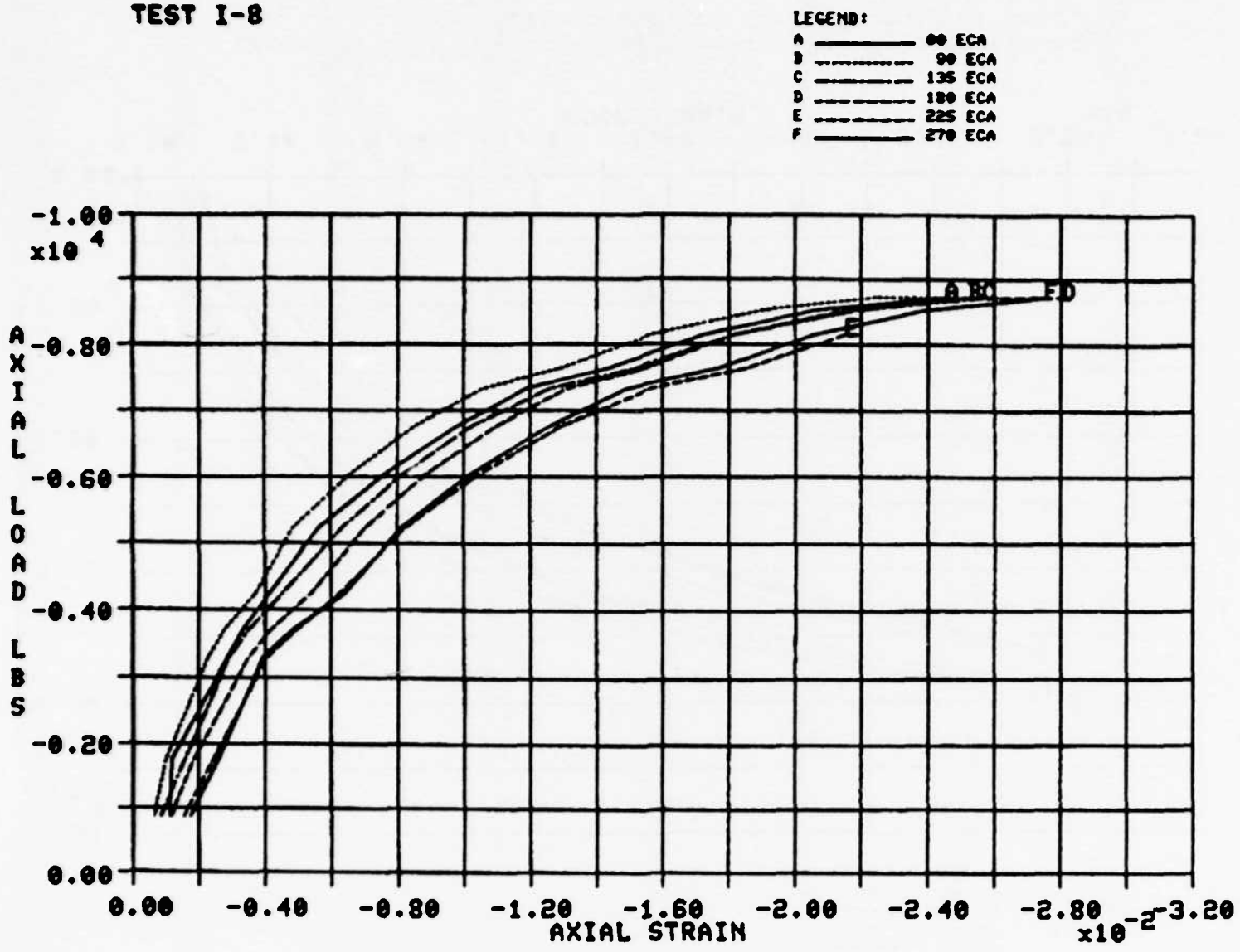

Figure 79 Plot of Axial Load vs. Axial Strain at Mid-length Around the Circumference of Test No. I-8

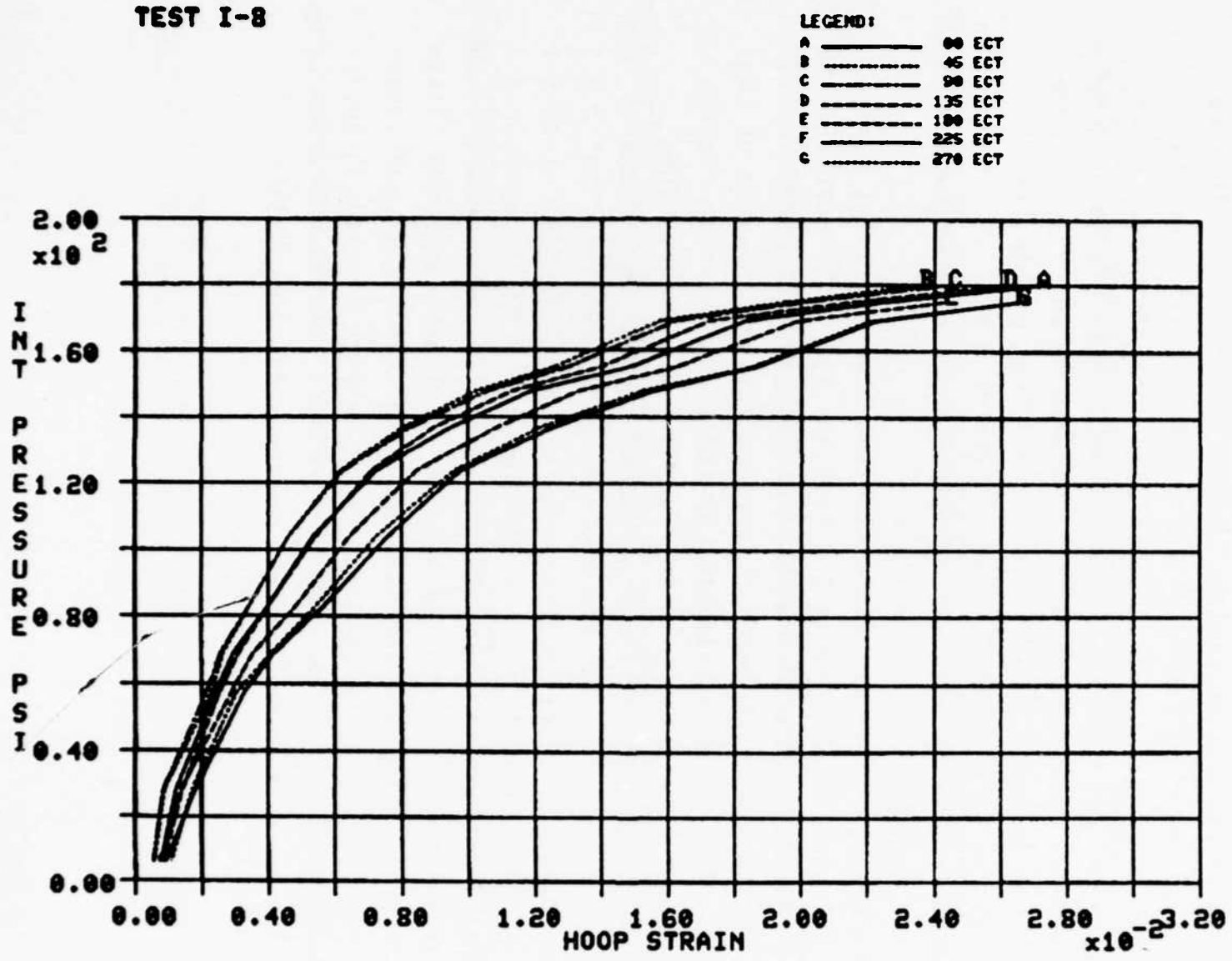

Figure 80 Plot of Internal Pressure vs. Hoop Strain at Mid-length Around the Circumference of Test No. I-8

plots for Test I-7 are shown in Figures 81 through 83. These plots suggest that the applied load was eccentric with respect to the specimen axis. The strain readings are higher at the 00° and 45° locations and low at the 180° and 225° locations. This is better illustrated in Figure 84 with a plot of axial strain at -5,000 lbs. vs. gage location around the circumference. It is also important to note that the ultimate failure of the specimen was between 00° and 45° locations. Figures 85 and 86 are plots of axial and pressure loads vs. axial and hoop strain, respectively, at the 90° and 180° locations for Test No. I-9. The difference in strain gage readings also indicates there was some eccentric loading of this specimen.

Figures 87 and 88 are plots of axial load vs. axial strain at the 90° and 180° locations for Test No. I-6. There appears to be good agreement between the internal and external gages indicating relatively small bending stresses through the wall of the specimen. This is also indicated by the plots shown in Figures 89 through 91 of external strain vs. internal strain. These plots have slopes close to unity. Similar plots for Test Nos. I-7, I-8 and I-9 for the 90° and 180° locations (90° and 315° for Test No. I-7) are shown in Figures 92 through 104. The plots for Test I-7 indicate there is some bending at the 90° location and very little at the 315° location. The data for Test Nos. I-8 and I-9 indicate there was some bending at mid-length and very little at the ends. It appears that the amount of bending in each specimen does not correspond with the ratio between biaxial stresses. This would suggest that the amount of bending stress or barreling of the specimen is more dependent on the variations between specimens than loading conditions.

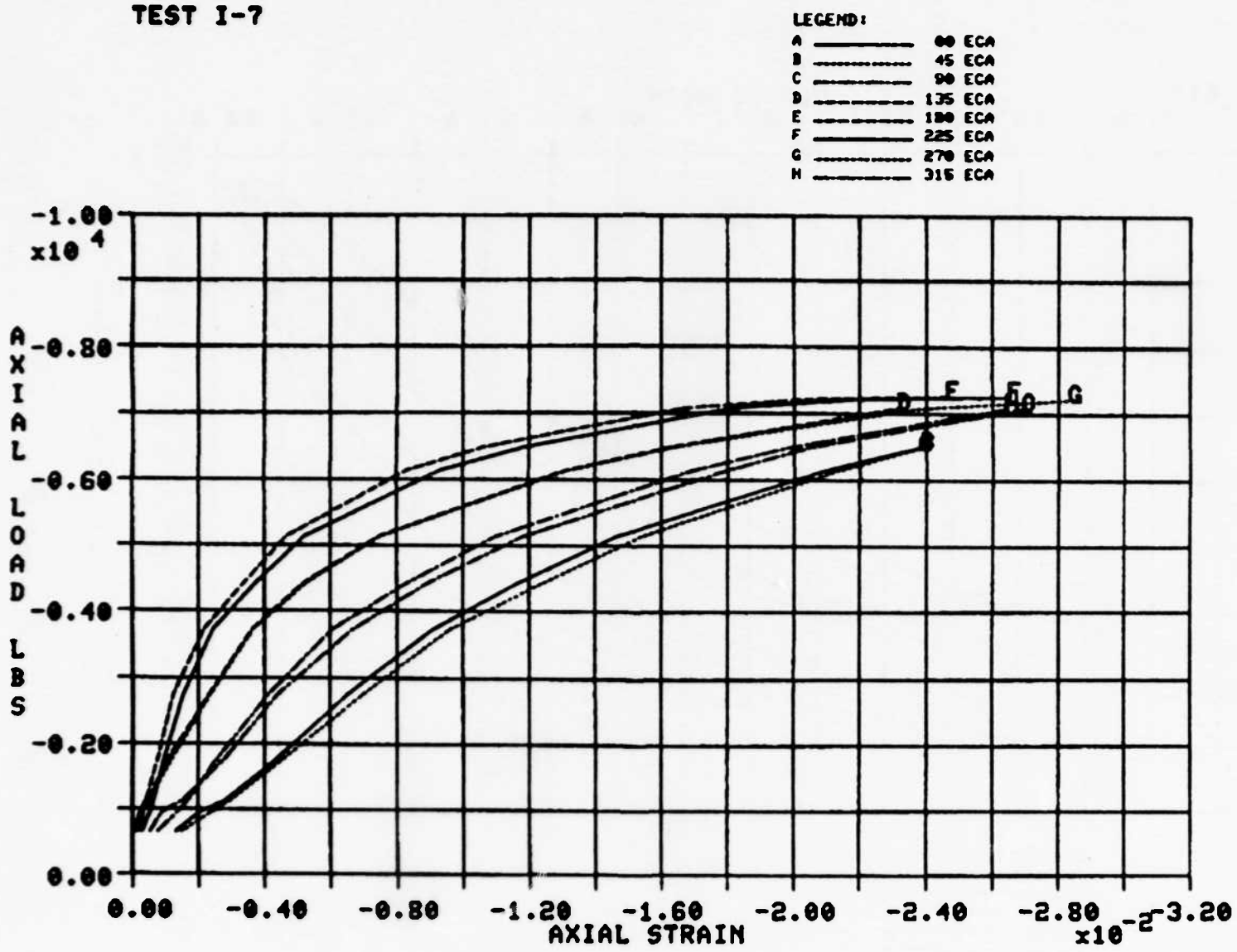

Figure 81 Plot of Axial Load vs. Axial Strain at Mid-length Around the Circumference of Test No. I-7

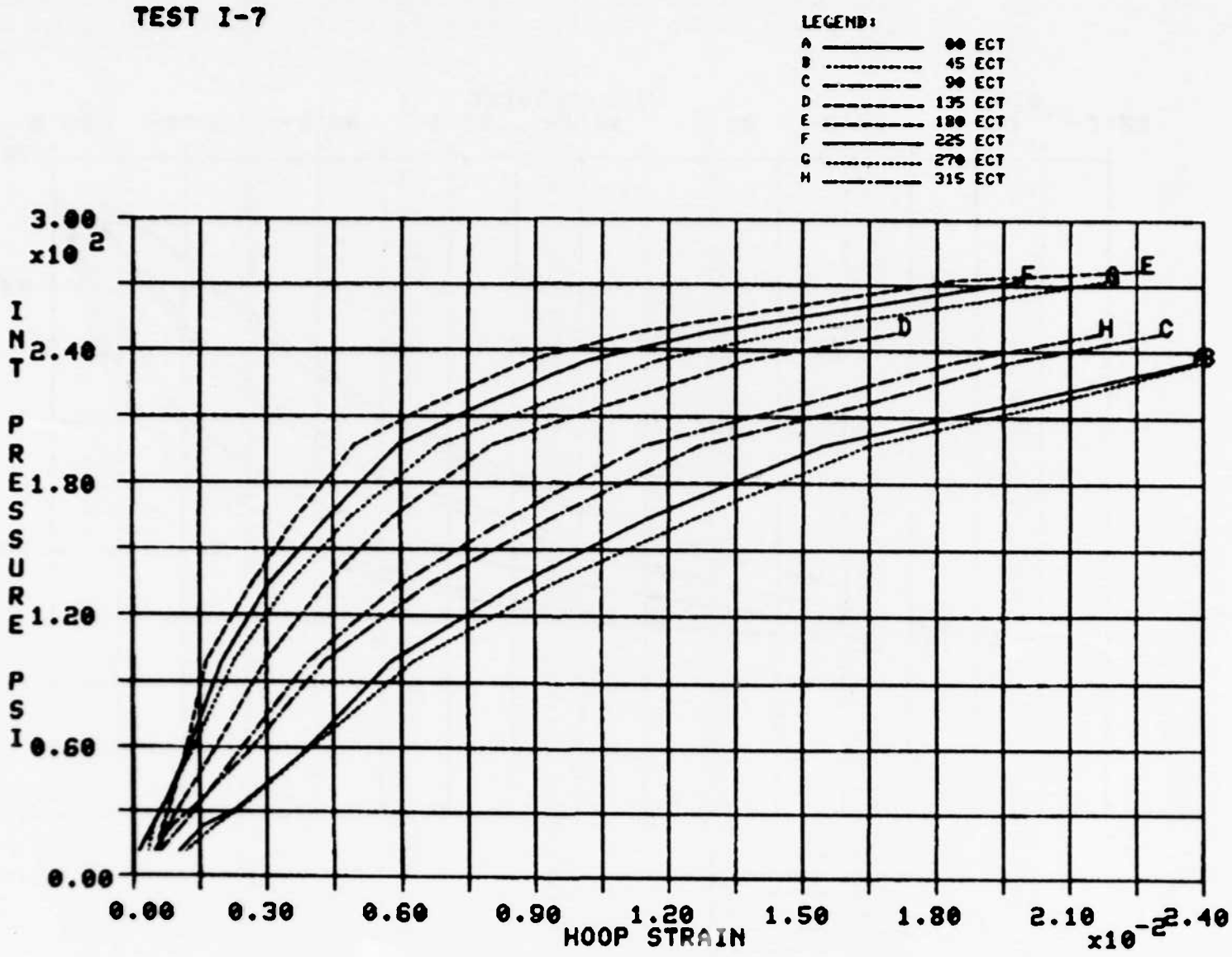

Figure 82 Plot of Internal Pressure vs. Hoop Strain at Mid-length Around the Circumference of Test No. I-7

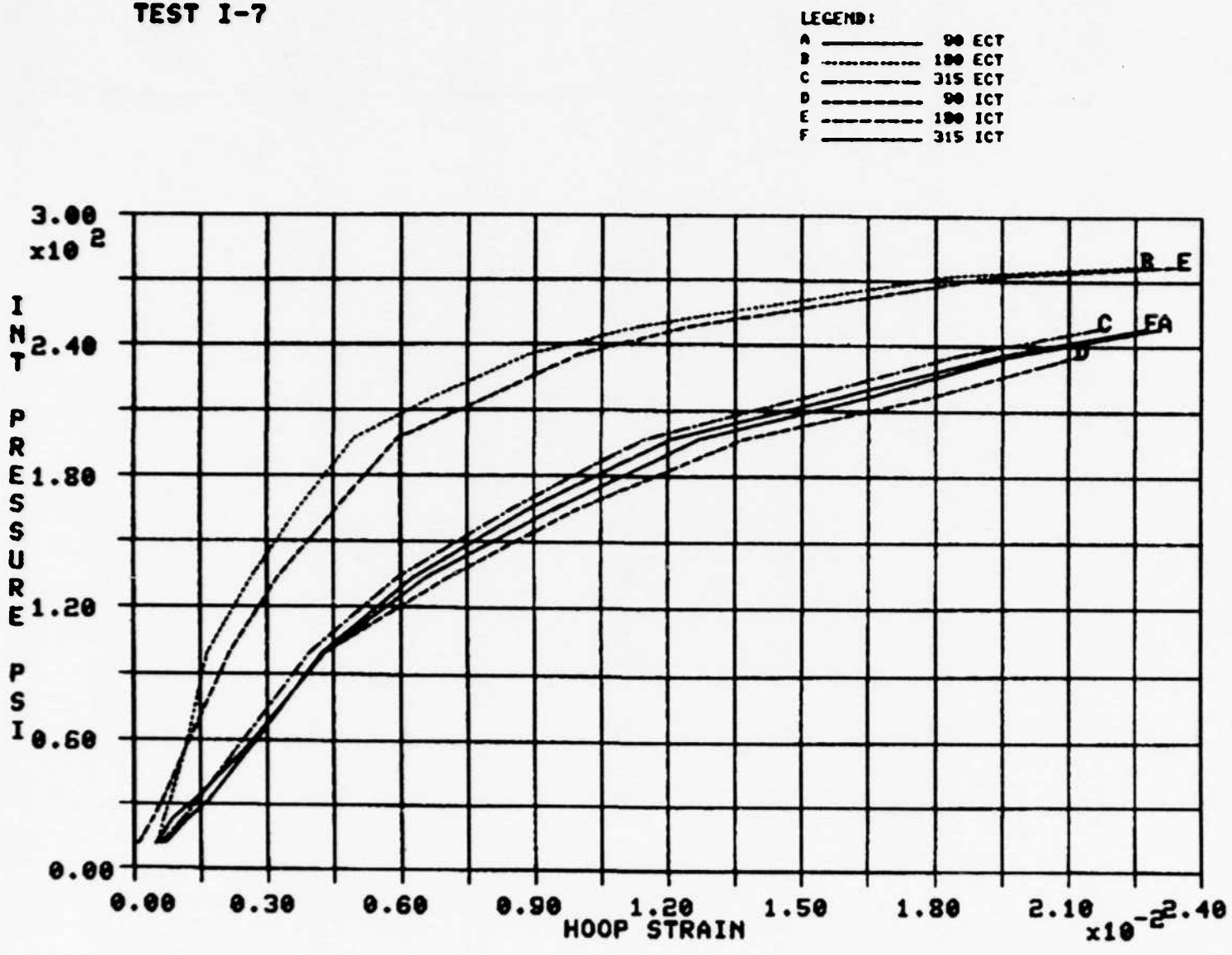

Figure 83 Plot of Internal Pressure vs. Hoop Strain at Mid-length Around the Circumference of Test No. I-7

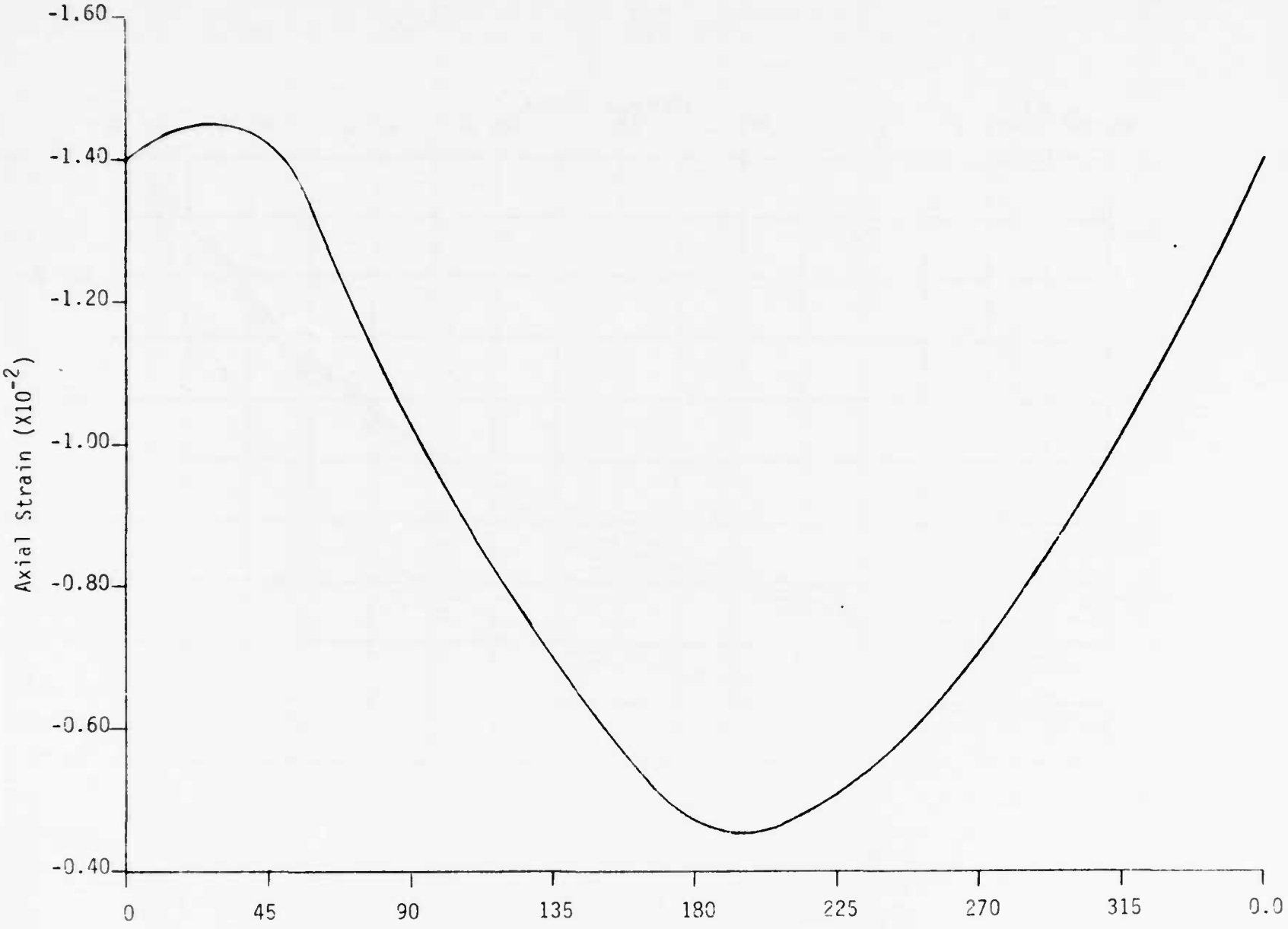

Figure 84 Axial Strain vs. Gage Location for Test No. I-7

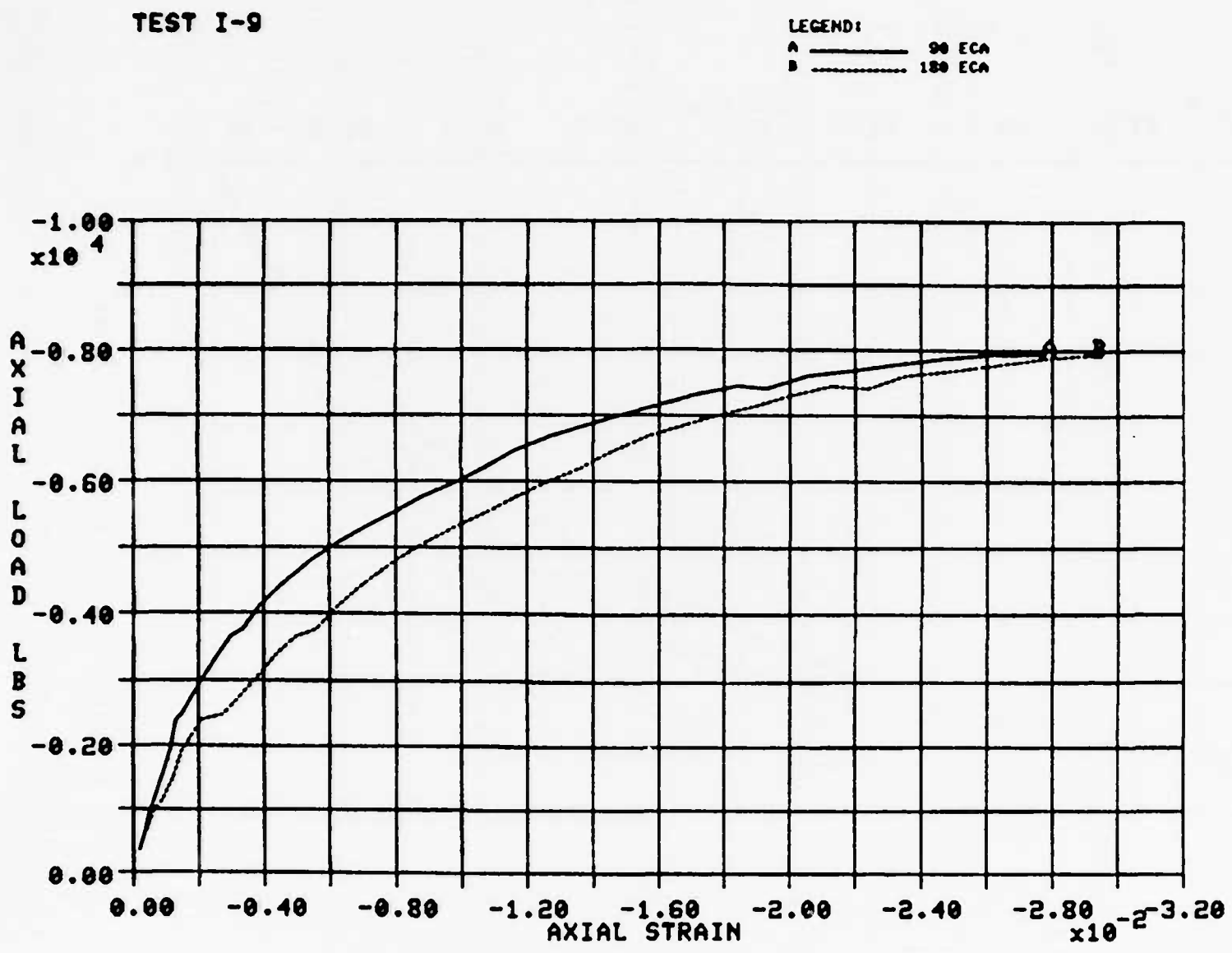

Figure 85 Plot of Axial Load vs. Axial Strain at Mid-length of Test No. I-9

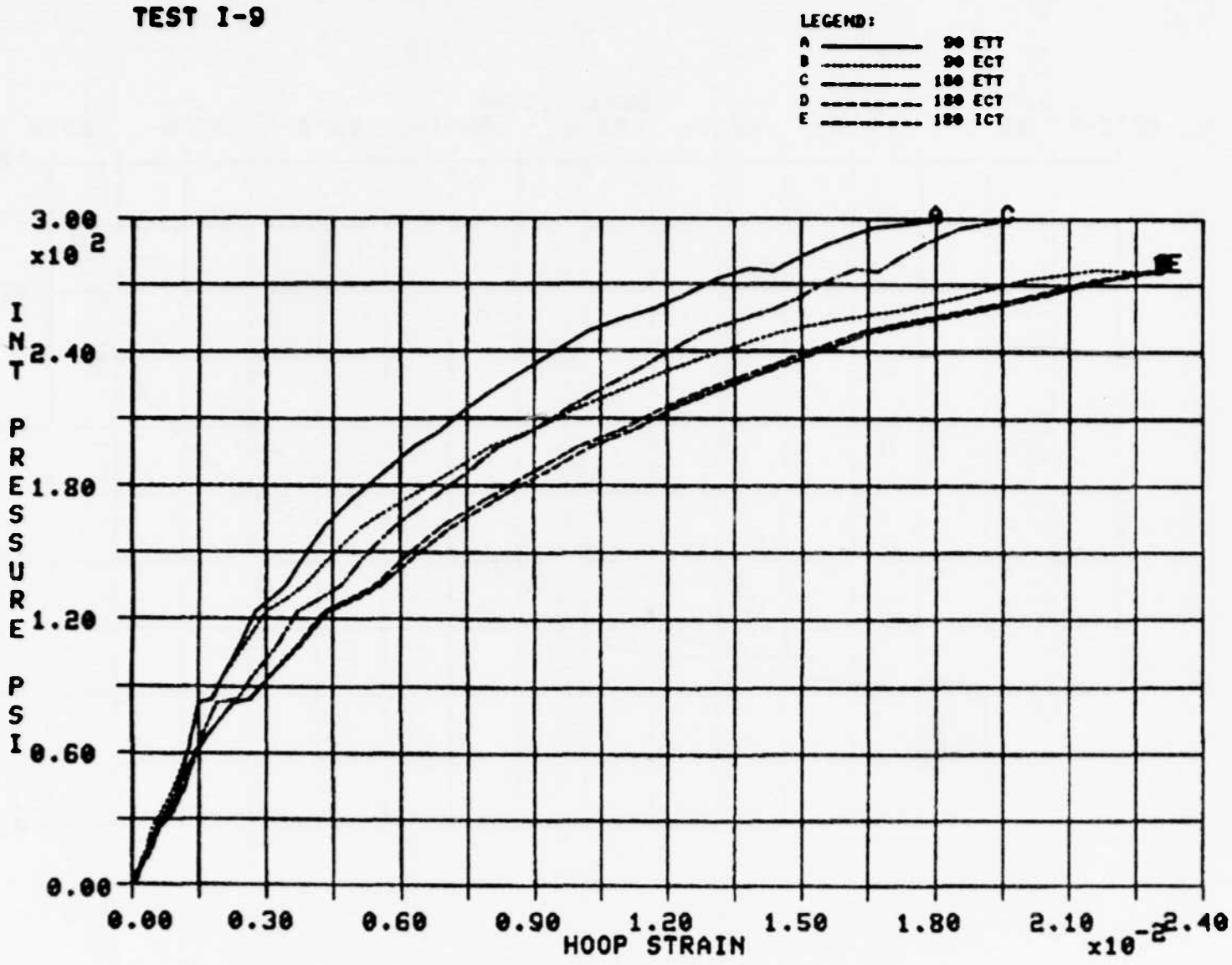

Figure 86 Plot of Internal Pressure and Hoop Strain for Test No. I-9

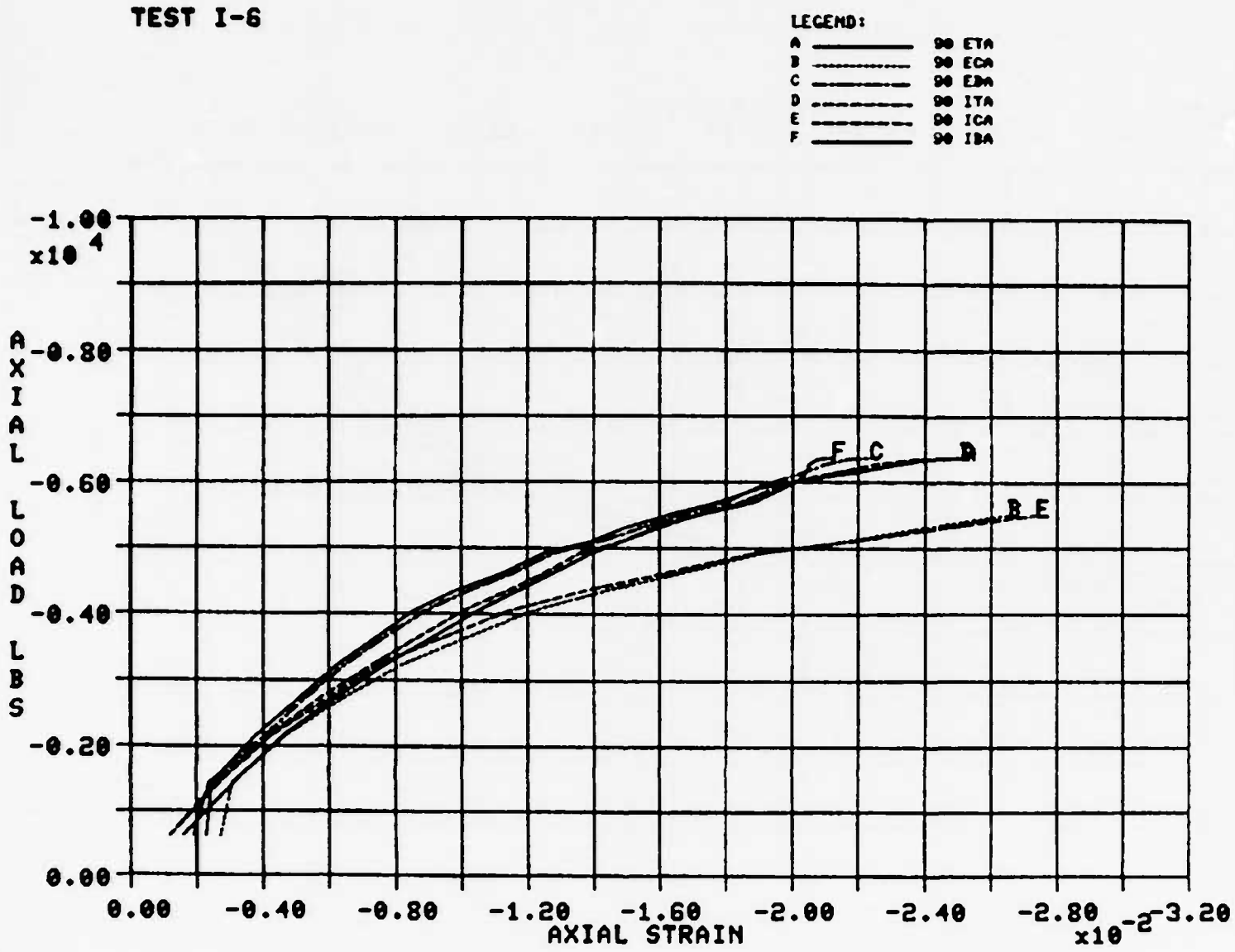

Figure 87 Plot of Axial Load vs. Axial Strain at the 90° Location for Test No. I-6

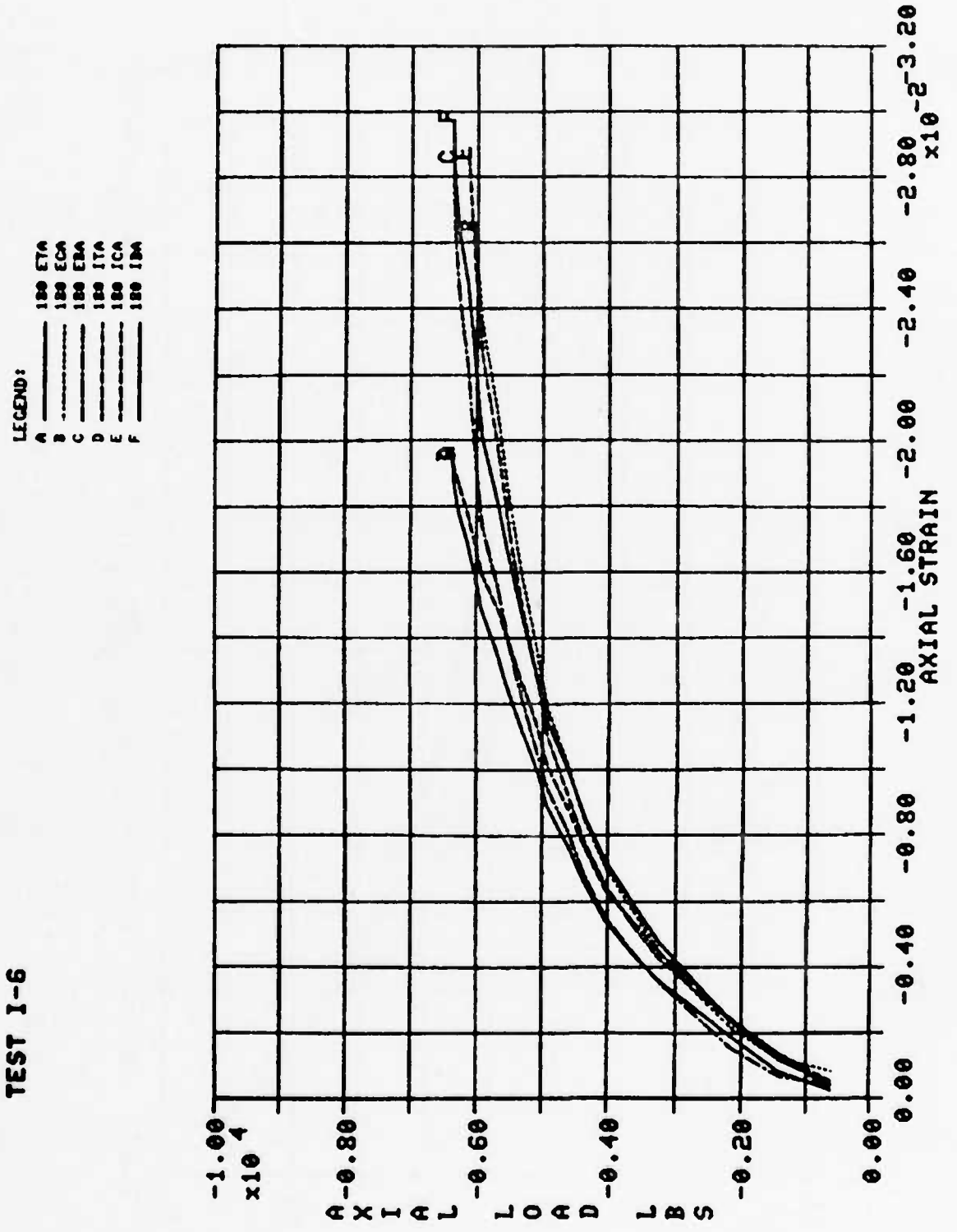

Figure 88 Plot of Axial Load vs. Axial Strain at the 180° Location for Test No. I-6

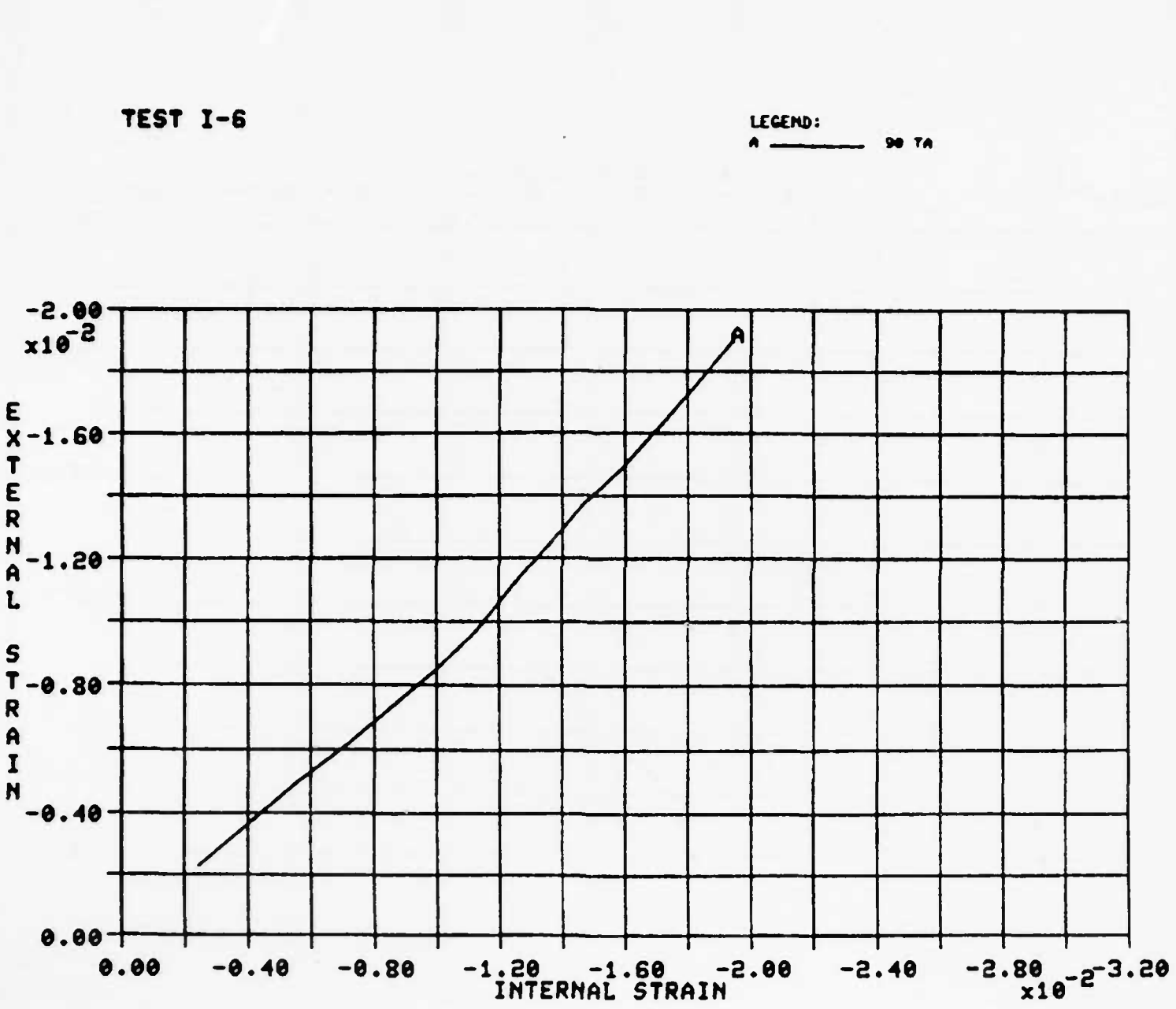

Figure 89 Plot of External vs. Internal Axial Strain at the 90° Location Near the Top Edge of Test No. I-6

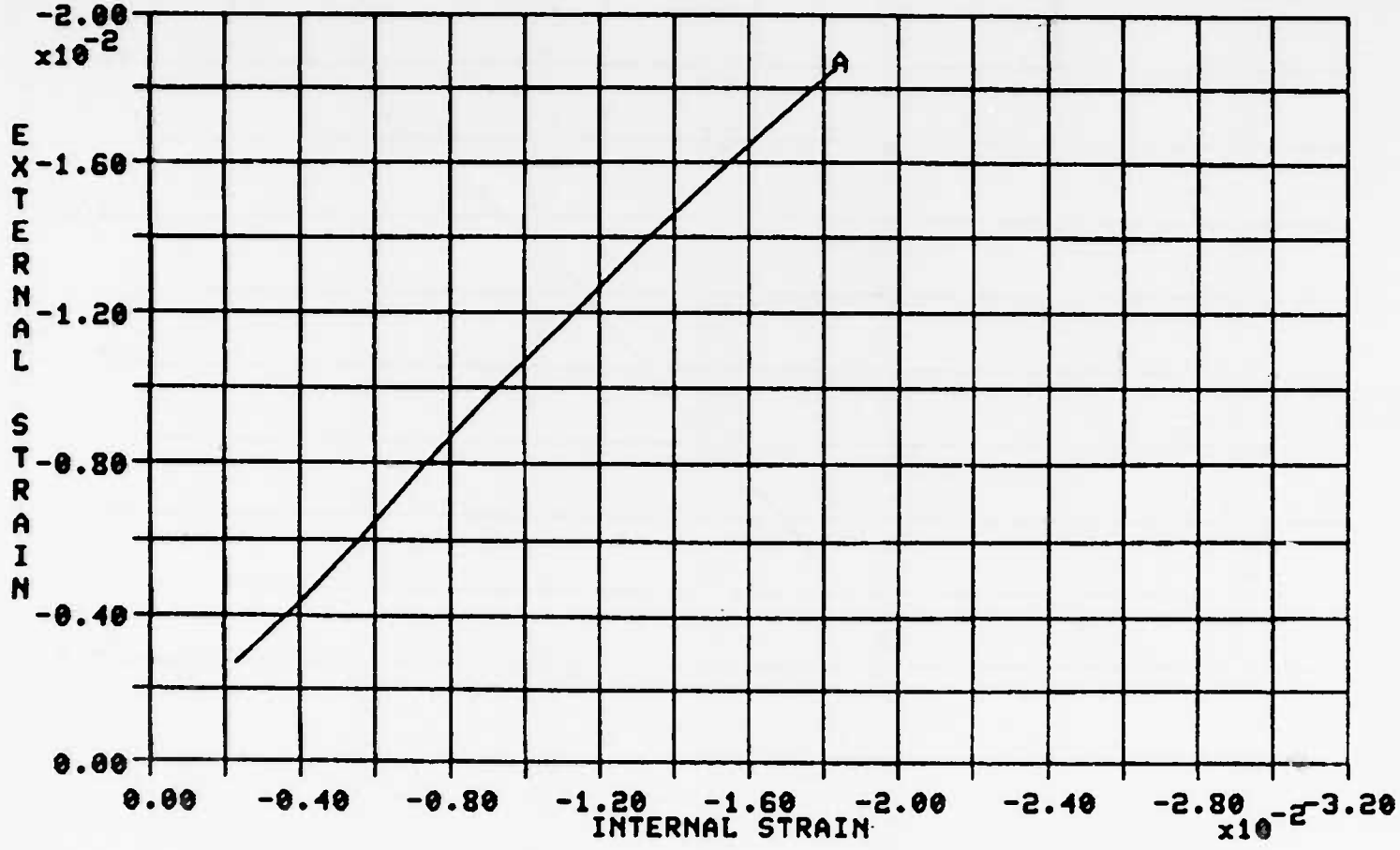

Figure 90 Plot of External vs. Internal Axial Strain at the 90° Location Near the Center or Mid-length for Test No. I-6

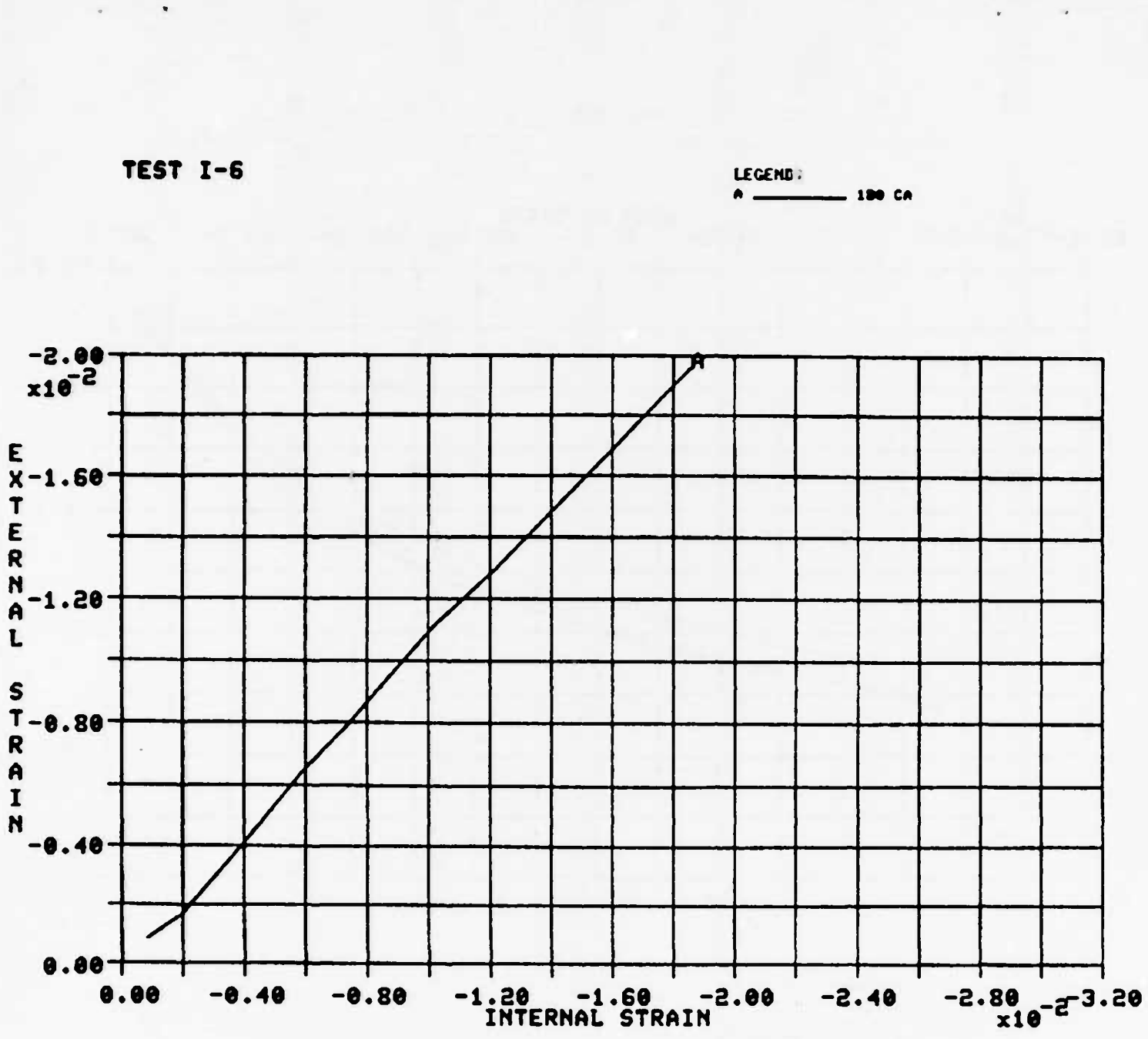

Figure 91 Plot of External vs. Internal Axial Strain at the 180° Location Near the Center or Mid-length of Test No. I-6

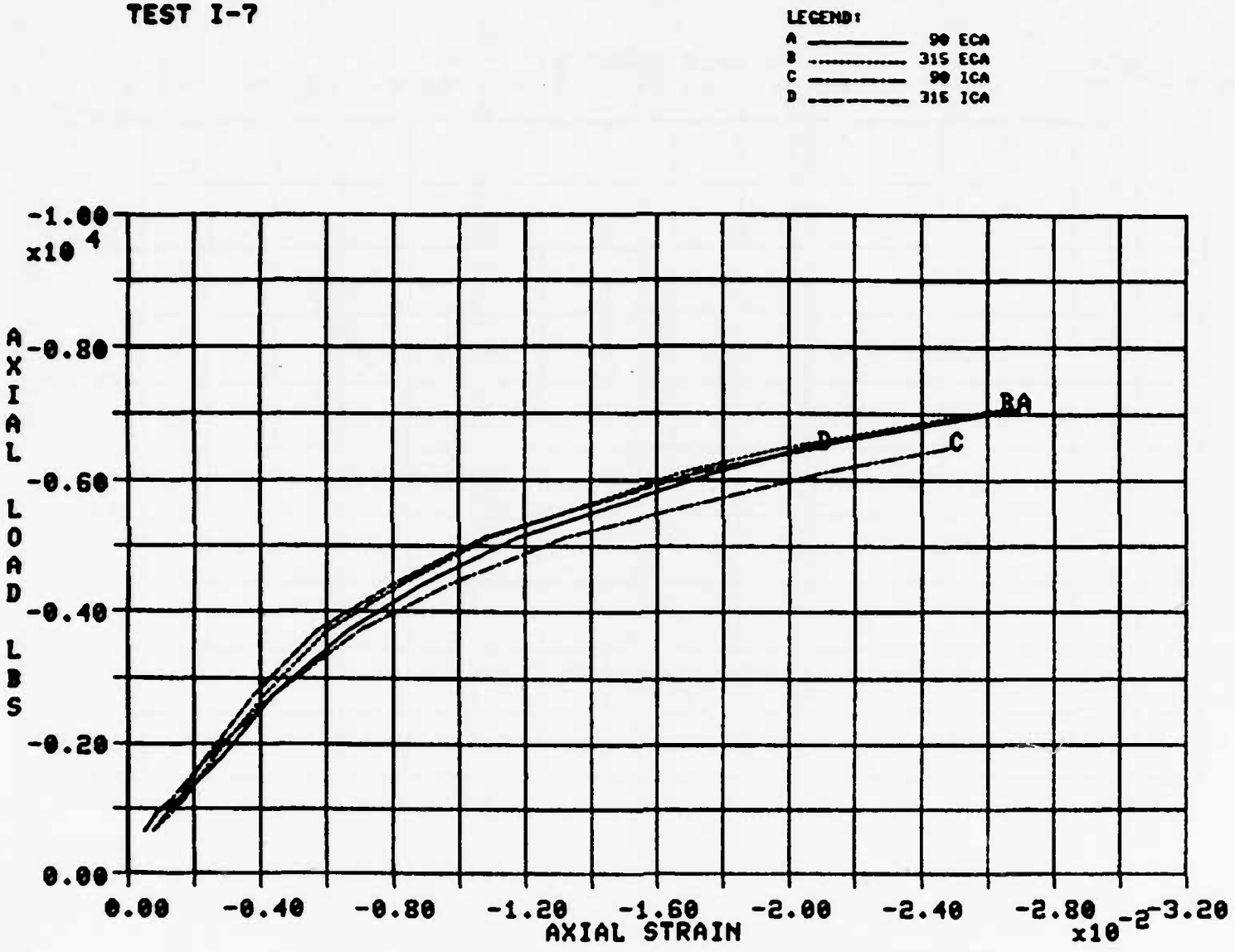

Figure 92 Plot of Axial Load vs. Axial Strain at the 90° and 315° Locations for Test No. I-7

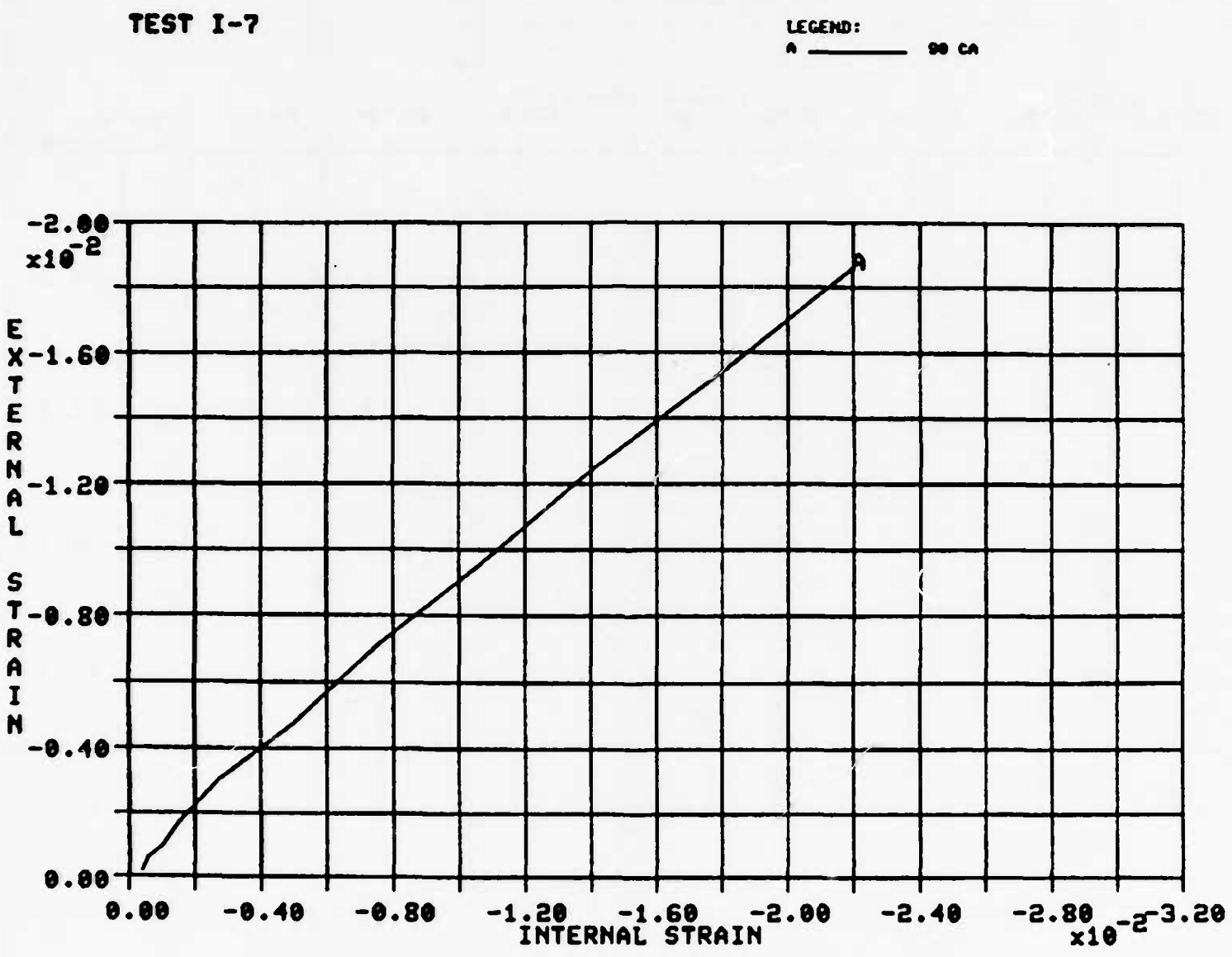

Figure 93 Plot of External vs. Internal Axial Strain at the 90° Location Near the Center or Mid-length of Test No. I-7

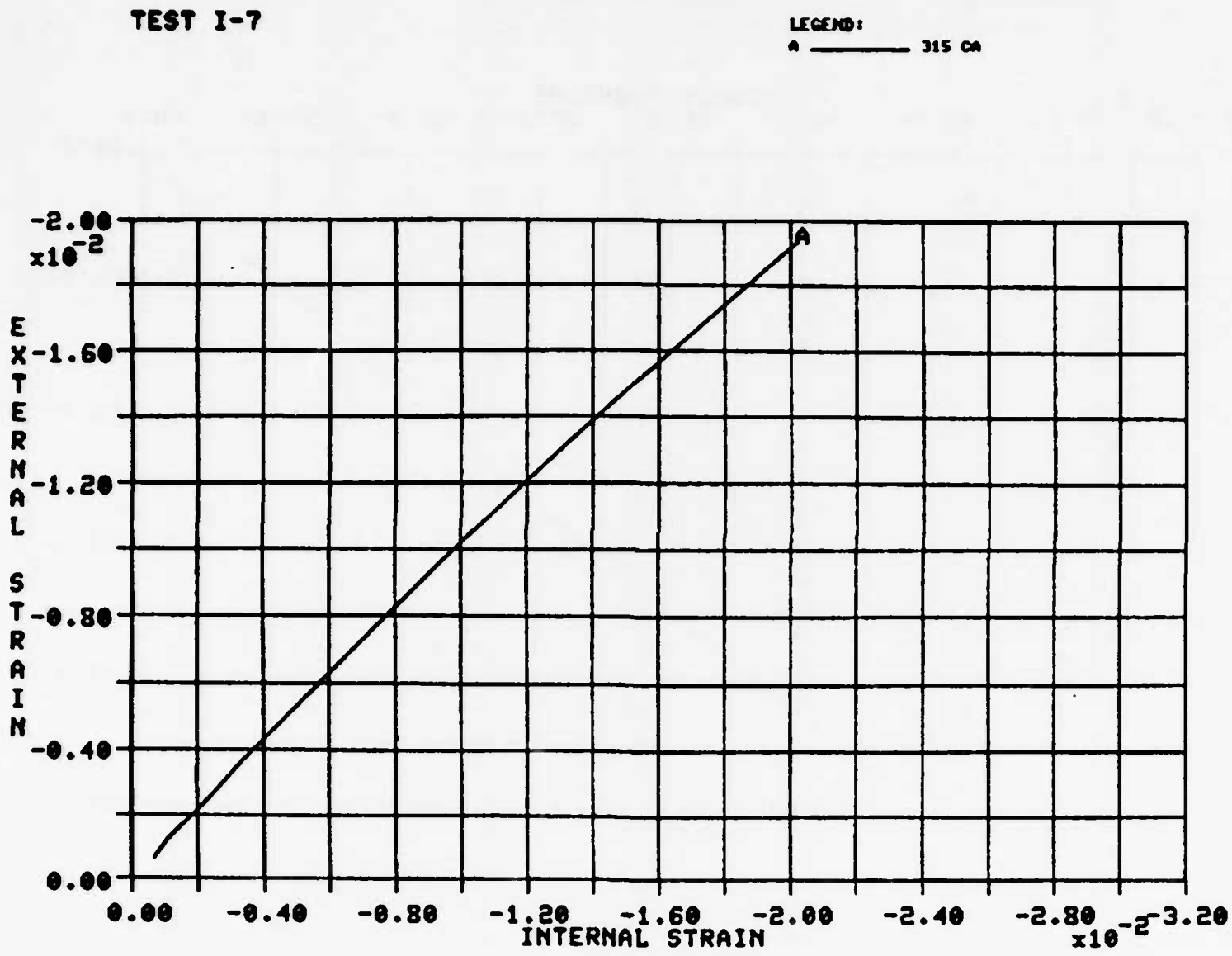

Figure 94 Plot of External vs. Internal Axial Strain at the 315° Location Near the Center or Mid-length of Test No. I-7

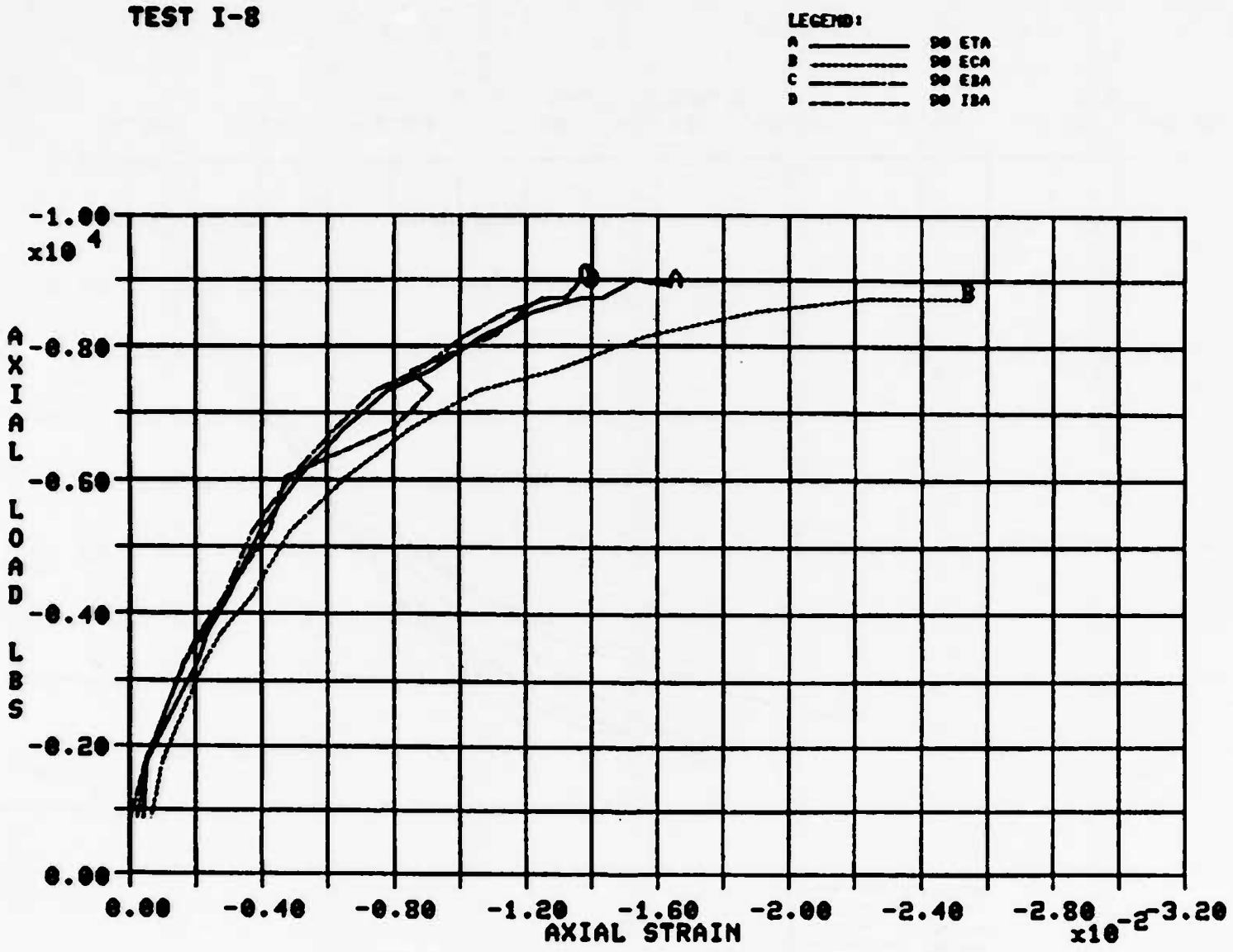

Figure 95 Plot of Axial Load vs. Axial Strain at the 90° Location for Test No. I-8

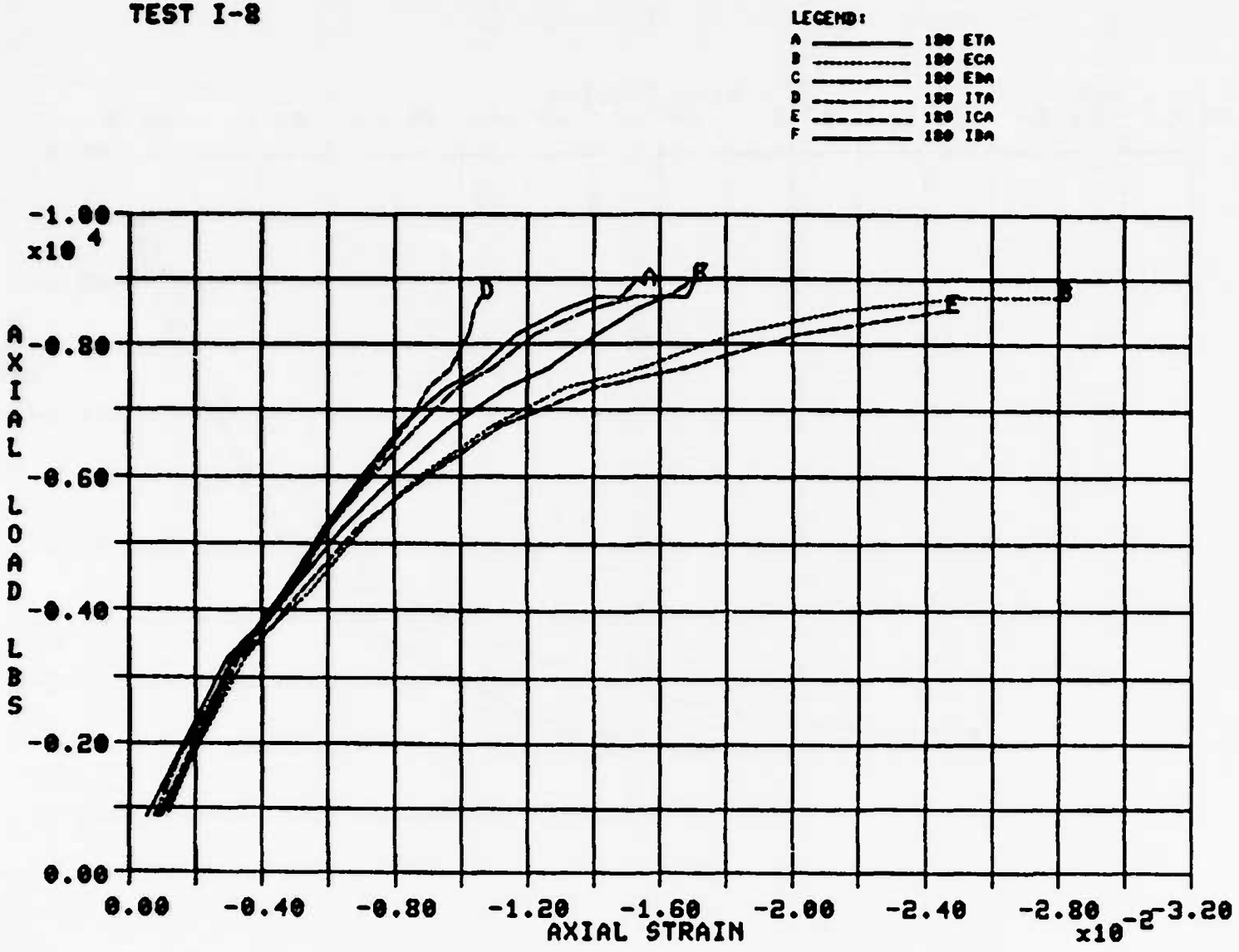

Figure 96 Plot of Axial Load vs. Axial Strain at the 180° Location for Test No. I-8

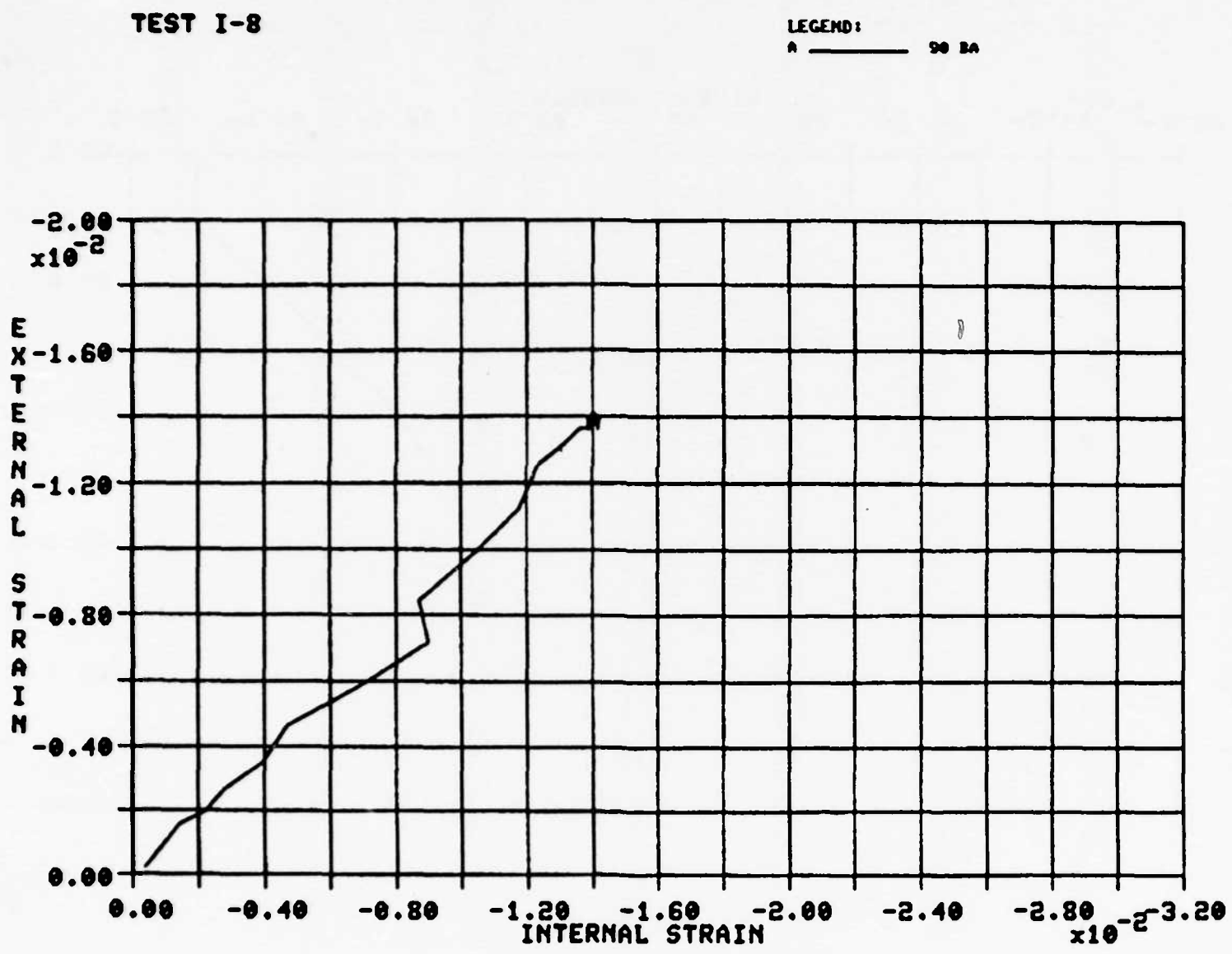

Figure 97 Plot of External vs. Internal Axial Strain at the 90° Location Near the Bottom Edge of Test No. I-8

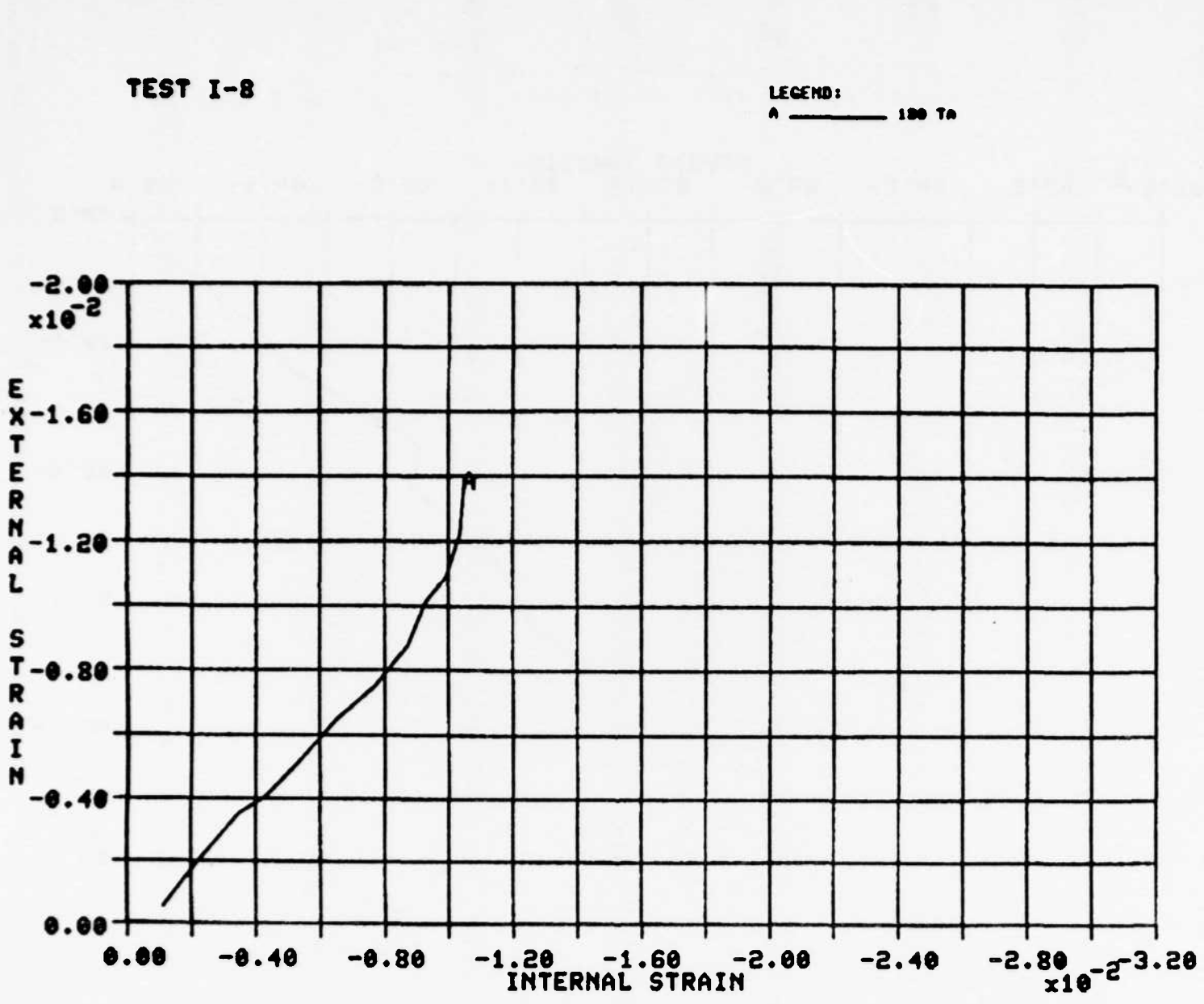

Figure 98 Plot of External vs. Internal Axial Strain at the 180° Location Near the Top Edge of Test No. I-8

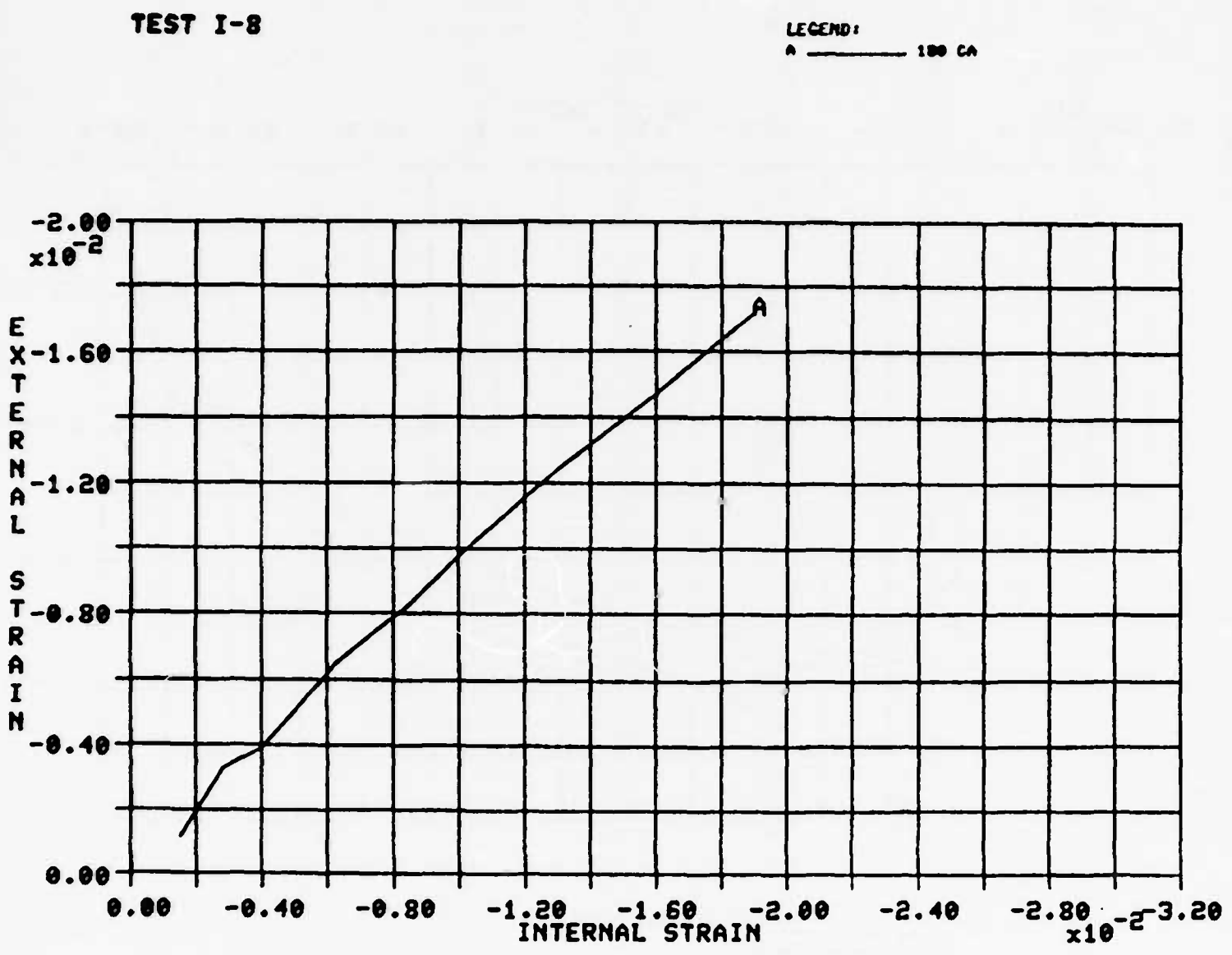

Figure 99 Plot of External vs. Internal Axial Strain at the 180° Location Near the Center or Mid-length of Test No. I-8

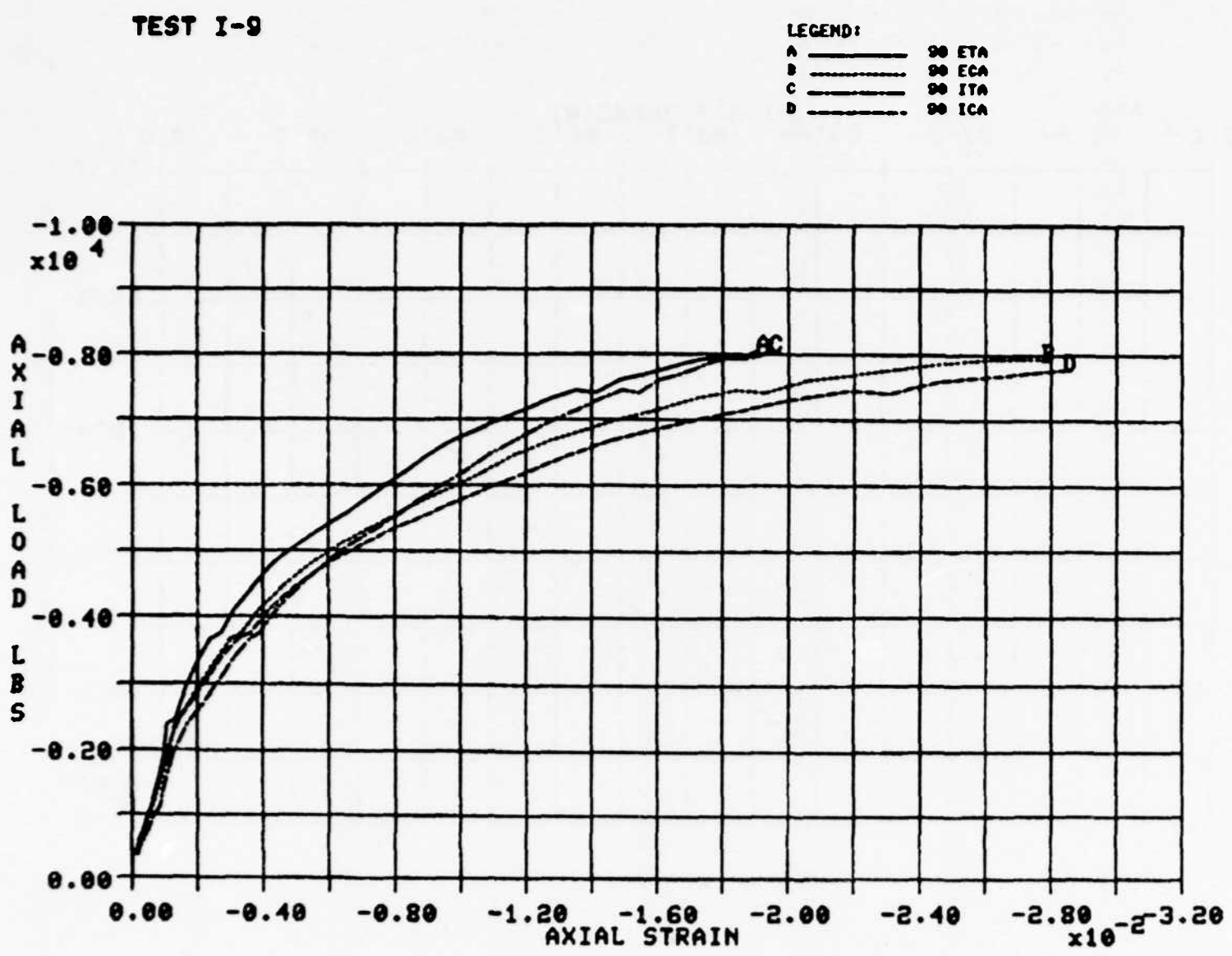

Figure 100 Plot of Axial Load vs. Axial Strain at the 90° Location for Test No. I-9

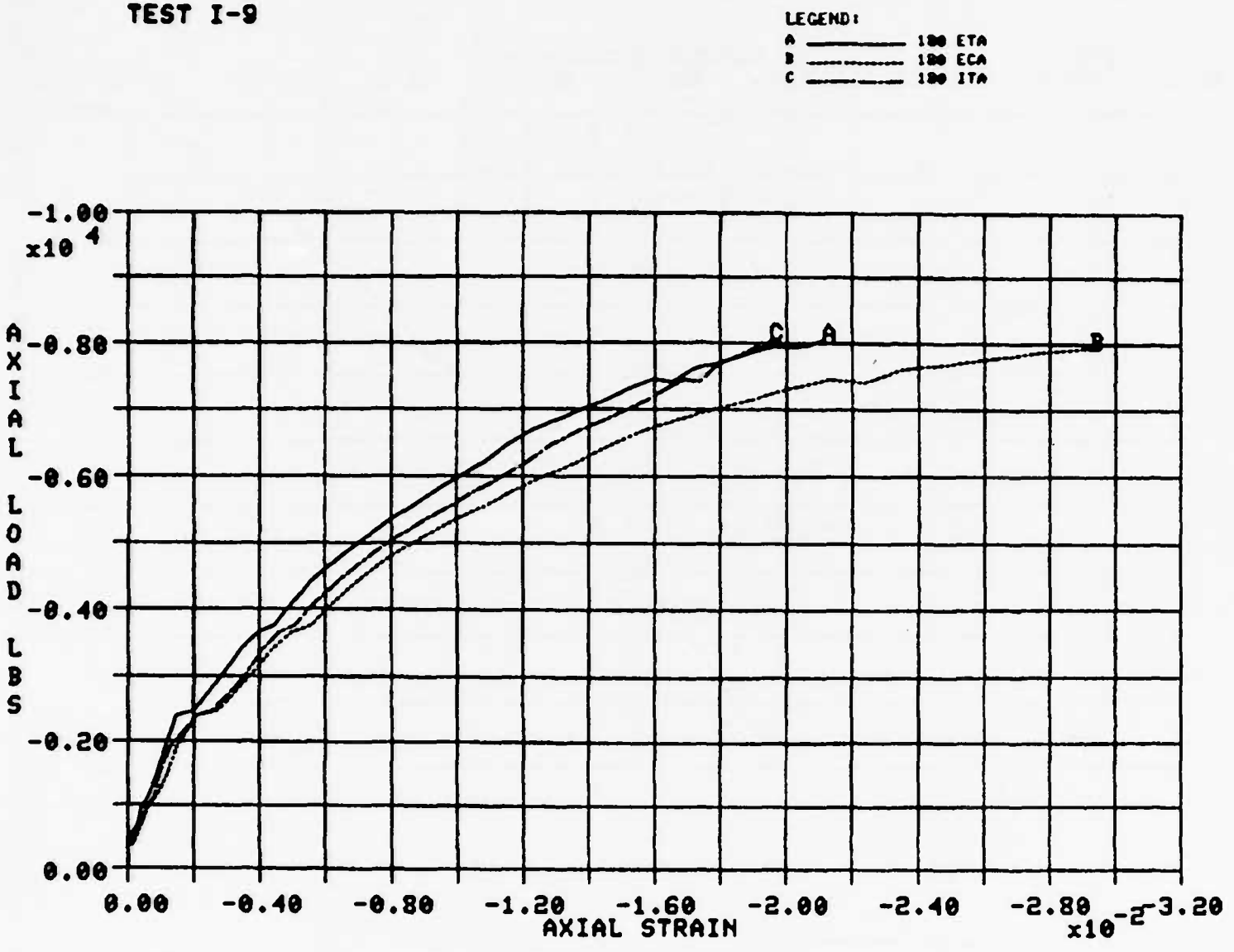

Figure 101 Plot of Axial Load vs. Axial Strain at the 180° Location for Test No. I-9

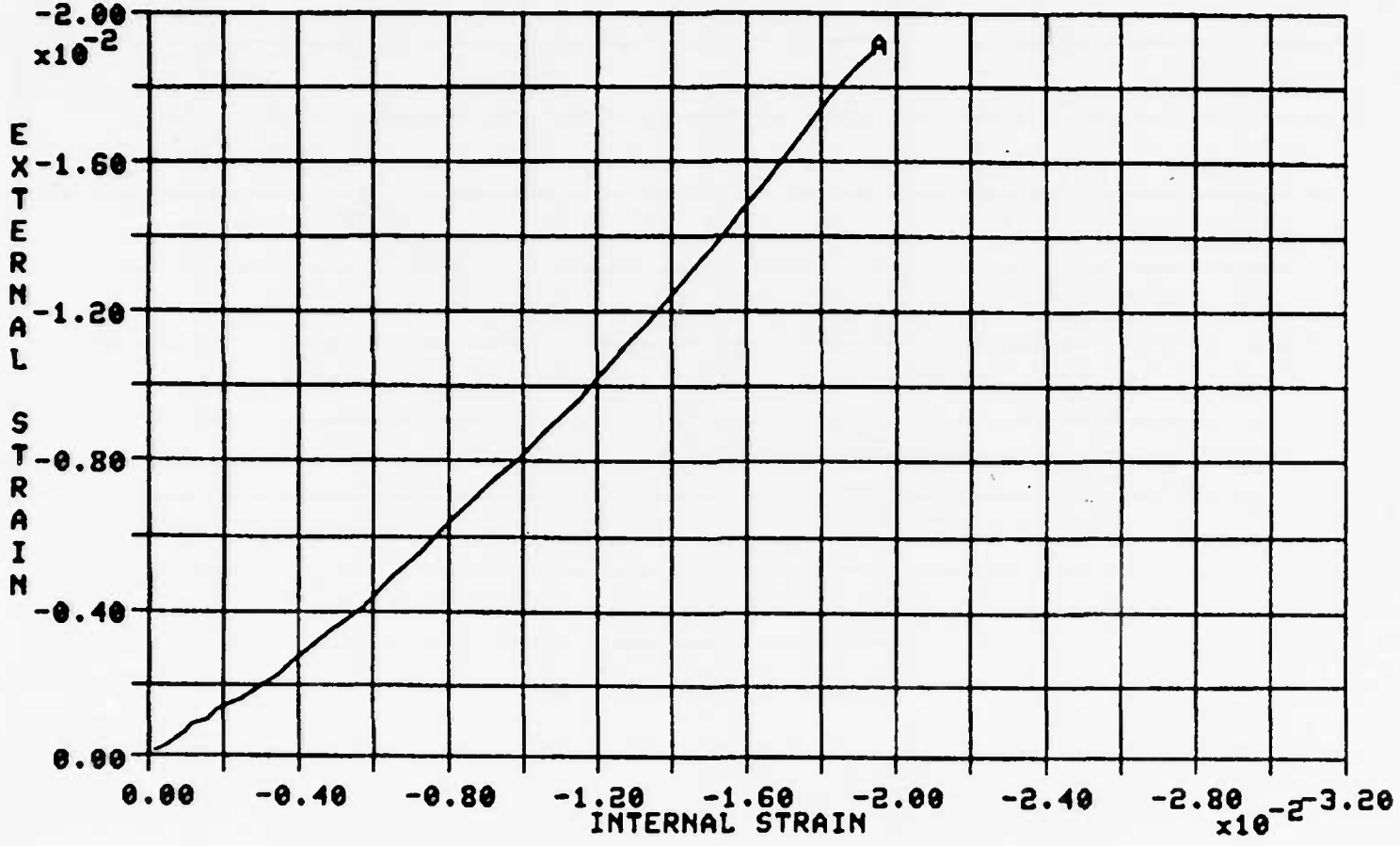

Figure 102 Plot of External vs. Internal Axial Strain at the 90° Location Near the Top Edge of Test No. I-9

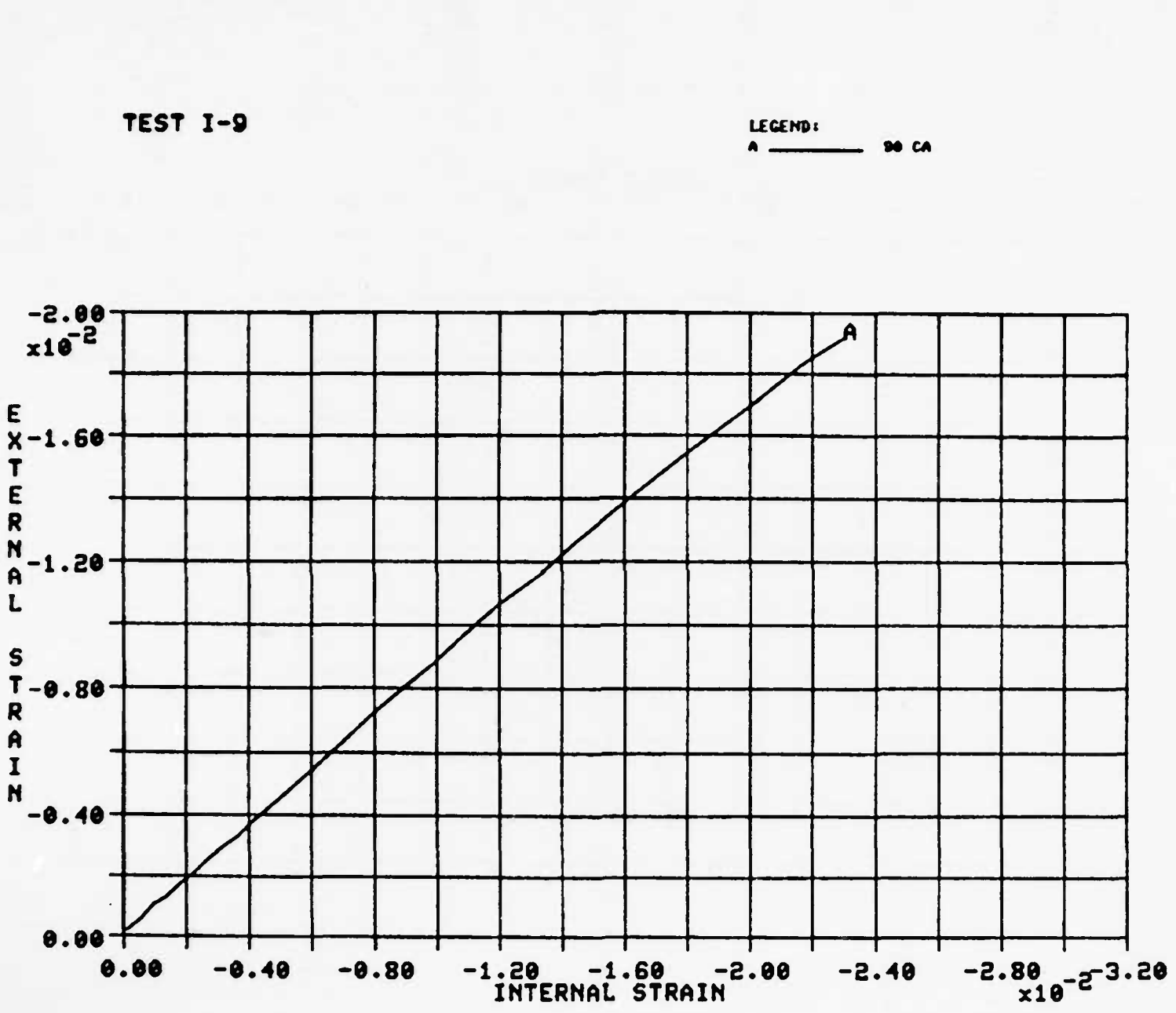

Figure 103 Plot of External vs. Internal Axial Strain at the 90° Location Near the Center or Mid-length of Test No. I-9

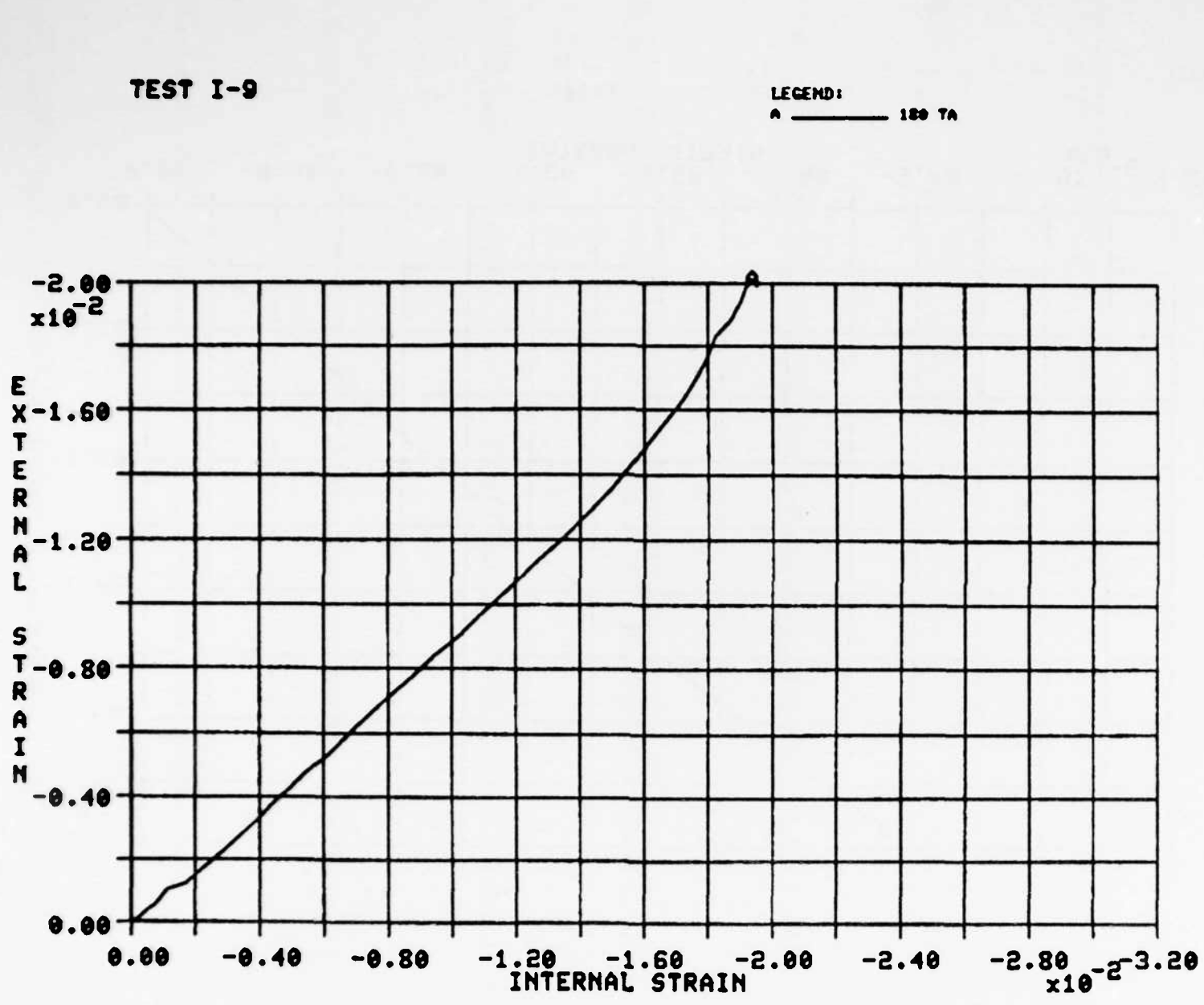

Figure 104 Plot of External vs. Internal Axial Strain at the 180° Location Near the Top Edge of Test No. I-9

VIII. EXTERNAL PRESSURE TESTS

Two instrumented specimens were tested with external pressure only. These were Test Nos. II-10 and II-11. Both specimens were 2 inches in length. Specimen No. II-10 was instrumented with thirty-nine strain gage elements using the gage layout listed in Table 10. The gages were spaced 45° apart around the circumference of the specimen. Specimen No. II-11 was instrumented with twelve strain gage elements using the gage layout listed in Table 11. The gages were at the 90° and 180° locations.

Two strips of special-made rubber gasket material were used on the external surface of the specimens. The two strips laid side by side were slightly wider than the length of the specimen. The two strips were cut to a length equal to the circumference of the specimens. Cut-outs were made in the gaskets for instrumentation wires. The gaskets were bonded side by side around the circumference of the specimens with silicone rubber. Seams and cut-outs were also sealed with silicone rubber. Because of the extra width of the gasket material, the gaskets could be preloaded between the two platens of the biaxial test fixture with only a small axial load applied to the specimens. This axial preload provides the seal necessary for external pressurization. The lead/polyethelene/lead sandwich gasket lubrication was also used at the platen surfaces. An external pressure collet was placed around the specimen and biaxial test fixture. This cylindrical collet was sealed with O-rings between the upper and lower platen sides. The volume between the pressure collet, upper and lower platens, and the specimen was pressurized using a handwheel-operated, single-stroke piston pump. The axial preload was provided by the MTS system. Both the pressure and load sugnal were sent to the MTS system controller. The ratio in gain between the load and pressure signal was adjusted such that the system would produce a constant preload on the specimen plus the force required to overcome the pressure load acting on the external surface area of the platens inside the pressure collet. The

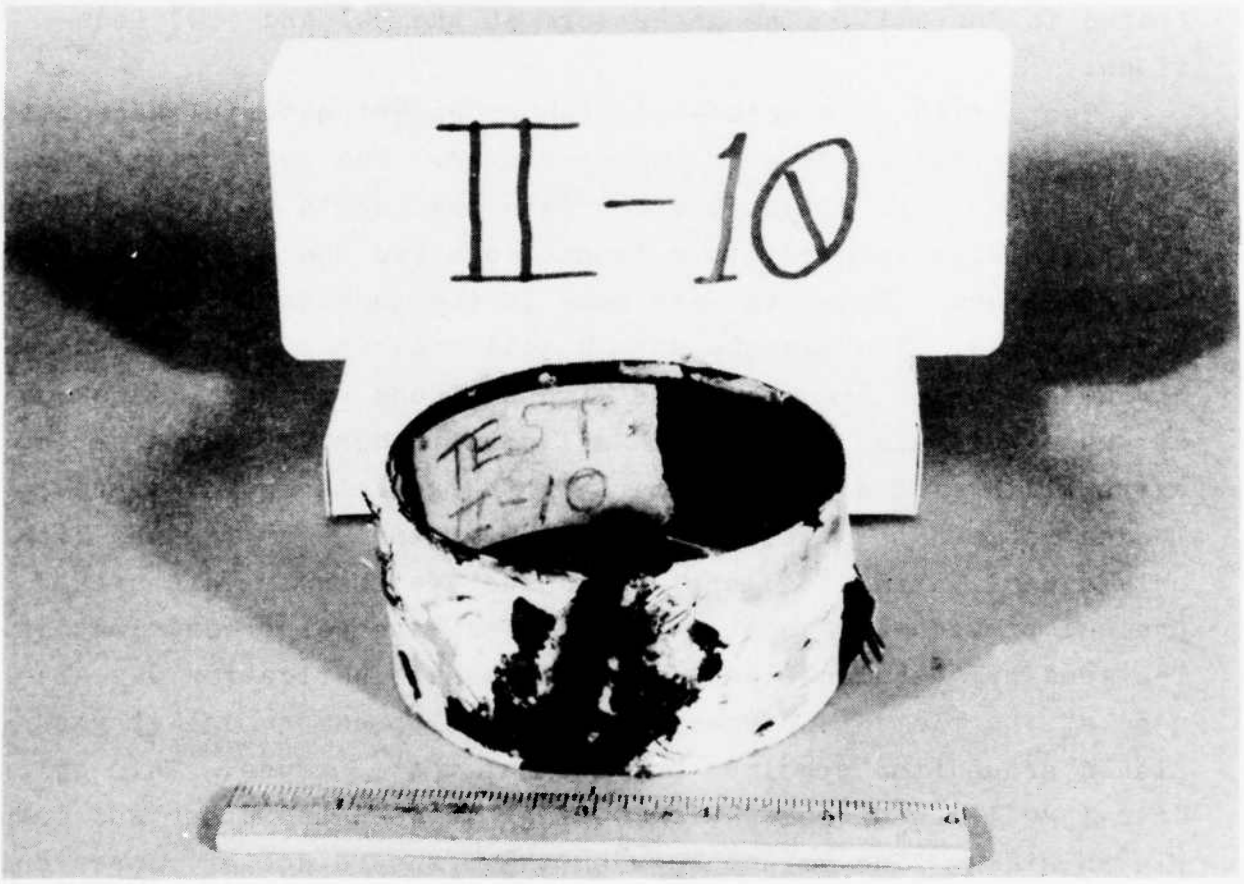

Figure 105 Photograph of Specimen No. II-10 After Testing

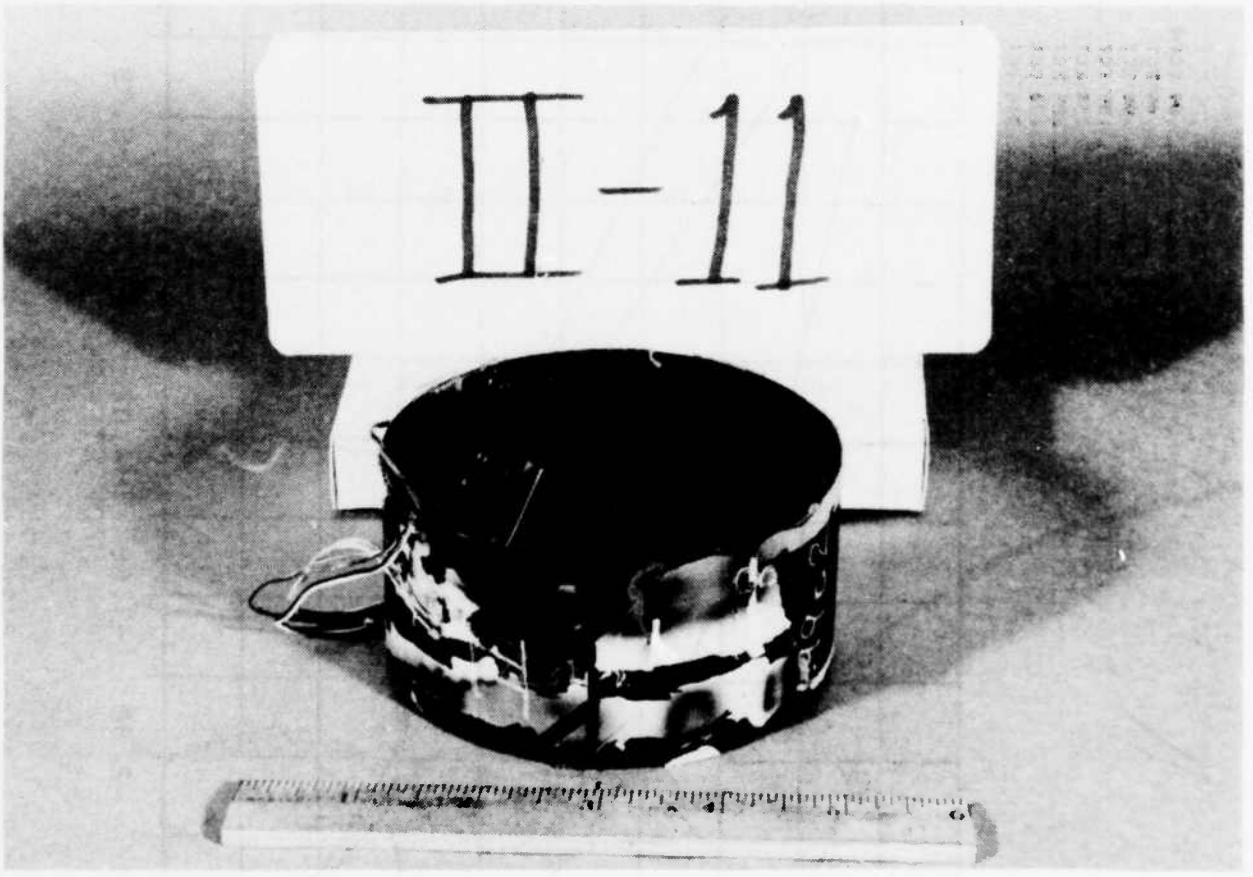

Figure 106 Photograph of Specimen No. II-11 After Testing

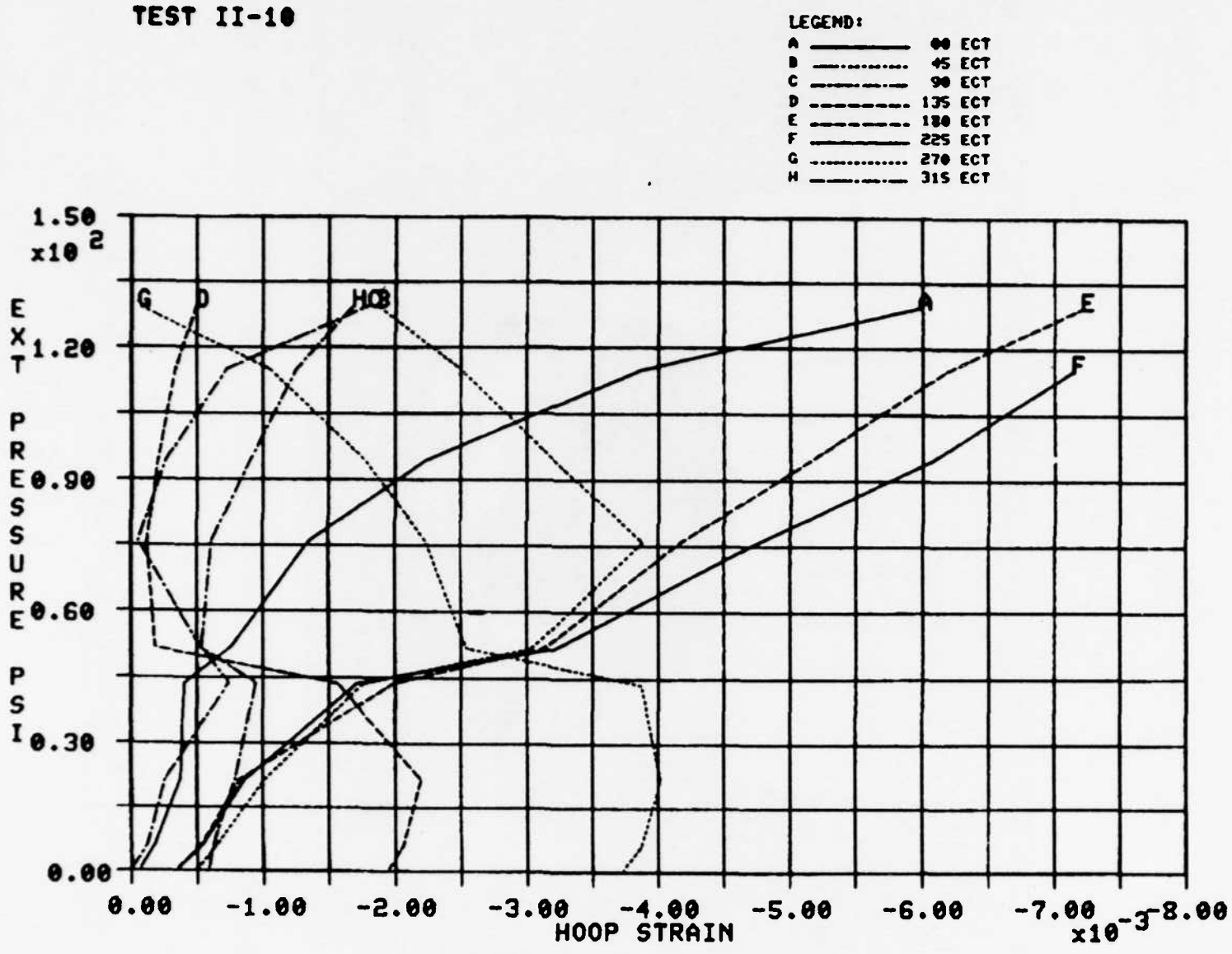

Figure 107 Plot of External Pressure vs. External Hoop Strain at Mid-length Around the Circumference of Test No. II-10

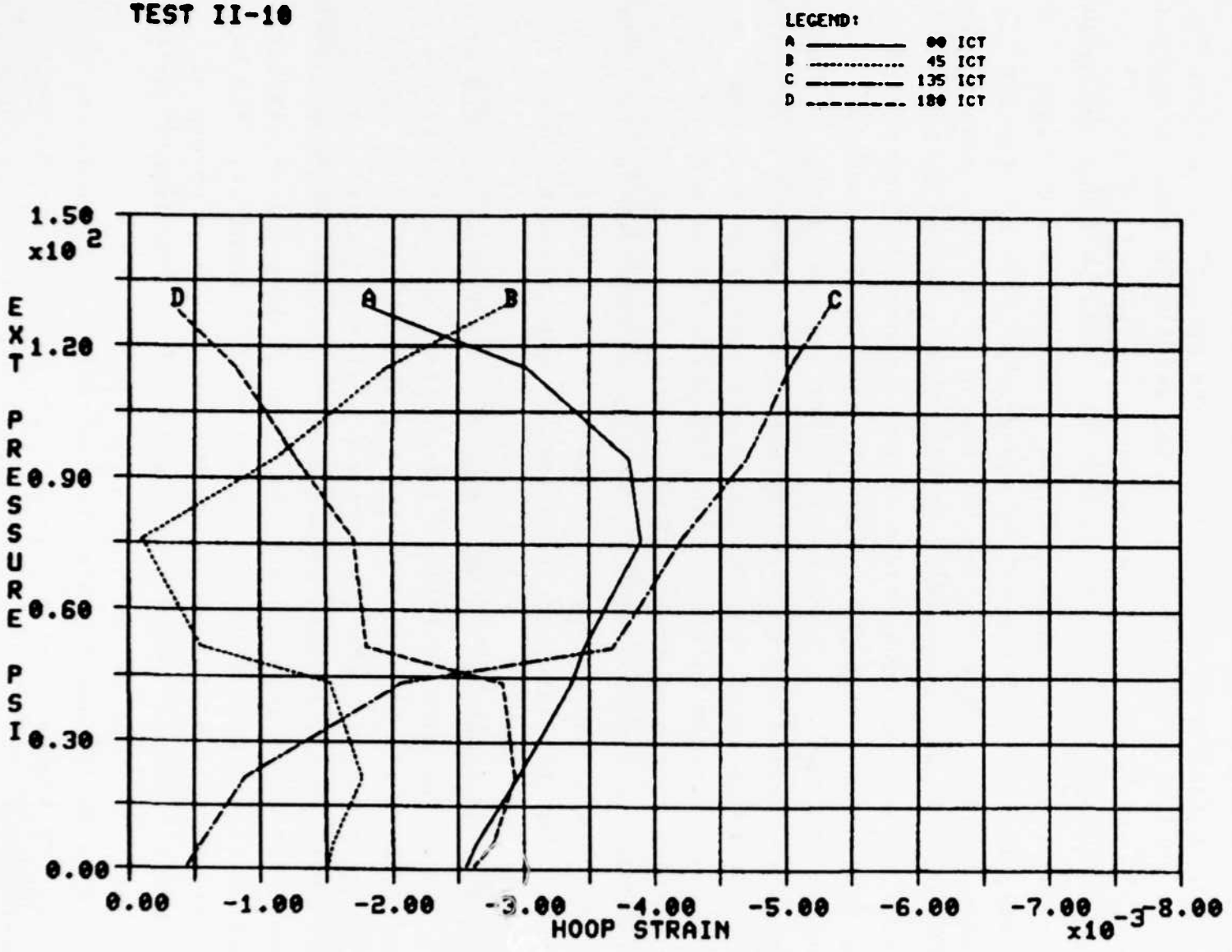

Figure 108 Plot of External Pressure vs. Internal Hoop Strain at Mid-length Around the Circumference of Test No. II-10

strain gage, axial load and pressure data were digitized via the SUN system and sent to the PDP 11/34 computer.

An initial preload of -250 lbs. was applied to specimen No. II-10. The external pressure was increased at a rate of approximately 5 psi per second. As the pressure reached 140 psi it dropped quickly to approximately 75 psi. The pressure was again increased to 175 psi where the rate of hydraulic fluid loss became excessive. The specimen was removed from the fixture and found to have fractured along the length of the wall between the 90° and 135° gage locations. The specimen appeared to have failed in buckling as a result of the compressive hoop stresses. The fracture was straight and smooth with local separation between ply layups. There was no other apparent damage to the specimen. Figure 105 is a photograph of the specimen after failure. It is believed that the first pressure drop at 140 psi is where the specimen buckled. This 140 psi external pressure is equivalent to a hoop stress of -6.10 ksi. The increase in pressure after that was retained by the gasket material on the external surface of the specimen. A review of the strain gage data reveals that the data was irregular and unintelligible after the first 140 psi peak.

Test No. II-11 was also tested with an initial preload of -250 lbs. The mode of failure was similar to Test No. II-10. The pressure was increased to 163 psi when the pressure quickly dropped to 80 psi. The pressure was again increased to 195 psi when hydraulic fluid loss became excessive. The specimen was removed from the test fixture and found to have failed similar to Test No. II-10 with a fracture along the 45° location. The external pressure of 163 psi is equivalent to a hoop stress of -7.10 ksi. Figure 106 is a photograph of the specimen after testing.

Figures 107 and 108 are plots of external pressure vs. hoop strain for the gages at mid-length around the circumference of Specimen No. II-10. This data appears to be irregular indicating poor load distribution around the specimen circumference. This

irregular loading could be the result or cause of the buckling failure. Figures 109 and 110 are plots of the external pressure vs. hoop strain at the 90° and 180° locations. These plots compare the internal and external gages. In general, it can be seen that the gage readings follow each other up to approximately 45 psi, at which time the internal and external readings oppose each other at almost equal rates. This would indicate that at individual circumferential locations there was good radial and lengthwise stress distribution up to 45 psi where bending stresses or buckling first occured. It can also be seen that at the 90° location, bending stresses started to reverse at 75 psi. This would also indicate buckling in the specimen wall. As a result of Poisson's effect, the axial strain readings show respective data. Figure 111 and 112 are plots of external pressure vs. axial strain for Test No. II-10. The data is not sufficient to accurately evaluate the amount of barreling or hourglassing of the specimen. It should also be noted that some of the gage elements for Test No. II-10 failed to produce a signal.

Figures 113 and 114 are plots of external pressure vs. hoop strain for Test No. II-11. After comparing the magnitude and opposing signs between the two plots it can be seen that bending stresses were present from the start of the test. Note, however, that the bending has opposite signs between the 90° and 180° locations. Figures 115 and 116 are plots of external pressure vs. axial strain. These plots also show some indication of bending stresses with opposite signs between the 90° and 180° locations.

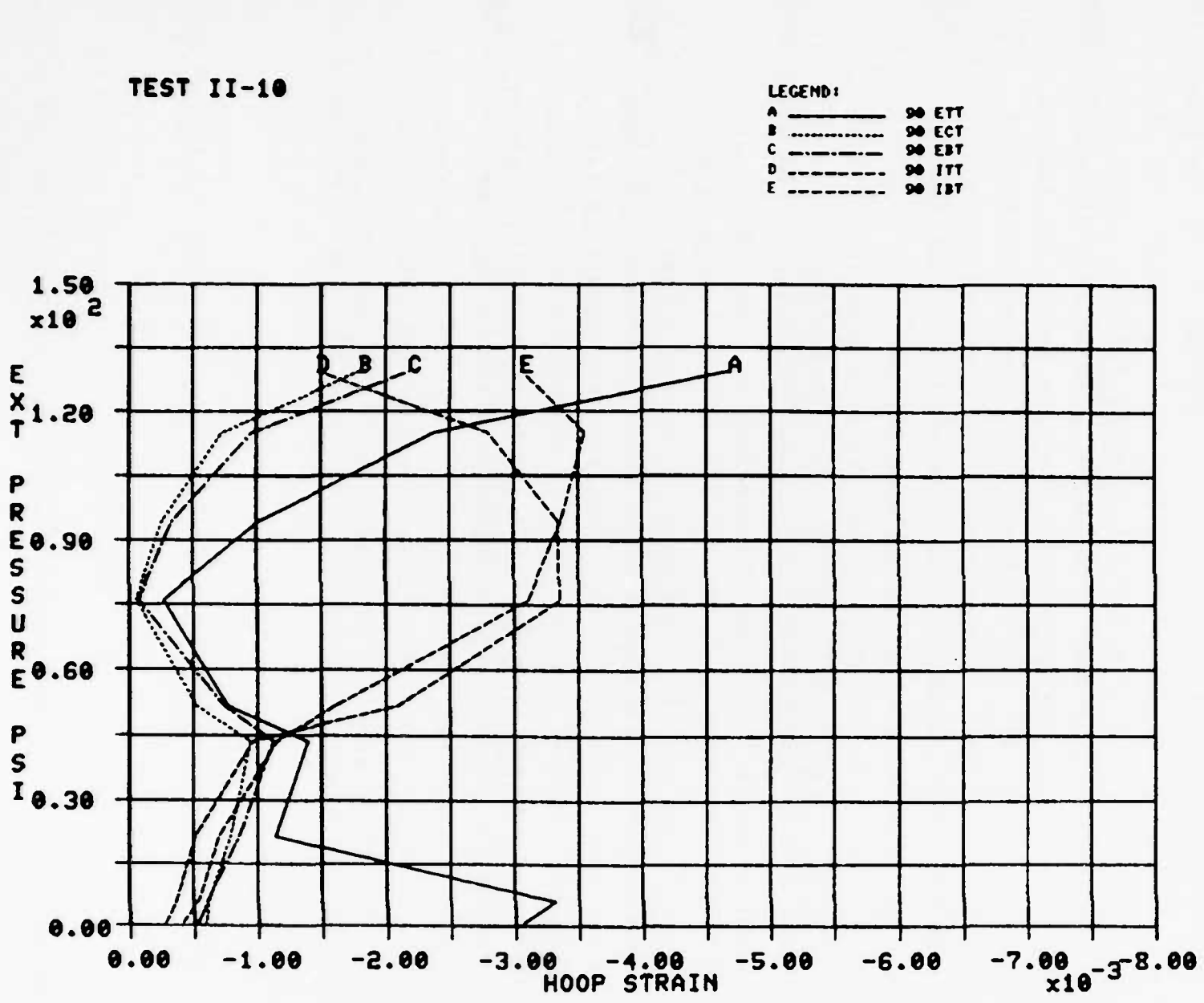

Figure 109 Plot of External Pressure vs. Hoop Strain at the 90° Location of Test No. II-10

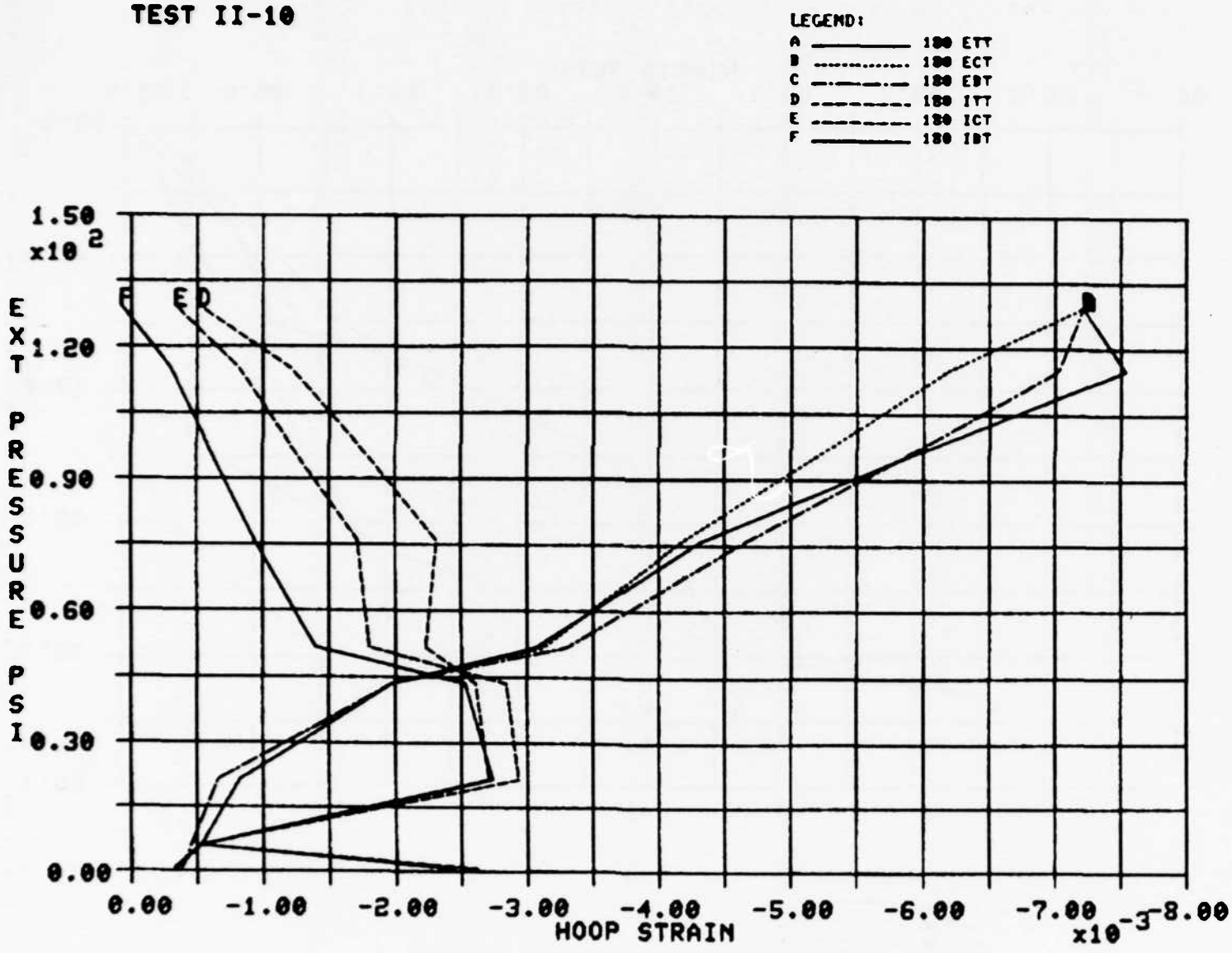

Figure 110 Plot of External Pressure vs. Hoop Strain at the 180° Location of Test No. II-10

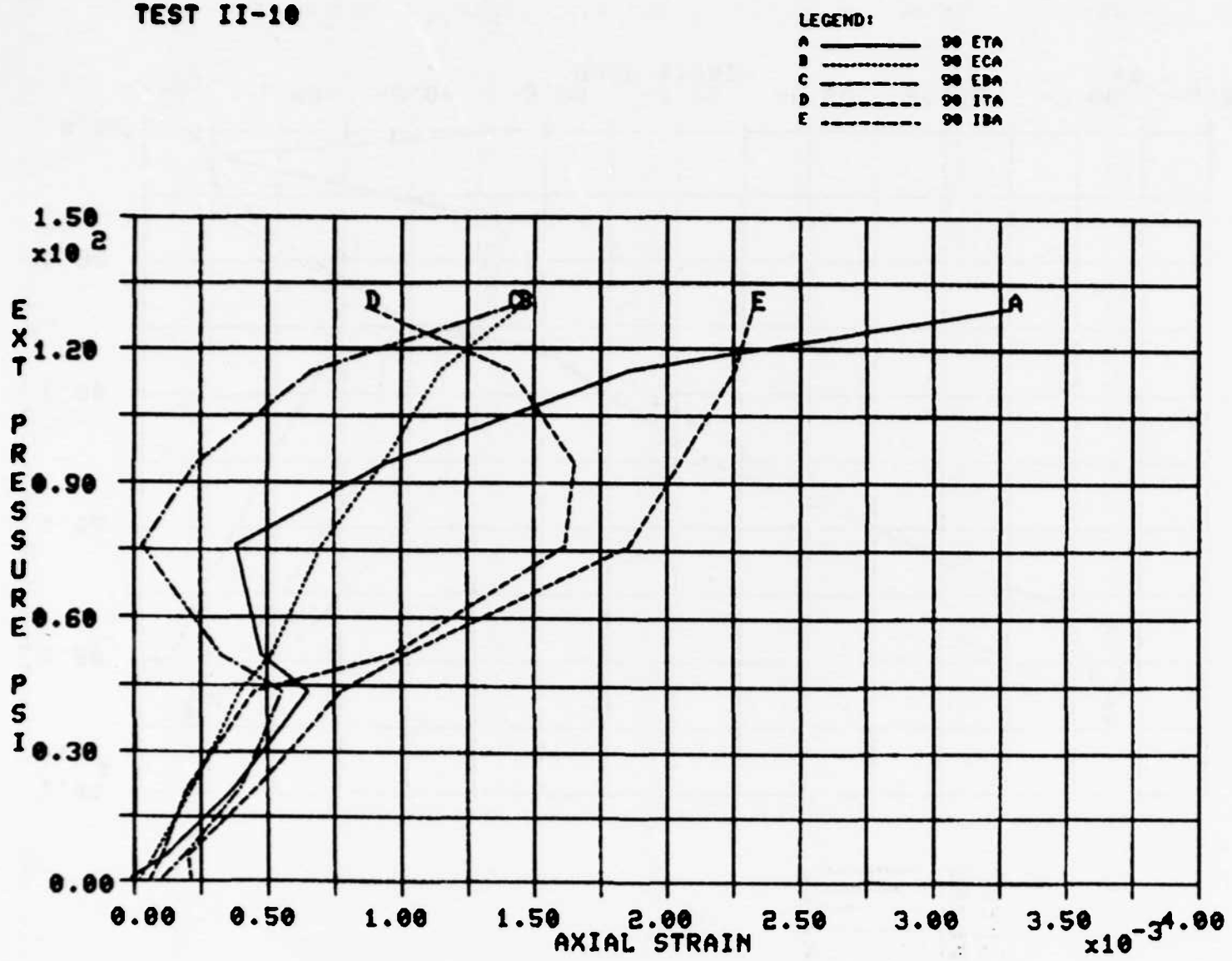

Figure 111 Plot of External Pressure vs. Axial Strain at the 90° Location for Test No. II-10

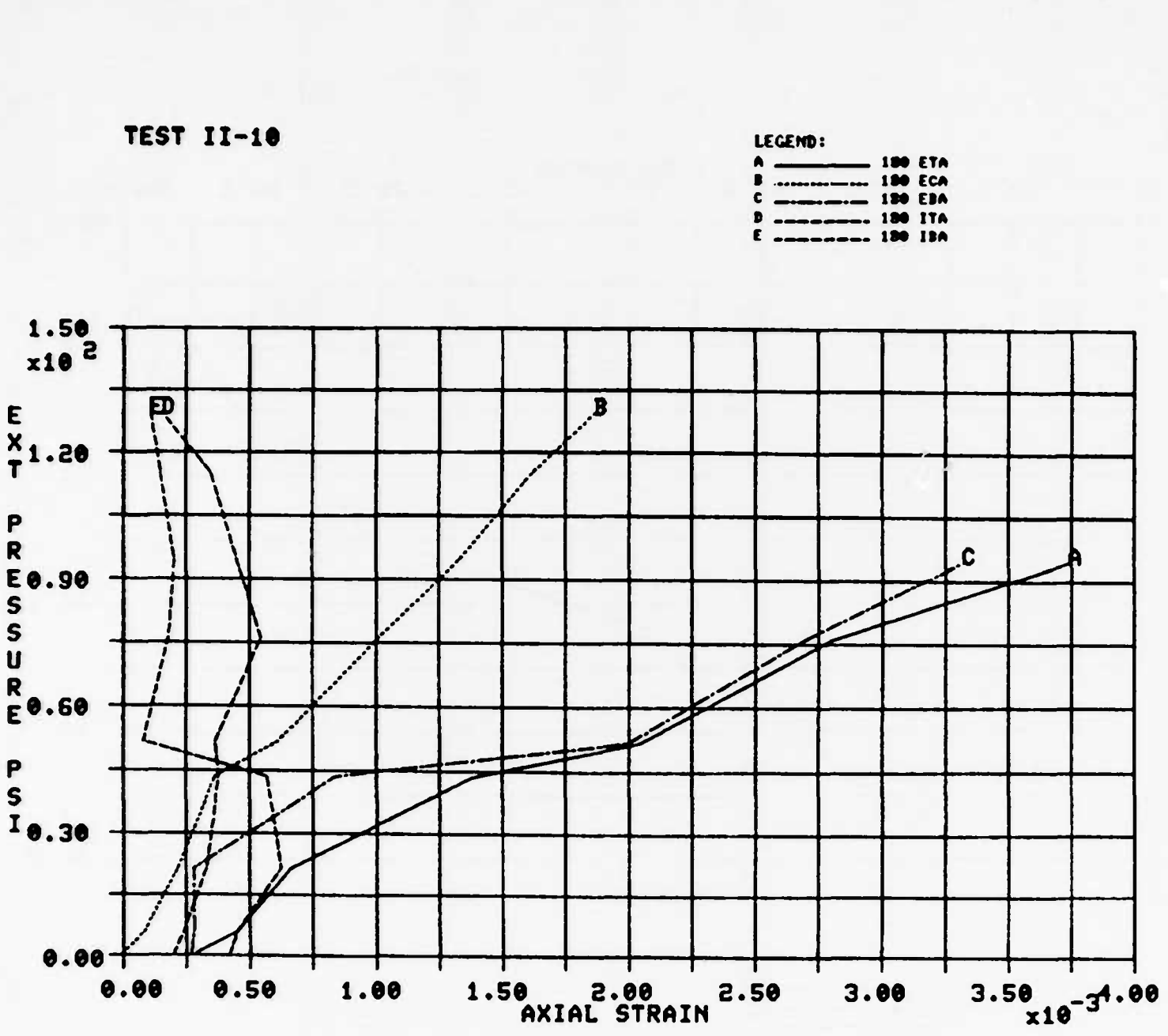

Figure 112 Plot of External Pressure vs. Axial Strain at the 180° Location for Test No. II-10

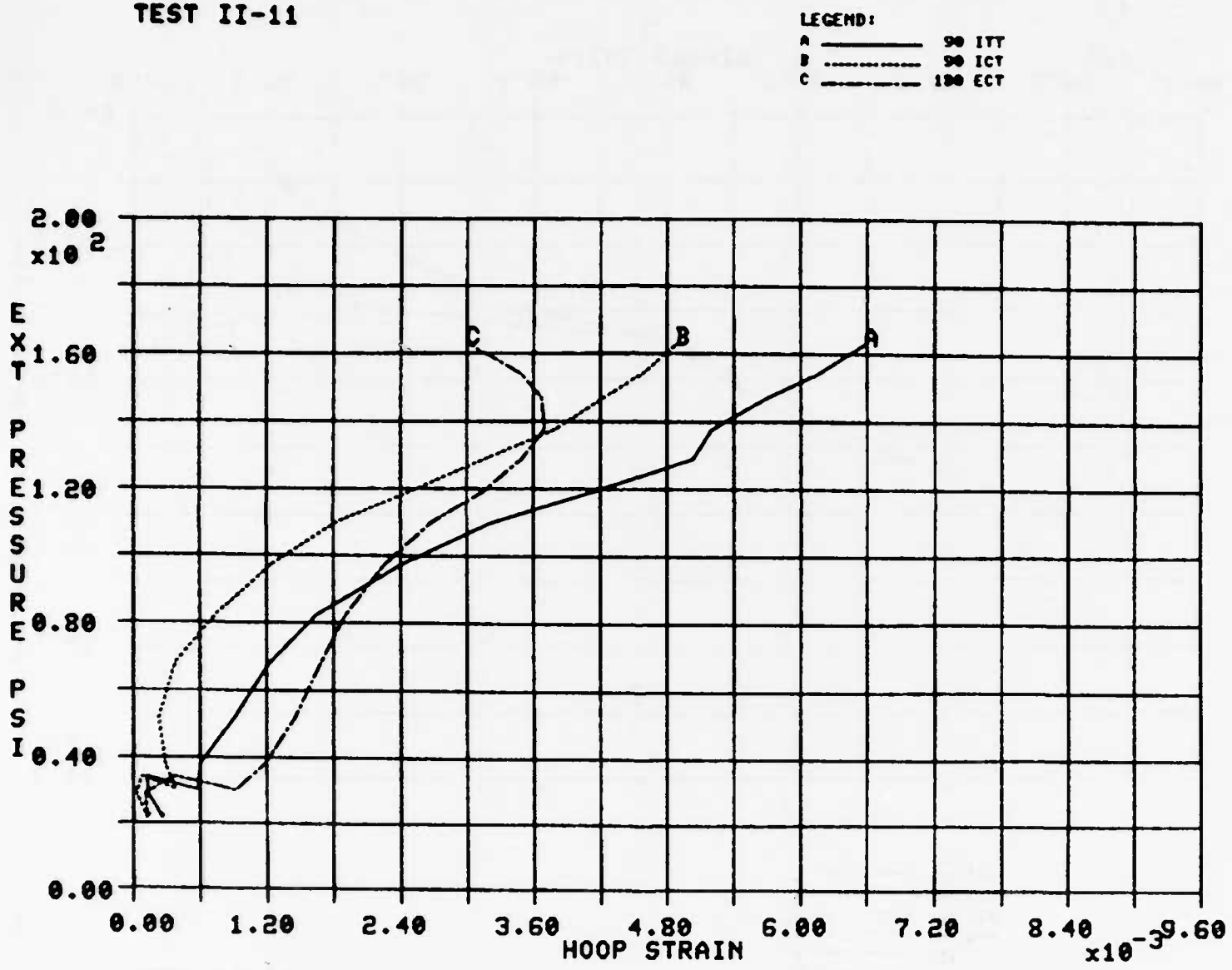

Figure 113 Plot of External Pressure vs. Hoop Strain for Test No. II-11

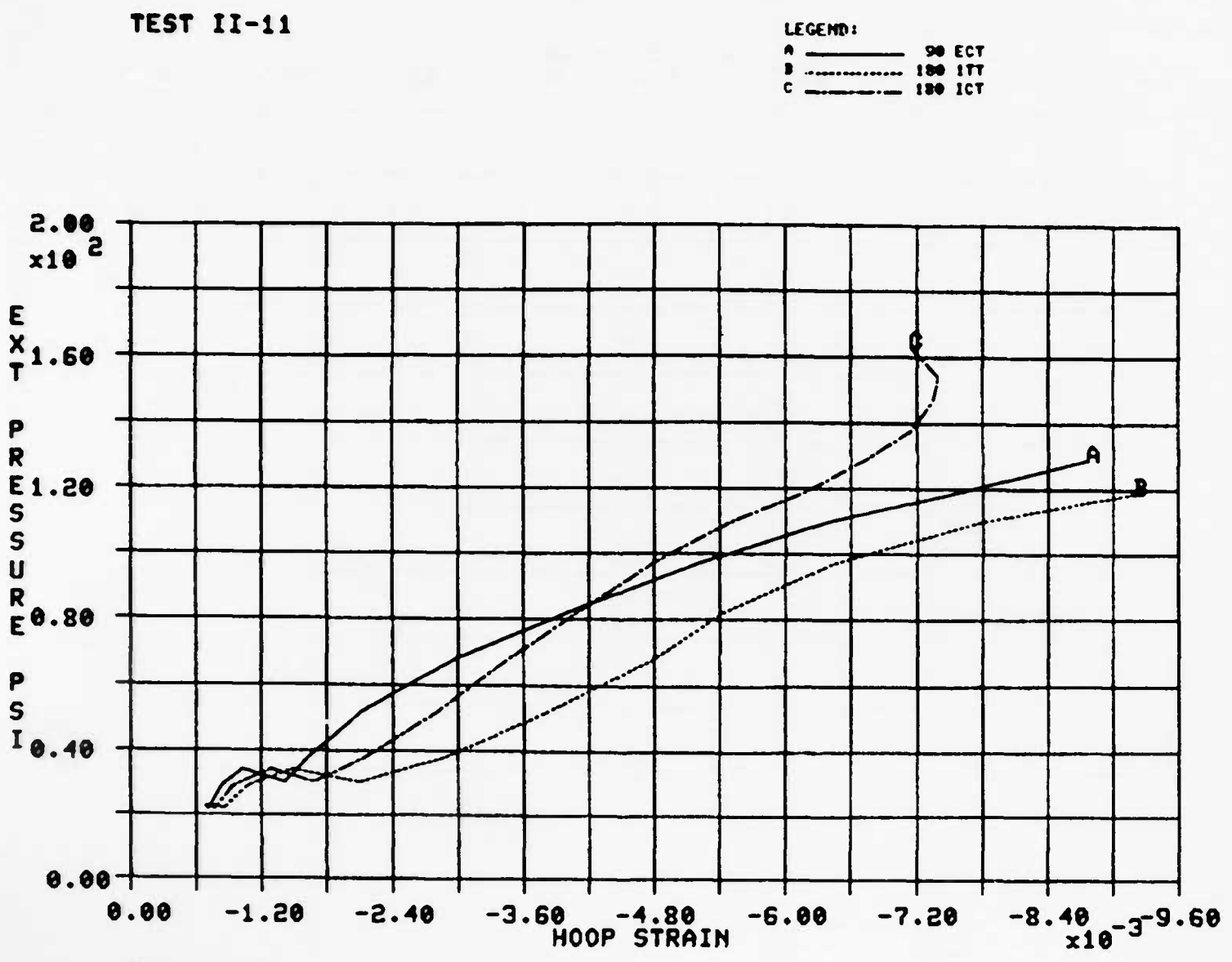

Figure 114 Plot of External Pressure vs. Hoop Strain for Test No. II-11

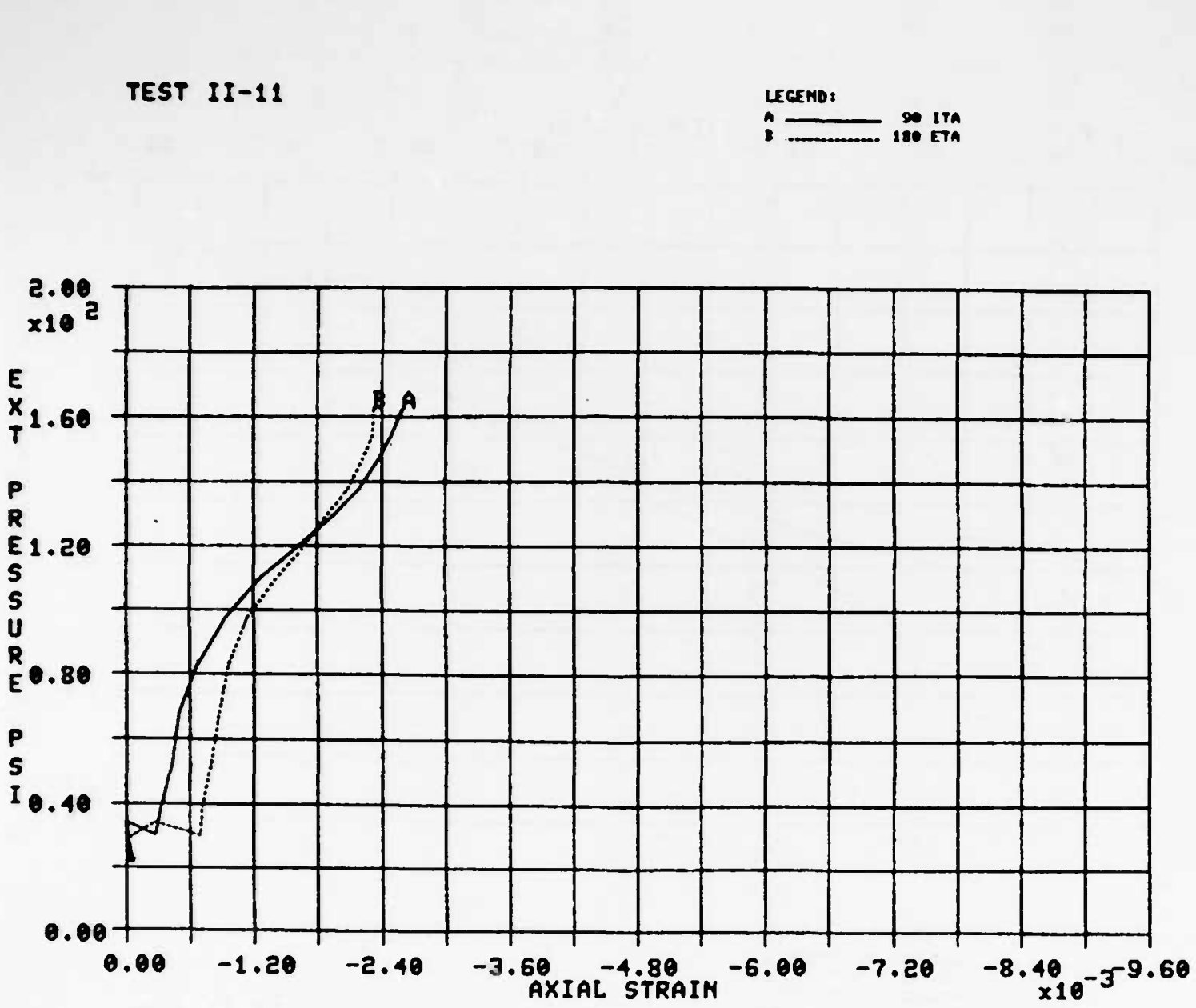

Figure 115 Plot of External Pressure vs. Axial Strain for Test No. II-11

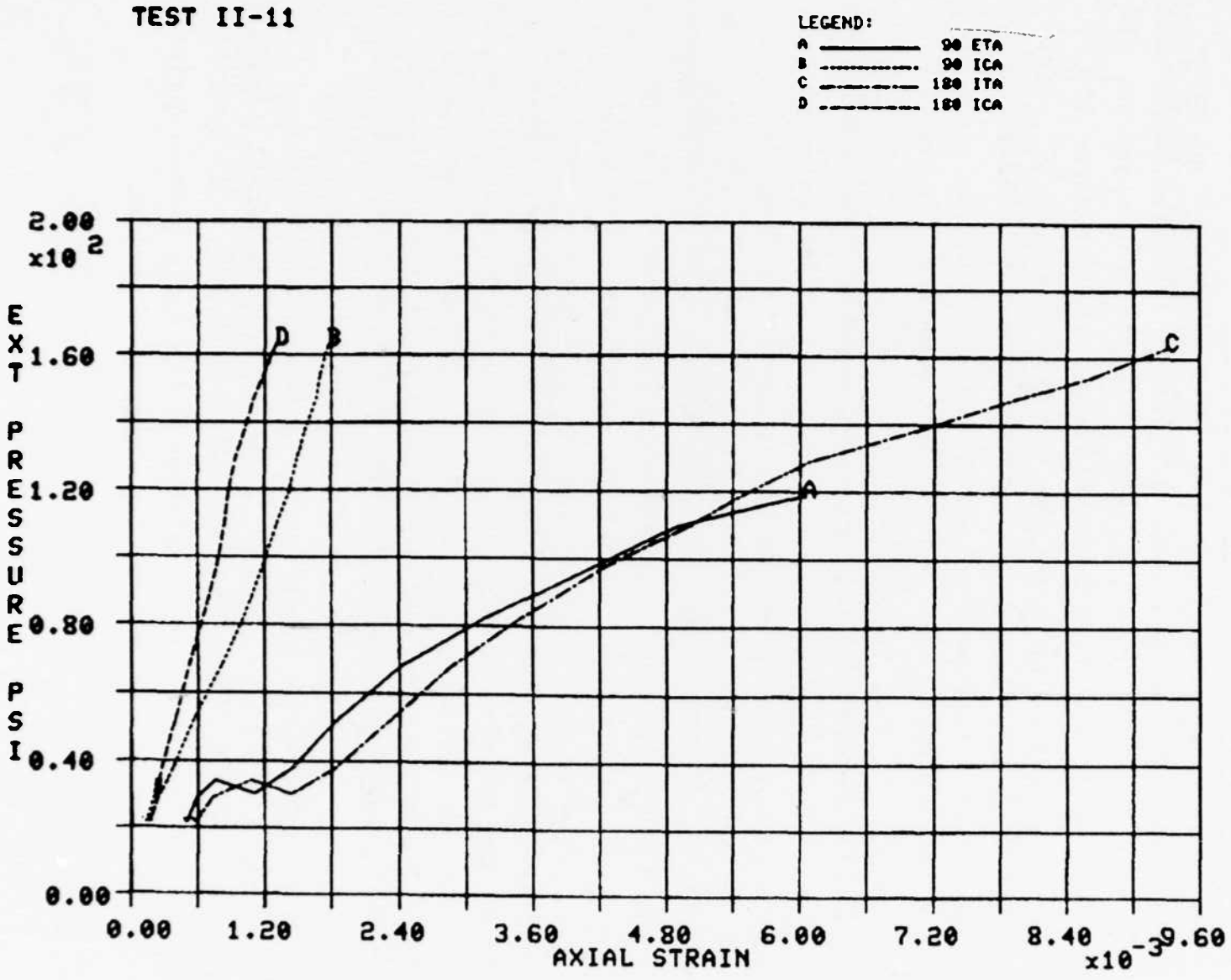

Figure 116 Plot of External Pressure vs. Axial Strain for Test No. II-11

IX EXTERNAL PRESSURE PLUS AXIAL LOAD TESTS

Two instrumented specimens were tested with external pressure plus axial compressive load. These were Test Nos. II-12 and II-13. Both specimens were 2 inches in length. Specimen No. II-12 was instrumented with forty strain gage elements using the gage layout listed in Table 8. The gages were spaced 45° apart around the circumference of the specimen. Specimen No. II-13 was instrumented with twelve strain gage elements using the gage layout listed in Table 12. The gages were at the 90° and 180° locations.

As in previous tests performed with external pressure only, special-made rubber gasket material was used on the external specimen surface as well as the lead/polyethelene/lead sandwich gasket lubrication at the platen surfaces. The external pressure collet was also utilized for external pressurization. The axial load and external pressure signals were both sent to the MTS controller through two variable gain amplifiers. The amplifier gain was adjusted such that the system would produce the correct ratio between axial and hoop stresses plus the force required to overcome the pressure load acting on the external surface area of the platens inside the pressure collet. The strain gage, axial load, and pressure data were digitized via the SUN system and sent to the PDP 11/34 computer.

The external pressure and compressive axial load were applied simultaneously producing a biaxial stress condition. Figures 117 and 118 are plots of axial load vs. external pressure for the two tests. Using the specimen geometry of 3.92 inch diameter and 0.045 inch wall thickness, the ratio between axial stress (σ_x) and hoop stress (σ_θ) is calculated as

$$\frac{-\sigma_x}{\sigma_\theta} = 1.01, \text{ Test No. II-12}$$

$$\frac{-\sigma_x}{\sigma_\theta} = 1.18, \text{ Test No. II-13}$$

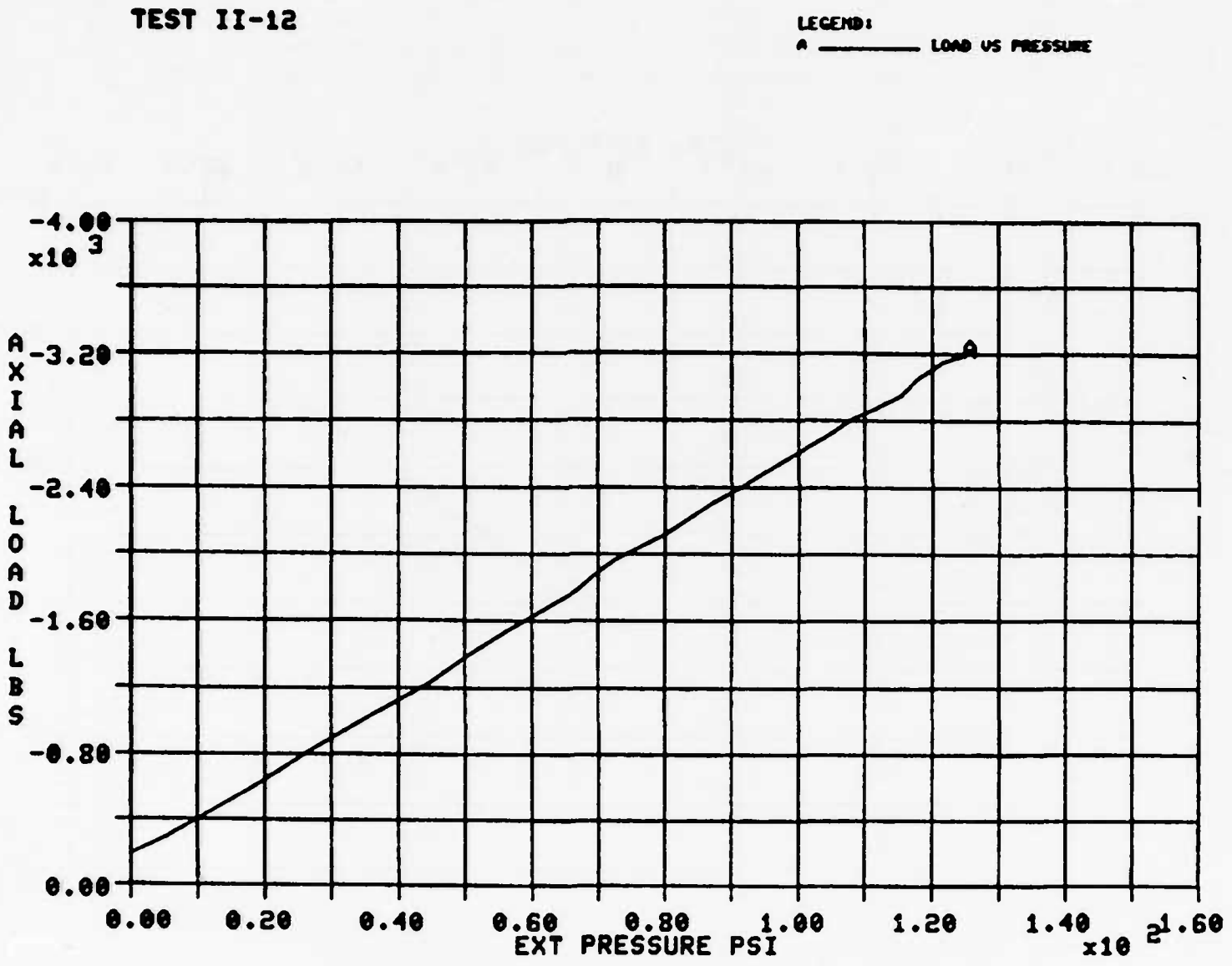

Figure 117 Plot of Axial Load vs. External Pressure for Test No. II-12

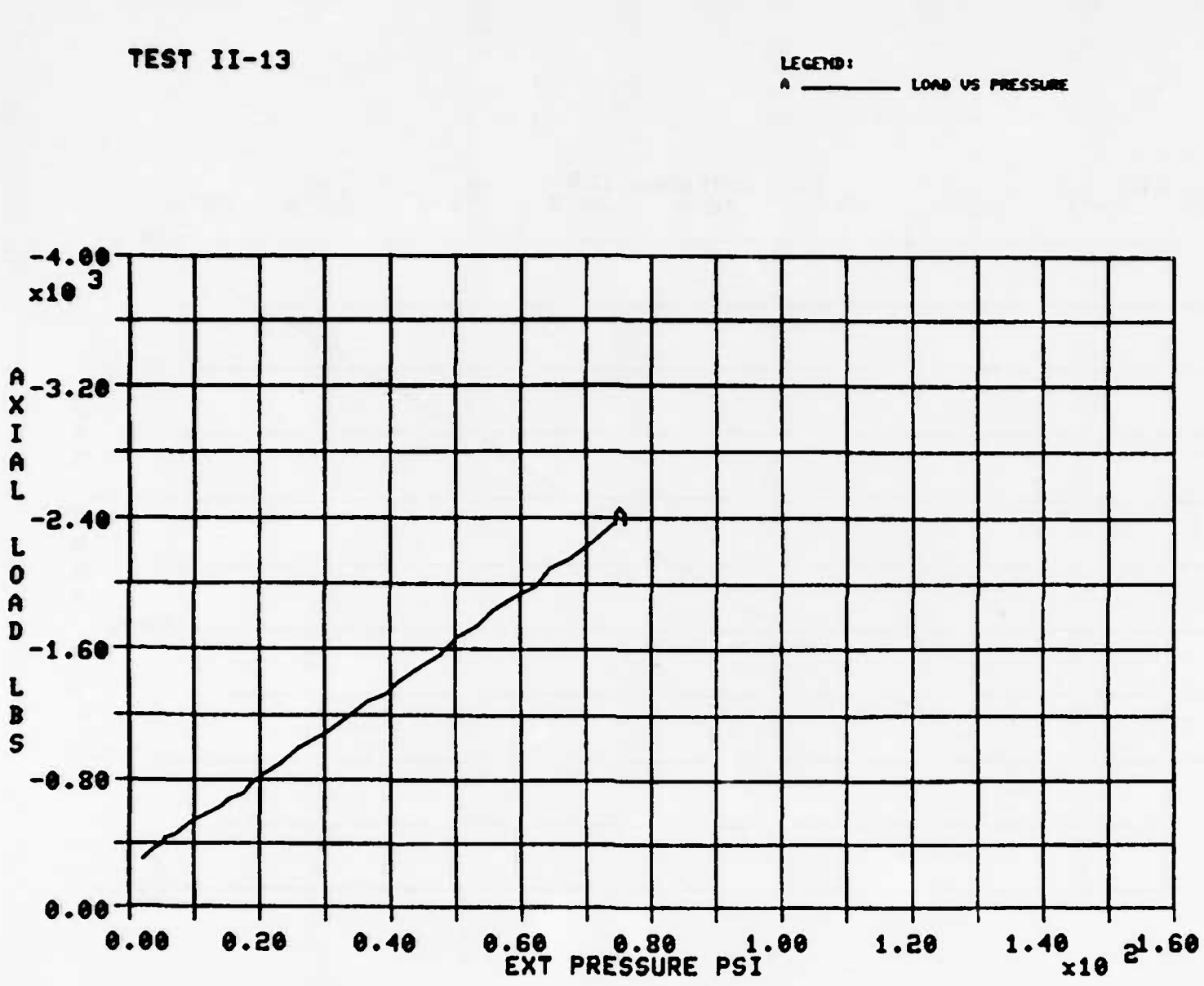

Figure 118 Plot of Axial Load vs. External Pressure for Test No. II-13

Both the axial and hoop stresses were compressive. Also, an axial preload of -250 lbs. was applied to both specimens. This preload produces the seal necessary for external pressurization and is equivalent to an initial axial stress of -0.45 ksi.

The external pressure was applied manually at an increasing rate of approximately 5 psi per second. The MTS system applied the axial load accordingly. As the pressure on Test No. II-12 reached 135 psi it became difficult to control. The load vs. strain gage data became very irregular after approximately 120 psi. It is suspected that the specimen started to fail at this load. The corresponding axial load at 120 psi was 3,200 lbs. This is equivalent to a hoop stress (σ_θ) of -5.23 ksi and an axial stress (σ_x) of -5.78 ksi. The maximum pressure obtained before losing the pressure seal was 175 psi. After testing Specimen No. II-12 it was removed from the test fixture and found to have failed in buckling as a result of compressive hoop stresses. The specimen had fractured through the wall at the 270° gage location. The fracture left some local separation between ply layups. There was no apparent damage resulting from axial stresses. Test No. II-13 had a similar failure mode to Test No. II-12. As the pressure reached 75 psi it became difficult to control and irregular. The maximum pressure obtained was 160 psi before losing the pressure seal. After a review of the data it appears that the specimen failed with an external pressure of 75 psi and an axial load of -2,400 lbs. This corresponds to an axial stress (σ_x) of -4.33 ksi and a hoop stress (σ_θ) of -3.27 ksi. After the test, Specimen II-13 was removed from the test fixture. The damage was similar to Test No. II-12. Photographs of the specimens after testing are given in Figures 119 and 120.

Figures 121 through 124 are plots of external pressure vs. hoop strain and axial load vs. axial strain for Test Nos. II-12 and II-13. From this data the loading appears to be very irregular. Also, the axial strain data goes from negative to positive. This is in contradiction to the applied axial compressive load.

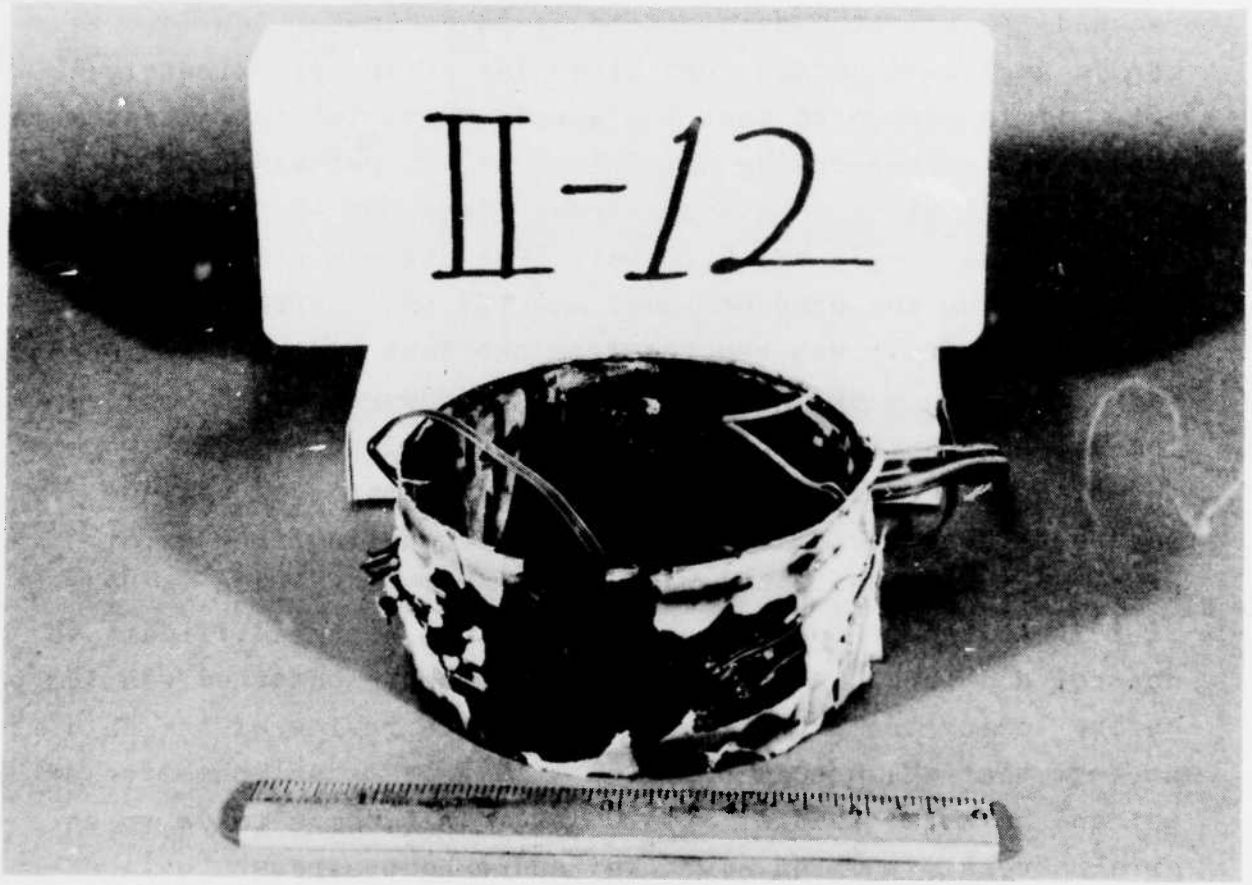

Figure 119 Photograph of Specimen No. II-12 After Testing

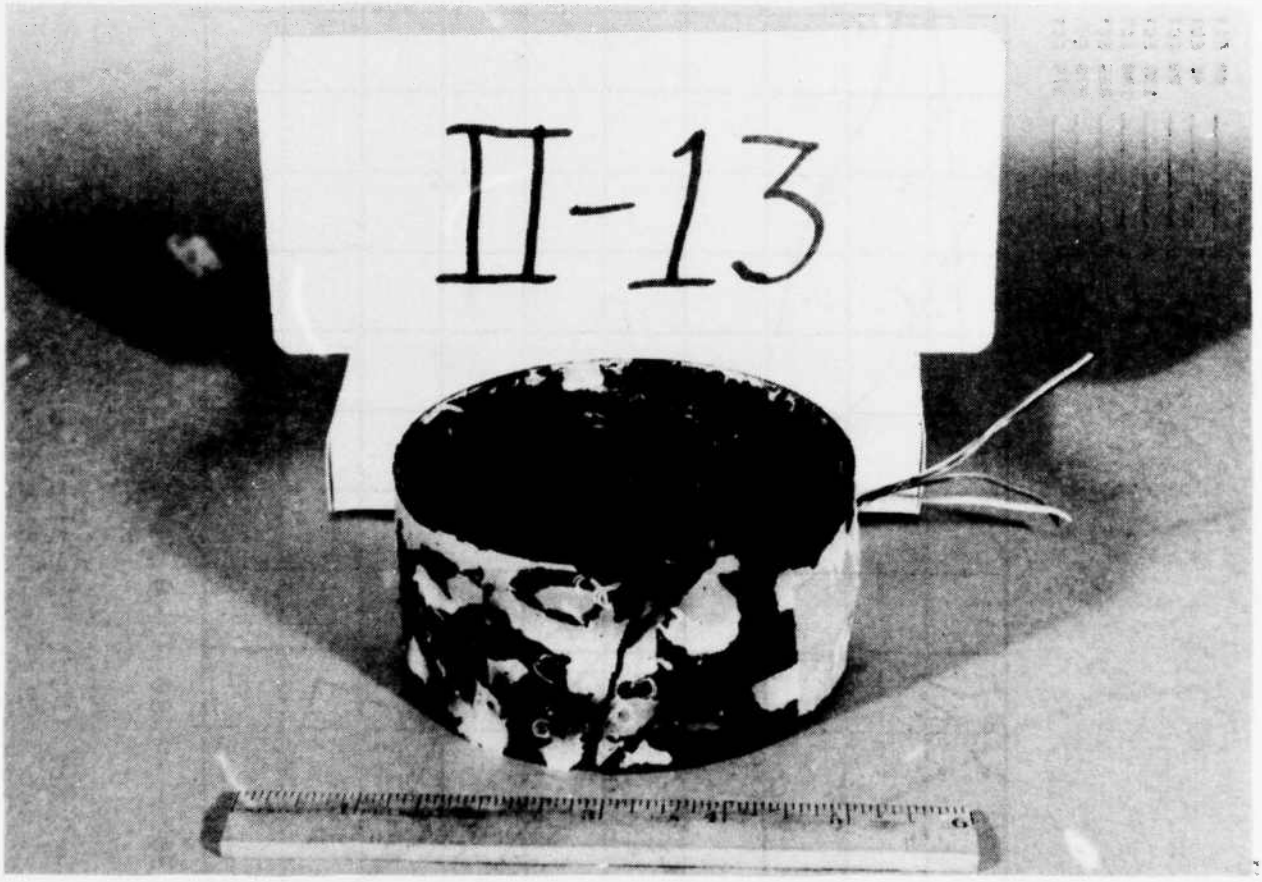

Figure 120 Photograph of Specimen No. II-13 After Testing

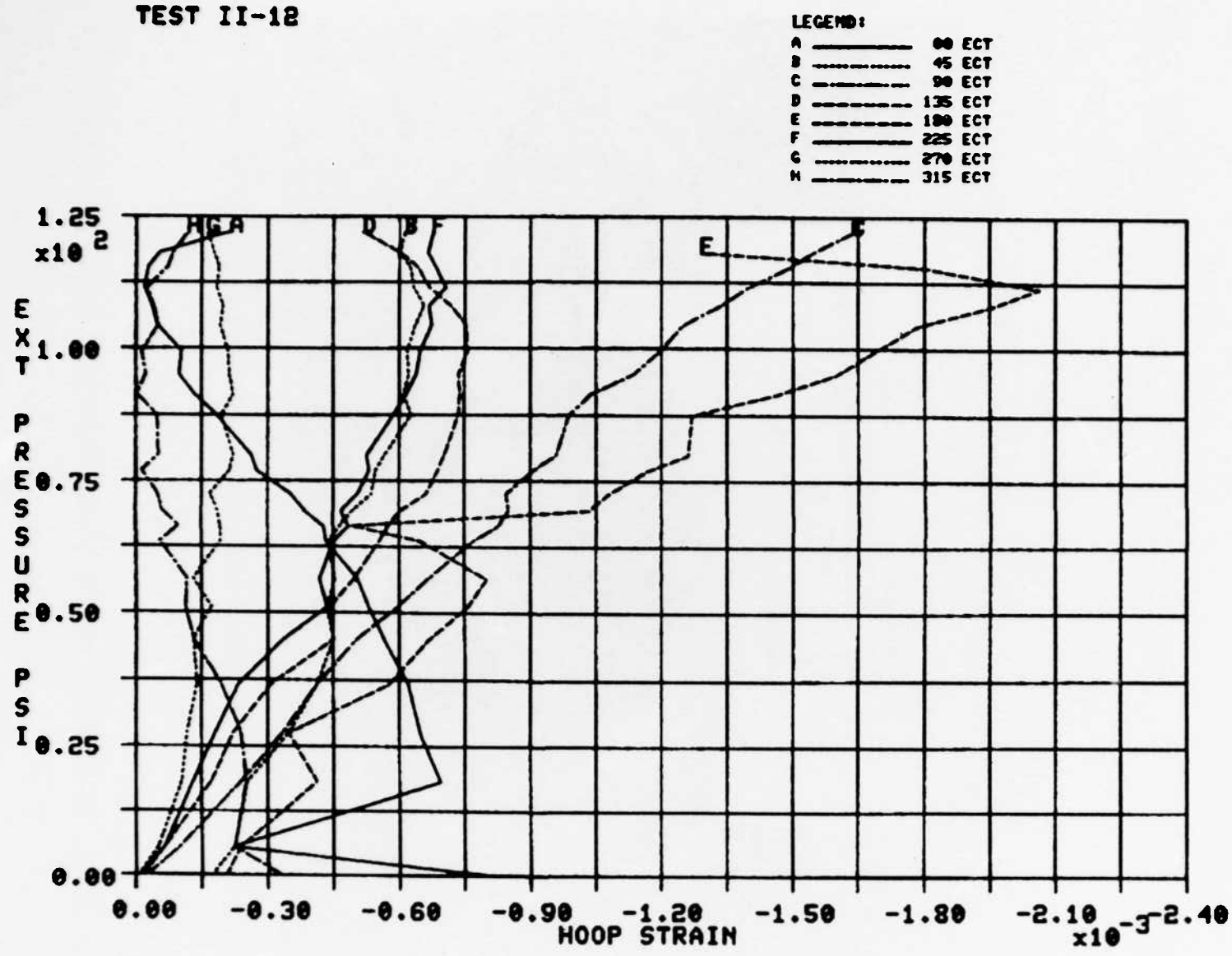

Figure 121 Plot of External Pressure vs. Hoop Strain at Mid-length Around the Circumference of Test No. II-12

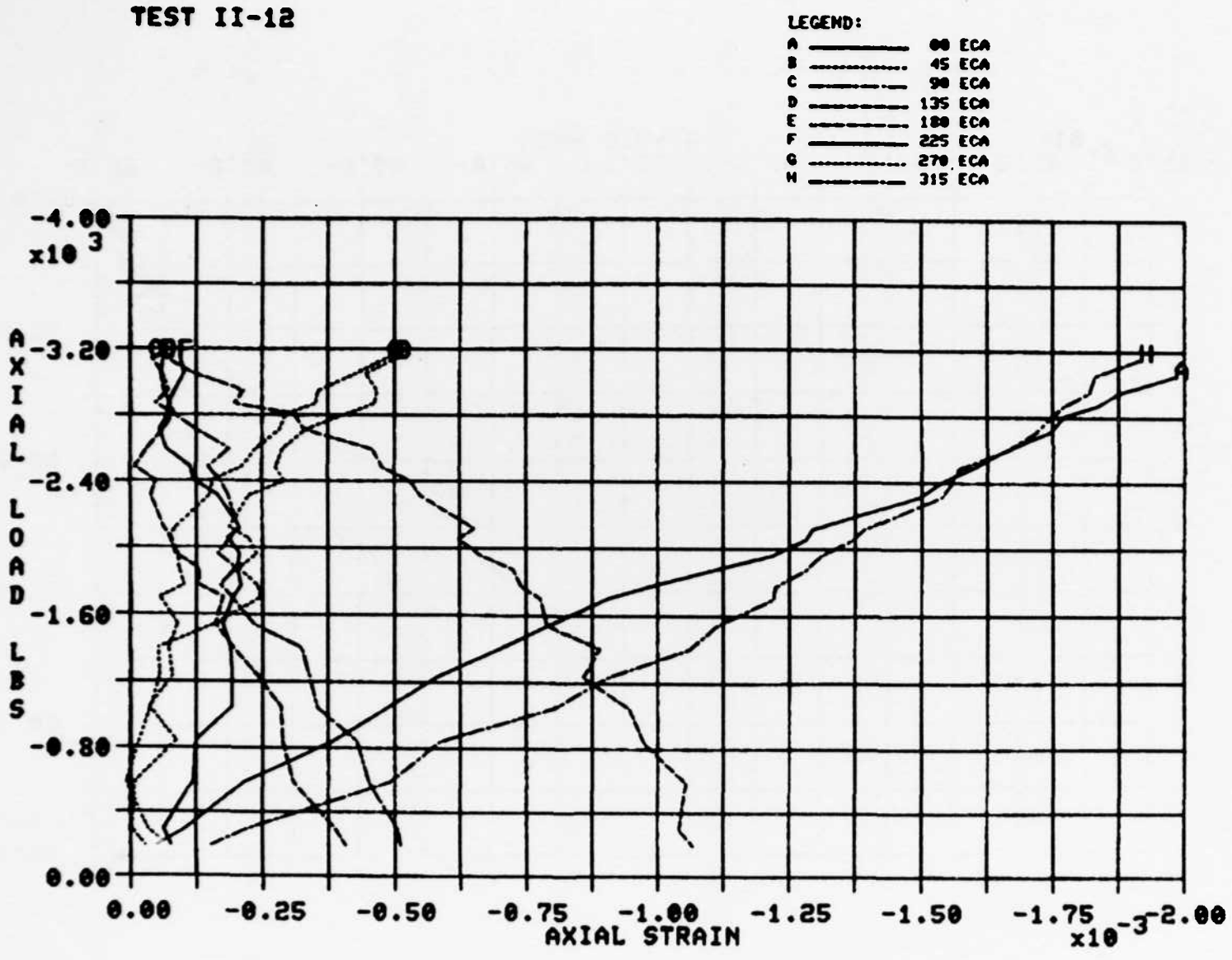

Figure 122 Plot of Axial Load vs. Axial Strain at Mid-length Around the Circumference of Test No. II-12

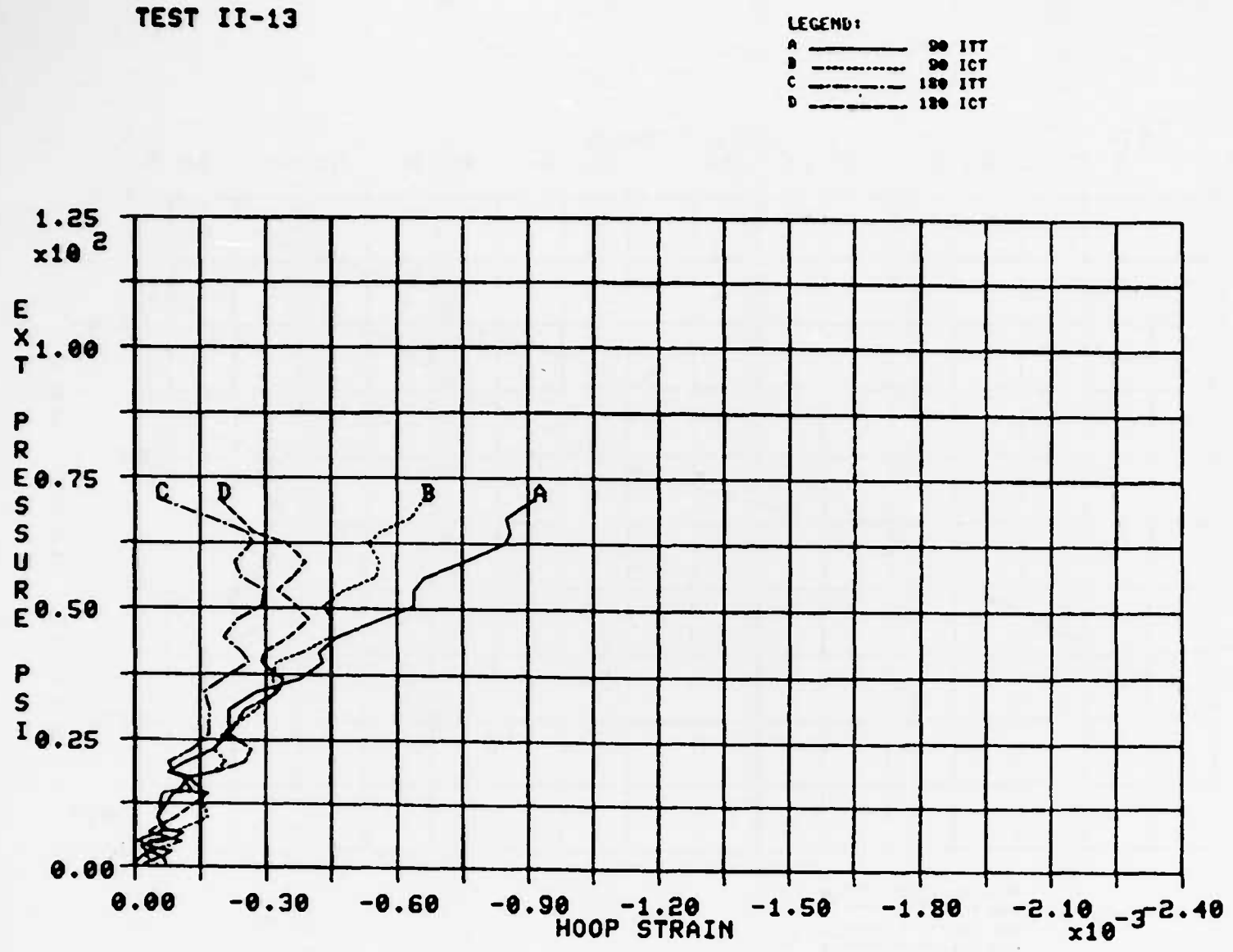

Figure 123 Plot of External Pressure vs. Hoop Strain for Test No. II-13

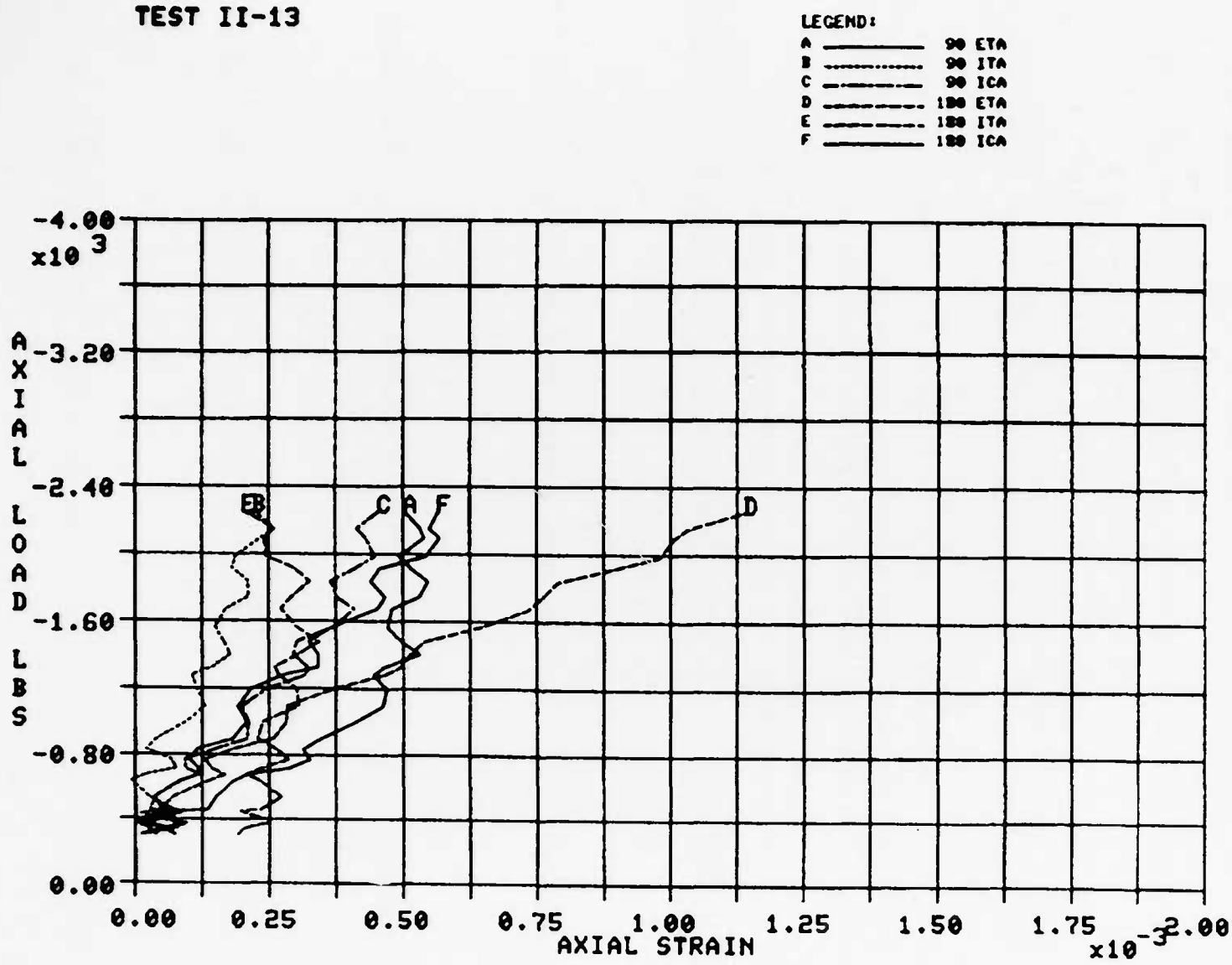

Figure 124 Plot of Axial Load vs. Axial Strain for Test No. II-13

With nearly equal stresses in the axial and hoop directions, this positive-going axial strain data could be the result of a slightly greater Poisson's ratio with respect to hoop stress than axial stress. This is only possible becaus the Poisson's ratio in both directions is very close to unity. The Poisson's ratios were measured previously with uniaxial loads applied. Figures 125 through 128 are plots of external pressure vs. hoop strain and axial load vs. axial strain at the 90° and 180° locations of Test No. II-12. In general, this data indicates the specimen was barreling under load. The hoop strain is more compressive at the ends than at mid-length. The axial strain on the external surface has a faster positive going rate than the internal surface. This was not expected with external pressure loads applied.

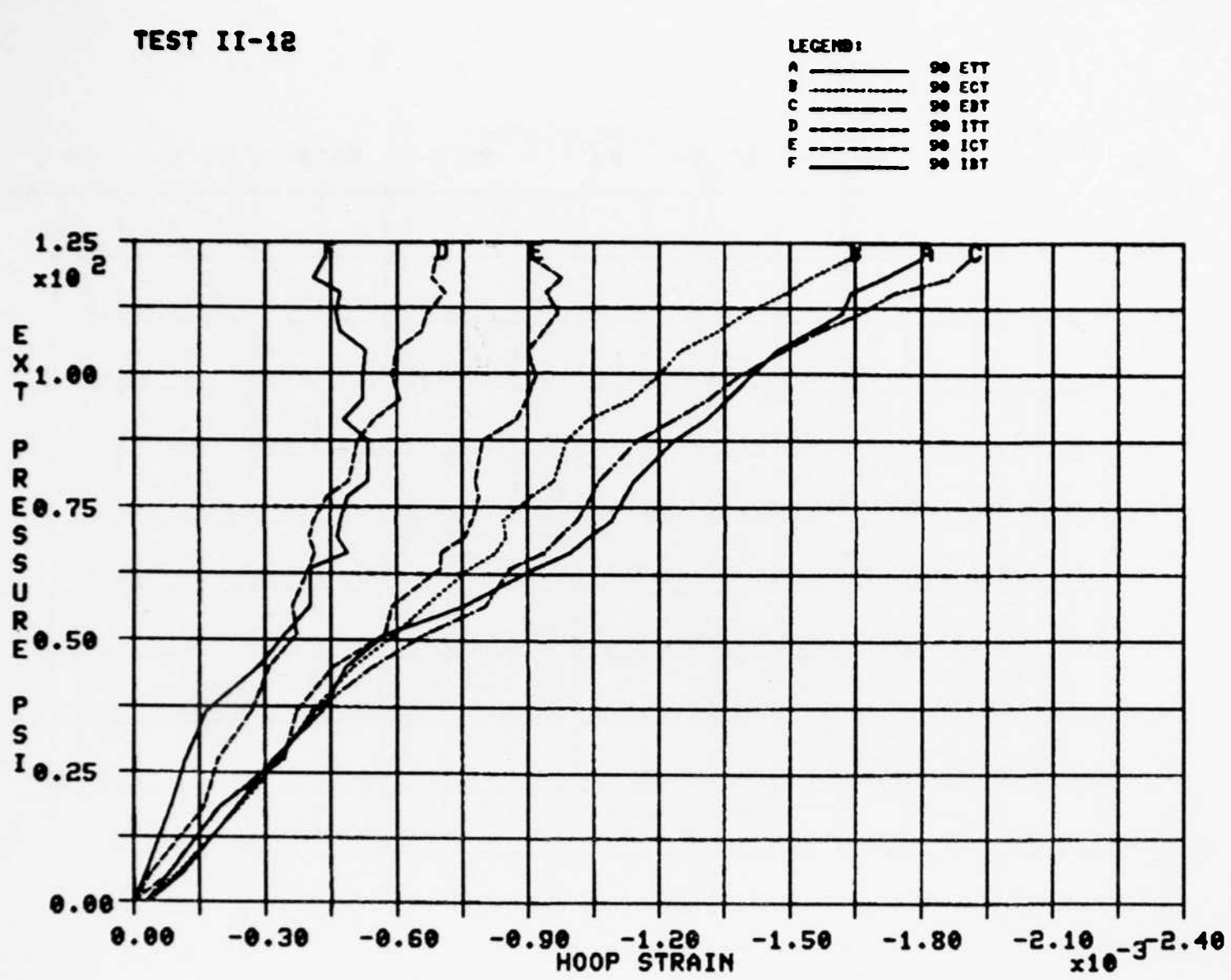

Figure 125 Plot of External Pressure vs. Hoop Strain at the 90° Location for Test No. II-12

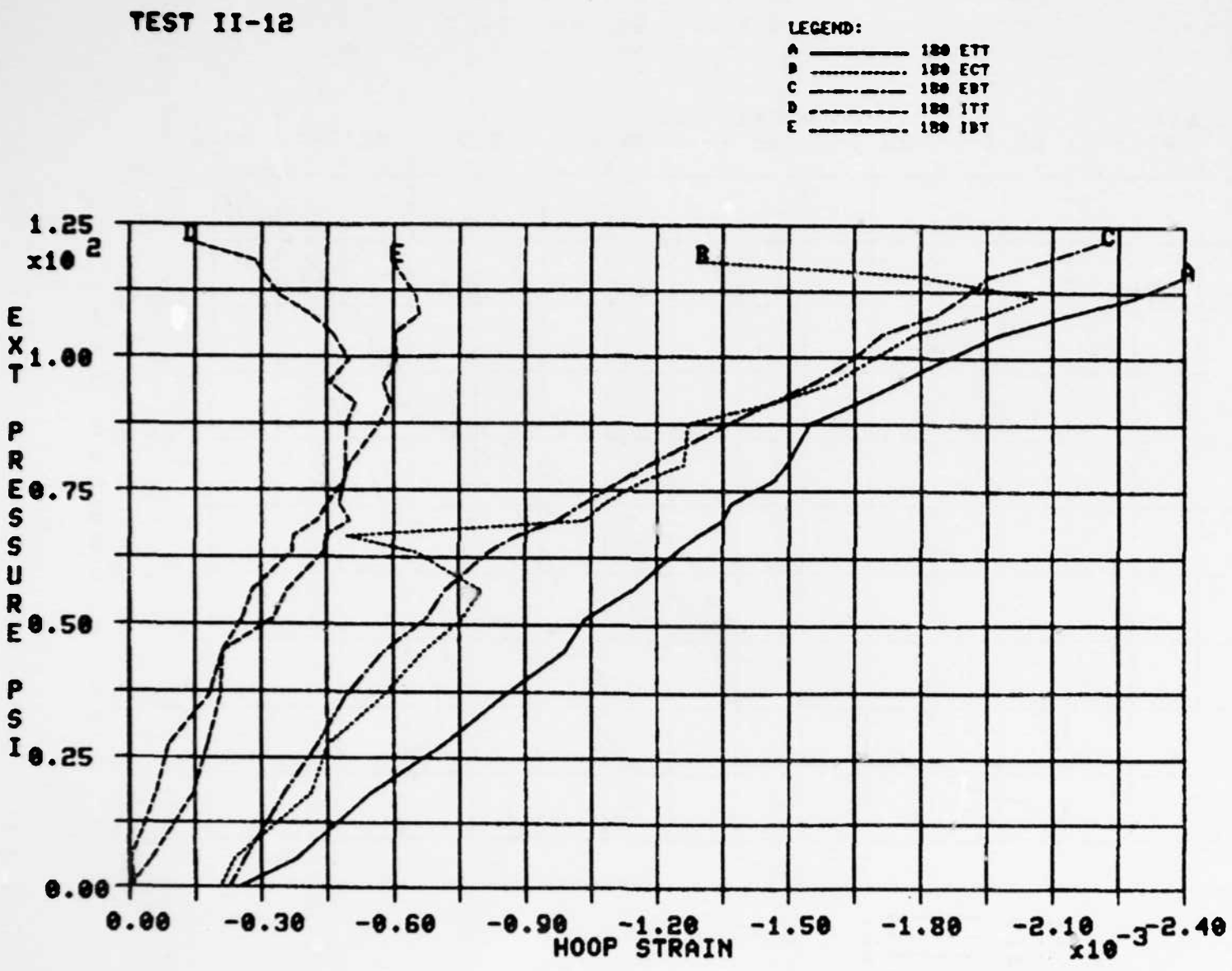

Figure 126 Plot of External Pressure vs. Hoop Strain at the 180° Location for Test No. II-12

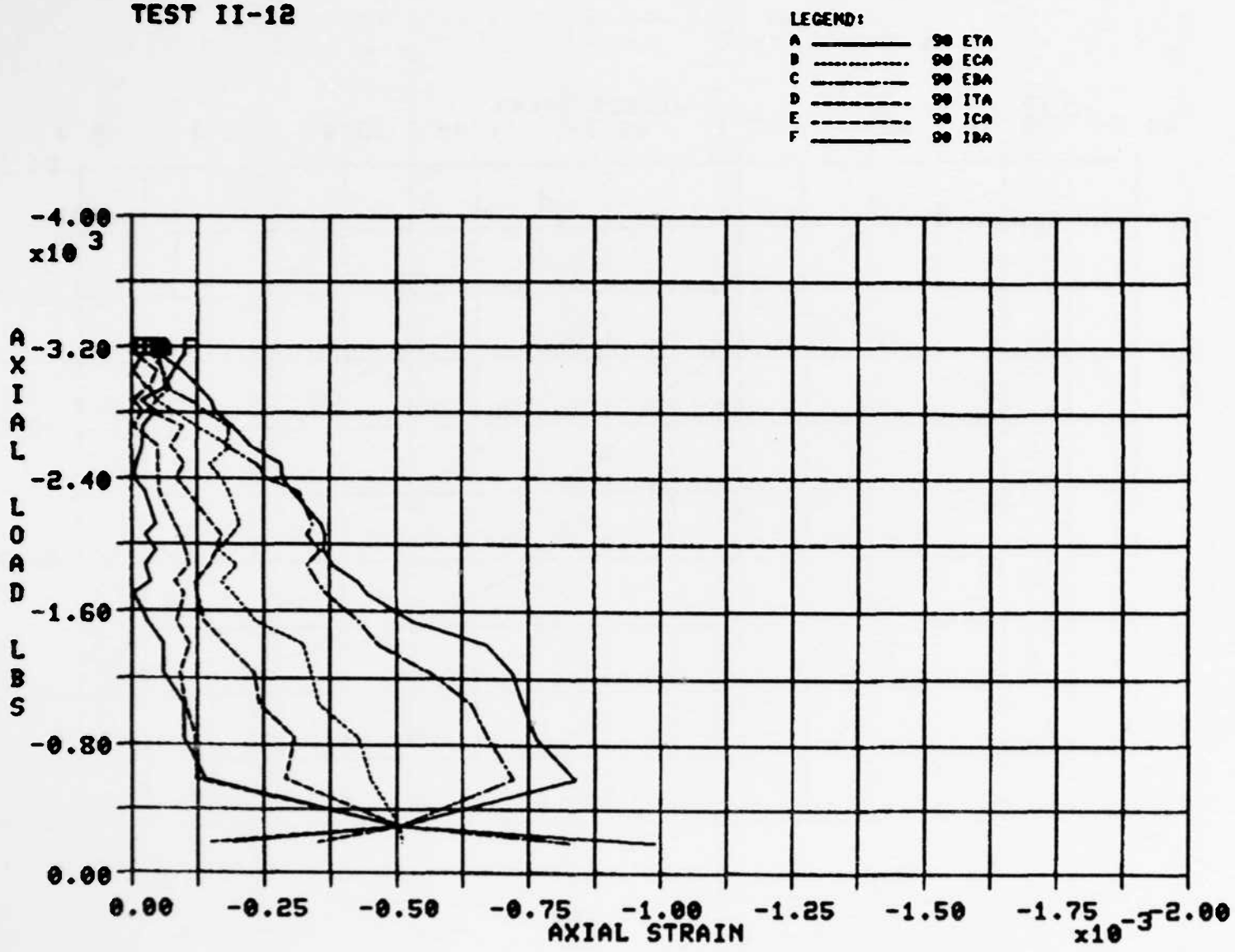

Figure 127 Plot of Axial Load vs. Axial Strain at the 90° Location for Test No. II-12

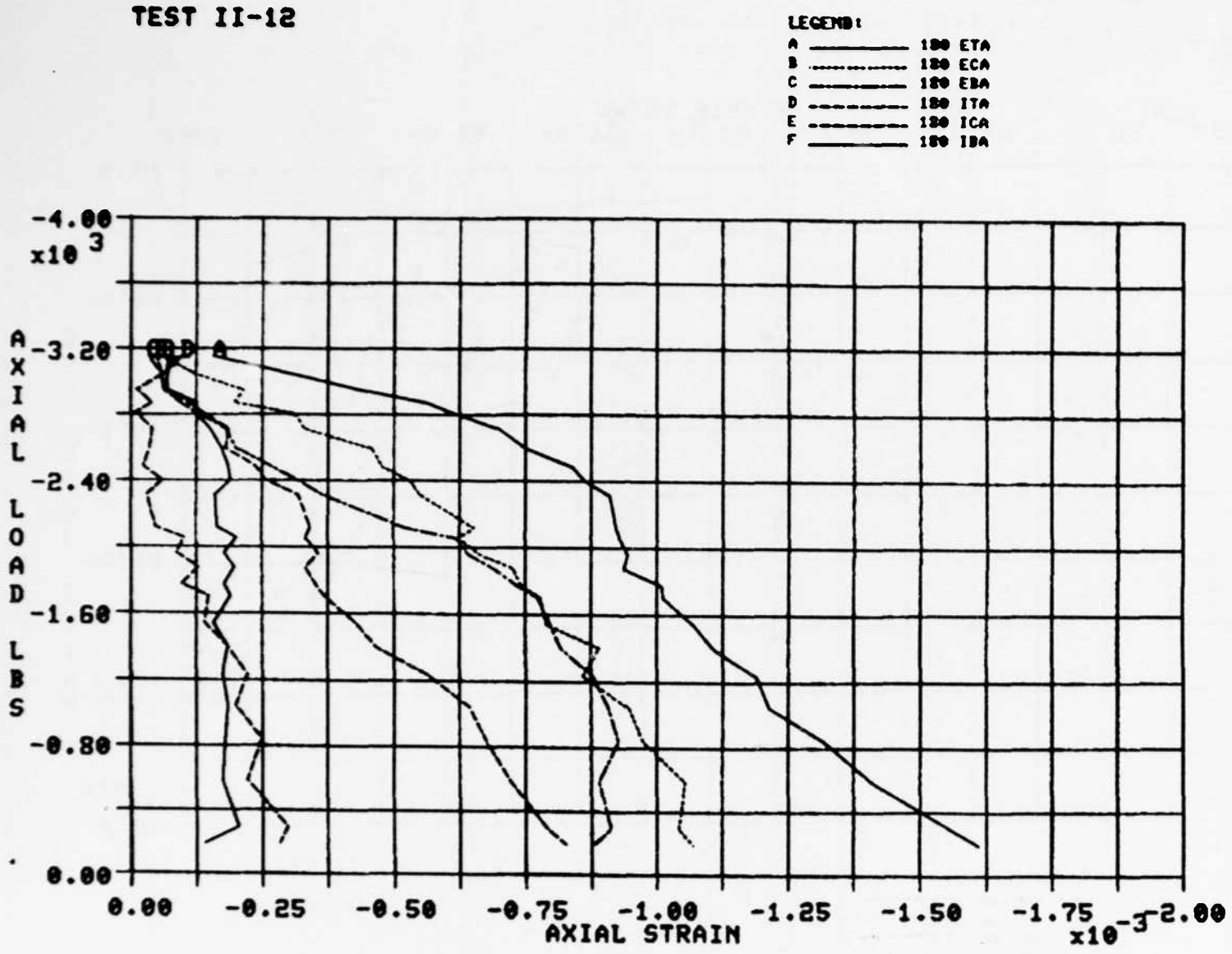

Figure 128 Plot of Axial Load vs. Axial Strain at the 180° Location for Test No. II-12

X. CONCLUSIONS

In the process of this evaluation many of the original problems with the test procedure have been solved; however, some new questions as well as old ones have not been resolved. In general, the system works well on specimens loaded with axial loads and internal pressure. Also, there seems to be no problem testing materials with high Poisson's ratios. There are many problems testing specimens with external pressure. Primarily the problem is premature buckling of the specimen due to compressive hoop stresses. This is a result of the specimen's geometry. In addition, installation of the external pressure collet is extremely difficult when the specimens are instrumented with external gages.

The system is best suited for testing specimens with internal pressure only. These test results indicated the best stress distribution for all the testing. The specimen installation and setup procedure is also very easy and simple. The lead/-polyethelene/lead gasket seems to provide a sufficiently free boundary while retaining hydraulic fluid pressure. The specimens showed no sign of failure resulting from boundary restraints. Because the platens of the test fixture move during testing, there is no problem testing specimens which decrease in length as a result of a high Poisson's ratio.

The next best test results were obtained with axial load only tests. There were some problems resulting from eccentric loading; however, there was good repeatability of the maximum failure load. Equal hoop and axial load strength would be expected for a material with a symmetrical ±45° ply layup; however, the axial load results were lower than the internal pressure test results. There were also some blooming and buckling at the specimen ends resulting from local end restraints. This problem would be less on materials with a lower Poisson's ratio. The setup and installation procedure for the axial load tests was easy and similar to the internal pressure tests.

Good results were also obtained from the biaxial testng with internal pressure plus axial loading. Generally the specimens tested with higher relative axial loads showed more damage resulting from end constraints; however, there was little correlation between the biaxial stress ratio and the shape of the failure envelope. The setup and installation was very easy and similar to the internal pressure and axial load tests.

Very poor and unpredictable results were obtained from the test using external pressure loads. The specimens failed in buckling at very low loads. The buckling was the result of compressive hoop stresses. Further studies should be made to find a better specimen geometry. Installation of the external pressure collet was very difficult when the specimens were instrumented with external gages. There was minimal space to maneuver instrumentation wires between the specimen and the pressure collet.

A more complete evaluation could be made of the validity of the test system by testing specimens with known material properties. Also, a better evaluation of the system's repeatability can be made by testing several uninstrumented specimens and comparing the maximum loads and types of failures.

END

FILMED

12-83

DTIC